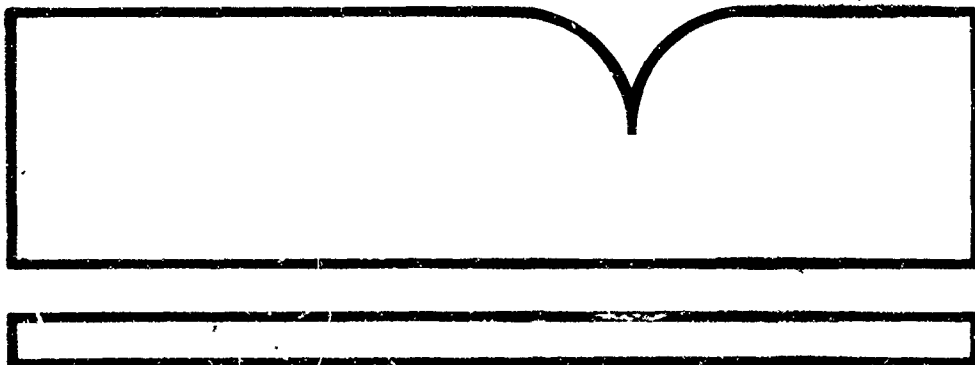AD-774-836

SUMMARY OF PROPELLER DESIGN PROCEDURES AND DATA. VOLUME II. STRUCTURAL
ANALYSIS AND BLADE DESIGN

William Amatt, et al

Henry V. Borst and Associates
Rosemont, Pennsylvania

Nov 73

AD-774 836

DOCUMENT CONTROL DATA - R & D

(Security classification of title, body of abstract and indexing annotation must be entered when the overall report is classified)

1. ORIGINATING ACTIVITY *(Corporate author)*	2a. REPORT SECURITY CLASSIFICATION
Henry V. Borst & Associates 353 Yorkshire Road Rosemont, Pennsylvania	Unclassified
	2b. GROUP

3. REPORT TITLE

SUMMARY OF PROPELLER DESIGN PROCEDURES AND DATA
VOLUME II - STRUCTURAL ANALYSIS AND BLADE DESIGN

4. DESCRIPTIVE NOTES *(Type of report and inclusive dates)*

Final Report

5. AUTHOR(S) *(First name, middle initial, last name)*

William Amatt
William E. Bates
Henry V. Borst

6. REPORT DATE	7a. NO. OF PAGES	7b. NO. OF REFS
November 1973		15

8a. CONTRACT OR GRANT NO. DAAJ02-72-C-0033	9a. ORIGINATOR'S REPORT NUMBER(S)
b. PROJECT NO	USAAMRDL Technical Report 73-34B
c. Task 1G162207AA7203	9b. OTHER REPORT NO(S) *(Any other numbers that may be assigned this report)*
d.	

10. DISTRIBUTION STATEMENT

Approved for public release; distribution unlimited.

11. SUPPLEMENTARY NOTES	12. SPONSORING MILITARY ACTIVITY
Volume II of a 3-volume report	Eustis Directorate U.S. Army Air Mobility R&D Laboratory Fort Eustis, Virginia

13. ABSTRACT

The technology needed for the design and installation of propellers is presented and summarized in three volumes.

Volume II (Structural Analysis and Blade Design) contains the theory and data for the detailed structural and vibration analysis of propellers. Included are estimating procedures for initial design purposes; the details for designing solid, hollow, and composite blades; and manufacturing techniques used. /

DD FORM 1473 REPLACES DD FORM 1473, 1 JAN 64, WHICH IS OBSOLETE FOR ARMY USE.

DISCLAIMERS

The findings in this report are not to be construed as an official Department of the Army position unless so designated by other authorized documents.

When Government drawings, specifications, or other data are used for any purpose other than in connection with a definitely related Government procurement operation, the United States Government thereby incurs no responsibility nor any obligation whatsoever: and the fact that the Government may have formulated, furnished, or in any way supplied the said drawings, specifications, or other data is not to be regarded by implication or otherwise as in any manner licensing the holder or any other person or corporation, or conveying any rights or permission, to manufacture, use, or sell any patented invention that may in any way be related thereto.

Trade names cited in this report do not constitute an official endorsement or approval of the use of such commercial hardware or software.

DISPOSITION INSTRUCTIONS

Destroy this report when no longer needed. Do not return it to the originator.

.

SUMMARY OF PROPELLER DESIGN
PROCEDURES AND DATA

VOLUME II
STRUCTURAL ANALYSIS AND BLADE DESIGN

By

William Amatt
William E. Bates
Henry V. Borst

Prepared by

HENRY V. BORST & ASSOCIATES
Rosemont, Pennsylvania

for

EUSTIS DIRECTORATE
U.S. ARMY AIR MOBILITY RESEARCH AND DEVELOPMENT LABORATORY
FORT EUSTIS, VIRGINIA

ii

SUMMARY

This volume presents the structural design and analysis of the high-performance aircraft propeller. The various types of blade structures used, including solid, hollow, and composite blades are analyzed. The effects of changes of the various blade parameters such as diameter, thickness ratio and solidity are considered.

So that an accurate analysis can be conducted, a complete discussion of loads that the propeller will encounter is presented. Included are the loads generated when operating at high inflow angles, aerodynamic loads and centrifugal loads.

Complete methods of analysis are presented along with estimating procedures for the early design phases. The estimating procedures given are particularly important during the aerodynamic design and analysis phase so that the proper trade-offs can be made. The methods of analysis given include the basic blade stress calculation, propeller vibration and resonant frequencies, blade and flexural resonance, blade flutter, stall flutter, etc.

The structural section includes material for analyzing the hub and blade retention, and discussion of the various types of materials is also presented.

Propeller blades are discussed, including the basic design criteria, material considerations and details of construction. The basic methods for designing a blade are presented as well as the details of section layout blade integral characteristics for the hollow types and the shank fairing details.

The methods for blade manufacturing are discussed for solid aluminum, hollow steel and composite blades, along with the relative costs of each.

Blade ice control methods and also other environmental problems associated with blades are covered.

TABLE OF CONTENTS

Preceding page blank

TABLE OF CONTENTS (Continued)

TABLE OF CONTENTS (Continued)

TABLE OF CONTENTS (Continued)

TABLE OF CONTENTS (Continued)

TABLE OF CONTENTS (Continued)

TABLE OF CONTENTS (Continued)

Page

TABLE OF CONTENTS (Continued)

;

.

LIST OF ILLUSTRATIONS

xiii

LIST OF ILLUSTRATIONS (Continued)

LIST OF TABLES

LIST OF SYMBOLS

A	Angularity of air inflow, deg
A	Area of section, $in.^2$
A_q	The 1xP excitation factor, degree $lb/in.^2$
AF	Activity factor per blade
AR	Aspect ratio of the wing
a	Slope of lift curve vs. apparent angle of attack, $radians^{-1}$
a_o	Slope of lift curve for infinite aspect ratio
B	Number of blades
b	Blade chord, in.
b	Wing span, ft
b'	Semi-chord, ft
b_e	Effective chord length, in.
C	Torsional stiffness of untwisted blade section, in.-lb/rad per inch of length
C'	Torsional stiffness due to blade twist, in.-lb/rad per inch of length
C_L	Coefficient of lift
C_T	Total torsional stiffness of section, in.-lb/rad per inch of length
CF	Centrifugal force at any blade station r, lb
D	Propeller diameter, ft
d	Bearing ball diameter, in.
e	The base of the natural logarithms
E	Modulus of elasticity, psi
F	Vertical force on shaft, lb

LIST OF SYMBOLS (Continued)

F	Blade shear force, lb
f	Intensity of stress, psi
G	Shear modulus of elasticity, psi
g	Gravitational constant, ft/sec^2
h	Maximum thickness of section, in.
h_e	Effective section thickness, in.
I	Moment of inertia of section, $in.^4$
I_h	Hub polar moment of inertia, $slug-ft^2$
I_{max}	Major moment of inertia of section, $in.^4$
I_{min}	Minor moment of inertia of section, $in.^4$
I_p	Polar moment of inertia, $slug-ft^2$
J	Polar moment of inertia of section, $in.^4$
k	Radius of gyration, in.
k	Section constant for torsional stiffness formula, in.
k	Constant of an elastic spring
L	Length, in.
L	Lift, lb
M	Bending moment, in.-lb
M	The 1xP couple, in.-lb
M	Mach number
M_G	Gyroscopic moment, in.-lb
$M_y(x)$	Bending moment (vibratory) in fore-aft plane, in.-lb
$M_z(x)$	Bending moment (vibratory) in torquewise plane, in.-lb

LIST OF SYMBOLS (Continued)

m	Mass, slugs
N	Propeller rotational speed, rpm
n	Propeller rotational speed, rps
P	Load on beam or column or spring, lb
P_y	Loading component, vibratory, fore-aft plane, lb/in.
P_z	Loading component, vibratory, torquewise plane, lb/in.
Q'	Friction transmissibility (retentions) lb/in.
Q_a	Aerodynamic twisting moment, in.-lb
Q	Centrifugal twisting moment, in.-lb
Q_u	Centrifugal untwisting moment, in.-lb
q	Dynamic pressure, psi
R	Tip radius of blade, in.
r	Radius to any given blade section, in.
r	Radius of gyration, in.
S	Wing area
S.F.	The 1xP side force, lb
s	Blade radius, variable, in.
s_e	Endurance limit stress, lb/in.^{2}
s_o	Steady stress, lb/in.^{2}
s_v	Alternating stress, lb/in.^{2}
T	Torque, in.-lb
t	Plate thickness, in.
t	Time, sec

V	Velocity, fps
V_o	Apparent wind velocity, fps
w_L	Blade solid lead edge width, in.
w_T	Blade solid trailing edge width, in.
x	Blade radius, fixed, in.
y	Blade deflection, fore-aft plane, in.
y_{max}	Deflection of beam
z	Blade deflection, torquewise plane, in.
α	Angle of attack, apparent, deg
α_i	Inflow angle, deg
β_x	Blade angle at any given radius, deg
β	Contact angle (bearing races)
β_{ref}	Blade angle at the blade reference radius, deg
δ	Weight density, $lb/in.^3$
Z	Induced torsional stiffness factor, $in.^6$
ϵ	Unit strain, in./in.
ϵ	Local upwash angle
ϵ_o	Average upwash angle
λ	Reduced frequency parameter (flutter), Poisson's ratio
μ	Coefficient of friction
ρ	Mass density, $slugs/in.^3$
σ	Intensity of stress, psi
σ	Solidity factor (flutter)
C.F.	Centrifugal stress, psi

LIST OF SYMBOLS (Continued)

τ Intensity of shear stress, $lb/in.^2$

ϕ True wind angle

ϕ_o Apparent wind angle, deg

ψ Phase angle

Ω Rotational speed, circular frequency of vibration, rad/sec

ω Rotational speed, rad/sec

ω Torsional frequency of oscillation, rad/sec

INTRODUCTION

The purpose of this volume is to present the structural details
which must be considered in the basic design of the high-per-
formance aircraft propeller. As such, the presentation will
be concerned with the primary structural elements, loads and
methods of analysis. It is intended that these discussions
will be general yet inclusive; however, no attempt is made to
categorize specific procedures with a specific type of pro-
peller. Therefore, some discretion will be required on the
part of the analyst to determine whether a given criterion is
or is not applicable to this particular problem. An obvious
example: secondary plate stresses can be important in a mono-
coque type blade, but is of no concern in a blade having solid
sections. It must be further advised that the structural anal-
ysis should not be designated as, "a quick check to be sure
that things will hold together." Structural detail requires
an in-depth study and is an equal partner with aerodynamics,
weight and cost in achieving the optimum design.

STRUCTURAL ELEMENTS

In an elementary structural sense, the aircraft propeller's
basic function is to transmit the aerodynamic thrust and torque
to the airframe. The propeller is also a rotating mass, and
its components are subjected to centrifugal effects which are
self-balancing within the structure. A sketch of this ele-
mentary system is shown in Figure 1. There are three basic
components to be considered: (1) the blade, (2) the blade
retention, and (3) the hub. A general discussion of these
elements is presented on the following pages. A more detailed
discussion of analysis is given in the section Methods of
Analysis.

It should be noted that some treatments of propeller design
list only two basic components - the blade and the hub - with
the retention considered as part of either or both. More
recent experience has shown that a better understanding can be
achieved by considering the retention separately. It is also
obvious that there are other components in the total propeller
that require structural analysis. Generally, however, these
are associated with the control system and their analysis is
relatively straightforward.
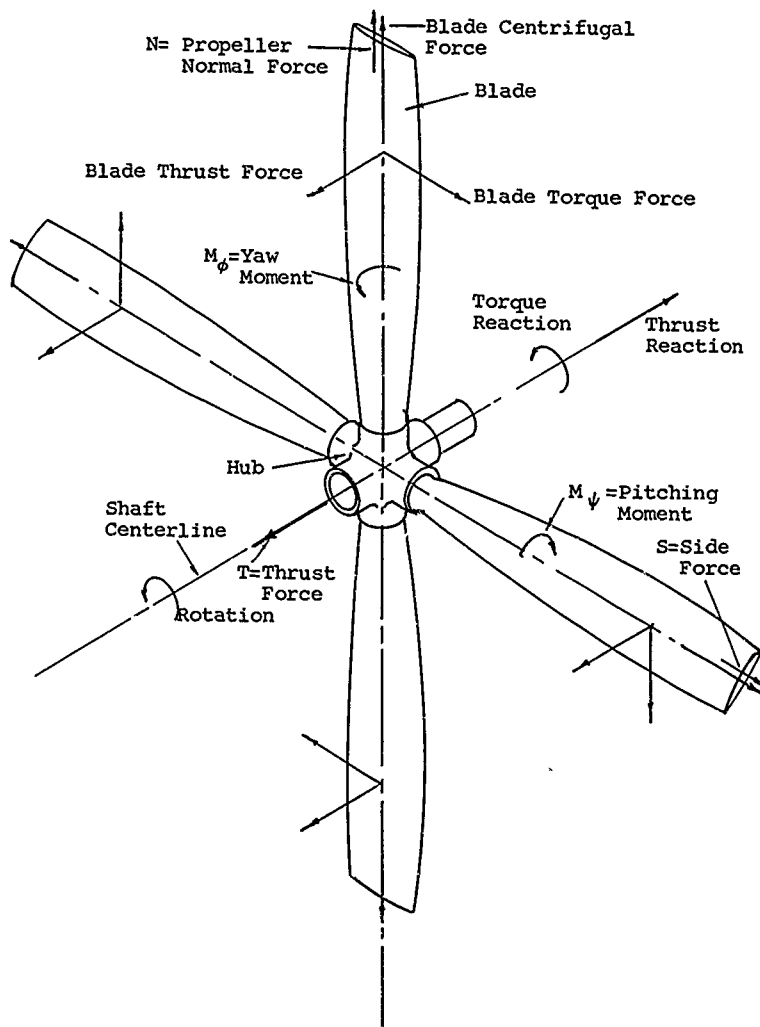
Figure 1. Typical Four-Bladed Propeller System.

THE PROPELLER BLADE

From a structural viewpoint the propeller blade can be con-
sidered as a cantilever beam fixed at the hub or shank end.
This beam is subjected to nonuniformly distributed axial and
lateral loads. Further, this beam has a varying cross-section
and a geometric twist along its length. Figure 2 illustrates
this beam configuration. Three basic parameters contribute to
the structural design: material, types of structure and aero-
dynamic parameters.

Material

A primary requirement of propeller material is a high strength-
to-weight ratio and a high fatigue strength. In the larger
high performance propeller, steel (SAE 4330, 4340; UTS=140000
psi and up) and aluminum alloys (2025S & 7075S) have been ex-
tensively used. The major background and experience is with
these materials, and their continued use would be recommended
for conventional application and where a material evaluation
program is not practical. Both magnesium and titanium alloys
have been considered in blade design studies. These materials
have not been extensively evaluated by practical application,
but they offer a potentially good material from a structural
standpoint. For future applications, composites appear to
offer the blade designer the best opportunity to achieve the
optimum weight-strength design. Fiber glass reinforced plas-
tic blades have been designed and built for prototype appli-
cations at a significant weight saving, as compared to their
metal equivalent. An extensive material evaluation program
would be required to select an optimum material from the com-
posites currently available.

Types of Structure

There are three primary types of blade structure: solid, hol-
low or monocoque, and spar type. Typical cross sections are
illustrated in Figure 3 .

Solid Section

The solid blade is the easiest to manufacture, and the struc-
tural analysis is relatively straightforward. The normal
service damage, nicks, scratches, etc., can be easily removed
by grinding or polishing without a significant loss of mate-
rial. As with all solid section structures a large portion of
the material is not being used to its full potential and there-
fore, this type of blade is not an optimum weight design.

Torque Loading

2 — Trailing Edge

1

Centrifugal Force

Axis

2 — Leading Edge

3

→ Shank — Transition — Airfoil →

(a) Planform View

Thrust Loading

Camber Side

Thrust Side
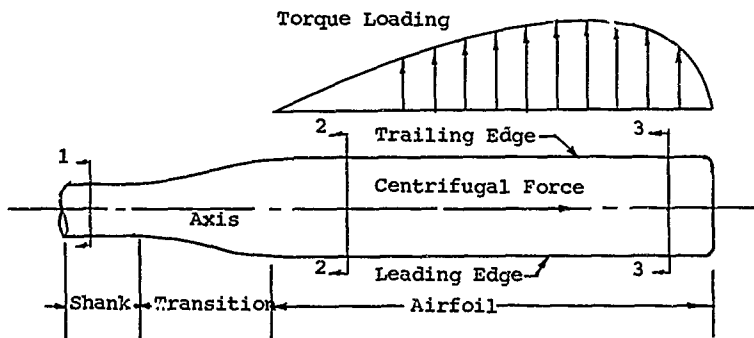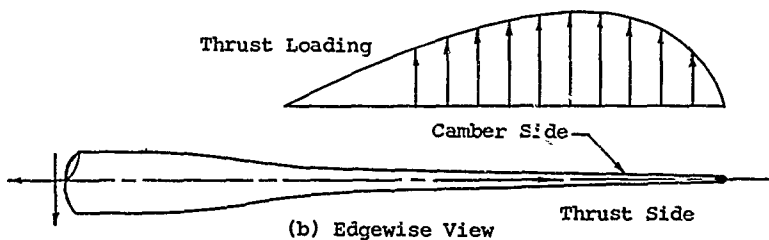
(b) Edgewise View
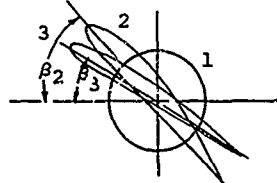
(c) Sections

Figure 2. The Blade Beam.
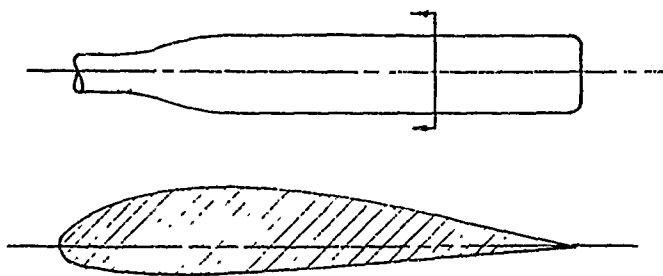
(a) Solid Section
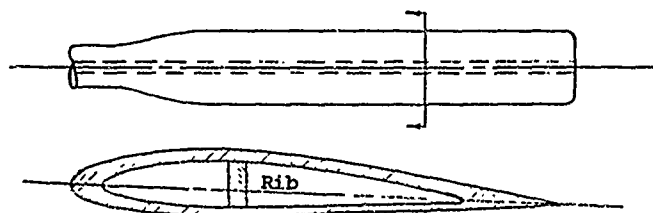
(b) Hollow Section
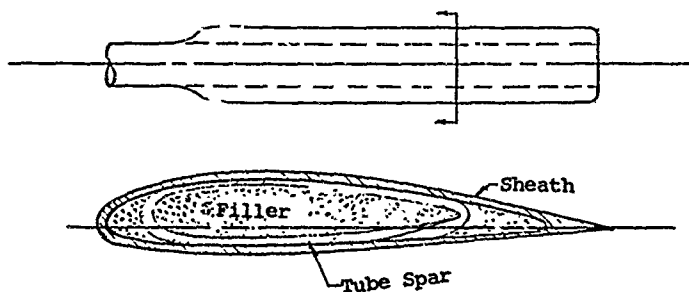
(c) Spar Section

Figure 3.   Blade Types.

However, in small diameters (up to 13-14 ft) the weight differential between the solid and other types of construction can be small. In fact, up to about 13½ ft, a solid aluminum blade is lighter than a comparable hollow steel design. Therefore, because of its simplicity the solid section type has been almost exclusively used in the smaller sized propellers on conventional aircraft installations. As the propeller size increases, the weight of the solid blade can become prohibitive. Also in special application, VTOL for example, where an optimum weight is essential, the solid blade would generally be undesirable.

Hollow Section

The hollow or monocoque design gives the designer considerable freedom to utilize the material to its design potential and therefore achieves a good strength-weight balance. The fabrication cycle of this type structure is more involved than in the solid design, and the various techniques (welding or forming in metal and filament orientation in composites) can influence material properties and therefore, the structural design. Manufacturing processes also have a significant influence in determining the size of the internal cavity; sharpness (stress concentration) at internal fillets, and minimum plate thickness, thereby imposing some limits on the design potential.

Structural analysis of the hollow type structure is considerably more complex than in the case of the solid design. The beam section is a plate or shell structure, and the associated problems of deformation, buckling and plate vibration must be considered by the analyst. In blades having a large plate span, these effects can be controlled by the use of longitudinal ribs, or by using a lightweight filler such as foam. The transition area, Figure 2, of this blade must also be carefully designed. An abrupt fairing from the airfoil to the round shank section can induce very high local stresses.

Hollow blades also contain a volume of trapped air which under rotation develops a centrifugal head, subjecting the plates to a high internal pressure in the tip region. For this reason the tip of the hollow blade is usually vented. Further, if the blade material is prone to atmospheric corrosion, the internal surfaces, which are not readily accessible for inspection, must be protected to prevent such corrosion and resulting stress concentration. Service damage becomes a significant factor in the hollow type blade design. In the thin plate the normal nicks and scratches can become serious stress-raisers and it is essential to provide extra plate thickness so that normal damage can be safely blended out.

6

Spar Section

The spar type of blade is a modification of the monocoque design. It consists of a main spar or structural member which is a simple round or elliptical tube. The airfoil is then formed by bonding a thin sheath to the spar structure; stainless steel and composites have been used in prototype designs. Generally, the cavities are filled to provide plate stability. The design and analysis of the spar is essentially the same as in the case of the hollow design. However, the simpler tube shape is generally easier to fabricate than in the case of forming a tube airfoil section. A significant advantage is that the primary structure is protected from service damage and a design allowance for the resulting stress concentration and material removal for repair are not required. Therefore, the only limitations imposed on designing the spar to an optimum strength-weight ratio are those that may be imposed by manufacturing processes. Another unique feature of this type of design is that when the sheath is damaged beyond acceptable limits, it can be removed and replaced without loss of the main structural element. The major design criteria with this type of construction is to provide adequate bond between the spar and the sheath. If a sheath is lost due to bond failure, the aerodynamic and mass balance of the propeller is destroyed. The resulting force unbalance could be catastrophic.

Aerodynamic Parameters

The aerodynamic parameters are, for purposes of this discussion, defined as those blade dimensions or characteristics which are established primarily to obtain the specified propeller performance. These factors influence the structural design of the blade and include airfoil section, activity factor, thickness ratio, and pitch distribution.

Airfoil Shape

The selection of the blade cross section or aerodynamic shape is the primary responsibility of the aerodynamicist. However, it does define the structural characteristics, area, moments of inertia, etc. In present-day propellers the NACA series 16 or series 65 sections are commonly used. A representative plot of the thickness vs. the chord of these two sections is shown in Figure 4. It is obvious that the fuller trailing edge of the 16 series will provide slightly higher structural characteristics. In hollow sections particularly, small changes in stiffness and moments of inertia can be obtained without a significant mass increase by using the 16 section rather than the 65. The choice of section can therefore become a compromise.

7
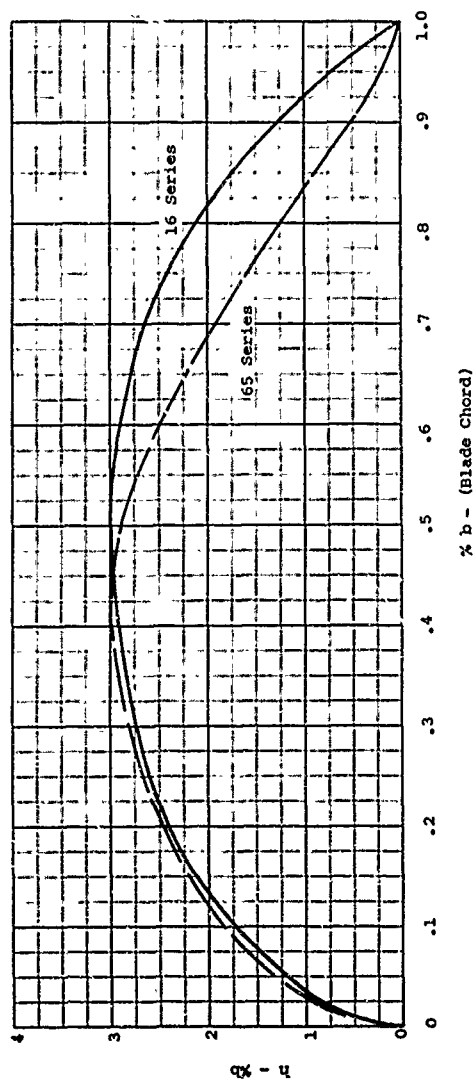
Figure 4. Thickness Distribution for Series 16 and 65 Airfoils.

8

Activity Factor, Thickness Ratio and Pitch Distribution

The blade activity factor, thickness ratio and pitch dis-
tribution define the basic blade dimensions and rate of
twist along the blade span. While being primarily de-
fined by aerodynamic performance requirements, these same
dimensions are fundamental to the strength and stiffness
characteristics of the design. It is therefore essential
that the aerodynamic and structural requirements are
fully coordinated early in the design phase. It has been
common experience to require some compromise of aero-
dynamic ideals, particularly with respect to thickness
ratio, in order to satisfy structural integrity.

BLADE RETENTION

The blade retention is basically a joint by which the propel-
ler blade is attached to the propeller hub. The function of
this joint is to transmit the blade loads to the hub structure
while permitting the blade freedom of rotation about the pitch
change axis. There are a multitude of retention designs and
a detailed discussion of all types would be impractical in
this report. Rather, a basic retention is presented in some
detail and other versions which have been used are shown to
illustrate various approaches to the design problem. The
essential components of any retention involve the blade shank,
a bearing, a hub attachment and the hub barrel. These elements
will be discussed primarily with respect to structural require-
ments. There are, however, numerous details such as provision
for lubrication, seals, etc., that must be considered in the
overall design. It must also be noted that provision must be
incorporated to permit a good preload to the bearing stack to
ensure an essentially fixed end restraint on the blade.

The so-called flanged shank type of retention, referred to as
the standard retention, has been one of the more popular de-
signs, and a typical configuration is shown in Figure 5 .
This type of retention is a simple design and has the advan-
tage of an extensive developmental history. It is easy to
assemble and provides for an easily accessible means of apply-
ing a solid preload to the bearing stack.

The Blade Shank

The typical flanged blade shank is shown in Figure
6 as a free body subjected to the blade forces. The blade
shank can be considered as a fundamental element in the over-
all design of the system. With the loads known, it is a rela-
tively simple procedure to establish a structurally adequate
tube section. However, the analyst has a considerable choice
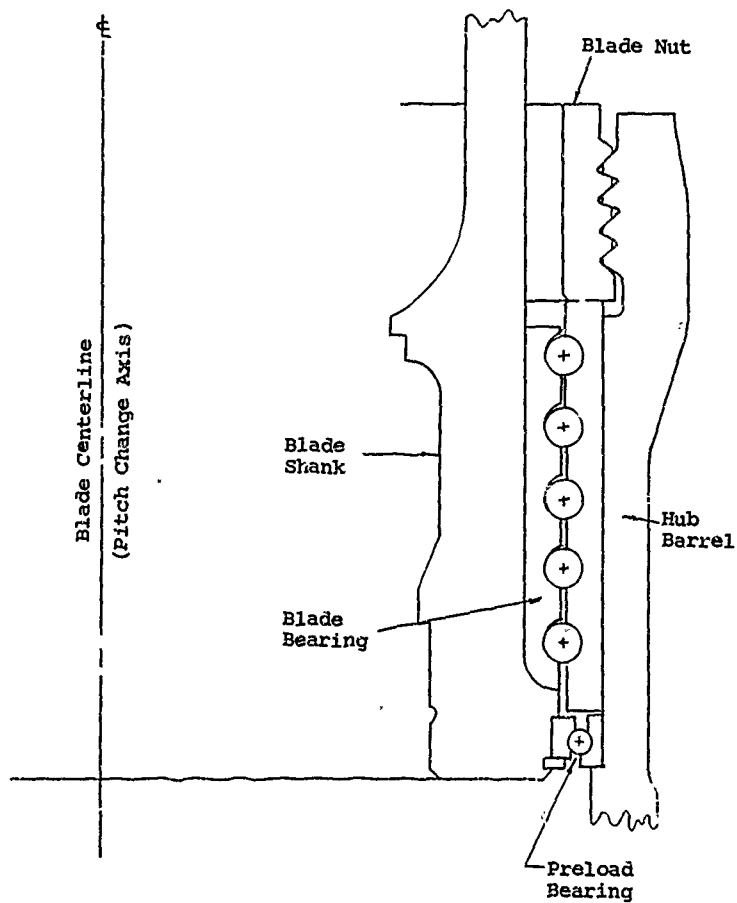
Figure 5. Typical Section
Standard Blade Retention.

10

between diameter and wall thickness. It is apparent from Figure 5 that the shank diameter establishes the bearing diameter and the hub barrel diameter, and is thus a primary factor in determining the hub size or a significant portion of the overall propeller weight. It may therefore be desirable in preliminary design phases to select more than one shank size and lay out the resulting bearing-hub structure to evaluate the most desirable configuration. For interchangeability reasons, the propeller industry has established standard shank sizes. These are measured by the outside diameter, diameter m, as in Figure 6, and these standard sizes are given in Table I . Generally a standard size is selected but this is not mandatory and bastard sizes have been used. The 4¾ shank (146.3 mm) diameter has been quite common. The inside diameter and the flange dimensions are selected to satisfy structured requirements. The high stress area of the shank is the flange fillet. Standard flange analysis methods are generally used,and extensive testing and photoelastic study have indicated a stress concentration in the order of 1.1 to 1.2 for the usual shank proportions. Typical shank dimensions for steel shanks are given in Table II.

As an added safety precaution, the fillet area is usually subjected to cold work, rolling and short peening to improve the fatigue strength of the material. With this type of design it should be noted that the inner bearing race is made in two halves. There is therefore, a high bearing stress against the blade shank and the under vibratory loads relative motion between race and shank. The shank bearing surface is therefore subject to galling,and the associated high stress concentration. To alleviate this condition, that area of the shank is usually short-peened. The short-peened surface is less susceptible to galling and further, the small pockets retain lubricant, giving further protection.

Blade Bearing

The blade bearing transmits loads from the blade shank to the blade nut while permitting rotation around the blade axis. For this type of retention a special angular contact thrust bearing is required. A typical bearing is shown in Figure 7. Figure 7a shows a single piece race, while Figure 7b shows a similar design with individual races; both types have been used. Generally, the single piece race provides a more rigid joint and minimizes galling on the blade shank and hub barrel. The individual race is,however, easier to install. The retention bearings are made as matched sets and the inner race is then split diametrically, so that it can be installed over the blade flange. The entire bearing is built up in place on the blade shank.

Figure 6. Typical Flanged Blade Shank.

12
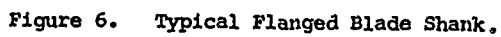
TABLE I.	SHANK SIZE – DIAMETER
Shank Size No.	Nominal Diameter (Millimeters)
2	115
3	130
4	140
5	165
6	175
7	190
8	205

TABLE II.   FLANGED SHANK DIMENSIONS, NOMINAL, STEEL BLADES, REFERENCE FIGURE 6

Shank Size	Dimension						
	m	l	d	p	h	h_1	r
2	4.5262	3.236	5.1160	5.25	.625	.644	.140
4	5.5101	4.220	6.1004	6.23	.625	.644	.140
$4\frac{1}{4}$	5.7713	4.220	6.2353	6.36	.750	.774	.140
5	6.5056	4.546	7.062	7.22	.850	.979	.140
6	6.8880	5.000	7.584	7.688	1.150	.941	.250
8	8.0720	6.401	8.880	8.880	1.165	.834	.250
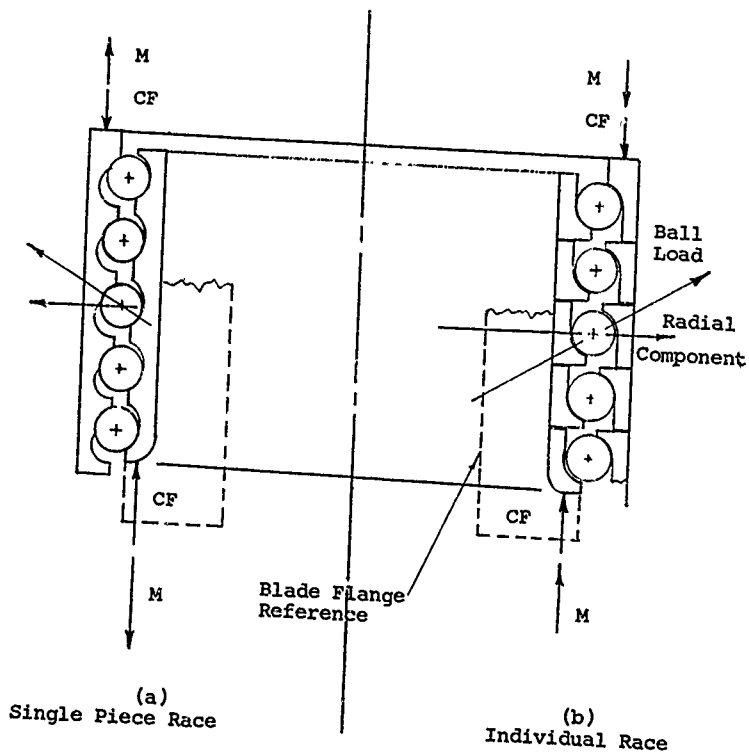
Figure 7.   Typical Blade Bearing.

14

The design of the bearing is primarily predicated on Hertzian stress and for this type of application, a mean stress of 350,000 psi with intermittent values up to 400,000 psi has proven satisfactory. However, the bearing analysis can become quite involved and it is recommended that standard references such as Jones, A., Reference 1 should be used.

In this type of bearing application, the bearing experiences a very low rotational speed, 20 to 30 degrees per second on conventional aircraft, and is subjected to high steady and vibrating loads. With extensive service time it is common to find light brinelling of the races. However, it is to be noted that in a sense this type of bearing can be considered a fail-safe design. The bearing can experience extreme damage, brinelling, spalling, cracked balls, etc., and still perform its function of keying the blade to the hub. This has been demonstrated numerous times on test installations where the blades have been locked at a fixed pitch and the propeller run under high loads. In such testing, bearing damage has been extreme without any serious effect on the propeller function. However, excessive damage should not be tolerated on a flight propeller. While there is no danger of throwing a blade with extensive damage, there is a possibility of jamming, thereby curtailing pitch control.

In addition to stress, there is another consideration which can influence the design of the retention bearing and also determine a minimum retention diameter. This is overturning. Referring to Figure 7, it is seen that on one side of the stack the moment couple force, M, is opposed to the centrifugal force. If the moment is relatively high this couple force can balance out the centrifugal effect and completely unload one side of the stack. This will produce an undesirable pounding. The condition can be alleviated by decreasing the couple, i.e., increase in the retention diameter.

A unique feature of this type of stack bearing is in the development of friction forces which tends to damp out vibrating forces and thereby relieving the hub thread loads. The angular contact bearing generates a radial force component, Figure 7, which expands the outer race against the hub-barrel. The contact pressure then provides a frictional force which absorbs a portion of the axial vibratory load components. To augment this effect, the outer race on some designs has been made with a single radial split. This eliminates the hoop restraint of the race and provides a higher hub-bearing contact pressure and higher frictional damping. Tests on such designs have shown that as much as 10 to 20 percent of the vibratory loads are absorbed and do not pass through the hub thread joint.

A design precaution should also be noted. The edges of the raceways adjacent to any split lines must be carefully blended

15

to assure smooth rolling of the balls over the split. Other-
wise a ball can hang-up and jam the bearing. On installation
it is also desirable to locate splits along the neutral axis
of the blade bending. For reference purposes, typical bearing
data is tabulated in Table III.

The Blade Nut

The blade nut provides the solid attachment between the blade
and the hub. The free-body is illustrated in Figure 8, and it
is essentially a ring subjected to a distributed twisting
moment, force times eccentricity e. The analysis is straight-
forward. The nut does, however, contain some type of locking
device, usually involving lugs with fillets, or tapped holes,
etc. These present stress concentrations and potential crack
origins. The thread itself is usually designed in conjunction
with the hub thread and is discussed in more detail in the
following paragraph.

Hub Barrel Thread

Experience with this type of retention has shown that the hub
thread is structurally the critical part of the retention.
The typical cross section is shown in Figure 9 . The high
stressed area is obviously at the thread relief fillet where
there is a combination of thread bending, local bending of the
hub barrel, and axial load. The design of this area is further
compounded by the well-known fact that a normal threaded con-
nection has unequal distribution of load between threads with
the first thread carrying a major portion of the total load.
A more uniform load distribution can be obtained by tapering
the nut thread as illustrated in Figure 9 . This design pro-
vides for the most outboard thread to provide the initial re-
action and as the structure deforms, successive turns pick up
their proportionate share of load. The tapered thread is usu-
ally incorporated in the more highly loaded installations. A
taper in the order of 0.025 inch   per inch of thread length
is generally required. However, establishing an optimum design
requires a detailed analysis involving deformations of the
threads, nut and hub.

A four-pitch modified buttress thread has been extensively
used for the hub-nut joint; in the order of three to four full
turns is generally required. Typical characteristics of the
hub thread relief area are given in Table IV.

Retention Variation

There have been several modifications to the basic retention

16

TABLE III. TYPICAL BLADE RETENTION BEARING DATA STEEL BLADES

Shank Size	No. Rows	Balls Per Row	Race Curvature Inner % Ball Diam.	Outer % Ball Diam.	Ball Diam. (In.)	Pitch Diam. (In.)	Outside Diam. (In.)	Inside Diam. (In.)	Race Inner (In.)	Length Outer (In.)
2	3	41	50.5	51.5	3/8	5.244	6.1056	4.530	2.16	2.10
4	3	42	↑	↑	.4375	6.228	7.0866	5.5118	2.325	2.10
4¾	5	63			5/16	6.41	7.0876	5.7688	2.83	3.2283
5	4	56			3/8	7.246	8.0697	6.496	2.95	2.95
6	3	42	50.5	51.5	9/16	7.972	9.0557	6.8892	3.1875	2.85

17
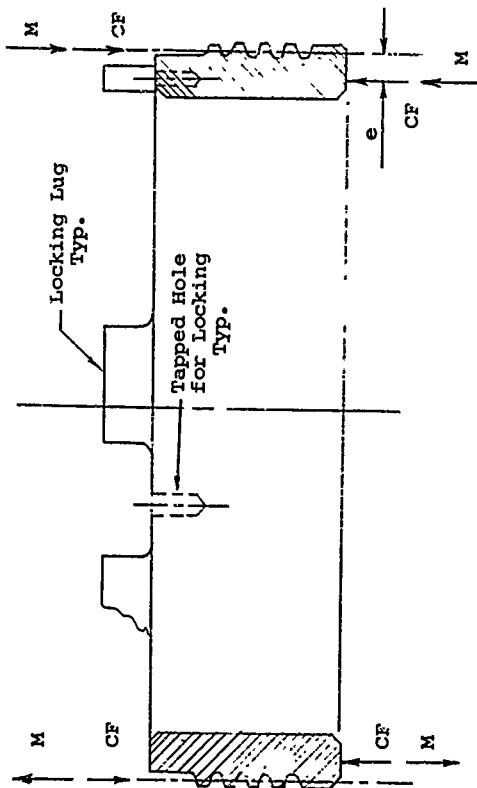
Figure 8. Typical Blade Nut Section.

18
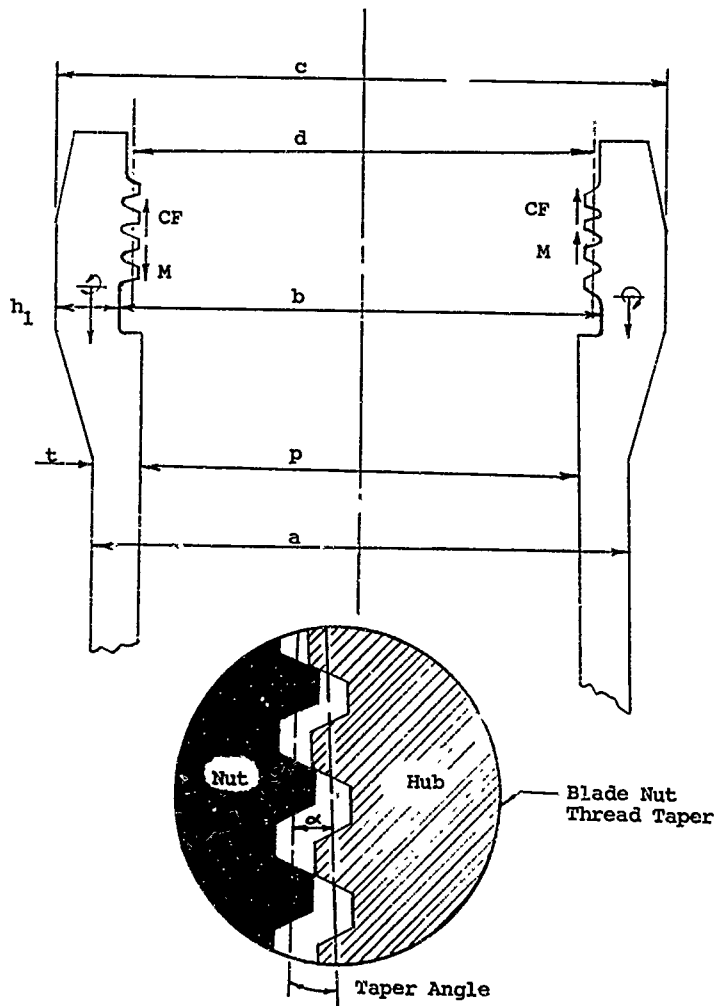
Figure 9. Typical Hub Barrel Section.

TABLE IV. TYPICAL HUB BARREL DIMENSIONS –
REFERENCE FIGURE 9

Shank Size	Thread P.D. (d) (in.)	Bore Diam. (p) (in.)	BBL O.D. (a) (in.)	BBL Thickness (t) (in.)	Thread Relief ID (b) (in.)	OD (c) (in.)	Thickness (h₁) (in.)	No. of Threads
2	6.243	6.105	6.645	.270	6.434	7.27	.423	2.9
4	7.227	7.089	7.83	.371	7.418	8.45	.521	3.9
5	8.06	7.923	8.67	.358	8.252	9.31	.529	4.0
6	9.19	9.057	9.81	.377	9.385	10.48	.552	3.0
8	9.98	9.845	10.625	.391	10.172	11.28	.559	3.0

as shown in Figure 5 . The following paragraphs will present
and discuss some of these adaptations which have been used in
various propeller designs.

The Dural Shank

In the recent propeller development a flanged shank type reten-
tion, essentially the same as shown in Figure 6 , has been
used with the dural propeller. The initial problem with the
dural flange is one of contact between the steel bearing race
and the softer aluminum, particularly a digging-in at the
split line of the bearing race. This situation is eliminated
by placing a continuous steel ring or washer around the shank
to provide a continuous bearing surface against the flange.
This is illustrated in Figure 10 . Obviously, the ring must
be installed on the shank before the upset and final machining
of the flange, complicating fabrication to some degree. The
design of the ring flange-bearing race should be carefully pro-
portioned so that the force line is essentially through the
ring centroid (more correctly the shear center), in order to
eliminate any twisting tendency of the ring. The galling
tendency between the inner race and shank is effectively con-
trolled by shot peening the shank, and generally the bearing
I.D. is silver plated. The lower strength aluminum requires a
heavier flange than the corresponding steel design. Table V
shows a dimensional comparison between similar sized shanks in
the two materials.

Integral Race Retention

This configuration is an attempt to reduce propeller weight by
eliminating the individual bearing races and the need for a
thread hub-nut joint. In this design the bearing races are
machined into the hub and blade shank. The design is shown
schematically in Figure 11 . The design has been used on some
designs but has not received widespread acceptance. Machining
and hardening the raceways obviously complicates the fabrica-
tion of the hub and blade shank. Further, a filler hole must
be provided in the barrel to permit assembly of the balls.
This hole is plugged after assembly. Preloading the assembly
presents a design problem, and this is generally accomplished
by providing some means of jacking the blade outward from in-
side the hub. Integral race retentions have been designed to
be used without preload, thus eliminating a difficult problem.

Structurally, this type of propeller introduces high local con-
tact stress on a structure which is also subjected to relatively
high bending and tension loads. The combined effects must be
considered by the analyst. Further, the filler hole in the hub
presents a potential stress concentration and it should be

21
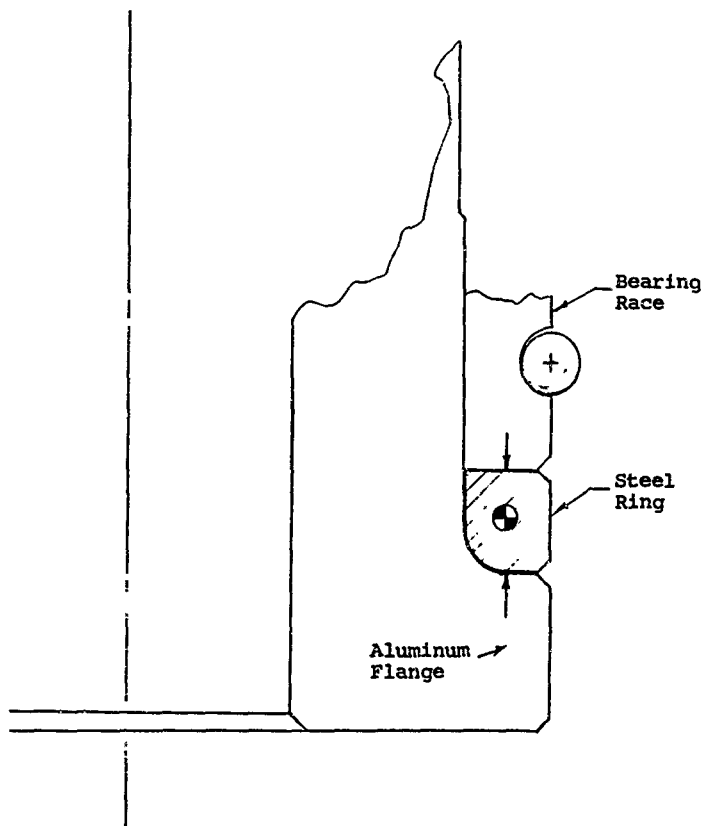
Figure 10.   Flanged Shank — Dural.

22

TABLE V.	DIMENSIONAL COMPARISON BETWEEN DURAL AND STEEL BLADE SHANK (REFERENCE FIGURE 6 FOR DIMENSIONS)					
Shank	m (in.)	l (in.)	d (in.)	h (in.)	h_1 (in.)	r (in.)
Steel	5.510	4.221	6.101	.626	.644	.135
Dural	5.501	2.685	6.921	1.251	1.408	.630
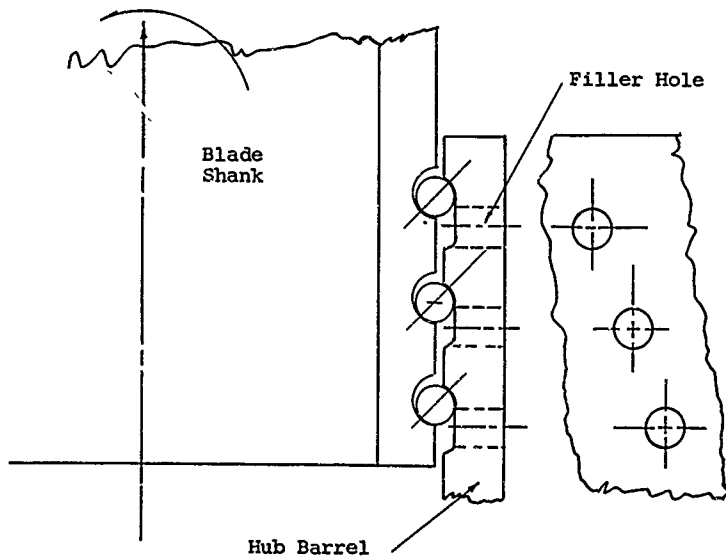
Figure 11. Typical Section - Integral Race Retention.

23

located in a relatively low stress area, i.e., close to the
neutral axis bending. This integral type bearing cannot be
considered a fail-safe design. Since the shank and hub are
subjected to high bending and tension stress, pitting or gal-
ling of the raceway introduces a stress concentration and
potential crack origin,and failure of the hub or blade shank
would be catastrophic. It is also apparent that with this type
of design, any significant damage to a bearing race requires
scrapping an entire hub and/or blade rather than replacing a
relatively inexpensive bearing stack.

Flanged Hub Retention

In this configuration of the basic retention, the threaded hub-
nut joint is eliminated by incorporating an internal flange
with the hub barrel. A typical section is shown in Figure 12.
Structurally this retention is essentially the same as the
standard design and it presents no special consideration since
the hub flange is a common analysis problem. The retention
bearing of this type has to be assembled on the shank from in-
side the hub, which can be an assembly problem. Preload as in
the case of the integral race design, is generally accomplished
by jacking the blades outward from inside the hub. Another
type of preload system has been used on these types of propel-
lers, and is shown schematically in Figure 13 . This system
uses a series of compression springs between the hub and blade.
It has the advantage of being external and therefore, readily
accessible. This system has proven satisfactory in limited
service, but it does not provide as rigid a system as the stan-
dard design and results in significantly less damping with
respect to blade vibration.

PROPELLER HUB

The propeller hub provides the necessary reaction for the
blade loads. Some of the load components,such as centrifugal
force, are balanced out within the structure; other components,
such as aero loads, are transmitted by the hub to the
airframe. Structurally, the hub can be regarded as a series
of intersecting cylinders hub barrels, hub body, and the rear
extension. This system is shown schematically in Figure 14.
As will be shown later in the section on Loads, the summation
of the blade aerodynamic loads at the hub results in six com-
ponents of load that must be reacted by the hub supporting
structure. These reactions are shown in Figure 14. For a
given power and speed, the thrust and torque are constant, but
the other load components can change in direction and magnitude
depending upon the propeller attitude with respect to free-
stream velocity. The magnitude can vary from a negligible
value to a significant design parameter.

24
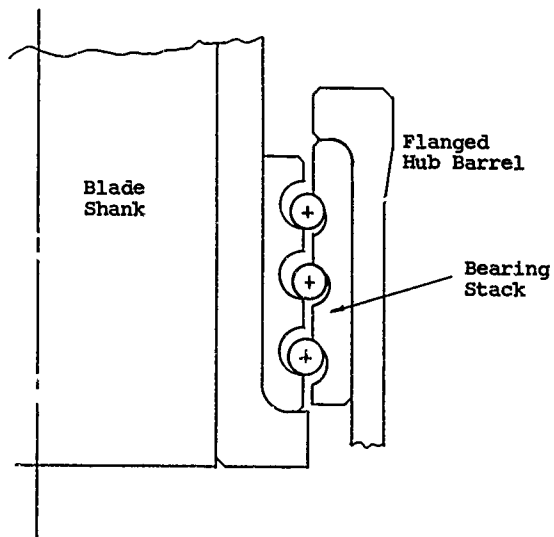
Figure 12. Typical Section - Flanged Hub Retention.
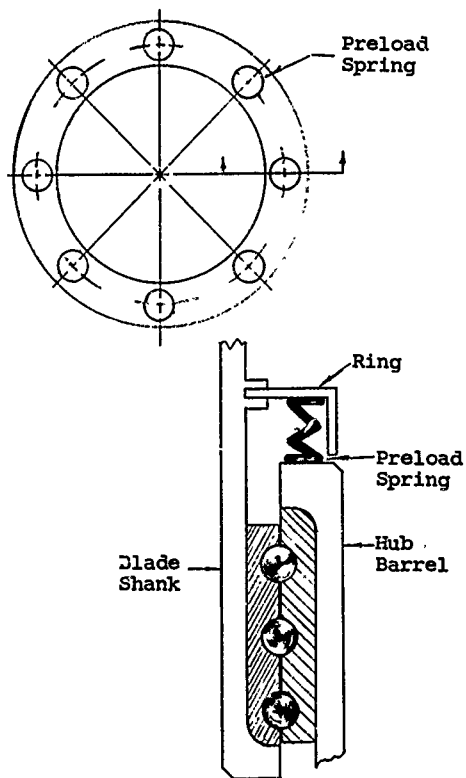
Figure 13. Spring Type Retention Preload.
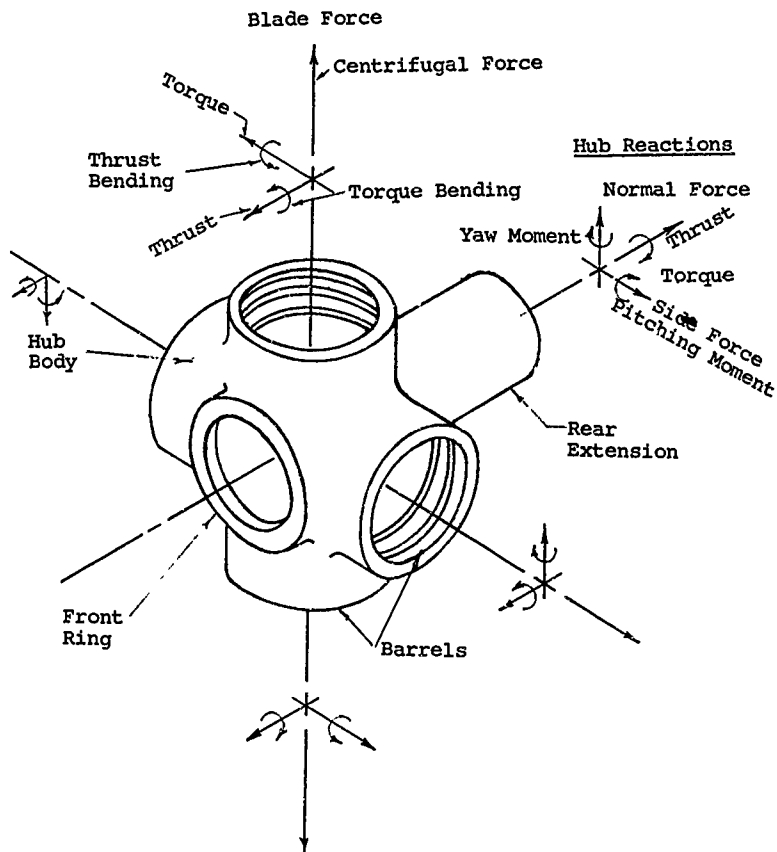
Figure 14.   Schematic Hub Load System.

The hub body, in addition to its structural function, generally serves as a housing for gearing, linkages, etc., associated with the blade pitch change system, and its envelope and internal structure depend to a large extent on the design details of a given pitch change mechanism. The front face of the hub often serves as a mounting surface for pitch change motors and other propeller accessories, and the electrical or hydraulic lines necessary to the function of these components are carried through holes or tunnels in the main body of the hub. The rear extension transmits the propeller loads to some aircraft supporting structure, such as the propeller shaft. In addition, this extension provides a convenient mounting surface for slip rings or other rotating joints.

It is obvious that with the type of structure and loading, the hub presents a highly redundant structure, and a detailed theoretical analysis presents a very complex problem. The initial design is, therefore, generally accomplished by comparison with similar existing models, and the final analysis is accomplished by experimental techniques using combinations of strain sensitive coatings and strain gages on prototype or model. Experience has shown that the most highly stressed areas are generally the front ring, and the region between the barrels. The rear extension can be considered as a tube subjected to tensions, torques and bending. However, it is to be noted that the section is rotating under a fixed moment, and therefore, fatigue is an important design parameter.

In the past, hubs have been made exclusively using high-strength steel such as 4340, heat treated to an ultimate stress of 140,000 psi or higher. Titanium has been considered in some study programs and would appear to be a satisfactory material with a potential weight saving.

There are basically two types of hubs which have been designed and developed for aircraft use. These are the shaft-mounted hub, and the nose-mounted design. General comments on these two types are given in the following paragraphs.

Shaft-Mounted Hub

The shaft-mounted propeller is the most common type of propeller mounting. The propeller is mounted directly on the engine propeller shaft using accurately machined cones and is retained by the thrust nut. This system is illustrated in Figure 15. Standard specifications have been established for the details of the cones, cone spacing and shaft details. This type of propeller is a relatively straightforward design and has proven to be entirely satisfactory for installations where the propeller moment, Figure 15, is not a predominant design factor. Referring to Figure 15, it is seen that the prop loads are

28
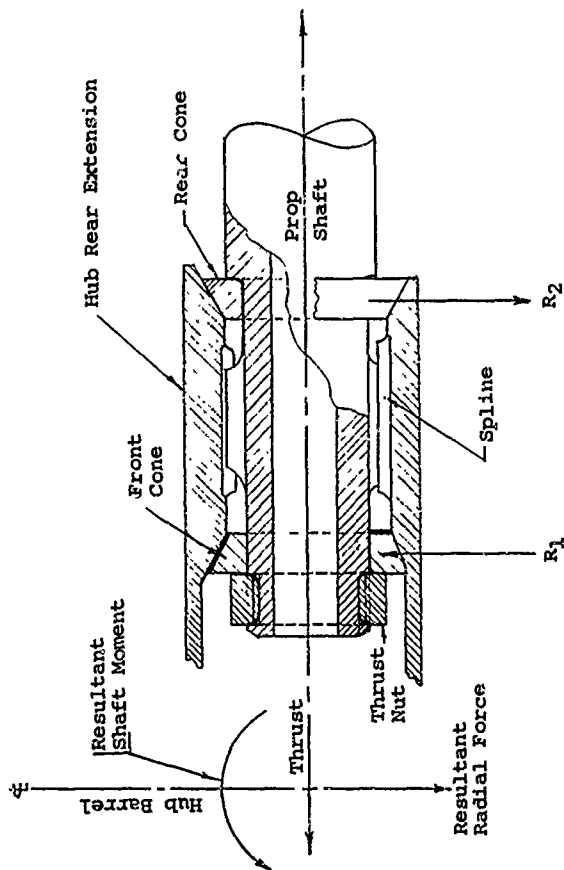
Figure 15. Shaft-Mounted Propeller Schematic.

29

transmitted directly to the shaft as a combination of bending, tension and torque, and through the shaft directly to the engine gearbox. It is further noted that under the bending load the rotating shaft is in fact a R-R Moore fatigue specimen. The propeller shaft therefore must be designed to satisfy this fatigue loading, and in those installations where the moment is large, the shaft, and its associated hardware, bearings, etc., can become unrealistically heavy with respect to its basic size requirement of transmitting thrust and torque. There has been a significant history of propeller shaft fatigue failures due to high propeller moments. In general, the simple shaft-mounted design would be selected for use on those applications where the magnitude of the propeller moment does not overly influence the size of the propeller shaft.

The Nose-Mounted Hub

The nose-mounted propeller was developed as one means of eliminating the need for larger propeller shafts to transmit the shaft moments on the more conventional shaft mounted design. A typical nose-mounted system is shown in Figure 16 . As seen, the propeller hub is mounted through a bearing directly to the engine nose, nacelle, or other convenient structure; the thrust and bending loads thereby by-pass the shaft completely. The primary propeller thrust and moment are transmitted directly to the propeller support as steady-state loads, and the shaft only transmits torque. The engine-shaft assembly using this style propeller can be a relatively light design as compared to more conventional shaft-mounted types. However, the large propeller bearing and supporting structure tend to compensate for the lighter shaft, and the overall propeller-engine weight may not be significantly different between the two types of propellers.

The major advantage of the nose-mounted system is that it eliminates the potentially serious combination of a prime structural member subjected to high fatigue loading.

The nose-mounted propeller requires a special bearing. Procedures have been developed for approximate sizing, but it is generally recommended that the final design be coordinated with a reputable bearing manufacturer to assure a satisfactory design for the application.

Development history of propellers, such as shown in Figure 16, has conclusively demonstrated an important design requirement. The inner bearing race is an interference fit on the hub, but in spite of the tight fit this race tends to walk, and in so doing tends to turn the thrust nut. Experience has shown this tendency to be quite pronounced, and a substantial lock must be provided between the nut and the hub.

30
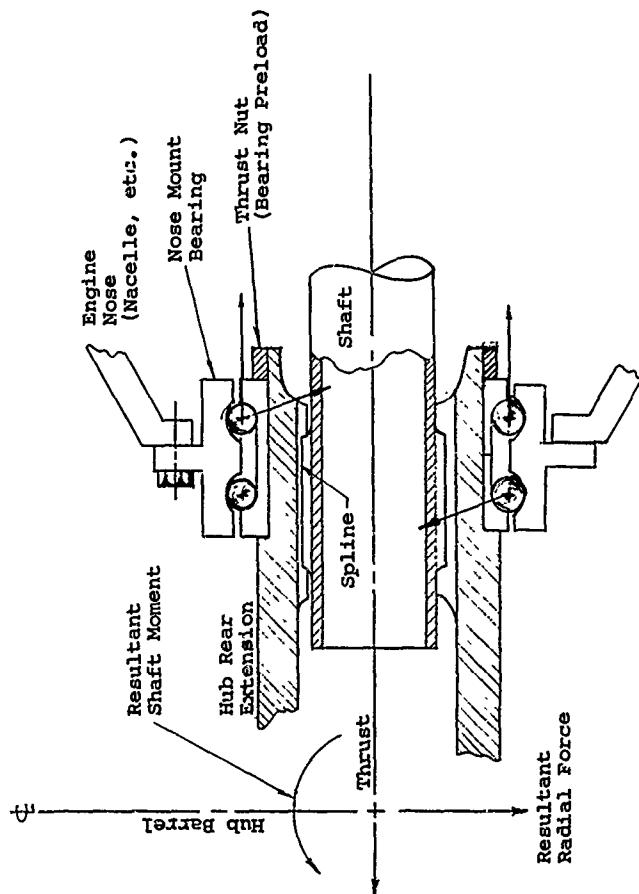
Figure 16. Nose-Mounted Propeller Schematic.

31

ESTIMATING PROCEDURES

Preliminary design and proposal effort often requires approxi-
mate size data well in advance of a detailed design effort.
The usual procedure is to determine the new design by a ratio
of an existing reference propeller system which has design
characteristics similar to those required in the new design.
To facilitate this estimating process, expressions have been
derived, some of which are based upon dimensional analysis and
others are empirical relationships. Constants have also been
established by averaging accumulated propeller data, and these
constants can be used when a suitable reference design is not
available.

From a structural consideration, the major effort has been on
establishing estimating procedures for blade properties and
loads, since with these quantities, it is a relatively easy
problem to rough size the retention and basic hub dimensions.
The basic blade parameters generally required are weight, sec-
tion data, loads and natural frequencies. These may be esti-
mated using the procedures given in the following paragraphs.

For the most part, only the estimating expressions are listed,
and no attempt is made to present the basic logic involved in
their development. However, some discussion will be given
when clarification is considered necessary. The accuracy of
these techniques will depend upon how they are applied. If
they are used to ratio from an appropriate reference design,
the results should be very good. Past experience has shown
that use of the given constants generally results in an error
within 10%.

ESTIMATING PROCEDURE - WEIGHT

The following expressions can be used to estimate the weight
of the high-performance aircraft propeller blade. It is to be
noted that these expressions are based upon a conventional
blade of the stated material with a generally rectangular plan-
form shape, and a standard flanged shank. It should also be
noted that the blade weight relations are given for the most
common materials, aluminum and steel. If other materials are
contemplated, a ratio of material densities can be applied as a
first approximation. However, allowable working stresses and
moduli (blade stiffness) are involved and some judgment of the
part of the analyst is required to compensate for these effects.

Solid Blade

$$\text{Blade weight} = K_W (AF)^2 (D)^3 \tag{1}$$

for aluminum $K_W = 3.28 \times 10^{-6}$

AF = Blade Activity Factor

D = Blade Diameter – ft

Hollow Blade

$$\text{Blade weight} = K_W (AF)(D)^2 \tag{2}$$

for steel $K_W = 4.35 \times 10^{-3}$

$$\text{Blade weight} = 1.2 \times 10^{-3} (AF)(D)^{2.3} \left(3.2 \frac{M}{(AF)(D)^3} - 1.84 \left(\frac{h}{b}\right)_{.4} + 1 \right) \tag{3}$$

where M = the total design vibratory shank moment $\pm$in.-lb
$(h/b)_{.4}$ = thickness ratio at the 0.4 blade radius.

Equation (2) is suitable for ratioing from a good reference blade or for obtaining a rough weight estimate. Equation (3) is considered the most reliable and has allowance for variations in thickness ratio and design load.

Hollow Fiber Glass Blade (Foam Filled)

Based upon a limited amount of design data, Equation (3) has been reevaluated for a fiber glass reinforced plastic blade, incorporating a flanged steel shank. The steel shank of these designs is in the order of 25 to 30% of the total blade weight. This relation is given as Equation (4) below as a rough guide for the use of a composite material.

$$W_T = 2.2 \times 10^{-3} (D)^{2.3} \left(0.228(AF) + \frac{M}{(D)^3} \right) \tag{4}$$

Total Propeller Weight

As a rule-of-thumb, the total weight of a propeller assembly, using metal blades, is in the order of twice the total blade weight.

33

Prop $W_T = 2$ x No. Blades x Blade Wt.   (5)

From limited data, the use of a fiber glass composite blade
results in a total prop weight in the order of 1.6 times the
total blade weight. The total propeller weight involves sev-
eral factors, such as retention, pitch change, mechanism,
shaft or nose mounted. Several expressions have been gener-
ated for estimating total propeller weight, but no expression
has been established which gives consistently more accurate
predictions than the above expression. Experience has shown
that a rough layout and sizing of the retention, hub and pitch
change components based upon the estimated blade loads, is the
most satisfactory way to estimate total propeller weight.

ESTIMATING PROCEDURES - BLADE SECTION DATA

A preliminary structural analysis requires blade section data
including area, moments of inertia, etc. Accurate data can
only be obtained from a section layout and integration. This
is a very time-consuming process and therefore expressions
have been derived for approximating the essential character-
istics. These estimating expressions are given in the fol-
lowing paragraphs.

When a suitable reference blade is available, the expressions
shown below can be used to ratio the properties of the new
design from that reference. With no blade reference available
the various constants developed are used to approximate the
desired section data. The given constants represent averaged
data and are adequate for initial sizing. However, the air-
foil thickness ratio and camber, design C_L influence the
section properties and the constants are more correctly form
factors.

Curves of these several factors are given in later sections
and by the use of those curves, section data can be estimated
quite accurately. The following data applies only to the
usual NACA 16 and 65 series airfoils. For other airfoil
shapes similar constants or form factors could be evaluated.
Data for round or elliptical sections can be obtained from any
structural handbook. Figure 17 is given as a reference for
basic data and definitions.

34

$$\text{Area} = \int dA$$
$$I_{min} = \int y^2 dA$$
$$I_{max} = \int x^2 dA$$
$$Z = \int x^4 dA$$
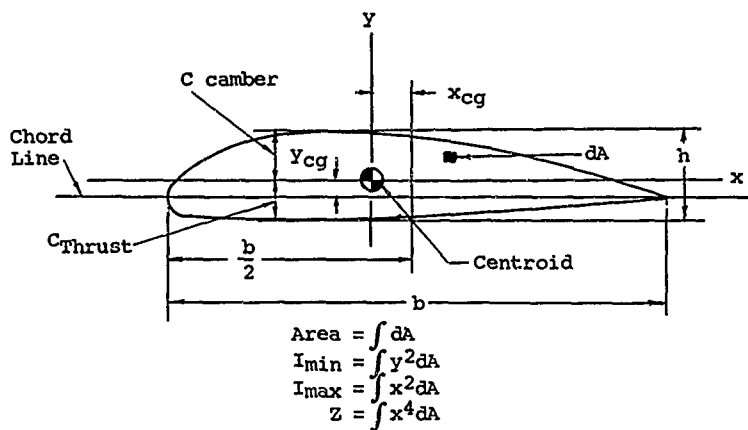
(a) General ordinates
and dimensions
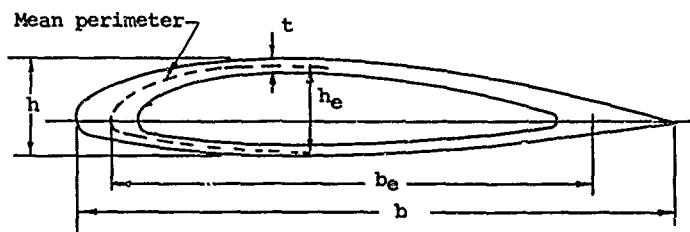
(b) Hollow section
specific dimensions

Figure 17.   Basic Airfoil Dimensions.

35

Solid Sections

PROPERTY	SERIES 16	SERIES 65
A = Area	.733 bh	.676 bh
I_{Min}	.0465 bh^3	.042 bh^3
I_{Max}	.0414 hb^3	.037 hb^3
Z	.0058 hb^5	.00454 hb^5
X_{cg}	-.018 b	.048 b
Y_{cg}	.046 bC_{Li}	.045 bC_{Li}

where C_{Li} = Section design lift coefficient

          h = Section thickness

          b = Section chord

Torsional stiffness is estimated from the equation

$$C_T = C \; + \; E\left(\frac{d\beta}{dr}\right)^2\left[Z \, - \, \frac{(I_{max})^2}{A}\right] \tag{6}$$

where C_T = Section torsional stiffness, $\frac{in.-lb}{rad/in.}$

        C = Kbh^3G

        K = .1793 Series 16 Airfoil

        K = .1492 Series 65 Airfoil

        G = Modulus of rigidity $lb/in.^2$

        E = Modulus of elasticity $lb/in.^2$

        $\frac{d\beta}{dr}$ = Rate of change of pitch distribution – rad/in.

The second term in Equation (6) generally contributes less than 10% to the total stiffness and can therefore be neglected in preliminary calculation. It is suggested, however, that the contribution of this factor be evaluated f'r at least two or

three sections to verify its importance.

Hollow Sections

The section properties of the hollow section are significantly influenced by factors other than airfoil shape. These include the number and spacing of longitudinal ribs and the fairing of the internal surface in the vicinity of the leading and trailing edge. As a consequence, the averaging of a considerable amount of airfoil data has shown that the same relationships can be used for either the NACA 16 or 65 hollow section, it is preferable however to ratio section data from an existing reference design. The constants given in the following expressions are considered good first approximation up to a thickness ratio of 0.40, and more accurate values can be obtained by referring to the curves in later sections. For specific dimensions peculiar to the hollow section see Figure 17.

$$A = \text{Area} = 2.23 \ bt \tag{7}$$

$$I_{min} = 0.320 \ bt(h-t)^2 \tag{8}$$

$$I_{max} = 0.210 \ b^3 t \tag{9}$$

$$Z = kb^5 t \tag{10}$$

$$k = 0.32 \quad 16 \text{ series}$$

$$k = 0.25 \quad 65 \text{ series}$$

$$(c/h) \text{ camber} = 0.56 \ h \tag{11}$$

$$(c/h) \text{ thrust} = 0.44 \ h \tag{12}$$

The torsional stiffness is estimated using Equation (6). For hollow sections the values of C can be obtained from Figure 18.

ESTIMATING PROCEDURES - PROPELLER LOADS

The basic propeller loads are the blade centrifugal and aerodynamic loads, and the shaft loads. Procedures for estimating these various load components are given in the following sections.

In order that estimates can be made, some basic knowledge about the intended propeller installation must be known or assumed. The fundamental installation data required are the horsepower, propeller rpm and the aircraft velocity associated

37

$$C_{solid} = kbh^3G \text{ (page 36)}$$
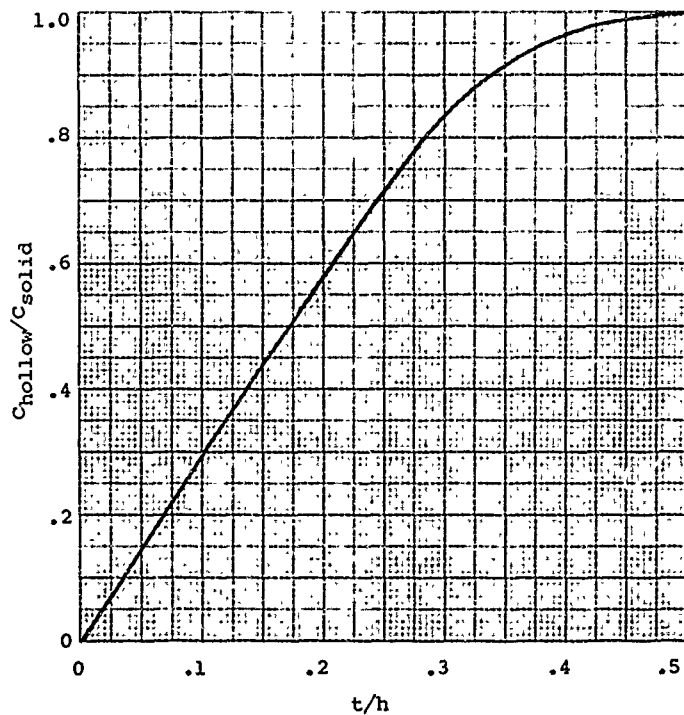
Figure 18. Ratio Of Torsional Stiffness – Hollow Blade to Solid Blade.

with the expected flight envelope of the aircraft. In addition, the angle between the propeller thrust axis and the velocity vector of the airstream entering the disc must be known. This angle is commonly known as the A angle or the propeller angle of attack.

Blade Centrifugal or Mass Loads

The centrifugal force, CF, is calculated at the blade but from the equation

$$CF = \frac{W_T}{g} \, \bar{r} \, \frac{2\pi N}{60}^2 \tag{13}$$

where W_T = blade weight - lb

g = gravity constant - ft/sec^2

$\bar{r}$ = radius to blade mass center - ft

= (0.38 blade radius)

N = propeller rpm

for hollow steel and solid dural blades

The distribution of this force along the blade can be estimated from Figure 19.

The centrifugal twisting moment $Q_{r \, max}$ is the torque required to rotate the blade in the hub at the blade butt and is needed for the design of the propeller pitch change system. The total twisting at the blade butt is the sum of the aerodynamic torque moment and the centrifugal twisting moments. Conservatively the aerodynamic torque loads are generally neglected in preliminary design studies since it subtracts from the centrifugal twisting moment.

For solid blades the centrifugal twisting moment is estimated from the equation

$$Q_{r \, max} = K_{QS}(AF)^2 \, w_T \tag{14}$$

where K_{QS} = 0.0126 at πnD = 1000 ft/sec
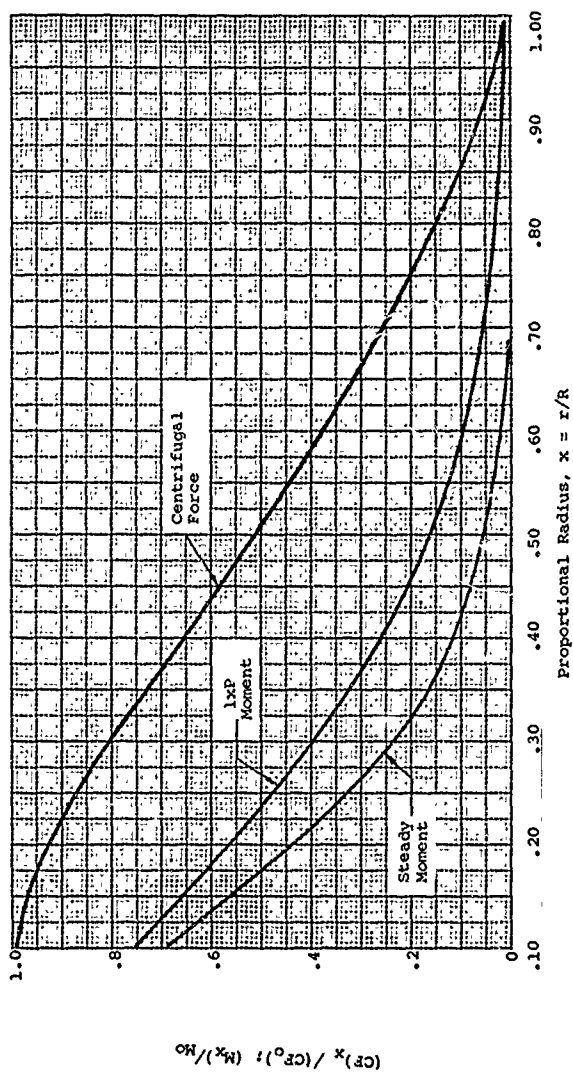
Figure 19. Normalized Blade Force and Moment Distribution.

For hollow blades,

$$Q_{r\ max} = K_{QH}\ (AF)^3\ D^4 \left[.343 - \left(\frac{h}{b}\right)_{.4}\right] \qquad (15)$$

where $K_{QH} = .745 \times 10^{-6}$ at 1000 rpm

AF = blade activity factor

W_T = blade weight - lb

D = blade diameter - ft

$(h/b)_{.4}$ = thickness ratio at the 0.40 radius

The polar moment of inertia (I_p) is the blade mass moment of inertia about the center of propeller rotation and equals

$$I_p = K_I\ W_T\ D^2 \qquad (16)$$

For solid blades, $K_I = .124 \times 10^{-2}$

For hollow steel blades, $K_I = .155 \times 10^{-2}$

Blade Aerodynamic Loads - Steady State

The primary aerodynamic loads on the propeller blade needed
for preliminary sizing are the steady-state loads assosiated
with the thrust and torque, and the harmonic or vibratory load
due to first order aerodynamic excitation, commonly known as
the propeller 1xP loading.   Relationships or expressions for
estimating these loads are given in the following paragraphs.
Pertinent data is given in Figure 20.

The thrust and torque forces can be most accurately estimated
by the aerodynamic procedures given previously. For prelim-
inary purposes the following procedures can be used for known
conditions of hp and velocity.

41
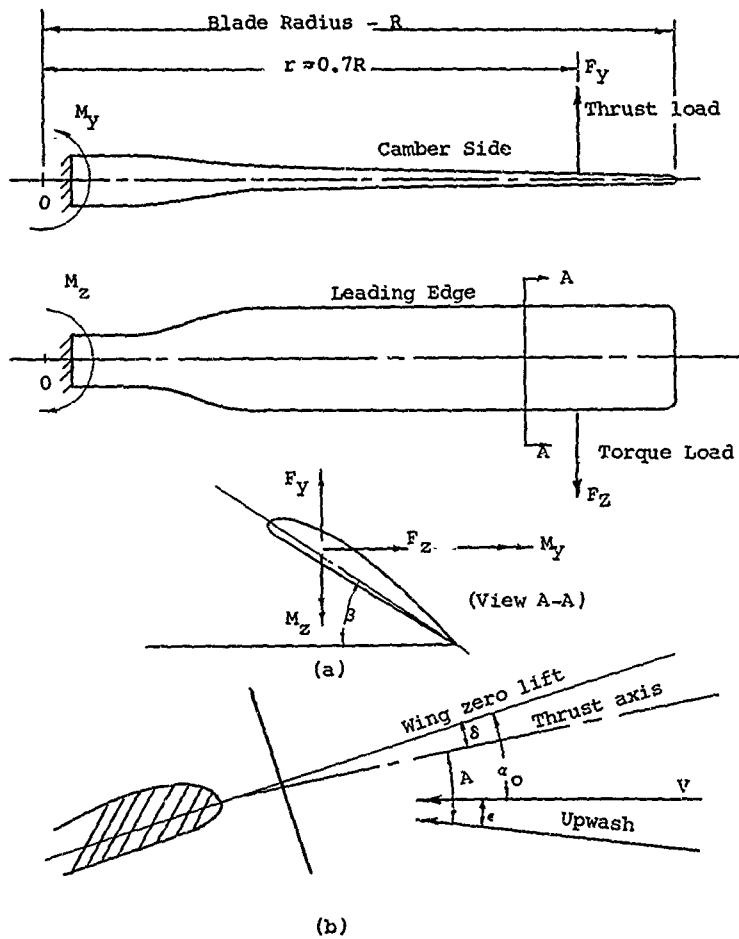
Figure 20. Aerodynamic Loads.

42

Propeller Thrust

$$\eta = \frac{T(V)}{HP \times 550} \tag{17}$$

where η = propeller efficiency, assume 75%

   T = propeller thrust – lb

   V = aircraft velocity – ft/sec

   HP = propeller horsepower

   Thrust/Blade = (T/B) = Thrust/No. Blades   (18)

The shank end moment due to this force can be estimated by
assuming that the center of the thrust force is at the 70%
radius.

$$M_{y_O} = (T/B) \ (.70)R \tag{19}$$

   M_{y_O} = Bending moment at the blade butt, 0 radius due to
        thrust load

The blade centrifugal restoring force reduces the above moment,
and as a preliminary estimate it can be assumed that the
thrustwise moment experienced at the blade butt is:

$$M_{y_O}^{1} = M_{y_O} \ (K_M) \tag{20}$$

where $M_{y_O}^{1}$ = the resultant thrust moment at the 0 radius
   K_M = .60 for metal blades

   K_M = .85 for low (density/modulus) materials,
        such as fiber glass

The total moment at the blade butt in the torque or edgewise
direction can be obtained from the basic torque expression:

$$M_{z_O} = \frac{63000 \ HP}{(B) \ N} \tag{21}$$

M_{z_O} = Blade torquewise moment

B   = Number of blades

N   = Propeller rpm

The resultant blade moment at the blade butt due to thrust
and torque is:

43

$$M_{RO} = \sqrt{(M'_{yo})^2 + (M_{zo})^2} \qquad (21)$$

As a first approximation, the blade bending stress can be found by assuming a moment distribution along the blade, M_{Rx} as given in Figure 19. Where M_R is the section resultant moment,

$$M_R = M_y \cos\beta + M_z \sin\beta \qquad (22)$$

Blade Aerodynamic Forces – Harmonic, 1xP

The first-order blade loads represent the predominate vibratory or harmonic loading on the propeller blade. On conventional aircraft, i.e., an aircraft where the angle A (Figure 20b) is less than 10 to 15 degrees, this 1xP force is essentially simple harmonic, and for such a case the term Aq is used to describe the magnitude of the loading.

For the conventional aircraft the aerodynamic 1xP loads are proportional to the airplane Aq factor.

From Figure 20b

$$A = a_o + \epsilon - \delta \qquad (23)$$

q = airplane dynamic pressure = $\frac{1}{2}\rho V^2$

$$a_o = (C_L/_a)57.3$$

$$C_L = \frac{1}{q} \cdot \frac{W}{S} \quad \left(\equiv \frac{L}{\frac{1}{2}\rho V^2 S}\right)$$

$$a = \frac{a_o/\sqrt{1 - M^2}}{1 + \dfrac{a_o/\sqrt{1 - M^2}}{\pi AR}} \qquad\qquad (24)$$

$$\epsilon = \frac{k\, C_L}{\pi AR}\ 57.3$$

$$k = \epsilon/\epsilon_o \quad \text{(see Figure 21)}$$

$$AR = b^2/S$$

44
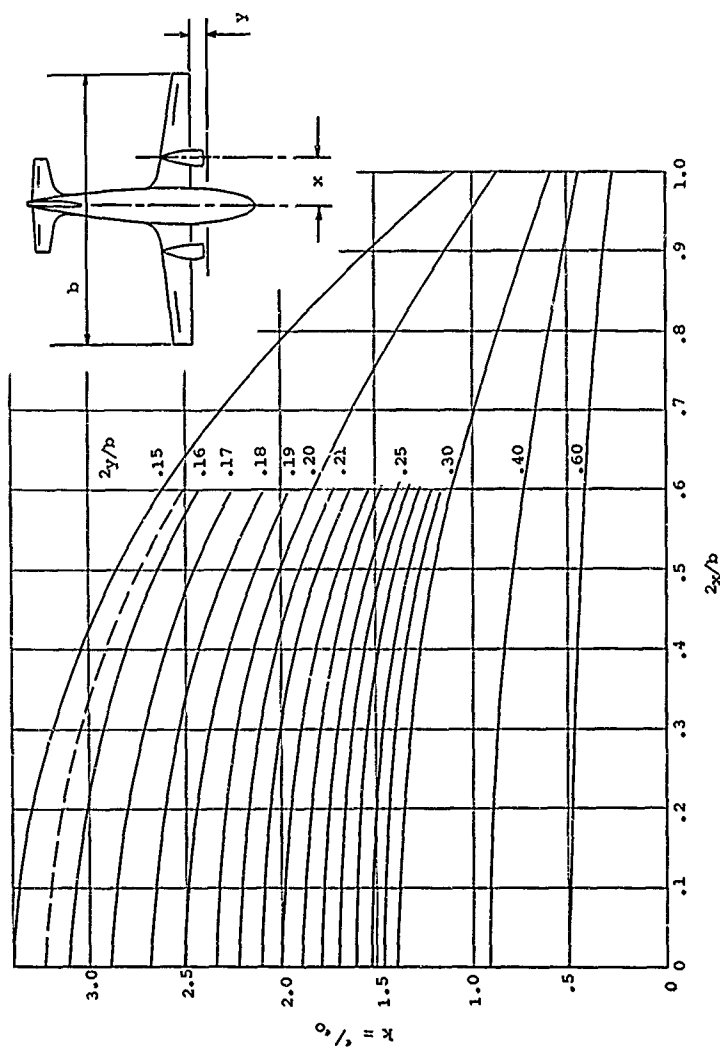
Figure 21. Variation Of Upwash Along Semi-Span.

45

where   W = aircraft weight
          C_L = wing lift coefficient
          a = slope of the airplane lift curve of
              the wing (radians^{-1})
          a_O = slope of the airplane lift curve for
              infinite aspect ratio
          AR = aspect ratio of the wing
          b = wing span in feet
          S = wing area in square feet
          k = ratio of local to average upwash
          ϵ = local upwash angle
          ϵ_O = average upwash angle
          δ = angle between wing zero lift line and
              thrust

Shaft Forces - From 1xP

The 1xP aerodynamic forces produce a radial force, F, and bend-
ing moment on the propeller shaft. With respect to the shaft
these forces are steady state*, and are applied at the inter-
section of the shaft and blade centerlines. For an aircraft
in a pure pitch attitude they would correspond to the normal
force and yawing moment of Figure 14 . The value of these
loads is estimated by the equations,

$$F = \frac{K' B (A_q) AF\ D^2}{K_1}\ \sin\beta_{.7}\ (\alpha_{.7} + 2\ C_{L.7}\ \cot\beta_{.7})$$

(25)

$$M = \frac{K' B (A_q) AF\ D^3}{K_2}\ \cos\beta_{.7}\ (\alpha_{.7} + 2\ C_{L.7}\ \cot\beta_{.7})$$

(26)

where   F = 1xP shaft force, lb

         M = 1xP moment, in.-lb

         $a_{.7}$ = slope of the lift curve at 70% radius

         AF = activity factor

         A_q = 1xP excitation factor, deg-lb/ft^2

         B = number of blades

* This statement is true for propellers having more than two
blades. On a two-blade installation the 1xP shaft forces are
harmonic, and the resulting vibration is transmitted to the air-
frame.

46

$$
\left.\begin{array}{r} k' \\ K_1 \\ K_2 \end{array}\right\} = \text{constants}
$$

$\beta_{.7}$ = blade angle at 70% radius

$c_{L.7}$ = operational lift coefficient at 70% radius

D = propeller diameter, ft

Recommended Values for k'

        1.15 - for moderately stiff blades

        1.25 - for blades of normal stiffness

        1.35 - for moderately thin blades

Recommended Values for K_1 and K_2

Blade Planform	K_1	K_2
Round tip	438,000	102,000
Rectangular	495,000	124,000
Inverse taper	545,000	124,000

In the foregoing approximate relations, values of the slope of the lift curve and the average lift coefficient of the typical outboard station are required for the evaluation of the force and moment. Estimates of the slope of the lift curve and the lift coefficient are given in the following paragraphs.

The operating lift coefficient may be estimated from,

$$
c_{L.7} = \frac{\text{hp } \sin\phi_{o.7}}{0.00036 \text{ Bq } V_r D^2 (b/D)_{.7}} \tag{27}
$$

where   hp = shaft horsepower

       q = dynamic pressure, lb/sq ft

       V_r = rotational tip speed, ft/sec

$\phi_{o.7}$ = apparent wind angle at 70% radius

$(b/D)_{.7}$ = chord to diameter ratio at 70% radius;
AF/1560 for rectangular planform

Similarly, an approximate formula for the blade angle as meas-
ured to the zero lift line is,

$$\beta_{.7} = \phi_{o.7} + \frac{c_L}{a_{.7}} \qquad (28)$$

The slope of the lift curve can be found by one of two equa-
tions. In the case of a pure supersonic propeller the slope
is given by the Buseman-Ackeret relation, i.e.,

$$a_{.7} = \frac{4}{\sqrt{M^2 - 1}}$$

Whereas for subsonic and transonic flows the conventional
finite aspect ratio relation using the Prandtl-Glauert and
Lock-Goldstein corrections is employed. The formula for the
finite aspect ratio slope of the lift curve, which includes
the effect of three-dimensional flow, is

$$a_{.7} = \frac{a_{om.7}}{1 + \frac{a_{om.7}}{4 K_L \sin\phi}} \qquad \text{per radian} \qquad (29)$$

where $a_{.7}$ = finite aspect ratio slope of the lift
curve at 70% radius

$a_{om.7}$ = infinite aspect ratio slope of the lift
curve corrected for compressibility, Figure 22

K_L = solidity factor, $bB/2\pi r$

L = Lock variation of Goldstein's nondimensional
circulation K_g, $K_L = K_g/\cos^2\phi$, Figure 23

ϕ = true wind angle $\approx \phi_o$

48
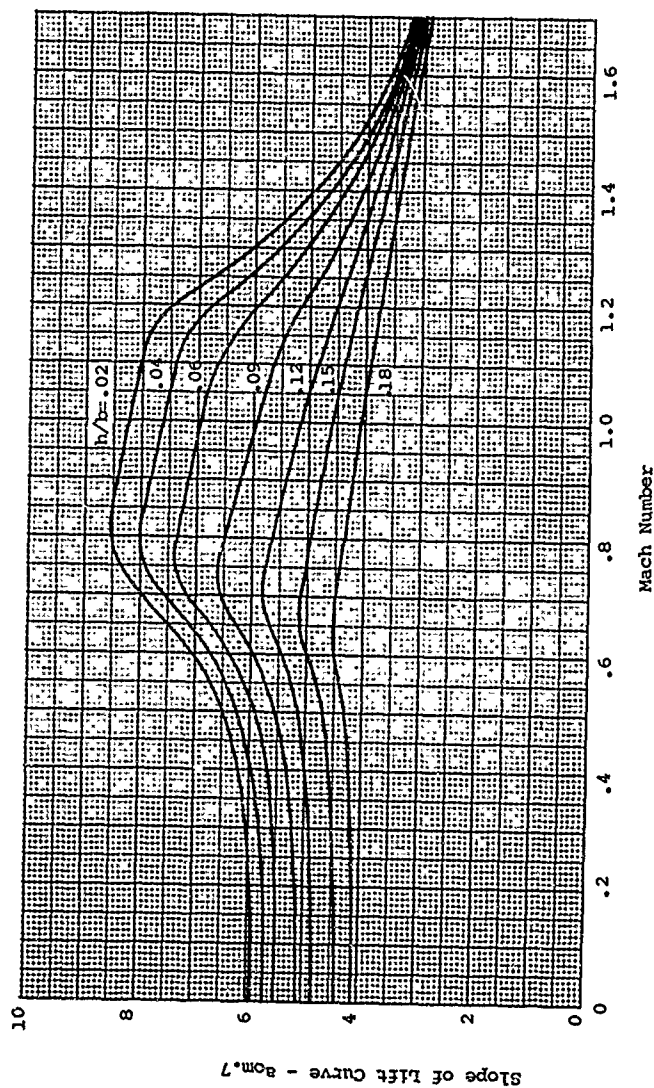
Figure 22. The Infinite Aspect Ratio of the Lift Curvature Variation With Mach Number.

49
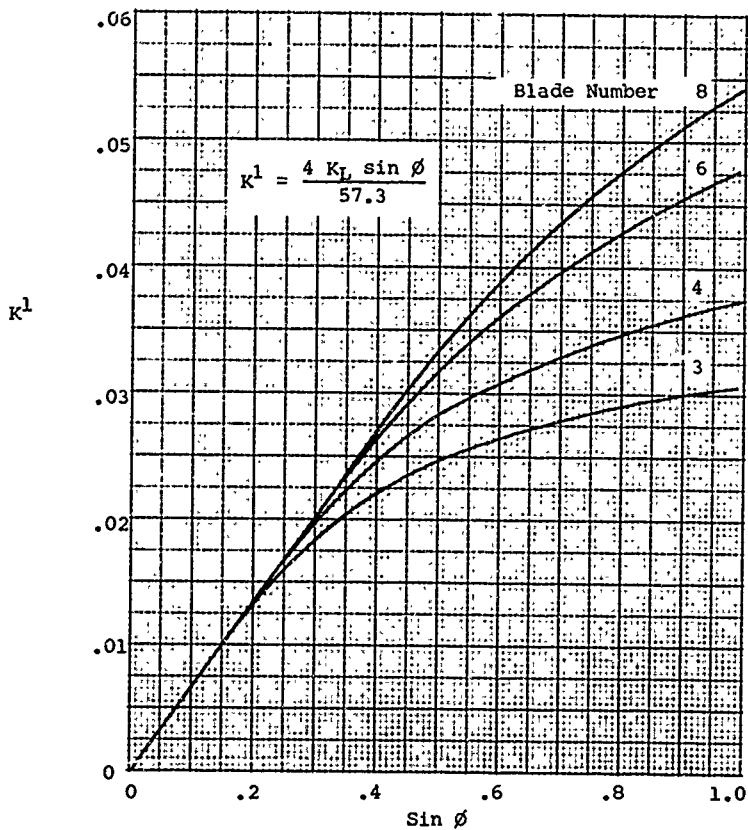
Figure 23. Lock-Goldstein Correction Versus Sin ∅ at 70 Percent Blade Station.

50

1xP Blade Moments

The blade 1xP loads are harmonic, and therefore, produce vibra-
tory loading on the blade retention and hub structure. The
thrustwise bending moment and torquewise force on the blade
butt can be found from the shaft force and moment.

$$\pm M_{yo} \ (1xP) = \frac{M \times 2}{B}$$

$$\pm F_{zo}(1xP) = \frac{F \times 2}{B}$$

(30)

$\pm M_{yo}(1xP)$ = Blade thrustwise vibrating moment in. lb

$\pm F_{zo}$ = Blade vibratory torque force, (1xP)

M = Shaft moment, from Equation (26)

F = Shaft force, from Equation (25)

The blade edgewise bending moment can be estimated by assuming
the force center at the 70% radius.

$$\pm M_{zo} \ (1xP) = F_{zo}(.7)R$$

(31)

The resultant moment on the blade shank end is

$$\pm M_{Ro} \ (1xP) = \sqrt{M_{yo}^2 + M_{zo}^2}$$

(32)

The radial distribution of the 1xP moment along the blade in-
volves both inertia and centrifugal forces. A first approx-
imation of the resulting moment distribution can be made from
Figure 19.

1xP Forces - Nonconventional Aircraft

On aircraft such as a tilting propeller VTOL, or other instal-
lation where the propeller inflow angle (A) can exceed the 10-15
degree range, the 1xP harmonic force becomes much more complex,
and the relatively simple force estimating equation given in
the previous section is no longer valid. The various propel-
ler forces and moments for this type of installation can best
be approximated by use of propeller coefficients obtained from
test data. Typical of such test data which has been used
quite extensively for preliminary estimates is that given in
Reference 2.
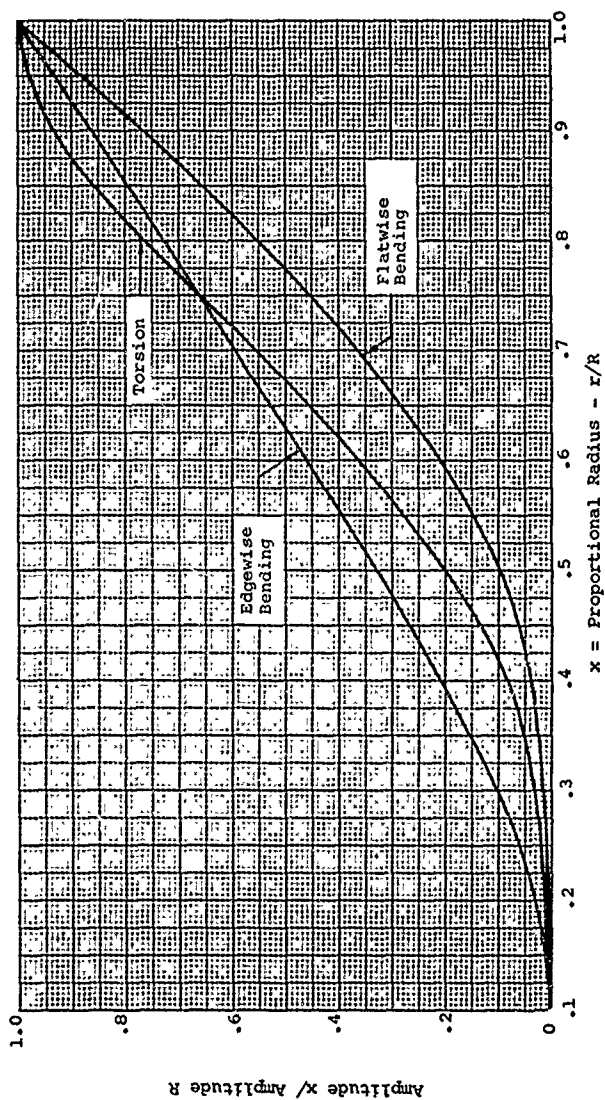
Figure 24. Normalized Blade Modes – Fundamental.

52

The various force coefficients involved are

Thrust $C_T = \dfrac{T}{\rho n^2 D^4}$

Normal forces $C_N = \dfrac{N}{\rho n^2 D^4}$

Side forces $C_S = \dfrac{S}{\rho n^2 D^4}$

Pitch moment $C_M = \dfrac{M}{\rho n^2 D^5}$ (33)

Yawing moment $C_Y = \dfrac{Y}{\rho n^2 D^5}$

Power $C_p = 550\,(hp)/\rho n^3 D^5$

These various forces are illustrated in Figure 14.

A typical procedure for estimating the forces from such test data is outlined below.

Given data:

1. Propeller diameter and activity factor, horsepower, rpm, aircraft velocity and propeller tilt angle.

2. Calculate,

   $J = \dfrac{V}{nD}$ and C_p

3. Convert C_p to an equivalent C_p of the test propeller

   $(C_p)_{test} = C_p \dfrac{(AF)\ test}{(AF)\ given}$

4. With $(C_p)_{test}$ and J, enter test data and obtain required force and moment coefficients.

5. Convert test coefficient to equivalent coefficients for given propeller.

53

$$\left.\begin{array}{c} C_T \\ C_N \\ C_S \end{array}\right\} = \left.\begin{array}{c} C_T \\ C_N \\ C_S \end{array}\right\}_{test} \cdot \frac{(AF)given}{(AF)test}$$

6. $$\left.\begin{array}{c} C_M \\ C_Y \end{array}\right\} = \left.\begin{array}{c} C_M \\ C_Y \end{array}\right\}_{test} \cdot \frac{(AF)given}{(AF)test}$$ \qquad (34)

7. From estimated coefficients, compute propeller forces and moments, Equations (33).

8. The corresponding blade force and moments can be computed by use of Equations (30) and (31). These individual components must be combined vectorally to obtain the maximum blade loads.

ESTIMATING PROCEDURES - RESONANT FREQUENCIES

The blade modes most generally involved in propeller vibration are the fundamental flapping, fundamental edgewise, and the first torsion. If a reference blade is available which has geometric proportions close to a proposed design these fundamental frequencies can be estimated by the following proportionalities:

$$\frac{f\ new}{f\ ref} = \frac{AF\ new}{D\ new} \quad \frac{D\ ref}{AF\ ref} \qquad (35)$$

Torsion modes:

$$\frac{f\ new}{f\ ref} = \frac{AF\ new}{AF\ ref} \qquad (36)$$

It has, however, proved to be more reliable to perform a relatively simple computation of the static (nonrotating blade) natural frequencies and correct for the effect of rotation by the familiar Southwell equation.

With the blade section properties (Area, Moments of Inertia, Torsional Stiffness) known or estimated, the fundamental frequencies can be estimated by assuming an untwisted cantilever by use of any of several methods available. The following expressions based on energy considerations have proven quite satisfactory.

54

Static natural frequency, bending modes:

$$\omega_o^{\,2} = \frac{\int_0^{1.0} A_{(s)}\left(Y_{(s)}\right)^2 ds}{\dfrac{\rho}{g} R^4 \int_0^{1.0} \dfrac{\left(\int_x^{1.0} \int_s^{1.0} A_{(s)} Y_{(s)} ds ds\right)^2}{(EI)_x} ds} \tag{37}$$

Static natural frequency, torsion modes:

$$\omega_o^{\,2} = \frac{\int_0^{1.0} (I_P)_s \,(\theta_s)^2\, ds}{\dfrac{\rho}{g} R^2 \int_0^{1.0} \dfrac{\left(\int_x^{1.0} (I_P)_s \,(\theta_s)\, ds\right)^2}{(C_T)_x} ds} \tag{38}$$

where X = proportional radius, $X = \dfrac{r}{R}$, fixed

ρ = mass density, $lb/in.^3$

g = gravitational constant, $in./sec^2$

R = blade radius, in.

A_s = section area at station x, $in.^2$

$(I_p)_s = (I_{max} + I_{min})$ at station x, $in.^4$

I = moment of inertia, $in.^4$

$I = I_{min}$ for flapping mode

$I = I_{max}$ for edgewise mode

C_T = torsional stiffness, $\dfrac{in. - lb}{rad}$ in.

ω_o = fundamental frequency nonrotating b de, rad/sec

$\left.\begin{matrix} Y_s \\ s \end{matrix}\right\}$ = mode shape

s = proportional radius, variable

Equations (37) and (38) may at first glance seem formidable,
but the various integrations are readily evaluated by tubular
integration using standard calculating machines. However, the
mode shape for the respective mode must first be estimated,
and as a first approximation the curves given in Figure 24
can be used.

The effect of rotation on the fundamental frequency can be
estimated from the Southwell equation,

$$f_R = f_O + (c)(n) \tag{39}$$

where f_R = fundamental blade frequency at n, cps

   f_O = fundamental blade nonrotating frequency, cps

   C = constant

   n = propeller speed, rps

Values of C are:

   first flapping mode $C = 1.5 - 2.0$

   first edgewise mode $C = 0.8 - 1.0$

The frequency of first torsion mode is for all practical pur-
poses unaffected by rotational speed.

PROPELLER LOADS

The ultimate structural design of the aircraft propeller re-
quires an accurate evaluation of the various loads generated
by the propeller system. These loads have two basic sources:
(1) the aerodynamic components developed by the airfoil sec-
tions of the blade, and (2) the components developed by the
mass of the propeller subjected to various accelerations.

It is the purpose of this section to present in some detail
procedures by which these various loads can be computed. In
many instances the complete mathematical development is not
presented. However, in all cases the initial steps and final
results are given and the intermediate steps can be easily
developed, or in the case of the more complex problems, ade-
quate references are indicated.

PROPELLER LOADS - AERODYNAMIC

The first requirement in establishing the aerodynamic loads
is the definition of the structural design conditions. Basic-
ally, two areas of propeller operation must be considered.
First, the static takeoff condition, i.e., just prior to brake
release, the aircraft velocity is zero, the propeller is oper-
ating at maximum horsepower and generating maximum thrust.
The magnitudes of the loads and stresses is generally a maxi-
mum at this takeoff condition, but they are essentially steady
state. The second area of interest is during flight. The
total load or stress magnitude is generally lower than at the
static condition, but a large component of the total load is
harmonic at predominantly 1xP frequency (one load cycle per
propeller revolution). Fatigue, therefore, becomes a design
criterion, and long life fatigue requirements at flight con-
ditions generally dictate the propeller design.

As will be shown later, the 1xP harmonic loading, at least on
conventional aircraft, is approximately proportional to the
so-called airplane Aq factor, where A is the propeller angle-
of-attack and q is the airplane dynamic pressure. The criti-
cal flight design conditions, therefore, occur at the maximum
Aq values and this quantity must be evaluated over the flight
envelope. There are generally two flight conditions that are
of concern: (1) Early climb at maximum gross weight, where
the propeller inflow angle A, is relatively high and q is low,
(2) Minimum gross weight at maximum velocity which results in
a small value of A but a maximum value of q. Highly maneuver-
able aircraft may require the evaluation of loads at other
high load factor conditions defined by the airplane V-n dia-
gram. Special aircraft such as propeller driven V/STOL types
may also require load studies at conditions of propeller oper-
ation peculiar to the specific type of application.

Airplane Aq Factor

In order to evaluate the structured design condition for a
given propeller, the airplane Aq factor must be established.
This factor is a characteristic of a given aircraft configur-
ation, and therefore an accurate evaluation requires that cer-
tain basic aircraft data be made available. The data required
will be enumerated later in this section. Referring to Figure
25, it is apparent that the airflow enters the propeller disc
at some angle with respect to the direction of flight. The
angle between the local velocity and the thrust line is the
propeller angle of attack or Angle A. Figure 26 shows the
conventional propeller wing layout and the angle A is seen to
be:

$$A = \alpha - \delta + \epsilon \tag{40}$$

57

Direction of Thrust

Plane of Rotation

Direction of
Flight

L.E.

Air
Stream
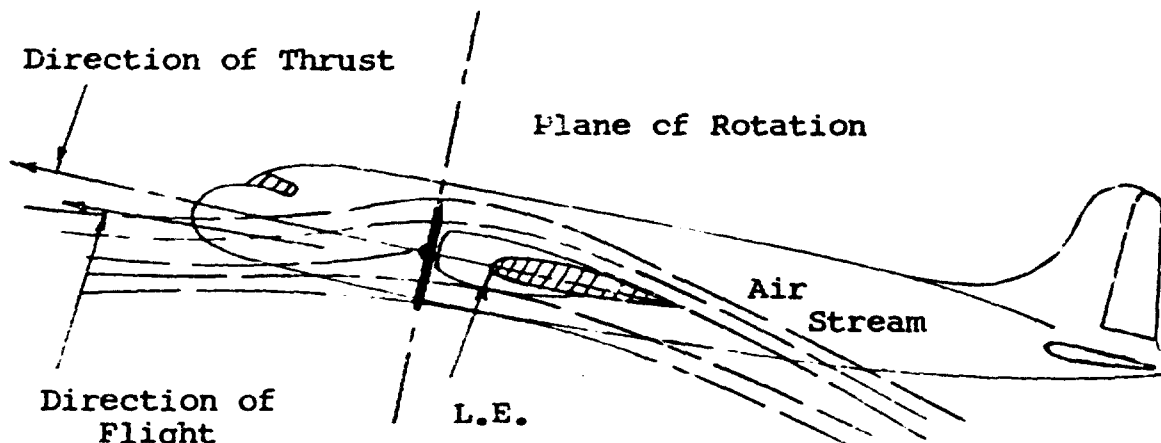
Figure 25. Airplane in Climbing Attitude.

Propeller Disc

Absolute Angle of Attack

δ

α

A

ε = Upward Angle

V

Direction of Flight
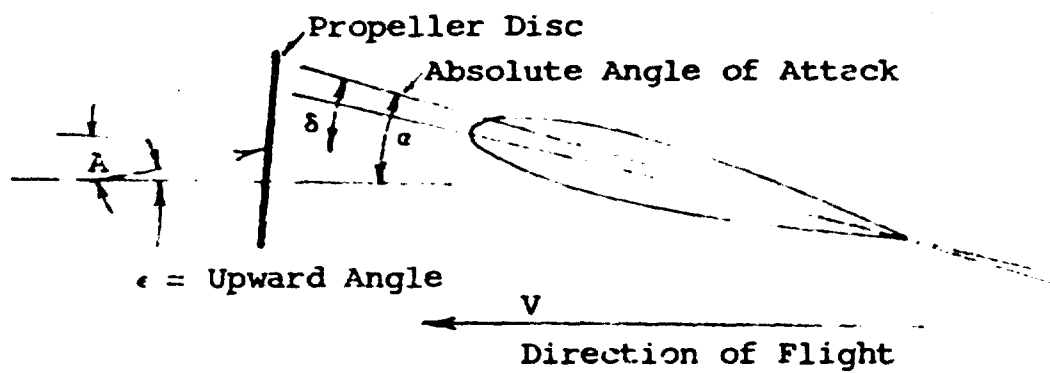
Figure 26. Components of Inflow Angle.

58

where α = the wing angle of attack - degrees*

         δ = angle between the propeller
thrust line and the zero
lift line - degrees*

         ϵ = upwash angle - degrees*

The wing angle of attack, α, can be found from elementary
aerodynamics noting that airplane lift = the airplane weight.

$$L = W = \tfrac{1}{2}\rho V^2 \frac{dC_L}{d\alpha}\alpha S$$

$$\alpha = \frac{W}{S\, q(dC_L/d\alpha)} \tag{41}$$

W = aircraft weight - lb

S = wing area - ft^2

$q = \tfrac{1}{2}\rho V^2 = (V_i)^2/29$ -   lb/ft^2

V_i = airplane indicated velocity - kn

$\dfrac{dC_L}{d\alpha}$ = slope of the aircraft lift curve with
respect to the zero lift line.

The angle δ is a fixed quantity and is determined by the air-
craft geometry.

The angle ϵ is dependent upon the proximity of the propeller
to the wing leading edge, proximity to the fuselage and other
aircraft characteristics. Evaluation of this angle obviously
requires a detailed evaluation of the airflow characteristics
in the proximity of the propeller disc. It is also obvious
that this angle will vary at different points in the propeller
plane. Experience has shown that an averaged value taken at
the 0.70 propeller radius is a good representative value for
purposes of estimating the airplane Aq factor.

From the foregoing, it is apparent that the evaluation of the
Aq factor is a simple calculation, but the following data

---

* Aq values as generally referred to, i.e., 1200 Aq, are in
deg-lb/ft^2 units.   When used in load equations the value is
converted to radian units.

59

must be supplied:

1. Velocity range

2. Gross weight and Wing Area (or wing loading, W/S)

3. Slope of the aircraft lift curve $dC_L/d\alpha$ including the effects of flaps, etc.

4. Average upwash angle as a function of airplane angle of attack and/or other pertinent parameters.

It has been common practice to evaluate the Aq factor for the maximum and minimum gross weight over the speed range of the airplane. A typical plot of the computed results will give a curve such as is shown in Figure 27a. Experience has shown that due to extraneous factors, a value of zero Aq seldom exists, and in fact the computed values are generally in the order of 150 to 200 Aq too low. Further, the change in sign indicates a 180° phase shift in the harmonic load. Since only the magnitude of Aq is important, the change in sign is neglected. Therefore, ignoring the phase shift and applying the experience correction factor, the resulting Aq curve for a given aircraft will have the form shown in Figure 27b.

The Aq curve illustrated is essentially balanced, i.e., the maximum value at low speed is approximately the same as the maximum value at high speed, with a minimum value at cruise. This would be an optimum design which is not usually obtained. The shape of the curve can be adjusted by small changes in the angle δ of Equation (40). A low value of δ will give higher Aq climb. Increasing the value of δ will result in the maximum value of Aq at high speed. Therefore, it is usually necessary for the airframe and propeller designers to coordinate the thrust line orientation in order to establish the best Aq for the given installation.

Examination of Equations (40) and (41) shows that the Aq curve, thus established, represents the 1xP excitation factor that exists on the propeller during normal 1-g flight. It is therefore usually referred to as the nominal Aq. The effects of aircraft maneuvers such as yaw, sideslip, high-g pull outs, etc., must be combined with this nominal. Referring to Figure 28, the aircraft in a yaw attitude will generate a 1xP excitation factor equal to ψq where ψ is the given yaw angle. Ideally, the harmonic forces generated by this factor will have a 90° phasing with respect to the forces attributable to the nominal Aq and the magnitude of the resultant is the simple square root of the sum of the squares. Since the forces are proportional to Aq and ψq it is easily shown that for the case of yaw, the magnitude of the effective Aq is:

60
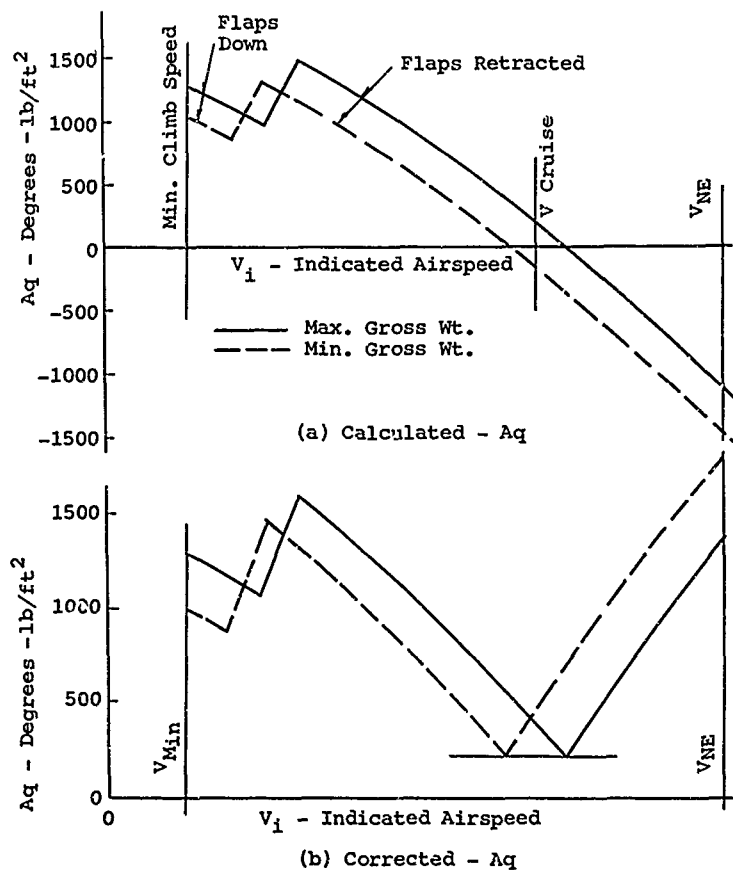
Figure 27.   Nominal Aq Diagram.

61
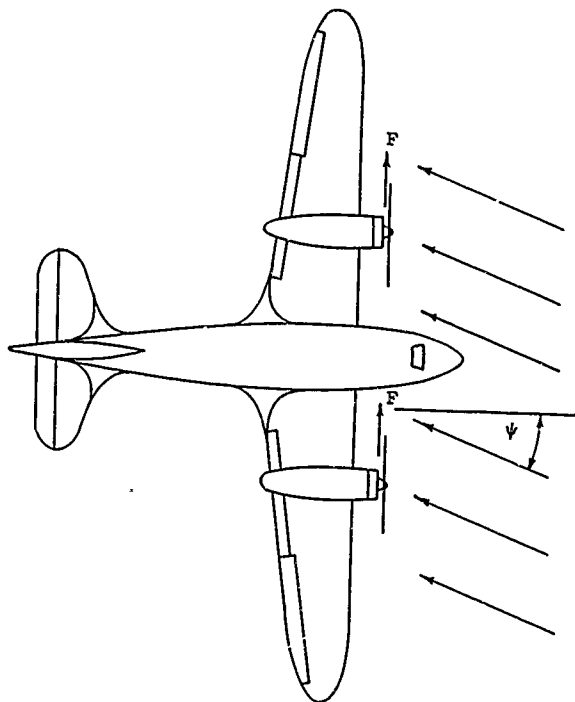
Figure 28. Airplane in Yaw.

$$\text{Aq}_{\text{eff}} = \sqrt{\left|\text{Aq}_{\text{nom}}\right|^2 + \left(\psi q\right)^2}$$

$$= q\sqrt{A^2 + \psi^2} \tag{42}$$

It should be noted that the nominal Aq is not in a pure pitch direction, nor is the value ψ pure yaw, and the phasing between the harmonic force vectors is not 90°. Equation (42) is therefore an approximation, but one which experience has proven to be adequate for design purposes.

For illustrative purposes, a simple development of the force factor resulting from the combinations of the nominal Aq at some assumed phase with yaw is shown in Figure 29. The correct phasing can only be obtained from extensive flow studies, either analytical or experimental, and such studies have not been carried out extensively in the past.

The Aq resulting from high -g pull outs or similar maneuvers can be computed by the use of Equations (40) and (41); Equation (41) is modified to

$$\alpha = \frac{nW}{S \; q(dD_L/d\alpha)} \tag{43}$$

where n = applicable load factor

Special conditions can exist on unconventional aircraft. On a tilting propeller type V/STOL, for example, during the transition of the propeller from hover attitude to conventional flight position, the flow is quite complex and a simple Aq evaluation such as given previously has not proven too reliable. This special type of propeller for VTOL airplanes will be covered in more detail in the next section.

First-Order Propeller Loads

One of the major design parameters on the present-day high-performance aircraft propellers is the magnitude of the first order or commonly called 1xP aerodynamic loading. This load is produced when the airstream enters the propeller disc at some angle with respect to the thrust line, in effect a propeller angle of attack. Under such a condition a harmonic aerodynamic force is generated by the blades with a frequency equal to the propeller rotational speed. Hence, the name first-order-propeller or 1xP.

63
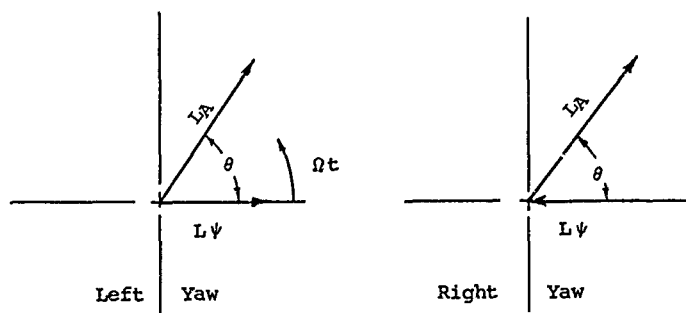
L_A = Blade Harmonic Force Vector Due To Aq

L_ψ = Blade Harmonic Force Vector Due To ψq

$L_A = K_A q; \quad L\psi = K\psi q$

$L_1 = L_A \sin (\Omega t + \theta); \quad L_2 = L\psi \sin \Omega t$

θ = Assumed Phase Angle

Resultant (Left Yaw)

$L_R = (L_A^2 + L\psi^2 + 2L_A L \cos)^{\frac{1}{2}}$

$L \sim Aq \sim q\psi$

$Aq_{eff} = (A^2 + \psi^2 + 2A\psi \cos \theta)^{\frac{1}{2}} q$

Similarly For Right Yaw:

$Aq_{eff} = (A^2 + \psi^2 - 2A\psi \cos \theta)^{\frac{1}{2}} q$

Figure 29. Resultant Aq.

64

Referring to Figure 30 and considering a conventional aircraft configuration where the angle A is small, the following assumptions can be made:

1. The velocity components are uniform over the disc.

2. $\cos A = 1.0$; $\sin A = A$ (44)

3. $\emptyset = \emptyset_o$; $W = W_o$

Then, the basic lift on a section at radius r is given as:

$$L_r = \tfrac{1}{2}\rho W_o^2\ C_L\ b\ \Delta r$$

where C_L = Section lift coef

  b = Section chord - ft

  W_o = Resultant velocity - ft/sec

  ρ = Mass density of air - slugs/ft^3

This basic lift will change with changes in velocity and changes in lift coefficient. The change in lift can be written

$$\Delta L_r = \left[\frac{1}{2}\ \rho 2\ W_o \Delta W_o + \frac{\rho}{2}W_o^2\ \frac{dC_L}{d\alpha}\ \Delta\alpha\right]b\ \Delta r \qquad (45)$$

From Figure 30 and the foregoing assumptions,

$$\Delta W = VA\ \cos\emptyset_o\ \sin\Omega t$$

$$\Delta\alpha = \frac{VA\ \sin\emptyset_o\ \sin\Omega t}{W_o}$$

Substituting these values in (45) the maximum value of the harmonic lift is

$$\left(\frac{\Delta L}{\Delta r}\right)_r = Aq\left[2C_L\ \cot\emptyset + \frac{dC_L}{d\alpha}\right]b \qquad (46)$$

Equation (46) shows that the periodic 1xP force is proportional to the excitation factor Aq.

The periodic lift can be evaluated for each station along the blade for any given flight condition. Aq must be known from page 61, and appropriate values of the C_L, $\emptyset$ and $dC_L/d\alpha$ must be established. Ideally these data should be determined by

Propeller
Disc

V cos A

A

V sin A

V

Ω

Ω

V sin A

Section at Radius r

f_y

L

f_z

W_o

β

ϕ_o

φ

V cos A

$2\pi n \, r$

V sin A sin Ωt
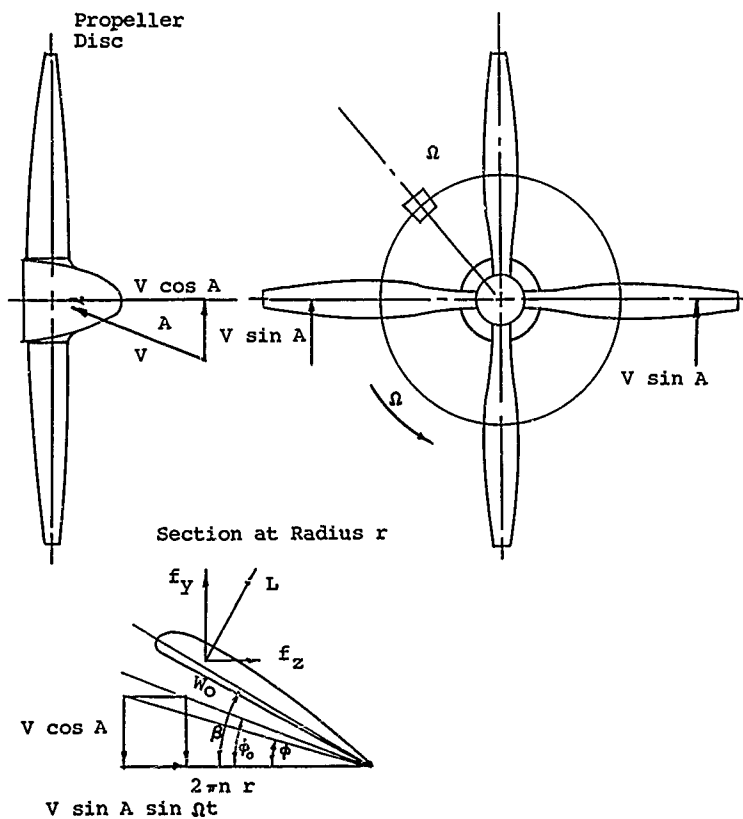
Figure 30. Development of Periodic Forces.

aerodynamic strip analysis.

The development of Equation (46) is obviously based on a quasi-steady flow assuming a rigid blade. The periodic force will produce corresponding periodic blade deflection in both bending and torsion. These will in turn influence both ΔW and $\Delta \alpha$, Equation (45). Considering all of these effects can become quite complex and there are several classic studies of the forces generated by oscillating airfoils, for example, Theodorsen, Reference 3. Also the helicopter industry has studied the problem extensively with respect to rotor design.

Fortunately, however, propeller experience to date has indicated that the effects of blade deflection on the 1xP harmonic load are negligble with the exception of the torsion.

Referring to Figure 31, the torque acting on the blade element at radius r is

$$\Delta Q = \Delta L(a) + b\ddot{y}\,dm + I\ddot{\alpha} \quad - \quad \Delta CF \frac{dy}{dr} b \qquad (47)$$

where y = flexural acceleration dy^2/dt_2 $in./sec^2$

α = torsional acceleration $d^2\alpha/dt^2$ rad/sec^2

dm = section mass

I = section polar moment of inertia - $in.lb/sec^2$

ΔCF = elemental centrifugal force - lb

The 1xP forced vibration on a propeller blade is well removed from resonance, and the inertia terms ydm and $I\alpha$ are relatively small. Further, in the more highly flexible tip regions the blade deflection is such that the centrifugal component is approximately equal to the lift components

$$\Delta CF \frac{dy}{dr} \approx \Delta L$$

Therefore, neglecting the inertia terms and using the equality expressed above, the effective torque on the section is essentially a couple and can be expressed as

$$\left(\frac{\Delta Q}{\Delta r}\right)_{1xP} = \frac{\Delta L}{\Delta r} x_{cp} \qquad (48)$$

67
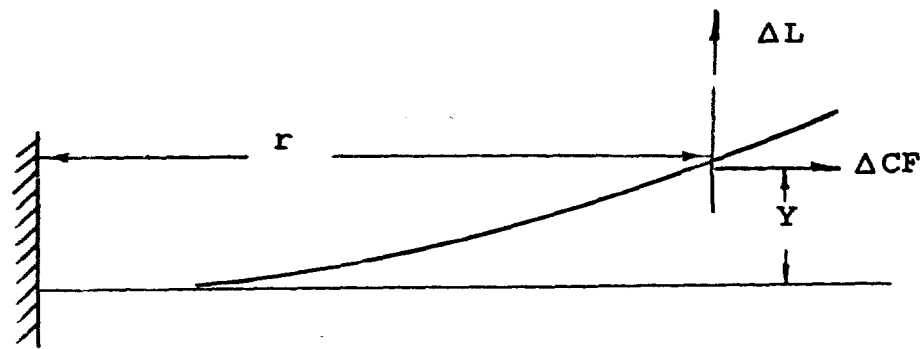
Blade Deflection
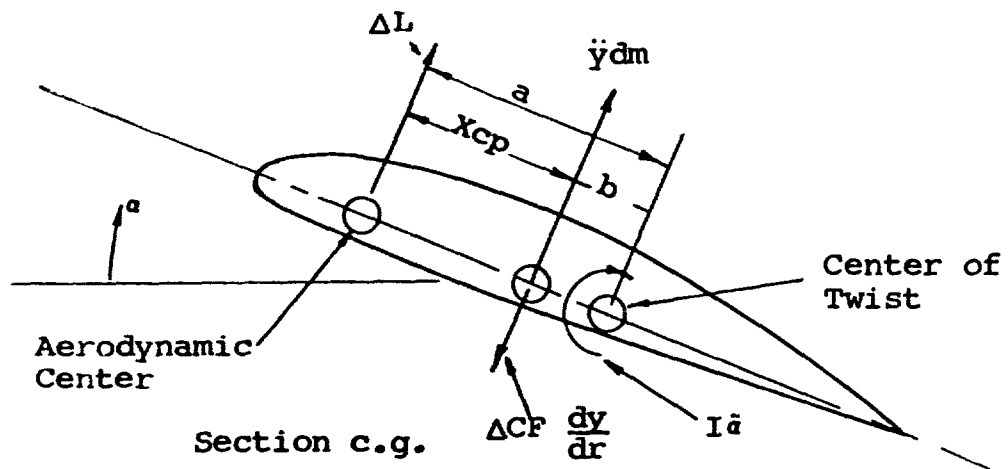
Figure 31. Blade Aero-Torsion.

where $(\Delta Q/\Delta r)_{1xP}$ = blade torque due to the 1xP harmonic lift, in.-lb/in.

x_{cp} = distance from the aerodynamic center to the section mass center, in.

The location of the center of pressure is often taken at the ¼ chord, but a more accurate location can be obtained from Figures 70 to 73 in the aerodynamics section, Volume I.

The blade torque at any station r is then

$$(Q_r)_{1xP} = \int_r^R \left|\frac{\Delta L}{\Delta r}\right| x_{cp} \, dr \tag{49}$$

and the corresponding deflection is

$$(\alpha_r)_{1xP} = \int_0^r \left|(Q_r)_{1xP}/C_T\right| dr \tag{50}$$

Then the change in harmonic lift is

$$\left|\frac{\Delta L}{\Delta r}\right|_\alpha = \frac{1}{2} \rho \, W^2 \frac{dC_L}{d\alpha} (\alpha_{1xP}) \tag{51}$$

where $(\Delta L/\Delta r)_\alpha$ = change in harmonic lift due to blade twist - lb/in.

α_{1xP} = angular deflection of the blade section at radius r due to harmonic lift - rad

C_T = blade section torsional stiffness constant, see Equation (6), in.-lb/rad/in.

W = the resultant velocity, ft/sec and is obtained from aerodynamic strip analysis or it can be estimated from the relation

$$W = V/\sin\phi \quad \text{(see Figure 30)}$$

R = tip radius

The total harmonic lift on the given section is therefore

$$\left|\frac{\Delta L}{\Delta r}\right|_t = \left|\frac{\Delta L}{\Delta r}\right|_{eq. (46)} + \left|\frac{\Delta L}{\Delta r}\right|_\alpha \tag{52}$$

69

It is usually necessary to take the results of (52) and repeat the calculations of Equations (49) and (51) and thus converge on a final value. Experience has shown that in the more recent blade developments, this torsional influence increases the basic lift of Equation (46) in the order of 15% in the more flexible outboard sections of the blade.

The final value of harmonic lift as computed by Equation (52) at the various radii along the blade can be resolved into thrust and torque components.

$$\left.\begin{array}{l} \text{Thrust force} = f_y = \left(\dfrac{\Delta L}{\Delta r}\right)_t \cos\phi \\[3mm] \text{Torque force} = f_z = \left(\dfrac{\Delta L}{\Delta r}\right)_t \sin\phi \end{array}\right\} \quad (53)$$

These components can then be integrated to obtain the blade shear and moments distribution in the thrust and torquewise directions.

$$\left.\begin{array}{ll} (F_y)_r = \displaystyle\int_r^R \left(\dfrac{\Delta L}{\Delta r}\right)_t \cos\phi\, dr & \text{thrust force} \\[5mm] (M_y)_r = \displaystyle\int_r^R \int_x^R \left(\dfrac{\Delta L}{\Delta r}\right)_t \cos\phi\, dr dr & \text{thrustwise moment} \\[5mm] (F_z)_r = \displaystyle\int_r^R \left(\dfrac{\Delta L}{\Delta r}\right)_t \sin\phi\, dr & \text{torque force} \\[5mm] (M_z)_r = \displaystyle\int_r^R \int_x^R \left(\dfrac{\Delta L}{\Delta r}\right)_t \sin\phi\, dr dr & \text{torquewise moment} \end{array}\right\} (54)$$

These aerodynamic forces and moments represent the forcing function on a blade spring mass system. In addition, inertia and centrifugal effects contribute to the total blade load. These additional influences are considered on pages 75 to 80. It should be noted at this point, however, that on a rotating blade subjected to a simple harmonic vibration at 1xP frequency, the effects of centrifugal and inertia loading cancel each other out at the center of rotation, i.e., the blade zero radius. Therefore, if Equations (54) are integrated to the zero radius, the resulting aerodynamic loads are essentially the total load at station zero due to the 1xP excitation.

Remembering that Equations (54) are actually harmonic forces, the force or moment on a given blade with respect to time is

70

$$F_t = F \sin \Omega t$$

$$M_t = M \sin \Omega t \qquad\qquad (55)$$

where the subscript t denotes the instantaneous value of a given force or moment.

Assuming Equation (55) represents the force or moment on a given blade, designated blade No. 1, then the force on the next adjacent blades at the same instant are

$$F_t \text{ (Blade 2)} = F \sin (\Omega t + \lambda)$$

$$F_t \text{ (Blade 3)} = F \sin (\Omega t + 2\lambda) \qquad (56)$$

etc.

where λ = spacing between blades, i.e., 120° on a 3-way, 90° on a 4-way

If the instantaneous forces, Equations (55) and (56), are evaluated on each blade for the zero radius, the summation of these individual blade forces will give the shaft loads produced by the 1xP harmonic blade load. The results give the following for a propeller having more than two blades. These forces are illustrated in Figure 14.

$$\sum (F_y)_o = \text{Thrust} = 0$$

$$\sum (F_z)_o = \text{Nonharmonic, i.e., steady-state radial} \\ \text{normal force}$$

$$= N = \frac{B(F_z)_o}{2} \qquad (57)$$

where B = No. blades

$$\sum (M_y)_o = \text{Nonharmonic steady-state yawing moment, } M_y.$$

$$= M_y = \frac{(M_y)_o B}{2} \qquad (58)$$

$$(M_z)_o = 0 = \text{Shaft torque } Q_s$$

On a two-way propeller, $N = 2(F_z)_o$, $M = 2(M_y)_o$ and the shaft forces and moment are harmonic with a frequency of twice propeller speed.

Equations (57) and (58) give the shaft forces for a pure pitch attitude, if the attitude is pure yaw, then

$$(F_z)_o = \text{Side force, } S = \frac{(F_z)_o \, B}{2}$$

$$(M_y)_o = \text{Pitching moment, } M = \frac{(M_{yo}) \, B}{2}$$

(59)

In those cases where the effective Aq is a combination of pitch and yaw, the resultant can be found by vector addition similar to Equation (42) . The direction of the shaft forces will depend upon the airplane attitude, pitch-up, pitch-down, left yaw or right yaw, and the direction of propeller rotation. A right-hand-rule and other schemes can be expressed to give these shaft force directions; however, once a basic understanding of the generations of these forces is attained, the directions are quite obvious.

In large propellers, and in propellers having high excitation factors, Aq, the foregoing shaft forces can be a significant factor in the design of the propeller shaft.

Throughout the previous development, only the lift vector has been considered. Obviously there will be a cyclic drag variation, and an expression similar to Equation (46) can be developed expressing the 1xP harmonic drag vector. However, experience has shown that in the case of the conventional aircraft, the cyclic drag is relatively small with respect to the lift component, and that it can be safely neglected for structural design purposes.

The previous development applies specifically to the propeller installations where the propeller's angle of attack is small, and correlation of calculated and flight test data on conventional aircraft has been very good. Such correlations indicate a maximum error in the order of 7%.

When the angle A exceeds the 10-15 degree range, the accuracy of Equation (46) decreases rapidly and for A values above 20° the use of that equation would be unreliable. Several studies have been made to develop a universal 1xP loading equation. A preliminary approach is given in detail in Reference 4. In that development the 1xP lift corresponding to Equation (46) is given as

$$\frac{\Delta L}{\Delta r}_r = \frac{q}{2}\left[\sin 2A\left[b\ C_L\ \cot\emptyset\,(2 - \frac{V_O}{\sigma W}\cos\emptyset) + ba\right]\right.$$

$$+ \frac{3}{4}\,ab\,\frac{V}{W}\cos^3 A\ \sin\emptyset\left.\right]\ \sin\Omega t$$

$$- qba\ \sin A\left[\frac{V_i r}{VR}\ (\cot\emptyset - 2a)\right]\cos\Omega t \qquad (60)$$

where the terms not previously defined are   (see Figure 30)

V_O, V_i = components of induced velocity defined in Reference 4 – ft/sec

W = resultant velocity   – ft/sec

V = free stream velocity – ft/sec

a = propeller section angle of attack – rad

The $\sin\Omega t$ and the $\cos\Omega t$ terms of the above equation can be considered separately. Considering the aircraft attitude to be pure pitch and integrating Equation (60) to the zero radius, it is easily shown that the following shaft force and moments are produced (see Figure 14):

Force component	Force	Moment
$\sin\ \Omega t$	Normal	Yaw
$\cos\ \Omega t$	Side	Pitch

Loads computed on the basis of Equation (60) have not given satisfactory results. The major problem appears to be in the determination of correct values for the induced velocity components, V_O and V_i. The more classical type studies have also been initiated where the flow is expressed as functions of propeller radius, and rotational angle, forces computed and the various harmonics obtained by Fourier Analysis. All of these studies have shown that the induced velocity distribution during high angle-of-attack operation of a propeller has a large effect on the loading. A major problem in propeller analysis has been the analytical and/or experimental evaluation of this inflow velocity distribution.

The lack of reliable theoretical loading, makes it necessary for the designer to resort to a semiempirical approach to establish propeller 1xP harmonic loads for the high angle-of-attack conditions.

Blade load distributions and resulting shaft loads can be computed on the basis of Equations (57), (58) and (60). The corresponding shaft loads are also obtained from data such as given in Reference 4 or other model test data. The calculated blade load distributions can then be proportioned by the ratio of test loads to calculated loads. This technique has been proven very satisfactory in correlations calculated and flight test data on prototype V/STOL propellers.

Higher Order Loads

The relatively simple development of Reference 5 and the more complex flow studies show that in addition to 1xP the aerodynamic load on the propeller blade contains harmonic components at frequencies corresponding several multiples of the rotational speed, i.e., 2xP 3xP, 4xP etc., and the existence of such a loading has been verified in flight test. Indications are, at least on conventional aircraft, that these higher order components are small and have generally been neglected in evaluating design loads, but it has been common practice to make allowance for such extraneous factors when establishing a desired factor of safety.

The higher harmonics can become significant if the propeller operating speed is such that the exciting 2xP, 3xP, etc., frequency is in the proximity of a natural blade frequency. Further, the resulting propeller shaft forces due to the higher frequency loads are generally harmonic and a corresponding vibration will be transmitted to the propeller supporting structure. A more detailed discussion of these aspects will be covered in a later section. However, it might be noted at this point, that the imposed shaft forces will be of the following form:

$$
\left.
\begin{aligned}
T &= A_1 \cos n\Omega t & n &= KB \\
T &= 0 & n &\neq KB \\
N &= A_2 \cos (n+1)\Omega t & n+1 &= KB \\
&= A_2 \cos (n-1)\Omega t & n-1 &= KB \\
N &= 0 & n \pm 1 &\neq KB \\
M &= A_3 \cos (n+1)\Omega t & n+1 &= KB \\
M &= A_4 \cos (n-1)\Omega t & n-1 &= KB \\
M &= 0 & n \pm 1 &\neq KB
\end{aligned}
\right\} \quad (61)
$$

74

where T, N, M are harmonic components of the shaft thrust, radial force and moment.

A_1, A_2, A_3 = Represent the max. values of thrust, normal force, moment

           n = order of vibration

           Ω = propeller rotational speed, radians

           K = integers, 0, 1, 2, 3, etc.

           B = the number of blades in the propeller.

There have been some flight test data on V/STOL aircraft with the propeller operating at high angles-of-attack, which indicated a significantly high 2xP harmonic load. The evidence, however, has not been conclusive and the preliminary attempts to define the airflow through the disc and the subsequent harmonic analysis of the resulting loads, have not shown comparable high values of excitation due to higher orders. These factors indicate a need for better definition of the propeller inflow velocity distribution, particularly at the higher propeller angles of attack.

Steady-State Aerodynamic Loads

The steady-state aerodynamic loads are those force components associated with the nominal velocity of the blade airfoil section, i.e., the resultant of the rotation speed and the forward velocity of the aircraft. This in effect represents the mean velocity through the disc, and the resulting loads are the mean loads upon which the 1xP and other harmonics are superimposed. Further, it is the steady-state loads which provide the net thrust to satisfy the velocity requirements of a given flight condition and also provide the reaction for the horsepower input to the propeller.

Referring to Figure 32, the basic lift and drag forces on a blade of elemental length, Δr, is

$$\left. \begin{array}{l} L = \tfrac{1}{2} \rho W^2 \; C_L \; b \; dr \\[2mm] D = \tfrac{1}{2} \rho W^2 \; C_D \; b \; dr \end{array} \right\} \quad (62)$$

Figure 32. Nominal Blade Forces.
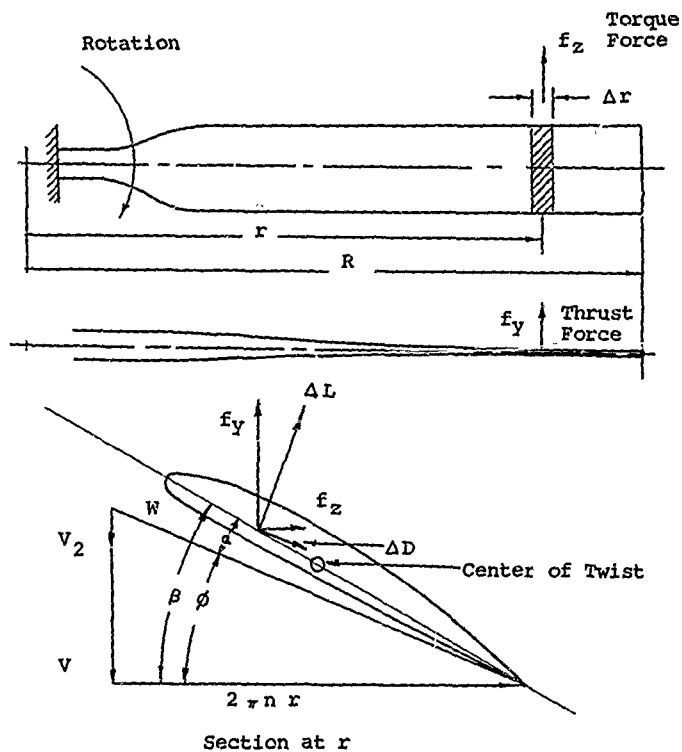
V = Free-Stream Velocity β = Blade Angle

V_2 = Induced Velocity ϕ = Wind Angle

2 nr = Rotational Velocity α = Angle of Attack

W = Resultant Velocity

Section at r

76

The thrust and torque forces are

$$f_y = \frac{\Delta L}{\Delta r} \cos\phi - \frac{\Delta D}{\Delta r} \sin\phi$$

$$f_z = \frac{\Delta D}{\Delta r} \cos\phi + \frac{\Delta L}{\Delta r} \sin\phi$$

$$\left.\right\}(63)$$

where f_y = thrust loading   lb/in.

f_z = torque loading   lb/in.

The resulting blade shears forces and moments can be obtained by integrating Equations

$$\text{Thrust force} \quad = (F_y)_r = \int_{r_R}^{R} f_y\, dr$$

$$\text{Thrust bending} = (M_y)_r = \int_{r_R}^{R} \int_{r}^{R} f_y\, dr\, dr$$

$$\text{Torque force} \quad = (F_z)_r = \int_{r_R}^{R} f_z\, dr$$

$$\text{Torque bending} = (M_z)_r = \int_{r}^{R} \int_{r}^{R} f_z\, dr\, dr$$

$$\left.\right\}(64)$$

It should be obvious that the total propeller thrust is equal to the thrust per blade times the number of blades, and that the torque moment per blade times the number of blades must be compatible with the input horsepower. That is,

$$B \int_{0}^{R} f_y\, dr = \text{Propeller thrust}$$

$$B \int_{0}^{R} \int_{x}^{r} f_z\, dr = \frac{63025 \text{ (input horsepower)}}{\text{Propeller rpm}}$$

$$\left.\right\}(65)$$

The accurate evaluation of the section thrust and torque, Equation (63), for a given condition of propeller operation, requires an aerodynamic strip analysis. The results of such a study are often provided in terms of an incremental thrust coefficient ΔC_T, and an incremental torque coefficient ΔC_Q. The corresponding forces can be evaluated from the following expression:

77

Thrust: $\left(\dfrac{\Delta C_T}{\Delta r}\right)_r = (f_y)_r \rho n^2 D^4$

Torque: $\left(\dfrac{C_Q}{\Delta r}\right)_r = (f_z)_r \, r \rho n^2 D^5$

$\left.\begin{array}{c}\\\\\\\\\end{array}\right\}$ (66)

With reference to Figure 32, it is apparent that aerodynamic forces will produce a twisting of the blade section. This will in turn change the angle of attack, α, thus increasing the aerodynamic forces in a manner similar to that discussed previously, Equations (49) and (52). However, in the case of the steady-state loading it must be remembered that the aerodynamic analysis by which the loads are determined is performed to satisfy given conditions of operation. Therefore, the required blade angle distributions as established by aerodynamic analyses must represent the final torsionally deflected position or the so-called live blade angle distribution.

In order to allow for the torsional deflection, the blade twist is subtracted from the aerodynamic pitch distribution, and the resulting angle is specific for manufacturing.

$$\beta_{mfg} = \beta_{aero} - \theta_{twist} \tag{67}$$

The two-blade angle distribution is illustrated in Figure 33. By this technique, the blade will under load deflect torsionally to the angle necessary to produce the required aerodynamic loads. However, it should be obvious that this process can only be optimized for one flight condition. Therefore, only one condition can be selected, such as takeoff, cruise, etc., as the most desirable for optimum performance of the given installation. The procedures for calculating the blade twist under steady-state loads are given in detail in the section on Methods of Analysis.

Propeller Mass Loads

The rotating mass of the propeller generates inertia forces which must be evaluated in establishing the total force system on the propeller. The development of these forces is presented in some detail in the following sections.

Blade Centrifugal Force

Consider a blade element as shown at some radius r, Figure 34; the centrifugal force on that element is

78
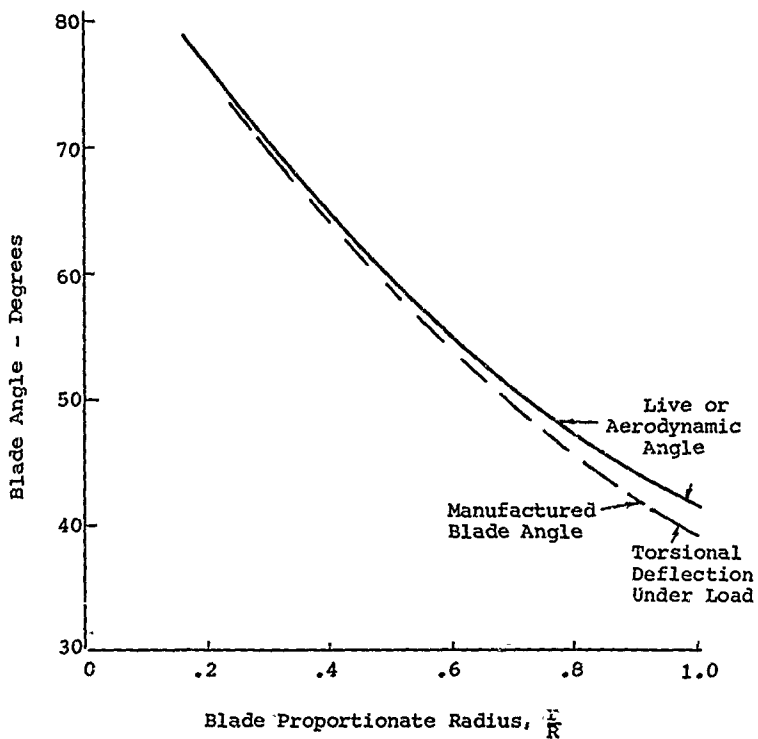
Figure 33. Typical Blade Pitch Distribution.

79

$$\Delta CF = dm r_1 \omega^2 \tag{68}$$

where dm = element mass considered concentrated at the c.g., lb-sec^2/in.

         r_1 = radius from the center of rotation to the section centroid, in.

         ω = rotational velocity, rad/sec

         $\omega = 2\pi N/60$, N = prop rpm

In propeller blades, the angle λ is very small, and r_1 can be taken equal to r.

Also, $dm = \dfrac{\delta}{g} A_r dx$

         δ = material density, lb/in.^{3}

       (A_r) = section area @ radius r, in.^{2}

         dr = elemental length, in.

Substituting in Equation (68)

$$(\Delta CF)_r = \frac{\delta}{g} \omega^2 (A_r) r \, dr$$

and the total centrifugal force at any given radius r^1

$$CF_r 1 = \frac{\delta}{g} \omega^2 \int_r^R A r \, dr \tag{69}$$

Noting that $\omega = 2\pi N/60$ where N is the propeller rpm, and g equals 386 in/sec^2, Equation (69) can be written

$$CF_r 1 = 28.4 \left[\frac{N}{1000}\right]^2 \int_r^R A r \, dr \tag{70}$$

Evaluating the above integral to the blade butt, $r^1 = r_b$, gives the total blade centrifugal force that must be reacted by the hub-blade retention.

Blade Centrifugal Restoring Moments

Since the propeller blade is essentially a cantilever beam, it deflects in the direction of the resultant load. The deflection therefore has components in both the thrust, y, and torque, z, directions, and the deflected blade axis is illustrated in Figure 34. This deflection provides a moment arm for the centrifugal force and the sense of the moment is such as to tend to return the axis to its undeflected position.

Considering the centrifugal force of the elemental mass dm at radius r, the angle λ, is small and therefore

$$r = r_1, \cos \lambda = 1.0, \sin \lambda = \lambda$$

$$\Delta CF_1 = \Delta CF \cos \lambda = \Delta CF$$

$$\Delta CF_2 = \Delta CF \sin \lambda = \Delta CF \frac{z_r}{r}$$

In the thrust direction, the moment at r^1 due to the force ΔCF is

$$(\Delta M_{yCF})_{r1} = \Delta CF(y_r - y_r^1) \tag{71}$$

and the total moment due to the centrifugal force on all blade elements outboard of r^1 is

$$(M_{yCF})_r^1 = \int_r^R (y_r - y_{r1}) \, dCF \tag{72}$$

Integrating the above by parts, it can be shown that

$$\Delta (M_{yCF})_r^1 = \int_r^R \left(\frac{dy}{dr}\right)_r (CF)_r \, dr \tag{73}$$

where   (CF) is the total centrifugal force at any station r

$(d\, y/dr)_r$ = the slope of the thrustwise deflection curve at any station r.

In the torquewise direction, Figure 34,

$$(\Delta M_{CF_z})_r^1 = \Delta CF(z_r - z_r^1) - \Delta CF_2(r - r^1) \tag{74}$$

81

Integrating the total centrifugal moment at r^1 is

$$(M_{CF_z})r^1 = \int_r^R (dz/dr)_r \, (CF)_r \, dr - \frac{\delta}{g} \omega^2 \int_r^R \int_r^R z_r A_r dr^2 \quad (75)$$

where z and (dz/dr) are the magnitude and slope of
the torquewise deflection curve.

The first term is similar to the thrust bending component, and
the second term is in the same form as Equation (69). It will
be noted that in Figure 34 the force ΔCF passes through the
center of rotation. Therefore,

$$(M_{CF_z})_0 = 0 \text{ or,} \quad \int_0^R (dz/dz)(CF)dr = \frac{\delta}{g} \omega^2 \int_0^R \int_r^R zA \, dr dr$$

It should be apparent that these centrifugal moments cannot be
evaluated unless the blade deflection is known. They cannot,
therefore, be readily computed as an isolated blade load com-
ponent. Techniques for evaluating these components will be
presented in the Methods of Analysis section.

Blade Tilt

The principle involved above provides a potential means by
which the bending moments on the blade can be controlled to a
desired magnitude. As previously shown the moment caused by
the centrifugal force acting through a deflection of the blade
axis produces a moment tending to restore the blade to its un-
deflected position. In other words, a moment which subtracts
from the aerodynamic moments, and is particularly effective in
the thrust-wise direction. Therefore, if an artificial deflec-
tion or tilt is manufactured into the blade, the result can be
a significant reduction in the net moment as felt by the blade-
beam. This elementary concept is illustrated in Figure 35a,
which shows the blade axis tilted forward, i.e., in the thrust
direction by the angle θ. Usually θ is a very small angle and
therefore, $r_1 = r \cos\theta = r$.

The slope of the tilted blade axis is

$$dy/dr = \tan\theta = \text{constant}$$

Figure 34. Blade Centrifugal Force.
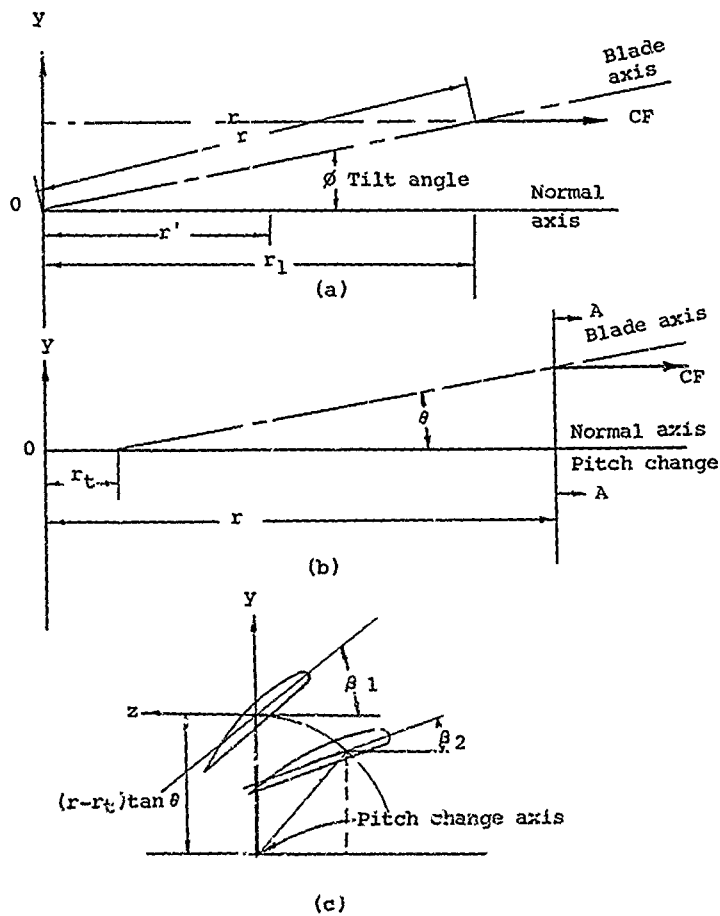
Figure 35. Blade Tilt.
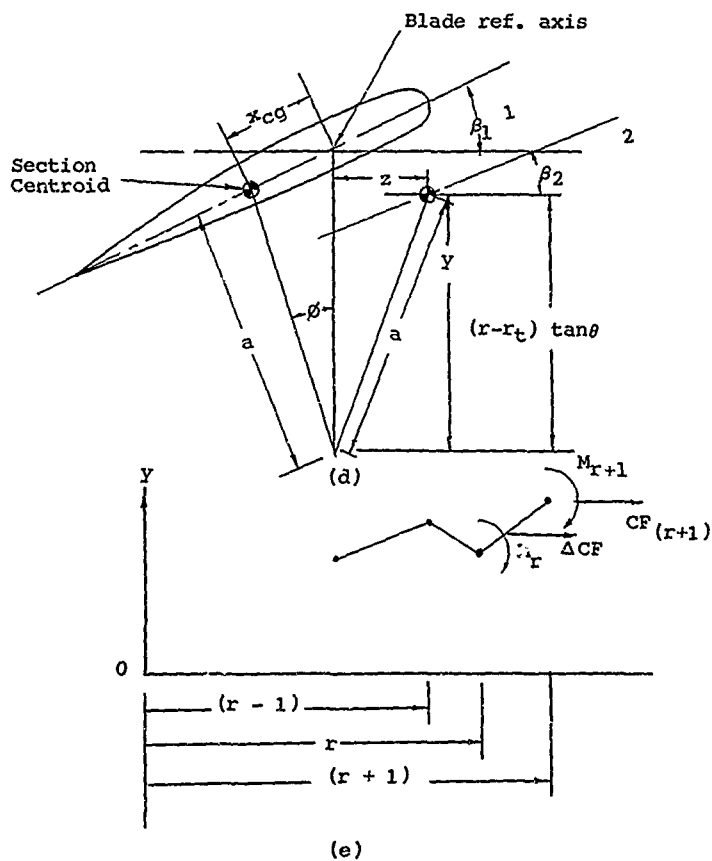
Figure 35. Continued.

85

Therefore, from Equation (73)

$$(M_{tilt})_{r1} = \tan \theta \int_{r}^{R} CF \, dr \qquad (76)$$

This elementary consideration would be very desirable if the tilt is pure thrust and the pitch change axis and the blade axis are coincident. This condition can be achieved by incorporating the tilt angle in the hub barrel. This, however, presents some difficulty in manufacturing and can influence the design of the pitch change system. It is therefore more common to introduce tilt into the blade by kinking the shank at some radius r_t just outboard of the hub barrel. This configuration is illustrated in Figure 35b.

For tilt in a pure thrust direction, Equation (76) is valid, but the maximum value of the tilt moment will be

$$M_{tilt_{max.}} = \tan \theta \int_{r_t}^{R} CF \, dr \qquad (77)$$

and the value is constant from r_t inboard.

Figure 35c shows the geometric relationships of a blade section at radius r. It should be quite apparent that for this type of tilt there is only one blade angle setting at which the tilted blade axis is in the pure pitch direction, and it is designated β_1 in Figure 35c. At this blade angle setting, Equation (77) is valid.

Now assuming that the flight condition changes and a new blade angle setting β_2 is required, the section rotates about the pitch change axis by $\Delta\beta$, where $\Delta\beta = \beta_1 - \beta_2$. The section is then tilted in both the thrust and torque direction.

$$y_2 = (r - r_t) \tan \theta \cos\Delta\beta$$

$$z_2 = (r - r_t) \tan \theta \sin \Delta\beta$$

and

$$dy/dt = \tan \theta \cos \Delta\beta$$

$$dz/dt = -\tan\theta \sin\Delta\beta$$

Substituting in Equations (73) and (75), the tilt moments become

$$(M_y) \text{ tilt} = \tan\theta \, \cos\Delta\beta \int_0^R CF \, dr$$

$$(M_z) \text{ tilt} = (-)\left[\tan\theta \, \sin\Delta\beta \int_0^R CF \, dr - \right.$$
$$\left. \omega^2 \, \frac{\delta}{g} \, \tan\theta\sin\Delta\beta \int_{r'}^R \int_r^R (r - r_t)A \, drdr\right]$$

$$(78)$$

where the (-) sign indicates that for the case shown, i.e., a decrease in pitch from the optimum position β_1, the torquewise tilt moment will add to the torque aerodynamic moment.

It is also to be noted that in a condition of reverse thrust, the moments due to forward tilt will also add to the aerodynamic moments. Obviously, therefore, with tilt incorporated in the blade shank, the analyst must consider the effects over the entire pitch range of the propeller in order to achieve the most practical benefit.

The foregoing development has assumed that the blade axis which is a manufacturing reference and also defines the tilt, is essentially coincident with the centroidal axis. For the conventional propeller blade this is approximately true, and the previous equations can be used without significant error. However, there have been designs where this is not the case, as illustrated in Figure 35d . This is essentially the same section as shown in Figure 35c, but with the centroid displaced from the reference axis. The radius (a) to the centroid and its angle ϕ with respect to the tilt plane can be determined from section layouts or

$$a = \left((x_{cg} \cos \beta_1)^2 + \left[(r - r_1) \tan\theta - x_{cg} \sin\beta_1\right]^2\right)^{\frac{1}{2}}$$
$$\sin^{-1}\phi = x_{cg} \cos\beta_1/a$$

where the distance x_{cg} must be taken from section design details.

The tilted position of the centroidal axis now becomes

$$y = a \cos (\Delta\beta - \phi)$$
$$z = a \sin (\Delta\beta - \phi)$$

If the blade geometry is such that the displacements as computed at the various blade radii form a reasonably straight line, Equations 78a and 78b can be easily modified to

incorporate the average centroidal slope. It is possible how-
ever for the centroidal displacements to form a very irregular
curve when plotted against the blade radius as illustrated in
Figure 35e.   In such a case the displacements are not
smooth curves and may have significant discontinuities, there-
fore the foregoing equations could be quite inaccurate. For
such cases it is desirable to compute the tilt moments by the
basic Equations (71) and (72).   The general equation for
the tilt moment at any radius r' is then

$$(M_Y)_{r'tilt} = \sum_r^R (y_r - y_{r'})(\Delta CF)_r$$

$$(M_Z)_{r'tilt} = \sum_r^R (z_r - z_{r'})(\Delta CF)_r - \sum_r^R (r - r')(\Delta CF_2)_r$$

(79)

where $\Delta CF = \delta/g\ \omega^2(A_r)r\ \Delta r$

$\Delta CF_1 = \Delta CF\ z/r = \delta/g\ \omega^2(A_r)z \Delta r$

Δr - the incremental blade length between
         selected radii.

Obviously, the more radii used to evaluate the above equation
i.e., the smaller the value of Δr, the greater the accuracy.

To simplify the calculations , Equation (79) can be put in
simple matrix form, which is illustrated below for the M_y
relation.

$$
\begin{vmatrix} M_{y_0} \\ M_{y_1} \\ M_{y_2} \\ \vdots \\ M_{y_R} \end{vmatrix}
=
\begin{vmatrix}
0 & (y_1 - y_0) & (y_2 - y_0) & - - - & (y_R - y_0) \\
0 & 0 & (y_2 - y_1) & - - - & (y_R - y_1) \\
0 & 0 & 0 & - - - & (y_R - y_2) \\
 & & & & \\
 & & & & \theta \\
\end{vmatrix}
\begin{vmatrix} \Delta CF_0 \\ \Delta CF_1 \\ \Delta CF_2 \\ \\ \Delta CF_R \end{vmatrix}
$$

Blade Centrifugal Twisting Moment

The centrifugal force generated by the rotating propeller
blade produces a torque or twisting moment on the blade sec-
tion. The sense of this twist is always in the direction

88

such as to turn the blade to flat pitch. The magnitude can be quite large and it is the major torque reacted by the pitch change mechanism of the propeller.

Figure 36 shows the centrifugal force, ΔCF, developed by an element of mass, dm, on a blade section at radius r. The section is considered to be displaced by the distances a & b from the pitch change axis.

$$\Delta CF = dm \; r_1 \omega^2 \tag{80}$$

$$\Delta CF_2 = CF \sin \lambda$$

$$\lambda \; \text{small}, \; \therefore \; r = r_1$$

$$\sin \lambda \; \frac{a + x \cos\beta - y \sin\beta}{r} \tag{81}$$

$$dm = \frac{\delta}{g} \; dA \; dr \tag{82}$$

where $\qquad$ dA = elemental area

The torque of this elemental force about the point "0" will be

$$\Delta Q_O = \Delta CF_2 \Big[b + x \; (\sin\beta + y \; \cos\beta) \Big]$$

Substituting Equations (81)-(82) in the above, expanding and integrating over the section, and also noting that x and y are taken with respect to the section centroid, the following is obtained:

$$\frac{\Delta Q_O}{\Delta r} = \frac{\delta}{2g} \omega^2 \Big[I_{max} - I_{min} \Big] \sin \beta + abA \tag{83}$$

where $\quad$ A $\quad$ = section area $\qquad$ in.^{2}

$$I_{max} = \int x^2 dA \qquad\qquad \text{in.}^4$$

$$I_{min} = \int y^2 dA \qquad\qquad \text{in.}^4$$

The total torque at any station r' can be found by integrating Equation (83) from r' to the blade tip.
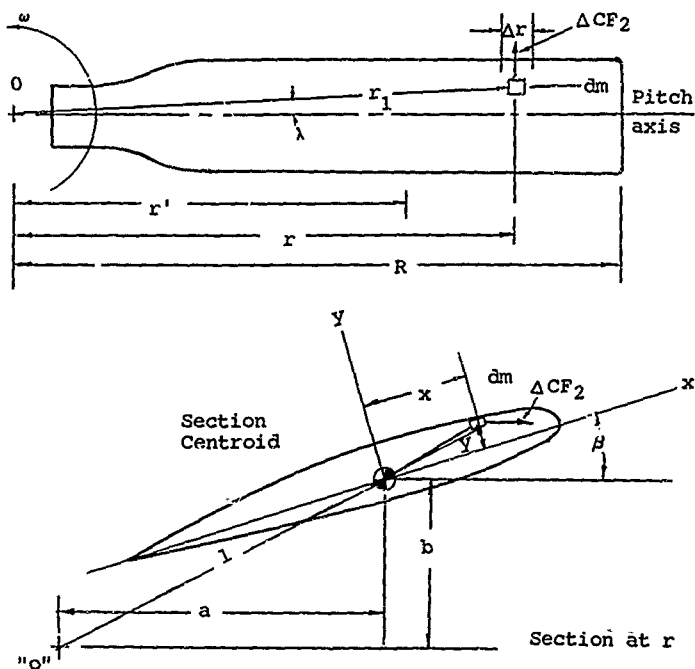
Figure 36. Centrifugal Twisting Moment.

$$Q_{r'} = \frac{\delta}{2g} \, \omega^2 \left[\int_{r'}^{R} (I_{max} - I_{min}) \sin 2\beta_r dr + \int_{r'}^{R} (abA)_r \, dr \right] \quad (84)$$

The above expression is dependent upon the pitch distribution and blade angle setting. Generally, the designer is primarily interested in the maximum value, and to simplify the evaluation, Equation (84) can be put into a more convenient form.

Let β_{ref} be the blade angle at some fixed reference radius, r_{ref}, then the blade angle at any radius r is

$$\beta_r = (\beta_r - \beta_{ref}) + \beta_{ref} \quad (85)$$

where $(\beta_r - \beta_{ref})$ can be easily obtained from the design pitch distribution of the blade. Substituting the above in Equation (84), the blade torque becomes

$$Q_{r'} = \frac{\delta}{2g} \, \omega^2 \left[B^2_{r'} + C^2_{r'} \right]^{\frac{1}{2}} \sin \left(2\beta_{ref} + \tan^{-1} \frac{B_{r'}}{C_{r'}} \right.$$
$$+ \left. \int_{r'}^{R} (abA)_r dr \right) \quad (86)$$

where
$$B_{r'} = \int_{r'}^{R} (I_{max} - I_{min})_r \sin 2 (\beta_r - \beta_{ref}) \, dr$$
$$C_{r'} = \int_{r}^{R} (I_{max} - I_{min})_r \cos 2 (\beta_r - \beta_{ref}) \, dr$$

The total twisting moment for the entire blade is obtained by taking the integration from the zero radius, $r' = 0$, and the total centrifugal blade torque reacted by the propeller pitch control system is

$$Q_O = \frac{\delta}{2g} \, \omega^2 \left[B^2_O + C^2_O \right]^{\frac{1}{2}} \sin \left(2\beta_{ref} + \tan^{-1} \frac{B_O}{C_O} \right.$$
$$+ \left. \int_{0}^{R} (abA)_r \, dr \right) \quad (87)$$

The maximum value of Equation (87) will occur when the value of the sine term equals 1.0. Therefore,

$$Q_{max} = \frac{\delta}{2g} \ \omega^2 \left[(B_o^2 + C_o^2)^{\frac{1}{2}} + \int_0^R (abA)_r \ dr \right] \qquad (88)$$

and since

$$\sin (2\beta_{ref} + \tan^{-1} \frac{B_o}{C_o}) = 1.0$$

$$(\beta_{ref})_{max} = (90 - \tan^{-1} \frac{B_o}{C_o})/2 \qquad (89)$$

where $(\beta_{ref})_{max}$ is now the blade angle setting at the selected reference station which will produce the maximum value of Q_o.

Now if the blade angle setting is changed by an amount $\Delta\beta$ from the value of $\beta_{ref \ max}$, it is easily shown that the torque at the new angle $\beta_{ref \ max} - \Delta\beta$) is

$$(\Delta Q_o)_{\beta - \Delta\beta} = \left[Q_{o \ max} - \frac{\delta}{2g} \ \omega^2 \int_0^R abA \ dr \right] \cos 2\Delta\beta$$

$$+ \int_0^R abA \ dr \qquad (90)$$

Noting that $\omega = \frac{2\pi N}{60}$ and $g = 386 \ in./sec^2$

$$\frac{\delta}{2g} \omega^2 = 1.419 \ N^2 \text{ where } N = \text{propeller rpm}$$

Equation (90) provides a convenient expression for evaluating the centrifugal twisting moment as a function of blade angle setting.

It is to be noted that in the case of most propeller blade designs the dimensions a & b are relatively small, and the term $\int abA$ is generally neglected. However, this may not be true especially in the case of tilt, see previous section. Also, by displacing the blade axis with respect to the pitch change axis the designer can exercise some control over the magnitude of this centrifugal torque.

92

Centrifugal Straightening Moment

In the propeller blade or any twisted beam, an axial strain
tends to straighten out or untwist the section. This effect
is not an applied load in the usual sense, but it is rather a
torque induced at the blade sections as a result of the twist
or pitch distribution.

The action is readily understood with reference to Figure 37
and the following elementary development. Figure 37 shows
two adjacent blade sections separated by the incremental dis-
tance Δr. The force acting on an elemental area (dA) is

$$dF = \sigma \, dA \qquad (91)$$

where σ is the local axial stress.

This force has a component dF_1 acting normal to the fiber, con-
necting $(dA)_1$ with the corresponding elemental area $(dA)_2$ in
section 2 of Figure 37.

From the referenced Figure 37,

$$dF_1 = \sigma \, dA \, \tan \lambda \qquad (92)$$

$$= \sigma \, 1(d\beta/dr)dA$$

and the torque about "0" is

$$(dQ_\mu)_r = \sigma \, 1^2(d\beta/dr)dA \qquad (93)$$

If "0" is a centroidal axis, integrating over the area gives

$$(Q_\mu)_r = (\sigma_{CF})_r (d\beta/dr)_r (I_{max} + I_{min})_r \qquad (94)$$

where $(Q_\mu)_r$ = straightening moment at radius r - in./lb

σ_{CF} = axial stress due to the blade
centrifugal force - psi

σ_{CF} = CF/A

CF = centrifugal force at r - lb

A = section area at r - in.

$(d\beta/dr)_r$ = rate of change of pitch - rad/in.

I_{max}, I_{min} = section moments of inertia - in.^{4}

93
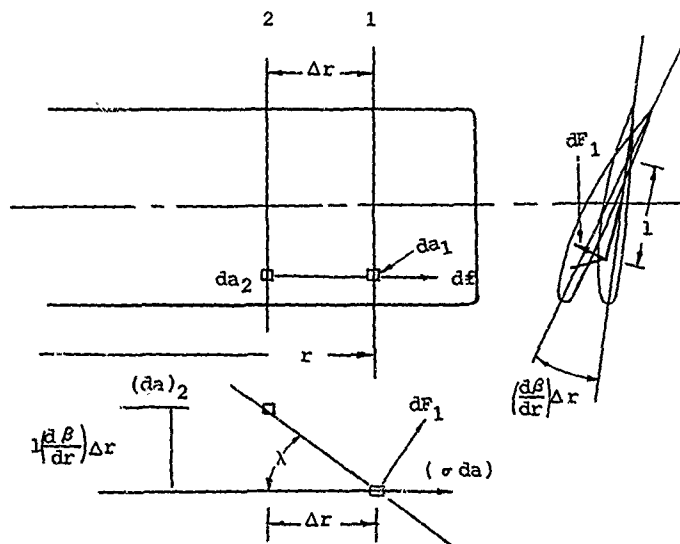
Figure 37.   Blade Straightening.

It will be noted that this torque is not an integrated effect, but is dependent only upon the local geometry. Usually this induced effect is small and is neglected. However, on very wide blades it can become significant.

Gyroscopic Forces

The rotating propeller is in effect a gyroscope and it generates all the forces and moments generally associated with that device. Figure 38 illustrates a propeller rotating about its own axis, Y-axis, with a constant velocity ω. At the same time this Y-axis is being rotated at some velocity Ω. At a given instant of time an element of mass, dm, on a given blade at radius r is at position (0). An incremental instant of time later, t, the mass element has moved through the angles $\omega \Delta t$ and $\Omega \Delta t$ to position (1). Considering the corresponding changes in velocity, it is easily shown that the magnitude of the acceleration acting on dm in the Y direction is

$$a = 2\Omega \omega r \cos(\omega \Delta t) \tag{95}$$

Consequently, there is a force acting on dm equal to

$$dF_g = (a) \, dm$$

$$dF_g = 2r \, \Omega \omega \cos \omega t \, dm \tag{96}$$

since $dm = \frac{\delta}{g} \, Adr$, and considering only maximum amplitudes, the shear force at any station r' is

$$\left. \begin{array}{l} (F_g)_{r'} = 2\Omega \, \omega \, \frac{\delta}{g} \int_{r'}^{R} Ardr \\[4mm] (M_g)_{r'} = 2 \, \Omega \, \omega \, \frac{\delta}{g} \int_{r'}^{R} \int_{r}^{R} Ardr \end{array} \right\} \tag{97}$$

and

where $(F_g)_{r'}$ = Blade shear force at radius r' due to gyroscopic action - lb

$(M_g)_{r'}$ = Blade moment at radius r' due to gyroscopic action - in.-lb

Ω = precessional velocity - rad/sec

ω = rotational velocity - rad/sec

Referring to Equation (69), Equations (97) can also be written
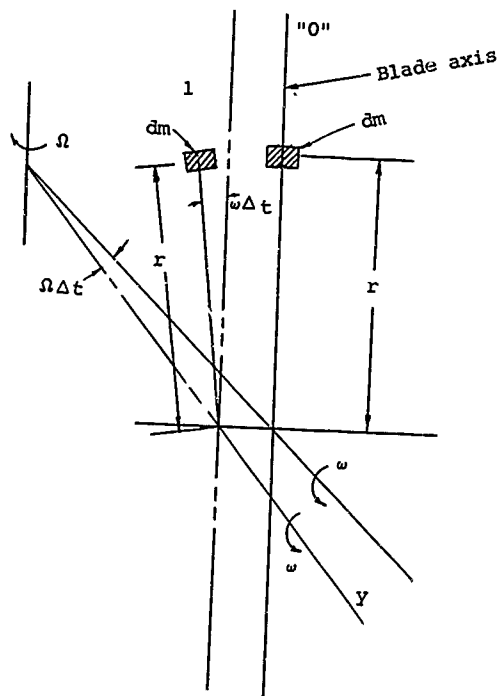
Figure 38. Gyroscopic Forces.

96

$$(F_g)_{r'} = \frac{2\Omega}{\omega}\,(CF)_{r'}$$

$$(M_g)_{r'} = \frac{2\Omega}{\omega}\int_0^R (CF)_r\,dr \tag{98}$$

It should be noted that the above forces are in the thrust or x direction.

Referring to Equation (96) it is seen that the blade is subjected to a forced vibration at a 1xP frequency. As in the case of the first-order aerodynamic forces, if the blade loads are integrated to the zero radius and summed, see Equations (57) and (58), the following shaft loads are obtained:

$$\left(\sum F_{gi}\right)_0 = 0$$

$$\left(\sum M_g\right)_0 = \frac{B(M_g)_0}{2} \tag{99}$$

As in the aerodynamic case the shaft moment is fixed or steady state. However, it should be noted that the above moment represents only the forces due to the blade mass. Actually there is a contribution due to the rotating mass of the hub and other propeller components. This contribution is small and is often neglected.

The gyroscopic forces occur on the propeller whenever the propeller axis is rotated, i.e., the aircraft pitches or yaws. The resulting 1xP gyroscopic excitation combines with the 1xP aerodynamic vibration. Fortunately, on most aircraft the rate of precession is relatively small. Further, an analysis of the aerodynamic and gyroscopic force vectors will show that in most cases the gyroscopic forces subtract from the aerodynamic forces, and it is therefore conservative from the structural standpoint to neglect the gyroscopic component. However, on highly maneuverable aircraft this may not be the case, and a careful analysis of the forces should be made to determine the gross effects.

The similarity between the gyroscopic and aerodynamic 1xP excitations provides a very effective means for endurance testing a full-scale propeller. If a test rig is so designed that a propeller can be mounted and driven at its design rotational speed, and the rig can simultaneously impart a precessional velocity, then gyroscopic forces will be generated. With the propeller rotating at its design speed, the centrifugal forces are exact. By selection of the blade angle setting, steady-state aerodynamic forces can be closely approximated. Selecting the precessional speed permits a selection of the magnitude

of the 1xP excitation to simulate the first-order design loads.
It must be noted that the gyroscopic forces are generated by
the blade mass, and generally the shear and moment load distri-
butions along the blade radius are not identical to the distri-
butions due to aerodynamic excitations. Therefore, on a gyro
test rig it is not possible to simultaneously match the maximum
design blade stress and the maximum design shank moment. Some
compromise is usually necessary in selecting the precessional
speed.

The gyro test rig has been sucessfully used for enduran~e test-
ing full-scale propellers for several years using a rig as
shown in Figure 139 in the section Propeller Blades.

Miscellaneous Factors

This section presents certain mass properties which are not in
themselves loads, but which are used to obtain certain propel-
ler forces.

Polar Moment of Inertia

By definition, the polar moment of inertia is mass times
the radius squared. Referring to Figure 36 the polar
moment of element dm is

$$I_p = r^2 \, dm \qquad (100)$$

$$dm = \frac{\delta}{g} \, Adr$$

$$\therefore \quad I_p = \frac{\delta}{g} \, r^2 Adr \qquad (101)$$

Integrating over the total blade length, the blade polar
moment of inertia is

$$(I_p)_b = \frac{\delta}{g} \int_0^R r^2 Adr \qquad (102)$$

The convention of the propeller industry to specify the
blade polar moment in slug-ft^2 units (ft - lb - sec^2),
therefore making the necessary substitutions

$$I_{p_b} = \frac{\delta}{12g} \int_0^R Ar^2 dr \qquad (\text{slug-ft}^2) \qquad (103)$$

98

where δ = material density $lb/in.^3$

        A = section area $in.^2$

        r = radius $in.$

        g = gravitational constant $in./sec^2$

The total moment of inertia of the propeller is

$$(I_p)_{prop} = B(I_p)_b + I_h \qquad (104)$$

where B = number of blades

             I_h = polar inertia of the hub

The value of I_h can be computed from a hub design layout using Equation (100). The evaluation must include the hub, retention components not considered in the blade and any pitch change system components that rotate with the hub about the propeller shaft. This value however is usually small with respect to the total blade value, and it has been common practice to use an estimated value. Experience has shown that a value of I_h in the order of 1.0 to 3.0 slug-ft^2 can be used as a good approximation.

From simple gyroscopic theory, it is known that the shaft moment is

$$M_S = I_p \Omega \omega \qquad (105)$$

Referring to Equation (99) the shaft moment due to gyroscopic forces was given as

$$M_S = \frac{B(M_q)_o}{2}$$

but $$(M_q)_o = \frac{\delta}{g} \, 2 \, \Omega \, \omega \int_0^R \int_r^R A r \, dr$$

Integrating the above by parts gives the equality

$$\frac{\delta}{g} 2 \Omega \omega \int_0^R \int_r^R A r \, dr = \frac{\delta}{g} \, 2 \, \Omega \, \omega \int_0^R A r^2 dr \qquad (106)$$

and therefore, except for the minor effect of the hub inertia included in the I_p term, Equations (105) and (99) are identical. The blade polar moment of inertia is usually given as one of the blade design parameters,

and therefore Equation (105) is usually the more conven-
ient form for obtaining the shaft moment.

Blade Inertia, Pitch Change Axis

In evaluating the dynamics of the pitch change system,
the blade inertia about the pitch change axis is required.
Referring to Figure 36 the inertia is by definition

$$\Delta I = 1^2 \ dm \tag{107}$$

$$1^2 = (a + x \cos\beta - y \sin\beta)^2 + (b + x \sin\beta + y \cos\beta)^2$$

$$dm = (dAdr) \ \delta/g$$

Substituting and integrating over the section

$$\Delta I = \frac{\delta}{g} \left[(a^2 + b^2)Adr + (I_{max} + I_{min})dr \right] \tag{108}$$

and for the total blade

$$I = \frac{\delta}{g} \left[\int_0^R (a^2 + b^2)Adr + \int_0^R (I_{max} + I_{min})dr \right] \tag{109}$$

In most propeller blades the pitch change axis is essenti-
ally coincident with the centroidal axis and the term
$\int_0^R (a^2 + b^2)Adr$ can be neglected.

METHODS OF ANALYSIS

Blade Section Properties

The accurate structural analysis of the propeller blade is,
like any beam, dependent upon the section properties. The
basic properties are necessary to define the primary blade
stresses, P/A and $M/(I/C)$. In addition it has been noted
that important propeller loads are mass effects which are func-
tions of the cross-section area and the moments of inertia.
Further, the bending moments acting on the blade are signifi-
cantly influenced by the blade deflection which is defined by
the (EI) distribution. Therefore, the accurate evaluation of
the basic blade section properties is fundamental to an ac-
curate structural analysis of the propeller.

Figure 39 shows the basic cross section of solid and hollow
blade sections and defines the primary blade dimensions. The
blade chord line and the perpendicular through the 50% chord
point are the common x - x and y - y reference axes. The ex-
ternal or aerodynamic shape is defined by the ordinated
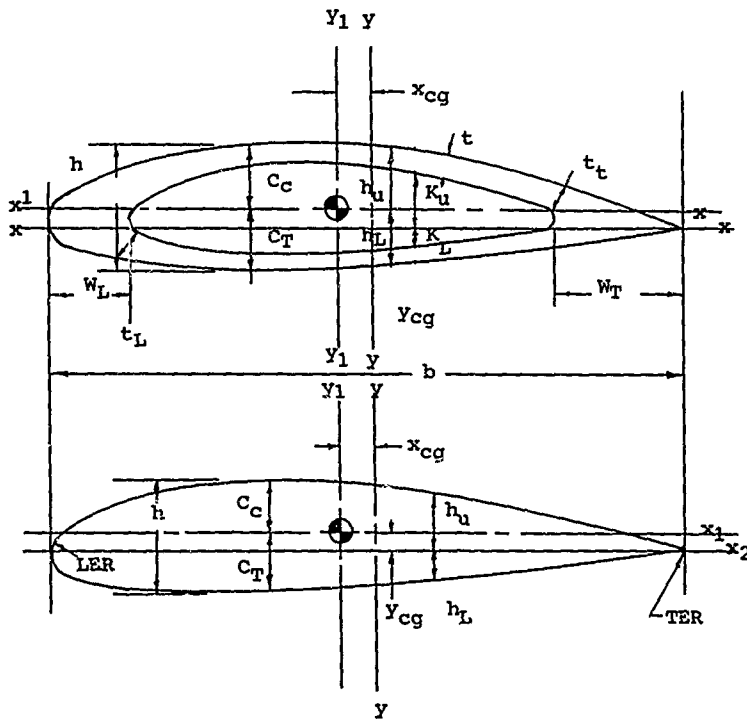
Figure 39. Basic Blade Dimensions.

101

h_u and h_L. These ordinates are, in turn, established by the selected airfoil shape, and for the common series 16 & 17 airfoils, they have been developed for evaluating the profile ordinates once the basic aerodynamic parameters of chord, thickness ratio and camber (design C_L) have been established. (See Tables X and XI in the section Propeller Blades).

The internal surface of the hollow section depends upon both structural requirements and manufacturing processes. Generally, definition of the internal contour requires some detailed preliminary analysis and section layouts. However, once the blade section has been defined the basic section properties are readily computed. The basic properties are by definition:

$$A = \text{Area} = \int dA$$

$$x_{cg} = \int x dA/A \qquad Y_{cg} = \int y dA/A$$

I_{min} = Minor moment of inertia about centrudal axis

$$I_{min} = \int y^2 dA - Y_{cg}^2(A)$$

I_{max} = Major moment of inertia about centroid

$$I_{max} = \int x^2 dA - x_{cg}^2(A)$$

Section moduli

$$(I/C) \text{ Thrustside} = I_{min}/C_T$$

$$(I/C) \text{ Camber} = I_{min}/C_C$$

$I_{x,y,}$ = Product of inertia = $I_{xy} - x_{cg} Y_{cg} A$

For the propeller sections, the x,y,axes can for all practical purposes be considered as the principal axis through the centroid.

z = Torsional stiffness factor = $\int x_1^4 dA$ where (x_1) is measured with respect to the centroid

These section data can be computed by the usual tubular integration. This process, while simple, is quite time-consuming and has therefore been programmed for high-speed computers. Most engineering computer program libraries have general section property programs that can be utilized. The input for such programs usually only requires a tabulation of the external and internal ordinates in accordance with a prescribed format. Accuracy therefore depends on carefully detailed section layouts from which ordinates can be selected.

102

Blade Section Properties - Composite Structures

In the more recent periods of propeller design and especially
with the development of composite blades, it is common to find
a blade section composed of more than one material. A typical
section of this type is illustrated in Figure 40. To facili-
tate the analysis of such a section, it is usually more conven-
ient to use an equivalent single material section which has the
same stiffness or mass properties as the composite section.
For the normal structural analysis, stress deflection, etc.,
the equivalent section is based upon compatibility of strain.
This is illustrated by a simple example. Figure 41 shows
a simple bar in tension, but the bar is made up of two mater-
ials, (1) and (2)

A_1 = Cross-section area of material (1)

A_2 = Cross-section area of material (2)

E_1 = Modulus of material (1)

E_2 = Modulus of material (2)

Now if a load P is applied to this composite bar, in order for
the total strain or elongation of each component to be equal,
the load will be so proportioned between the parts that

$$\delta = \frac{P_1 1}{A_1 E_1} = \frac{P_2 1}{A_2 E_2} \tag{110}$$

$$P = P_1 + P_2$$

For ease of analysis we can also say that

$$\delta = \frac{P1}{A_e E_{(1)}} \tag{111}$$

where A_e is the cross sectional area of an equivalent bar
made entirely of material (1).

By combining Equations (110) & (111) it is easily shown that

$$A_e = A_1 + A_2 \left(\frac{E_2}{E_1}\right) \tag{112}$$

The elongation of the bar is given by (111) and the stress com-
puted by the usual formula, $\sigma = P/A_e$ will be the stress in
material (1) but the stress in material (2) will be $\sigma_{(1)} E_2/E_1$.
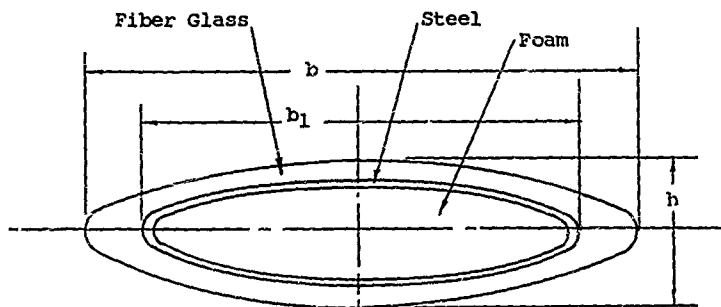
Figure 40.   Typical Composite Section.
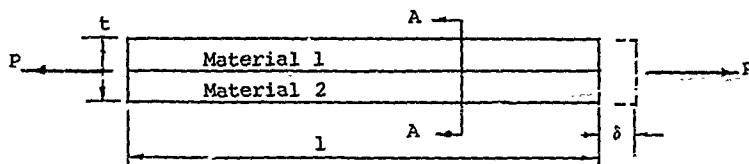
(a) Composite Bar
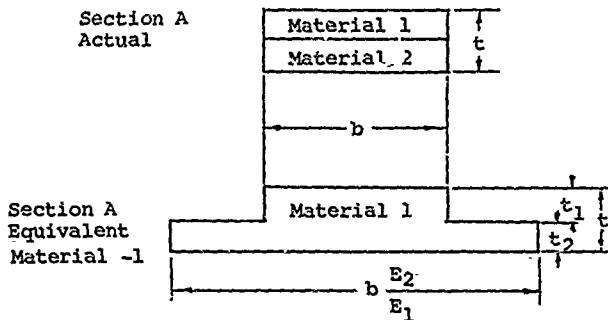
Figure 41.   Equivalent Structural Section.

In the case of bending, the bi-material bar can be replaced by the equivalent single material section as shown in Figure 41 . The equivalent section properties, x_{cg}, I and A, can now be computed in the unusual manner. The area is obviously equal to the value given in Equation (112) and the moment of inertia is

$$I_e = A_1(y_1)^2 + \frac{E_2}{E_1}(A_2)(y_2)^2 + I_1 + \frac{E_2}{E_1} I_2 - A_e(y_{cg})^2 \quad (113)$$

where I_1 & I_2 are the inertia of the original bar elements about their own centroid.

For calculating mass loads the equivalent blade section for the composite is computed in the same manner as indicated for the structural equivalent except that the ratio of material densities is used in place of the moduli ratio.

Applying this principle to the section shown in Figure 40 which is assumed symmetrical, the equivalent structural section with respect to the $x - x$ axis is shown in Figure 42 and the equivalent properties referred to material (1) are

$$A_{estr} = A_1 + \frac{E_2}{E_1} A_2 + \frac{E_3}{E_1} A_3$$

$$I_{e(xx)_{str}} = I_1 + \frac{E_2}{E_1} I_2 + \frac{E_3}{E_1} I_3$$

Similarly, the equivalent mass properties are   (114)

$$A_{e_{mass}} = A_1 + \frac{\delta_2}{\delta_1} A_2 + \frac{\delta_3}{\delta_1} A_3$$

$$I_{e(xx)_{mass}} = I_1 + \frac{\delta_2}{\delta_1} I_2 + \frac{\delta_3}{\delta_1} I_3$$

where δ is the material densities.

With composite sections, therefore, equivalent mass and structural properties are generally computed based upon the foregoing principle of equivalent sections. Usually the propeller section is sufficiently close to symmetrical that the equivalent properties can be closely approximated by relations such as Equations (114).
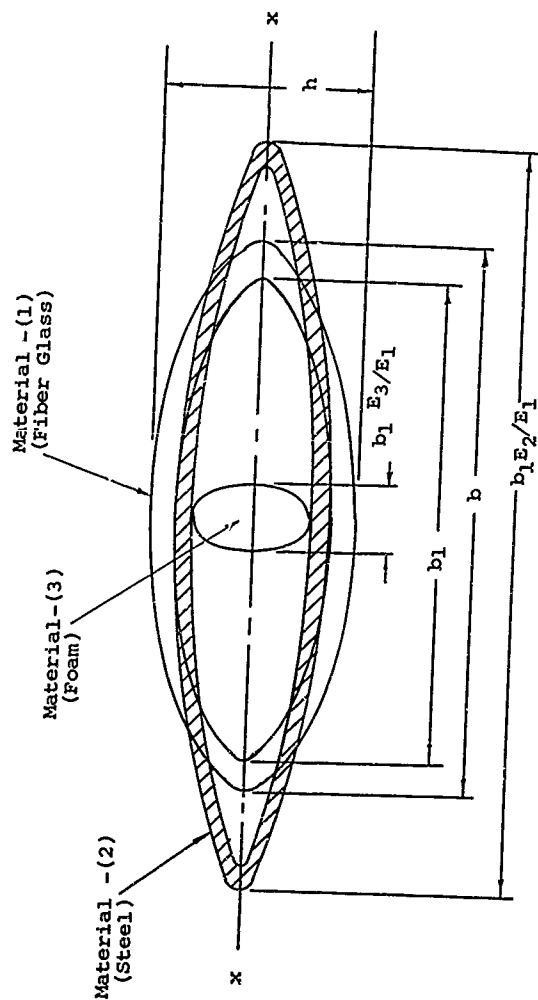
Figure 42. Equivalent Section of Figure 40 – Fiber Glass.

Blade Section Properties - Effect of Twist on Stiffness

The property Z was given in Equation (6) and is defined as a torsional stiffness factor. This section parameter may not be familiar, and some discussion is felt to be pertinent at this time.

The torsional deflection at some station x of a beam can be expressed as

$$\theta_x = \int_0^x \frac{T}{C_T}\, dr \qquad (115)$$

where θ_x = deflection at station x - rad

T = Torque - in.-lb

C_T = Stiffness - in.-lb/rad/in.

dr = differential length - in.

The stiffness, C_T, for an initially twisted beam is made up of two terms:

$$C_T = C + C_1$$

where C is the conventional stiffness, sometimes referred to as JG, J being a property of the cross section and G the shear modulus. The factor J is obtained from mathematical theory or membrane analogy and values are listed in most structural handbooks. For convenience, factors applicable to propeller sections are listed in Table VI.

The factor C_1 is an induced stiffness due to the twist or pitch distribution of the blade and is equal to

$$C_1 = E\left(\frac{d\beta}{dr}\right)^2 \left[Z - \frac{(I_{max})^2}{A} \right] \qquad (116)$$

where E = material modulus of elasticity - lb/in.^{2}

$d\beta/dr$ = rate of twist - rad/in.

$Z = \int x^4\, dA$ - in.^{6}

I_{max} = section Major moment of inertia - in.^{4}

A = section area - in.^{2}

107

TABLE VI. BLADE TORSIONAL STIFFNESS FACTORS

Hollow Section

Equation

$$C = \frac{(2 k b_e h_e t_{avg})^2 \, G}{A}$$

$$C_1 = E \left(\frac{d\beta}{dr}\right)^2 \left[\int x^4 dA - \frac{(I_{max})^2}{A} \right]$$

$$= E \left(\frac{d\beta}{dr}\right)^2 \left[Z - \frac{(I_{max})^2}{A} \right]$$

$$C_T = C + C_1$$

Values of k

0.785 round
elliptical
0.745 series 16 section
0.648 series 65 section

Solid Section

Equation

$$C = k b h^3 G$$

$$C_1 = k b^5 \, E \left(\frac{d\beta}{dr}\right)^2$$

$$C_T = C + C_1$$

Values of k

$\dfrac{\pi}{32}$ round section

$\dfrac{\pi}{16\left(1 + \left(\frac{h}{b}\right)^2\right)}$ elliptical section

.1793 series 16 section
.1492 series 65 section

.0026 series 16 section
.0025 series 65 section

$t_{avg} = (t_c \times t_t)/2$ G = Shear Modulus, lb/in.² E = Modulus of Elasticity, lb/in.²

A = Section Area (in.²) $(d\beta/dr)$ = Rate of pitch change, rad/in.

Note that the value for C for hollow sections is only valid for $(t/h)/$ 0.10 for t/h 0.1 (See Figure 18).

This induced effect with respect to twisted beams has been realized and is discussed in texts on structural design. One of the earlier references with specific application to the propeller blade is in Reference 5. For the sake of completeness, a brief development is given on the following pages.

Consider the blade segment shown in Figure 43 as having a length r. The change in angle between the outboard and inboard station is obviously $(d\beta/dr)\Delta r$. Considering a fiber of material near the leading edge a distance x from the c.g. of the section, the slope of this fiber will be, assuming $d\beta/dr$ to be small,

$$\alpha = \frac{d\beta}{dr}\Delta r \times \frac{1}{\Delta r}$$

$$\alpha = \frac{d\beta}{dr} x \tag{117}$$

If a torque is now applied to the segment, the angle distribution will change by an amount $d\theta/dr$, and the total angle between the inboard and outboard sections will be $d\theta/dr\,\Delta r$, as shown in Figure 43b; $d\theta/dr\,\Delta r$ is assumed to be much smaller than $d\beta/dr\,\Delta r$. In undergoing this twist it is obvious that the fiber at the leading or trailing edges will tend to elongate or compress, depending upon the direction of $d\theta/dr$. This is shown in Figure 43c, from which the expression for this change in length can be shown to be

$$\delta = \frac{d\theta}{dr}\Delta r \times \frac{d\beta}{dr} x$$

$$\delta = x^2 \frac{d\theta}{dr} \frac{d\beta}{dr} \Delta r \tag{118}$$

or the unit elongation will be

$$\frac{d\delta}{dr} = x^2 \frac{d\theta}{dr} \frac{d\beta}{dr} \tag{119}$$

From which the stress and corresponding force will be

$$\sigma = E\, x^2 \frac{d\theta}{dr} \frac{d\beta}{dr}$$

$$F_o = \int E x^2 \frac{d\theta}{dr} \frac{d\beta}{dr}\, dA \tag{120}$$
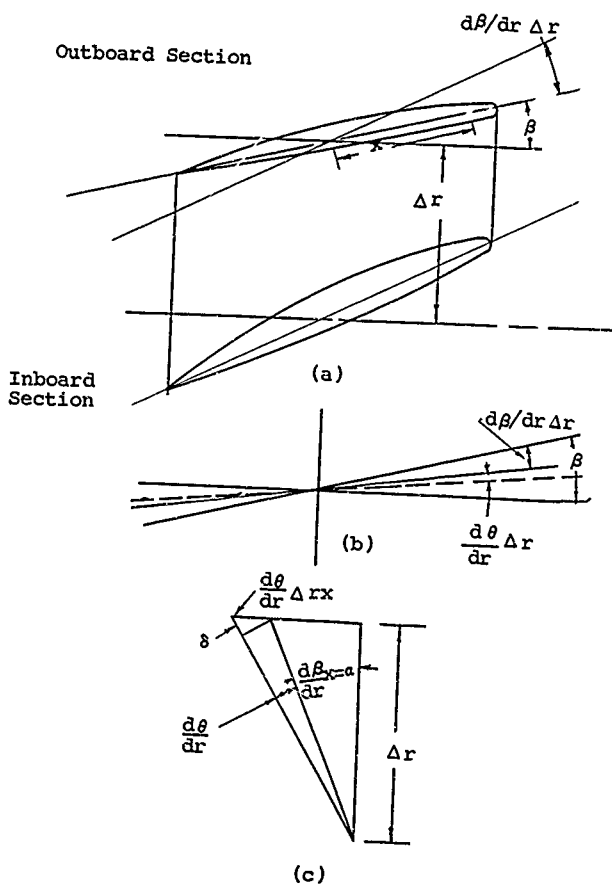
Figure 43.   Blade-Induced Effects.

Equation (120) represents the total undisturbed force on the
section. However, for equilibrium there will be a corresponding
uniformly distributed stress opposite to σ , Equation (119) and
equal to

$$\sigma_O = F_O/A$$

and the total stress will therefore be

$$\sigma = Ex^2 \frac{d\theta}{dr} \frac{d\beta}{dr} - \frac{\int Ex^2 \frac{d\theta}{dr} \frac{d\beta}{dr} dA}{A} \qquad (121)$$

Since $\int x^2 dA = I_{max}$ the above equation can be written

$$\sigma = E \frac{d\theta}{dr} \frac{d\beta}{dr} (x^2 - k^2) \qquad (122)$$

where $k = \sqrt{I_{max}/A}$ = radius of gyration

It is to be noted that Equation (122) represents a longitudi-
nal stress induced by torsion and is independent of any flexural
motion. It is also to be noted that for equilibrium of moments
about the major and minor axes, additional uniform stresses are
imposed but these are relatively small and can be neglected.

Knowing the stress distribution along the section the induced
torque acting on the segment of blade length Δr can be easily
shown to be

$$T = \int \sigma \frac{d\beta}{dr} x^2 \, dA$$

$$T = E \frac{d\theta}{dr} \left(\frac{d\beta}{dr}\right)^2 \int x^2 (x^2 - k^2) \, dA \qquad (123)$$

Now for a straight untwisted section the torque is equal to

$$T = C \frac{d\theta}{dr}$$

To this torque we can add the induced torque due to blade twist
Equation (123) to obtain the total torque on the section.

$$T_T = C \frac{d\theta}{dr} + E \frac{d\theta}{dr} \left(\frac{d\beta}{dr}\right)^2 \int x^2 (x^2 - k^2) dA \qquad (124)$$

111

from which the <u>total</u> torsional spring constant becomes

$$C_T = \frac{T}{d\theta/dr} = C + E\left(\frac{d\beta}{dr}\right)^2 \int x^2(x^2 - k^2) \, dA \quad (125)$$

Note that the integral in the above equation can be put in the form

$$\int x^2(x^2 - k^2)dA = \int x^4 \, dA - k^2 \int x^2 \, dA \qquad (126)$$

$$= \int x^4 \, dA - \frac{I^2_{max}}{A}$$

$$= Z - \frac{I^2_{max}}{A}$$

For a solid section, the integral of (126) can be expressed as

$$\int x^2(x^2 - k^2)dA = Kb^5h \qquad (127)$$

and appropriate values of the constant k are listed in Table VI.   On blades having a wide chord and a relatively low thickness ratio induced effects due to blade twist are significant.

It should be apparent that this same induced influence will also effect the bending or flexural stiffness. Following a similar type of development as given for torsion in the preceding pages, the total flexural stiffness of the blade can be shown as

$$\left[\frac{1}{(EI_{min})}\right]_{total} = \frac{1}{EI_{min}} + \frac{1}{C_T(I_{min})^2}\left(\frac{d\beta}{dr}\right)^2\left(\int x_1^2 \, y_1 \, dA\right)^2 \quad (128)$$

where x_1 & y_1 are the centroidal axes as defined by
          Figure 39.

For a symmetrical section the second term of (128) is equal to zero. Experience so far has shown that the indicated additional flexural stiffness is negligible.

Blade Steady-State Force and Moment Distribution

The basic individual forces and moments and their distributions on the propeller presented previously must be applied to the

propeller and the resultant combined loads developed. As was
implied in previous sections, the major problem · in evaluating
propeller loads is that of determining the final bending moment
on the propeller blade. As previously stated, the predominant
design conditions on the propeller are those associated with
the first-order harmonic aerodynamic excitations and the steady-
state aerodynamic loads. The following sections present a brief
development of the equation by which the resultant blade moments
can be determined.

Blade Steady-State Moments

Figure 44 shows the propeller with the blade in its deflec-
ted position. This blade is subjected to aerodynamic and cen-
trifugal moments in both the y and z directions. First consider
the case of the steady state loading,i.e., the aerodynamic loads
are constant with respect to time. Then the total moment at any
radius x along the x axis is

$$
\left.
\begin{aligned}
M_{y(x)} &= \int_{x}^{R}\int_{s}^{R} f_y \, dx \, dx - \int_{x}^{R} \frac{dy}{dr} \, CF \, ds \\
M_{z(x)} &= \int_{x}^{R}\int_{s}^{R} f_z \, dx \, dx - \int_{x}^{R} \frac{dz}{dx} \, CF \, ds \\
&\qquad\qquad + \omega^2 \int_{x}^{R}\int_{s}^{R} zA \, ds \, ds
\end{aligned}
\right\} \quad (129)
$$

where f_y & f_z are aerodynamic loads – lb/in.

CF = blade centrifugal force – lb

dy/dx, dz/dx = slope of y & z deflection
              curves – in./in.
ρ = material mass density – lb-sec^2/in.

A = section area – in.^{2}

ω = propeller rotational speed – rad/sec

R = tip radius – in.

x = intermedial radius (fixed) – in.

s = intermedial radius (variable) – in.

It will be noted that these moments are with respect to the y
and z axis; however, the blade section data are defined with
respect to the f & e axis, Figure 44.   The following rela-
tions are obtained:

113
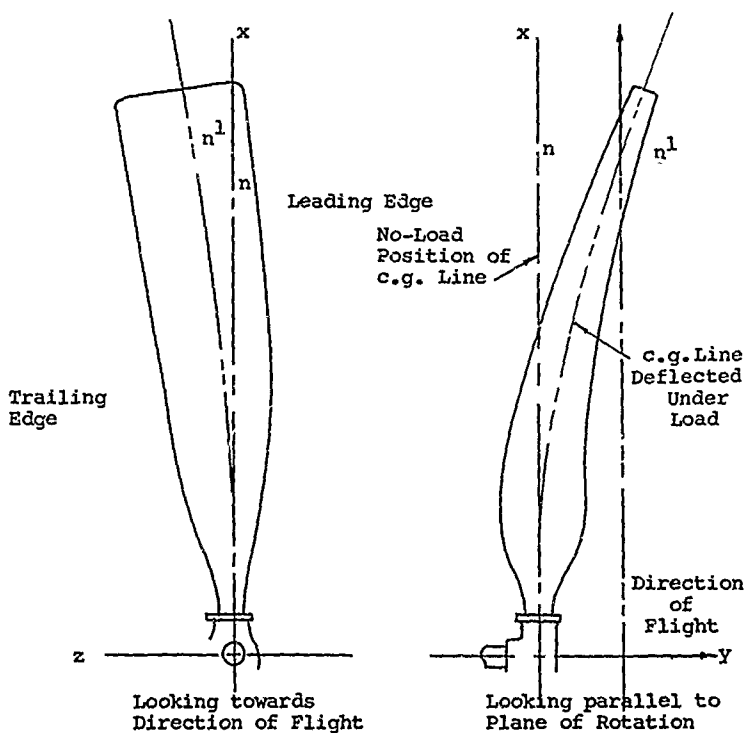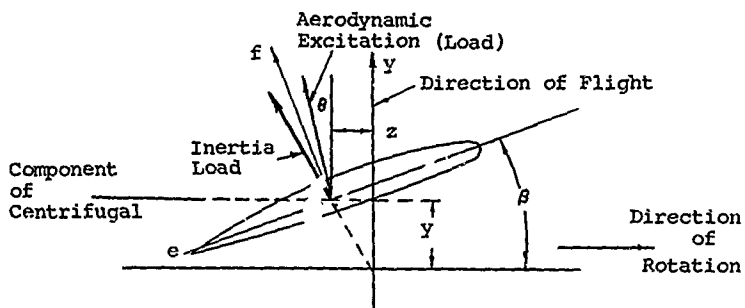
Figure 44. Blade Loads and Deflection.

114

$$(M_y)_x = (M_f)_x \cos \beta_x - (M_e)_x \sin \beta_x$$

$$(M_z)_x = (M_f)_x \sin \beta_x + (M_e)_x \cos \beta_x$$

$$y''_x = f''_x \cos \beta_x - e''_x \sin \beta_x \tag{130}$$

$$z''_x = f''_x \sin \beta_x + e''_x \cos \beta_x$$

$$y''_x = \frac{d^2 y}{dx^2} \; ; \; f''_x = \frac{d^2 f}{dx^2} \; ; \; e''_x = \frac{d^2 e}{dx^2}$$

where β_x = Blade angle at station x

The well known flexure formula with respect to the x, e, f blade axis is

$$(M_f)_x = (EI_f)_x \, f''$$

$$(M_e)_x = (EI_e)_x \, e'' \tag{131}$$

It is to be noted that I_f & I_e correspond to I_{min} and I_{max} in the conventional notation.

By combining (130) & (131) we can write:

$$y''_x = \left(\frac{1}{EI_{yy}}\right)_x (M_y)_x + \left(\frac{1}{EI_{yz}}\right)_x (M_z)_x$$

$$z''_x = \left(\frac{1}{EI_{yz}}\right)_x (M_y)_x + \left(\frac{1}{EI_{zz}}\right)_x (M_z)_x \tag{132}$$

where

$$\left(\frac{1}{EI_{yy}}\right)_x = \frac{\cos^2 \beta_x}{(EI_f)_x} + \frac{\sin^2 \beta_x}{(EI_e)_x}$$

$$\left(\frac{1}{EI_{yz}}\right)_x = \left(\frac{1}{EI_{zy}}\right)_x = \left[\left(\frac{1}{EI_f}\right)_x - \left(\frac{1}{EI_e}\right)_x\right] \sin \beta_x \cos \beta_x$$

$$\left(\frac{1}{EI_{zz}}\right)_x = \left(\frac{\sin^2 \beta_x}{(EI_f)_x}\right) + \frac{\cos^2 \beta_x}{(EI_e)_x}$$

Substituting 132 into 130 the blade moment equations become

$$(M_y)_x = \int_x^R \int_s^R f_y \ dsds - \int_x^R CF \int_0^s y'' \ dsds$$

$$(M_z)_x = \int_x^R \int_s^R f_z \ dsds - \int_x^R CF \int_0^s z'' \ dsds$$

$$+ \ \omega^2 \int_x^R \int_s^R \rho A \left[\int_0^s \int_0^s z'' \ dsds \right] dsds \quad (133)$$

where y'' & z'' are given by Equation (132)

Equations (133) can be transformed into linear integral equations of the second kind. The first term is a known applied load and in the steady-state case being considered they represent the combined aerodynamic and tilt moments as developed in previous sections. We can therefore designate these known applied moments as $(m_y)_x$ and $(m_z)_x$. The second term can be integrated by parts resulting in:

$$\int_x^R CF_x \int_0^s y'' \ dsds = \int_0^R K_2(x,s) \left[\left(\frac{M_y}{EI_{yy}} \right)_s + \left(\frac{M_z}{EI_{yz}} \right)_s \right] \quad (134)$$

$$\int_x^R CF_x \int_0^s z'' \ dsds = \int_0^R K_2(x,s) \ \left(\frac{M_y}{EI_{yz}} \right)_s + \left(\frac{M_z}{EI_{zz}} \right)_s$$

$$K_2(x,s) = D_1 - D_x \qquad 0 \leq s \leq x$$

$$= D_1 - D_s \qquad x \leq s \leq 1$$

$$D_s = \int_0^s (CF)_s \ ds$$

Also the third term in the M_z equation

$$\iint \rho A \left[\int_0^s \int_0^s z'' dx dx \right] dx dx = \int_0^R K_1(xs) \left[\left(\frac{M_y}{EI_{yy}} \right)_s + \left(\frac{M_z}{EI_{yz}} \right)_s \right] ds \quad (135)$$

116

where
$$K_{1(x,s)} = \left[k_{2(x,R)} - k_{2(x,s)} \right]$$

$$k_{2(x,s)} = \int_0^s k_{1(x,s)} \, ds$$

$$k_{1(x,s)} = B_{(x,R)} - B_{(x,x)}; 0 \leq s \leq x$$

$$k_{1(x,s)} = B_{(x,R)} - B_{x,s} \; ; \; x \leq s \leq R$$

$$B_{(x,s,)} = \int_0^s (s - x) \, \rho \, A \, ds$$

Equation (133) can now be written in the form:

$$
(M_y)_x = (m_y)_x + \int_0^R K_2{}_{(x,s)} \left[\left| \frac{M_y}{EI_{yz}} \right|_s + \left(\frac{M_z}{EI_{yz}} \right)_s \right] ds \left.\vphantom{\int_0^R}\right\}
$$
$$
(M_z)_x = (m_z)_x + \int_0^R K_3{}_{(x,s)} \left[\left| \frac{M_y}{EI_{yz}} \right|_s + \left(\frac{M_z}{EI_{yz}} \right)_s \right] ds \left.\vphantom{\int_0^R}\right\} \tag{136}
$$

where
$$K_3{}_{(x,s)} = \omega^2 K_1{}_{(x,s)} - K_2{}_{(x,s)}$$

Equations (136) are readily put into matrix form

$$
(M_y)_x = (m_y)_x + K_5{}_{(x,s)} (M_y)_s + K_6{}_{(x,s)} (M_z)_s \left.\vphantom{\int}\right\}
$$
$$
(M_z)_x = (m_z)_x + K_7{}_{(x,s)} (M_y)_s + K_8{}_{(x,s)} (M_z)_s \left.\vphantom{\int}\right\} \tag{137}
$$

where (M_y), (M_z), m_y & m_z are column matrices, and
K_5, K_6, K_7, and K_8 are square matrices.

$$
K_5{}_{(x,s)} = - \frac{\Delta .}{(EI_{yy})_s} \cdot K_2{}_{(x,s)} \left.\vphantom{\frac{\Delta}{(EI)}}\right\}
$$
$$
K_6{}_{(x,s)} = - \frac{\Delta s}{(EI_{yz})_s} \cdot K_2{}_{(x,s)} \left.\vphantom{\frac{\Delta}{(EI)}}\right\} \tag{137a}
$$

117

$$K_7(x,s) = \frac{\Delta s}{(EI_{yz})_s} \left[\omega^2 K_1(x,s) - K_2(x,s) \right]$$

<div align="right">(137a)Cont'd</div>

$$K_8(x,s) = \frac{\Delta s}{(EI_{zz})_s} \left[\omega^2 K_1(x,s) - K_2(x,s) \right]$$

Equation (137) represents 2n linear simultaneous equations, the number of which is dependent upon the degrees of freedom, n, that are chosen to represent the blade. The solutions of these equations will give the final moments (M_y) and (M_z) along the blade length. A detailed discussion with respect to the solution of these equations is given later in this section.

Blade First-Order Harmonic Moments

Consider the propeller blade shown in Figure 44 as being subjected to a harmonic aerodynamic loading. Assuming that damping is negligible and that the frequency of the applied load is well removed from resonance, then the deflections y and z are in phase with the applied load. The blade is also subjected to an inertia loading as illustrated in Figure 44.

For an assumed harmonic loading of frequency Ω , the following are valid:

$$\left. \begin{aligned} (f_y)_t &= f_y \cos \Omega t \\ (f_z)_t &= f_z \cos \Omega t \\ (y_t) &= y \cos \Omega t \\ (z_t) &= z \cos \Omega t \end{aligned} \right\} \quad (138)$$

where $\quad (f_y)_t$,etc., = variation of f_y ,etc., with respect to time.

At any station x along the radius, the inertia force component in the y direction will be

$$(f_i)_x = -\ddot{y}\, dm$$

Considering the maximum value $(f_i)_x = \Omega^2 y_{(x)}\, \rho\, A_{(x)} dx$ and its moment at a given radius x is

$$(M_{iy})_x = \Omega^2 \int_x^R \int_s^R Y_s\, \rho\, A_s\, ds\, ds \qquad (139)$$

<div align="center">118</div>

Similarly, $(M_{iz})_x = \Omega^2 \int_x^R \int_A^R z_{(s)} \rho A_{(s)}$ ds ds $\qquad$ (140)

For purposes of structural analysis we are only interested in the maximum value of the moment. Therefore, the maximum moment at any given station x along the blade is

$$(M_y)_x = \int_x^R \int_s^R f_{y_s} \text{ ds ds} + \Omega^2 \int_x^R \int_s^R \rho A_s y_s \text{ ds ds}$$
$$- \int_x^R \frac{(d_y)}{(d_x)_s} CF_s \text{ ds}$$

$$(M_z)_x = \int_x^R \int_s^R (f_z)_s \text{ ds ds} + \Omega^2 \int_x^R \int_s^R \rho A_s z_s \text{ ds ds} \Bigg\} (141)$$
$$+ \omega^2 \int_x^R \int_s^R \rho A_s z_s \text{ ds ds}$$
$$- \int_x^R \frac{(d_z)}{(d_x)_s} CF_s \text{ ds}$$

The form of Equation (141) is identical to (133) with the addition of the inertia term. It must be remembered that the terms M, f, y & z represent the maximum amplitude of the harmonic loads and amplitudes. As in the steady case the above equations can be transformed into linear integral equations and can be written in the same form as Equation (136)

$$(M_y)_x = (m_y)_x + \int_0^R K_5(xs) \ (M_y)_s \text{ ds}$$
$$+ \int_0^R K_6(xs) \ (M_z)_s \text{ ds} \Bigg\} (142)$$
$$(M_z)_x = (m_z)_x + \int_0^R K_7(xs) \ (M_y)_s \text{ ds}$$
$$+ \int_0^R K_8(xs) \ (M_y)_s \text{ ds}$$

where for the harmonic case

$$K_{5(xs)} = \frac{1}{(EI_{yy})_s} \left[\Omega^2 K_{1(xs)} - K_{2(xs)} \right]$$

$$K_{6(xs)} = \frac{1}{(EI_{yz})_s} \left[\Omega^2 K_{1(xs)} - K_{2(xs)} \right]$$

$$\text{(142a)}$$

$$K_{7(xs)} = \frac{1}{(EI_{yz})_s} \left[(\omega^2 + \Omega^2) K_{1(xs)} - K_{2(xs)} \right]$$

$$K_{8(xs)} = \frac{1}{(EI_{zz})_s} \left[(\omega^2 + \Omega^2) K_{1(xs)} - K_{2(xs)} \right]$$

The values of $1/EI$, K_1 and K_2 are the same as defined for Equation (137) and the values (m_y) and (m_z) are known applied harmonic loads.

Equation (142) can be put in matrix form similar to Equation (137)

$$M_{y_x} = (m_{y_x}) + K'_5 (M_y)_s + K'_6 M_{z_s}$$

$$M_{z_x} = (m_y)_x + K_7' M_y + K_8 . M_{z_s}$$

$$\left. \right\} \text{(143)}$$

For the specific case of the 1xP excitation (m_y) and (m_z) are known or can be determined by the procedure given on page 63. Further, the forcing function frequency is equal to the rotational frequency, therefore, $\Omega = \omega$. Using these values the solution of the simultaneous equations represented by (143) will give the resultant 1xP blade moments.

It is to be noted that Equation (143) is a general equation. As such it could be used to generate the resultant moments due to any known harmonic blade loading, providing that the assumption of negligible damping and the exciting frequency Ω is well removed from a blade's natural frequency. These assumptions are valid in the case of the 1xP loading.

Retention Flexibility - Effects on Blade Forces and Moments

The previous developments of the moment equation for the steady and 1xP loading conditions have assumed that the propeller blade

is fixed at the retention. However, tests have shown that there can be a significant flexibility due to bending of the hub barrel and deformations within the blade retention components. This effect can be incorporated quite easily into the Equations(134) to (142). Let the zero station or center of rotation of the propeller be the point of fixity and Δx the incremental blade length from this point. The hub retention flexibility is represented by a spring having a stiffness of k(in.-lb/rad). With the applied moment M_0 at Δx the slope of this element will be

$$\theta = \frac{M_0}{EI} \; \Delta x + \frac{M_0}{k} = \frac{M \; \Delta x}{EI_{eq}}$$

The equivalent EI, is therefore,

$$\frac{1}{EI_{eq}} = \frac{1}{EI} + \frac{1}{k \Delta x} \tag{144}$$

Therefore, the retention flexibility can be incorporated into the blade problem by modifying the flexibility factors at the most inboard blade station (assumed point of fixity). The flexibility factors are defind by Equation(132) then become

$$\frac{1}{(EI_{yy})_{eq0}} = \frac{1}{(EI_{yy})_0} + \frac{1}{k_y \Delta x}$$

$$\frac{1}{(EI_{zz})_{eq0}} \quad \frac{1}{(EI_{zz})_0} \quad \frac{1}{k_z \Delta x}$$

where   the subscript 0 refers to the assumed station of fixity generally taken as the center of the retention.

Δx = the incremental blade length

k_y = hub-retention flexibility, y direction in.-lb/rad

k_z = hub-retention flexibility, z direction in.-lb/rad

By introducing the above values of $1/(EI)_{eq0}$ into the $K_5 - K_8$ matrices, hub-retention flexibilities are taken into account. It will be noted that at the point of fixity, the blade is generally round, and therefore $1/(EI_{yz})_0 = 0$.

Values of k_y and k_z are usually difficult to calculate. Experience and experimental data have shown that for the standard type retention, see Figure 5, an average value of k_y is in the order of 35×10^6 in.-lb/rad., and k_z is in the order of

121

65×10^6 in.-lb/rad. The range in k_y has been from 22×10^6 to 44×10^6 in.-lb/rad and the range in k_z is 40×10^6 to 88×10^6 in.-lb/rad. Selecting an appropriate value is a matter of experience, and it is recommended that average values be used as a first approximation, pending experimental verification.

Solution of Blade Moment Equations

To obtain the moment distribution along the blade, it is necessary to solve the 2n simultaneous equation represented by Equations (137) and (143). The classic method for solving a set of simultaneous equations is by using determinants, Cramer's Rule, or Gauss Elimination. However, because of the large number of equations involved in the propeller moment problem, generally in the order of 40, these classic methods are impractical. The most attractive method of solution is the straight iterative procedure. This process is well-known in the solution of engineering problems; it is basically simple and is easily adapted to the automatic punched card calculators. This iterative procedure can be illustrated in shortened form as follows:

Representing the basic matrix equation as $M = b + A \cdot M$, where M & b are column matrices and A is square matrix. To solve this equation, initial values of M are chosen which can be called M_0; then

$$M_1 = b + AM_0$$

$$M_2 = b + AM_1$$

$$\cdot \quad \cdot \quad \cdot$$

$$\cdot \quad \cdot \quad \cdot$$

$$M_n = b + AM_{(n-1)}$$

After n cycles, the values of M_n and M_{n-1} have essentially converged to a common value representing the desired solution.

In adapting this process to the calculation, two basic steps are required: (1) generation of the matrices and (2) the iterative procedure. The solution of the blade moment equations can be programmed on high-speed computers. As a guide to this programming a brief outline of the techniques that have been used is presented on the following pages. It may be readily acknowledged that the basic kernels K_1 and K_2, pages 112 and 113, are always the same for any particular blade design.

Therefore, once they are calculated for a particular blade it is only necessary to start any analysis of the blade from these two kernels.

The K_2 matrix is calculated from the centrifugal force which is rpm related. From practical consideration this matrix is generally calculated for some reference speed, usually 1000 rpm. Then for the given operating speed, ω, of any specific problem it is only necessary to multiply the elements of the basic K_2 matrix, by the ratio $(\omega/\omega_0)^2$ where ω_0 is the reference speed for which the basic K_2 matrix was computed.

The kernels K_1 and K_2 are square matrices. Equations (137c) and (142a) indicate the operations which must be performed on the basic matrices K_1 and K_2 to get K_5, K_6, K_7, and K_8. It is obvious that the resulting matrices are likewise square matrices with n rows and n columns, n being the number of stations chosen to represent the blade. It was previously noted that there are two sets of variables along the same axis, these being x and s. In terms of the square matrices with n rows and columns the variables x and s have the following significance: values of x are constant along the rows of a matrix and values of s are constant along the columns of the matrix. Keeping this in mind, it is obvious that the moment of inertia terms, being functions of x, (I_x), will be multiplied into the square matrices by columns, i.e., they will be constant along the columns.

In the I.B.M. system a standard I.B.M. card represents each element of the matrices involved in a calculation. The cards must have index numbers punched in the last four card columns (card columns 77 to 80). The card columns 77-78 represent the row index, and card columns 79-80 represent the column index. These index numbers are in no way involved in the actual calculations but are only for sorting and identification purposes. However, each card must eventually have various quantities punched into specified card columns so that a calculating machine can read these quantities and calculate the new matrix element. For instance, consider the calculation of the K_7 matrix. There must be n^2 cards used in the calculation, one card for each matrix element. For the 1xP cases, Equation (142a), it is seen that in order to calculate an element of the K_7 matrix the following quantities must be used: a matrix element of both K_1 and K_2, $(\Omega^2 + \omega^2)$, $(\omega/\omega_0)^2$ and a particular $1/EI_{y\dot{z}}$. Therefore, each of these terms must appear on the punched card. The elements of the K_1 and K_2 matrix corresponding to the matrix element of K_7 to be calculated are punched into the card columns 1-7 and 8-12 respectively by means of the I.B.M. reproducer. The reproducer can be wired to reproduce specified quantities from one set of cards to any position on

123

another set of cards. The terms $(w/w_o)^2$ and $(\Omega^2 + w^2)$ are gang-punched into card columns 13-17 and 18-22 respectively of every card of the new matrix by means of the I.B.M. reproducer. It was previously stated that the $1/EI_{yz}$ will be constant along matrix columns; therefore, the cards must be sorted on card columns 79-80 to get the matrix sorted by columns. Then the $1/EI_{yz}$ terms are gang-punched into the card columns 23-20 of the proper matrix columns. The cards can then be inserted and the elements of the K_7 matrix will be calculated and punched into card columns 30-38. The matrices K_5, K_6 and K_8 are calculated in a similar manner.

At the start of the matrix iteration process the matrices K_5, K_6, K_7 and K_8 must be made up with their corresponding matrix elements punched in card columns 10-17 and the proper index numbers punched in card columns 77-80. Since there are at least three or more iterations necessary to obtain good convergence the card spacing of the moment distribution terms to be punched in can be arranged so that three iterations may be performed on one set of cards. The moment distribution for the first iteration are punched into columns 3-8, for the second they are punched into card columns 34-39, and for the third iteration they are punched in columns 55-60. By inspecting the pattern of matrix multiplications (a column matrix times a square matrix) it is to be noted that the first term of the column matrix will always multiply by the first column of elements of the square matrix; the second term of the column matrix will always multiply by the second column elements of the square matrix, etc. Therefore, since it is necessary to have all the terms involved in a particular calculation on one card, the matrix iterations are accomplished by putting the corresponding multiplier and multiplicand elements of the column and row matrices on the same card. This is accomplished by sorting the square matrices by columns and gang-punching the proper moment distribution terms (elements of the column matrix) in the proper matrix columns; i.e., the first term goes with the first column, the second term goes with the second column, etc. After this is accomplished the matrices must be sorted by rows (card columns 77-78), because the actual matrix calculation is a cumulative multiplication process to be performed by rows. By putting the cards through the calculator the desired answers are punched in the last cards of each row in card columns 18-27, 41-50, or 63-72, depending upon whether it is the first, second or third iteration on the set of cards.

The basic procedure is quite simple; however, to obtain a solution by straight iteration, there are rigid requirements that must be met by the system. For purposes of this report it is sufficient to say that in the propeller bending moment problem these requirements are seldom met and convergence solution by straight iteration is either extremely slow or the system is

124

nonconvergent. It is, therefore, necessary to utilize some
technique to alter the system and thereby force a convergent
solution. This situation is not uncommon in physical problems
and the literature contains several procedures which can be
applied. Over the years, several such techniques have been
used. However, the procedure which was eventually adopted is
commonly referred to as the Convergence Polynomial Method.
This procedure was developed by the Curtiss Propeller Division
and a simultaneous development was reported by D.A. Flanders
and G. Shortly, Reference 5.

Basic Blade Stress Calculation

The stress in the propeller blade as in many structural prob-
lems is easily determined once the loads and moments are evalu-
ated. With a known centrifugal force and a solution to the
applicable moment equations, the primary stress is found from
the usual P/A, MC/I relationship. However, it will be remem-
bered that blade section data is evaluated with respect to axes
parallel and perpendicular to the chord line, whereas the mom-
ents obtained from Equations (137)and(143) are in the thrust
and torque directions. Therefore, to calculate bending stress,
the moments must first be resolved to the appropriate axes, or
referring to Figure 44, from the x - y axes to the e - f axes:

$$M_f = M_y \cos\beta + M_z \sin\beta$$
$$M_e = M_z \cos\beta - M_y \sin\beta$$

(146)

At the inboard radius where the section is round, the resultant
moment can be used:

$$M_r = (M_y^2 + M_z^2)^{\frac{1}{2}}$$

(147)

The primary stress at a given point on the blade section at a
given radius x is

$$\sigma_x = \left(\frac{C_F}{A}\right)_x + \frac{M_f}{(I_{min}/f)_x} + \frac{M_e}{(I_{max}/e)}$$

(148)

where   CF = Centrifugal force - lb

M_f & M_e = Moment defined by Equation (146) - in./lb

A = Section area - in.^{2}

I_{min} = Minor moment of inertia - in.^{4}

125

I_{max} = Major moment of inertia – in.^{4}

f = Ordinate along the z axis – in.

e = Ordinate along the e axis – in.

Figure 46 shows a typical blade section and illustrates the distribution of the primary stress for the normal steady-state propeller loading. Conventionally the stress would be computed for several points in order to locate the maximum values. However, over the major length of the blade $I_{max} \gg I_{min}$, and therefore the stress component due to M_z is quite small. For all practical purposes, therefore, the maximum stress under steady-state load is

$$(\sigma_{max})_x = \left(\frac{CF}{A}\right)_x + \frac{M_y}{(I_{min}/C_T)} \tag{149}$$

where C_T is the maximum value of C measured to the thrust side of the section (see Figure 39)

$$\sigma_{CF} = CF/A$$
$$\sigma_y = M_y/(I_{min}/y)$$
$$\sigma = M_z/(I_{max}/z)$$
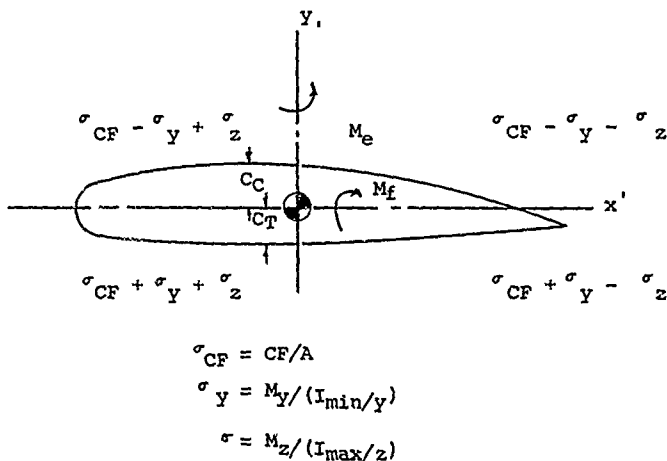
Figure 45.   Blade Stress Distribution.

At the inboard stations where the airfoil fairs into the round shank section, it is necessary to calculate the stress distribution around the section in order to locate the maximum.

For the 1xP blade loading (or other harmonic load condition) the harmonic components are superimposed on a mean or steady-state load. The total stress is therefore in the form

$$\sigma = \left[\frac{CF}{A} + \left(\frac{M_y}{I/C} + \frac{M_z}{I/C} \right) \text{mean} \right] \pm \left(\frac{M_z}{I/C} + \frac{M_z}{I/C} \right) 1xP \quad (150)$$

Now we have two combinations to consider. Neglecting the M_z components for the reason previously stated, the stress on the thrust side of the blade is (See Figure 45)

$$\sigma = \frac{CF}{A} + \frac{M_y}{I/C_T} - \frac{M_y 1xP}{I/C_T} \quad (151)$$

and on the camber side,

$$\sigma = \frac{CF}{A} - \frac{M_y}{I/C_C} + \frac{M_y 1xP}{I/C_C} \quad (152)$$

Usually $C_C > C_T$ and therefore on the thrust side, the stress is a combination of a high steady component with lower vibratory; whereas on the camber side, the steady component is low but combined with a higher harmonic stress. From a fatigue consideration the camber side is generally the more critical. Often as a matter of design conservatism the combination of the maximum thrust face steady stress in conjunction with the higher camber side vibratory stress is used as the fatigue design criteria.

The shear stress due to bending as in most beam problems can be neglected. Likewise, the shear stress due to torsion is generally low and neglected. An exception is in the case of blade flutter, which will be discussed in more detail in a later section.

The shear stress could be important in composite or other bonded designs. In such cases where it is necessary to evaluate shear, the shear due to bending is easily computed by the well-known formula

$$\tau = VQ/Ib \quad (153)$$

127

where τ = shear stress - psi

    Q = area moment - in.^{3}

    V = shear load - lb

    I = moment of inertia - in.^{4}

    b = appropriate section thickness in.

In the case of torsion, the shear stress can be approximated by the following:

solid section

hollow section

$$\tau_x = (Q_x h)G/(C_T)_x \qquad\qquad \tau_x = (Q_x/2At)_x \qquad (153)$$

where Q = torque in.-lb

    $A = kb_e h_e$

The other quantities in the above equations are defined in Table VI.

Referring to Equation (122) it is seen that torsion induces a longitudinal stress; the value as given is

$$\sigma_T = E(d\theta/dr)(d\beta/dr)(x^2 - k^2)$$

Since $d\theta/dr = Q/C_T$,

$$\sigma_T = E \cdot \frac{Q \, d\beta/dr}{(C_T)} (x^2 - k^2) \qquad\qquad (154)$$

Again, under normal circumstances, this component is small and generally neglected. However, on very wide-thin blades, this secondary tension can be significant, particularly in the area of the leading or trailing edge.

Another secondary stress component in hollow blades is generated by the rate of change in blade thickness, and can be particularly important in the inboard area where the blade is fairing more or less rapidly from airfoil to a circular section. Precise developments using elastic theory have been developed but as might be expected, these become cumbersome. Experience has shown that a simple semiempirical approach gives results which are quite adequate for blade design purposes. Consider Figure 46a which shows a longitudinal blade section of unit width along the axis of maximum thickness. For equilibrium the load, p, is expressed by

128

$$p = \frac{d(\sigma t \, dc/dr)}{dr}$$

The values of C_C or C_T are known from the blade section data and can be plotted, and the value of dc/dr for each plate is easily obtained graphically. σ can be taken as the basic stress, Equation (149).   The product ($\sigma t \, dc/dr$) is then plotted and the slope or, p, obtained graphically at each station along the blade. It is now assumed that the thrust or camber plates are subject to a uniform load equal to the appropriate value of p. Experience has shown that the maximum stress is in the internal fillets, points a and e, Figure 46b

(σ_c, σ_t = Nominal Stress)   (a) Longitudinal Section

(b) Section A
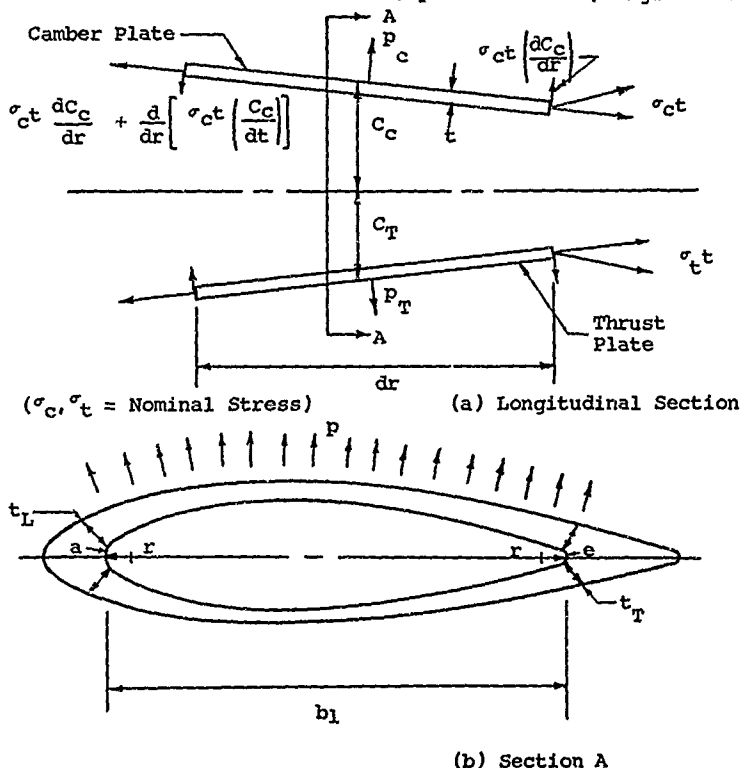
Figure 46.   Blade Transverse Stress.

The nominal stress can be taken as

$$\sigma_a = \frac{.31 \; p(b_1)^2}{(t_L)^2} \quad , \quad \sigma_e = \frac{.31 \; p(b_1)^2}{(t_T)^2} \tag{155}$$

where the values of (t_L), (t_T) and (b_1) are defined in Figure 47b.

There is obviously a stress concentration factor due to the internal fillet which must be considered, and Figure 47 gives a stress concentration curve that has been used in fillet design.

It was mentioned earlier that in the design of hollow metal blades the plate thickness must include some allowance for the cleanup or repair of service damage or inadvertent manufacturing thin spots. The results of these reworks, in effect, increase the local stress. Again from experience, a relatively simple relationship has been developed to estimate stress in such areas. Figure 48 shows a section of a blade plate which has been reworked to blend out a damaged area. An amount of Δt inches of material has been removed in the process. The basic stress in the center of such a thin spot is

$$\sigma_b = \sigma_n (1 + CR) \tag{156}$$

σ_n is the nominal stress in the unaffected plate area, Equations (151), (152)

$$R = 3t \, \Delta t / (t - \Delta t)^2$$

$$C = \text{factor given in Figure 49}$$

An appropriate stress concentration factor must be applied when applicable, and the experience derived values are also given in Figure 49. With a known blade material and working stresses, Equation (156) can be used to establish the safe maximum amount of material, Δt, that can be removed for rework of blade damage.

Propeller Vibration and Resonant Frequencies

Propeller vibrations are classified in the following manner:

1. Forced or resonant vibrations or flutter (flutter is treated separately in a later section)

2. The frequency and source of the external exciting
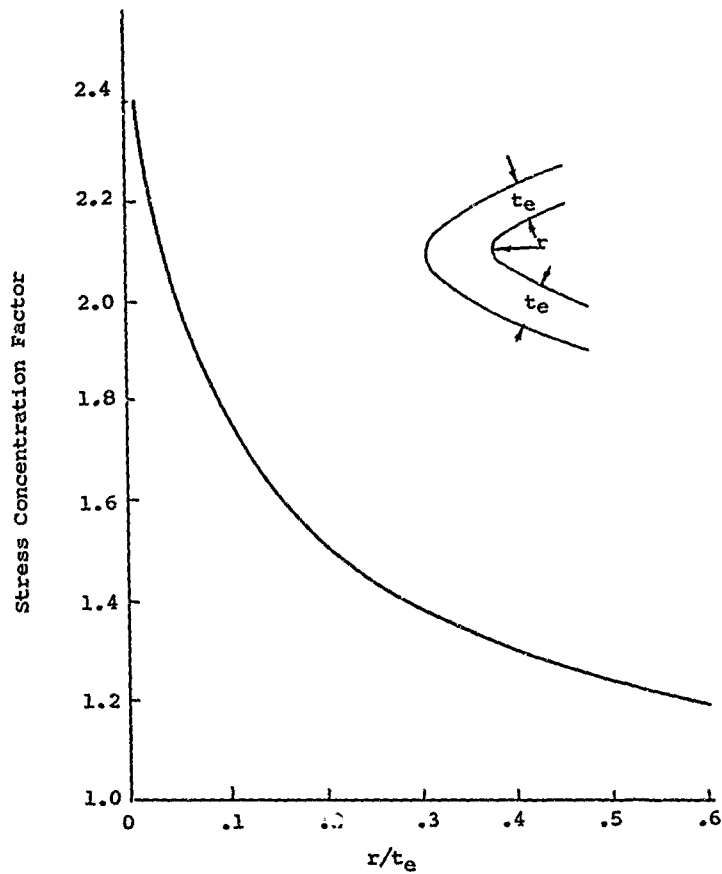
Figure 47. Fillet Stress Concentration Factor.

131

Damage Area

Section A
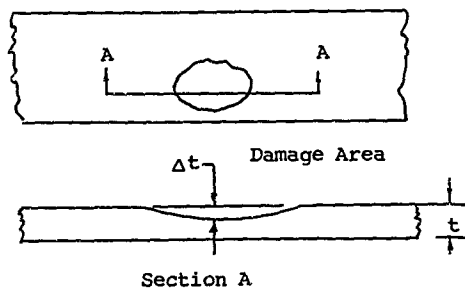
Figure 48. Blade Damage - Rework.

% Material Removed - $\frac{\Delta t}{t}$(100)
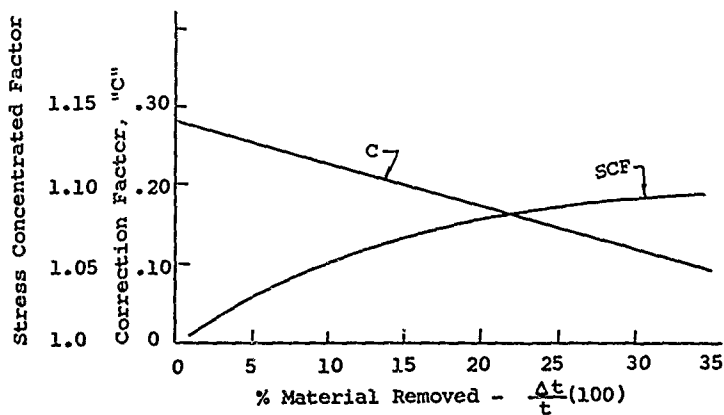
Figure 49. Factors Related to Plate Grind-Outs.

132

force or acceleration causing the vibration

3. The mode of vibration

Propeller vibrations arise from three main sources: First, periodic aerodynamic lift and drag forces on the airfoil sections of the blades can occur when the direction or magnitude of the air velocity with respect to the airfoil sections changes as the propeller rotates. Such nonuniformity of the air flowing into the propeller disc arises when the airflow is disturbed by the proximity of the wing or fuselage of the airplane to the propeller, or when the propeller axis is not coincident with the direction of flight. Such vibrations are called aerodynamic vibrations. The most predominate of such excitations is the 1xP which has been previously discussed.

Secondly, propeller vibrations will be created when the airplane motion deviates from a uniform, straight path. The most common of this type is the gyroscopic vibration induced by curvilinear motion of the airplane, see page 95.

With particular reference to reciprocating engine installations, a large number of propeller vibrations come from the engine. These vibrations can be induced in several ways. If the output torque of the engine is not uniform but varies periodically with time, the propeller blade will be subjected to periodic angular accelerations causing periodic inertia forces on the blades, which in turn excite vibrations of the blades. Another type of propeller vibration arises when the reaction of the engine on its mounts causes a whirling motion of the engine. This whirling motion occurs also on the blades if the propeller is rigidly connected to the engine, and it causes a periodic acceleration of the blade masses in the fore-aft direction. The frequency of this vibration can be shown to be equal to the engine whirling speed minus the propeller speed if the engine is whirling in the direction of the propeller rotation, and to the engine whirling speed plus the propeller speed if the two rotations are in opposite directions. On turbine installations engine excitation has been found to be virtually nonexistent.

Blade Resonance

The flexural vibrations of propeller blades are somewhat similar to those of an untwisted, cantilever beam. Propeller vibrations are influenced to a certain extent by the blade twist and the flexibility of the hub, engine and its mounting. Furthermore, the centrifugal force on the blade mass not only causes an increase in the natural frequencies over their values for the stationary cases, but also changes the shape of the deflection of the mode. In what follows, it will be assumed

133

that the propeller is mounted on a very rigid shaft. This condition is referred to as a fixed-root condition.

The lowest natural or principal mode of a fixed-root propeller blade is very similar to that of an untwisted cantilever. In this mode, commonly called the fundamental "flapping" mode, the blade sections are bending essentially about their minor principal axes, i.e., about lines which are roughly parallel to the section chords. In metal propellers the natural frequency of this mode usually occurs between 10 to 35 cycles per second. The higher frequency is characteristic of smaller diameters, and the value usually is smaller for the larger size propeller blades.

The next lowest mode of the propeller blades is generally not the same as the second mode of the normal cantilever, but is a mode where the outer sections are moving simultaneously in a flapping and edgewise direction, and where the blade is bending mainly in the narrow planform portion next to the hub.

Since the blade motion consists of a relatively large amount of edgewise or chordwise motion this mode is sometimes called the fundamental "edgewise" mode. It is, of course, the true second flexural mode of the blade. This mode is a particularly dangerous mode in propellers because the aerodynamic damping of an airfoil moving in the direction of the wind is very low. The next, or third, flexural mode of a blade is similar to the second mode of the untwisted cantilever. If the blade is unusually flexible in the flatwise direction, and is rigid in the edgewise direction on that portion next to the hub, the second mode of the blade will be this latter mode while the "edgewise" mode will occur at a higher frequency. The higher flexural modes of a blade are similar to the higher modes of the untwisted cantilever.

In addition to the flexural modes, propeller blades have torsional modes wherein the blade sections are twisting about some central line. In metal blades the natural frequency of the fundamental torsional mode is generally quite high with respect to that of the fundamental. The frequency ranges from 50 to 200 cps for metal blades having diameters from 10 to 20 feet. A knowledge of this frequency is important in determining the flutter characteristics of the blade. Resonance of the fundamental torsional mode is rarely excited in propellers although it may be excited in dual rotation propellers because the frequency of excitation arising from blade passage of the two propellers may be sufficiently high to cause resonance. Torsional modes higher than the fundamental are unimportant because of their high frequencies.

Complex plate vibrations can occur in hollow steel blades where no central supporting core or rib is employed in the designs.

134

The natural frequencies of these plate modes are usually high
and can only be excited by the higher harmonics of the engine
excitation.

Flexural Resonance

When a propeller is rotating, the blade elements are subjected
to centrifugal forces which introduce lateral restoring forces
when the sections bend out of the common plane of rotation.
That is, there is an additional stiffness imparted to a rota-
ting blade as compared to the stationary blade. There is a
simple well-known relation which approximates the natural
frequency of a rotating blade in terms of the frequency of the
same mode when the blade is stationary. This relation is given
by

$$f^2 = f_0^2 + c^2 n \qquad (157)$$

where the quantity, f, is the natural frequency of the rotating
blade and the frequency, f_0, is the static natural frequency.
The quantity, n, is the rotational speed of the propeller (in
revolutions per second if the frequency is in terms of cycles
per second). The quantity, C, is called the Southwell constant.
In the past the Southwell constant has been calculated on the
basis that the blade was untwisted and set at zero blade angle.
On this basis the following average values have been found for
metal propellers:

Mode	Flatwise Southwell Constant
Fundamental Flapping	1.5 to 2.0
Fundamental Edgewise	.8 to 1.0
Second Flapping	4 to 6
Third Flapping	10 to 12

When the blade is turned out of the plane of rotation there is
less centrifugal stiffening so that the natural frequency does
not increase so rapidly with increasing rpm. This means that
the Southwell constant decreases with increasing blade angle
for the normal flexural modes. An approximate relation for
fundamental rotating frequency is

$$f^2 = f_0^2 + (C - \sin^2 \beta_e) n^2 \qquad (158)$$

135

where β_e = an effective blade angle usually taken to be the angle at the 40 percent radius.

            C = flatwise Southwell constant for zero blade angle.

Use of the foregoing equations presupposes that the fundamental nonrotating frequencies are available, and these can be approximated with fair accuracy by assuming a flat untwisted beam and applying conventional beam theory. However, accurate calculation of blade resonances for the case of the fixed-root system can be made by utilizing a modified form of the basic Equation (142).

If the forcing function, m, is eliminated from that equation the equation then represents the case of a free vibration. Further, assume that the frequency of vibration is some ordered multiple of the rotational speed, or $\Omega = p\omega$, where as previously defined

$$\Omega = \text{frequency of vibration - rad/sec}$$

$$\omega = \text{propeller rotational speed - rad/sec}$$

Substituting this relationship into (142a), the values of K_5 - K_8 become

$$K_5 = \frac{\Omega^2}{EI_{yy}} \left[K_{1(xs)} - \frac{1}{p^2 \omega_o^2} K_{2(xs)} \right]$$

$$K_6 = \frac{\Omega^2}{EI_{yz}} \left[K_{1(xs)} - \frac{1}{p^2 \omega_o^2} K_2 \right]$$

$$K_7 = \frac{\Omega^2}{EI_{yz}} \left[(1 + \frac{1}{p^2}) K_1 - \frac{1}{p^2 \omega_o^2} K_2 \right] \Bigg\} \quad (159)$$

$$K_8 = \frac{\Omega^2}{EI_{zz}} \left[(1 + \frac{1}{p^2}) K_1 - \frac{1}{p^2 \omega_o^2} K_2 \right]$$

In these equations, ω_o is the rotational speed for which the basic K_2 matrix was originally evaluated.

Using the form given in (159), the resulting matrix equation corresponding to (143) for the case of the free vibration thus becomes

136

$$M_y = \Omega^2 \left[K'_5 \bar{M}_y - K'_6 \bar{M}_z \right]$$

$$M_z = \Omega^2 \left[K'_7 \bar{M} - K'_8 \bar{M}_z \right] \qquad (160)$$

$\bar{M}_y$ and $\bar{M}_z$ are assumed moment distributions. In principle, the calculation of the frequency is a common vibration problem, an initial normalized distribution of M_y and M_z are assumed and the iterative procedure is used to obtain a convergence on the shape of the moment distributions. With the converged shape, the frequency is easily calculated.

The procedure, therefore, is to take a series of values of p, p = 1, 2, 3, 4, and generate the K'5 - K'8 matrices per Equation (159). Then using Equation (160), evaluate the frequencies for the various blade modes. For the case of the static natural, zero rotational speed, Equations (159) and (160) can also be used. In this case the rotational effects are minimized by assuming a high value of "p" equal to 100,000.

In practice, the solution to Equation (160) can become quite involved due to convergence, particularly at the higher modes. As previously discussed some technique is required to force convergence of the desired modal shape. Again the "convergence polynomial method" has been found to be a very effective method for solving the free vibration case, see Reference 6.

Once the frequencies for the various modes have been found and noting that for any given value of p, $\omega = \Omega/p$, the frequencies can be plotted in the form such as given in Figure 50.

Plotted on the same graph are straight lines representing the frequencies of the exciting forces. The aerodynamic excitation can be resolved into its harmonic components with frequencies equal to or multiples of the propeller speed. For example, the line 1xP represents the exciting frequency of the first harmonic component of the aerodynamic excitation, so that if the propeller is turning at 10 rps this exciting component will have a frequency of 10 cycles per second. Generally, the 1xP line does not intersect any of the natural frequency curves of the blade in the operating range of the engine, and 1xP blade resonance will not occur.

The second harmonic frequency is shown by the 2xP line. This line, Figure 50, crosses both the fundamental and edgewise frequency lines, and the intersection points define a blade resonance. The strength of this excitation can be significant particularly during ground crosswind operation. The general design practice is to maintain a margin of at least 100 rpm between operating and resonant speeds. However, it is essential

137
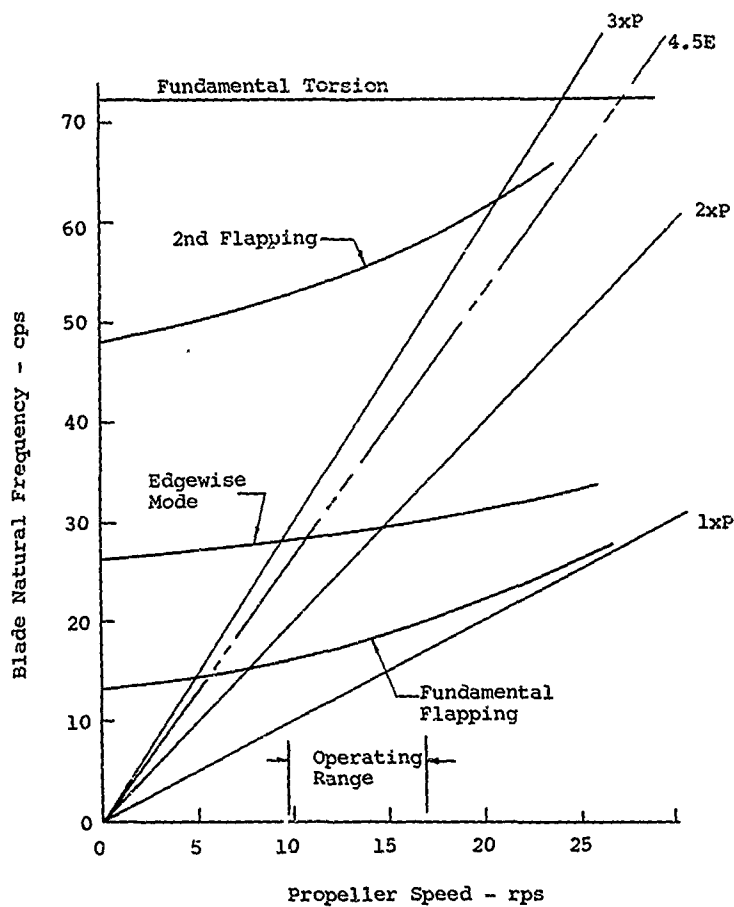
Figure 50. Blade Frequency Diagram.

to verify these resonances and blade response characteristics during propeller vibration surveys. Restrictions on rpm and crosswind operation have been required on several installations. The fundamental resonance is usually of concern with respect to ground idle speed, also a rapid acceleration through resonance may be required. The 2xP edgewise frequency for large metal blades is in the 25-50 cps range, 750-1500 rpm, and therefore in the normal takeoff or flight rpm range.

Likewise, the propeller may be subjected to periodic forces or torque arising from the engine. For reciprocating internal combustion engines, the frequencies of the harmonic components of the engine torque are multiples of half engine speed. In the nine cylinder radial engine a strong component is generally the firing frequency of $4\frac{1}{2}$ x E (four and a half times the engine speed). A line showing this frequency has been included in Figure 50.

By drawing all the expected exciting frequencies on the curve of natural frequencies, the possible resonances to be expected can be readily determined. However, in the actual installation certain resonances may not cause excessive stresses, and may be acceptable. 3xP resonances, Figure 50, are usually this type.

The foregoing natural frequencies are based on the assumption that the propeller is attached to a very rigid shaft. These frequencies are later corrected for the motion of the hub. However, it is suggested that in calculating resonant frequencies, the flexibility factors, Equation (132), include a correction for retention flexibility, page 120. It is also to be noted that these flexibility factors are functions of the blade angle setting. The resonant frequencies will therefore vary to some degree with pitch, and it is often desirable to evaluate the frequencies for two or three blade angle settings typical of the propeller operating range; for example, static takeoff, cruise, etc.

Reactionless and Nonreactionless Shaft Modes

When a propeller is subjected to periodic aerodynamic forces, there may or may not be a resultant periodic force or moment on the engine. Whether these forces and moments occur depends on the "order" of the aerodynamic excitation and the number of blades in the propeller. When the mode is such that there is no resulting periodic moment or force on the shaft the mode is said to be "reactionless". If a moment or force exists on the shaft, the mode is said to be nonreactionless. When the mode is not reactionless, the propeller vibration depends on the stiffness and mass characteristics of the engine and its mounts.

139

To show the effect of an aerodynamically excited vibration on
the engine, consider the vibratory lift on a blade element at
radius, r (see Figure 52) . Assume that the propeller con-
sists of B number of blades and is rotating at a speed equal
to the value, ω , in radians per second. Suppose that this
exciting force has a frequency equal to n times the rotational
speed of the propeller. The quantity, n, is called the "pro-
peller order" of the excitation. If the maximum periodic lift
on the element is denoted by ΔL_0 then the periodic lift is

$$\Delta L = \Delta L_0 \cos (n\omega)t \tag{161}$$

if it is so "phased" that it is a maximum in the zero angle
position (vertical) of blade number one (see Figure 51)
The quantity, ωt, is the positional angle of the first blade,
and this angle is increased by the angle between blades for
each succeeding blade. Therefore, the simultaneous lifts on
similar elements of the blades are as follows:

$$\left.\begin{aligned}
\Delta L_1 &= \Delta L_0 \cos n \cot \omega \\
\Delta L_2 &= \Delta L_0 \cos n \left(\omega t + \frac{2\pi}{B} \right) \\
\Delta L_3 &= \Delta L_0 \cos n \left(\omega t + 2\frac{2\pi}{B} \right) \\
\Delta L_B &= \Delta L_0 \cos n \left(\omega t + \frac{B-1}{B} 2\pi \right)
\end{aligned}\right\} \tag{162}$$

The resulting periodic <u>thrust</u> force is obtained by multiplying
these lift forces by the cosine of the wind angle at that sta-
tion, and adding. In summing these elementary periodic thrust
forces, the following general relation in trigonometric series
is employed:

$$\sum_{i=0}^{B-1} \cos n \left(\omega t + i \frac{2\pi}{B} \right) = 0 \qquad \text{for } n \neq KB$$
$$= B \cos n\omega t \qquad \text{for } n = KB$$
$$K = 0,1,2,3\cdots$$

$$\sum_{i=0}^{B-1} \sin n \left(\omega t + i \frac{2\pi}{B} \right) = 0 \qquad \text{for } n \neq KB$$
$$= B \sin n\omega t \qquad \text{for } n = KB$$
$$K = 0,1,2,3\cdots$$

On summing up the periodic thrust forces by making use of the
above relations, the following formula for the periodic thrust
on the propeller shaft is derived:

140
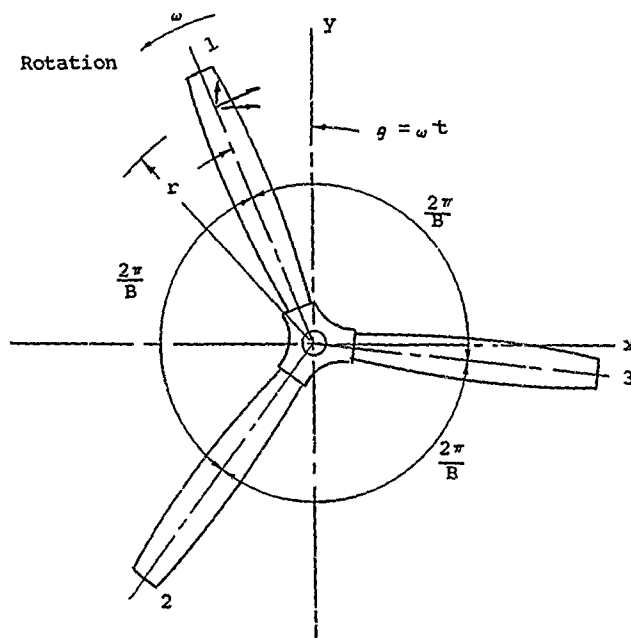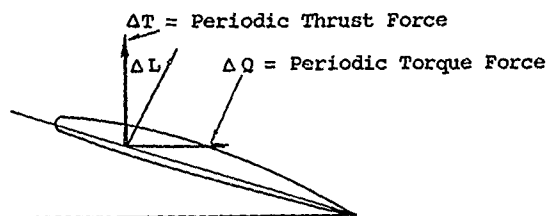
Figure 51. Resolution of Periodic Torque Force.

141

$$\Delta T = B \, \Delta T_O \cos n\omega t \qquad \text{for } n = KB$$

$$= 0 \qquad \text{for } n \neq KB \qquad\qquad K = 0,1,2,3\cdots\cdots \quad (163)$$

T_O = maximum periodic thrust of an element of one blade

The above relation proves that if there is an aerodynamic ex-
citation of order, n, there will be a periodic thrust on the
propeller shaft only if the order is zero or a multiple of the
number of blades in the propeller. For example, a 6xP excita-
tion will cause a periodic thrust on the shaft of a 3-bladed
propeller. When the order is not a multiple of the number of
blades there is no resulting periodic thrust on the shaft.
This same relation is also valid for the periodic torque on the
propeller shaft.

The bending moments induced by the periodic lift forces about
axes fixed to the engine (XOY in Figure 51) are calculated
by multiplying the thrust forces on the similar elements by
their arms to these respective axes. Assuming an excitation
of the nth order in the form used previously, the elementary
bending moment about the x-axis is

$$\Delta M_x = r\,\Delta T_O \cos n\omega t \cos \omega t + \cos n(\omega t + \tfrac{2\pi}{B})\cos(\omega t + \tfrac{2\pi}{B}) +$$

$$\cos n(\omega t + 2\tfrac{2\pi}{B}) \cos (\omega t + 2\tfrac{2\pi}{B}) + \cdots\cdots$$

$$\cos n(\omega t + \tfrac{B-1}{B}\, 2\pi) \cos (\omega t + \tfrac{B-1}{B}\, 2\pi)$$

$$(164)$$

The moment about the y-axis is the same except that the second
cosine in each term is replaced by the sine. The summation
may be performed by employing the following trigonometric
identity:

$$\sum_{i=0}^{B=1} \cos n(\omega t + i\tfrac{2\pi}{B}) \begin{cases} \sin(\omega t + i\tfrac{2\pi}{B}) \\ \cos(\omega t + i\tfrac{2\pi}{B}) \end{cases} = 0 \qquad \text{when } (n \overset{+}{\_} 1) \quad KB$$

$$K = 0,1,2,3 \cdots$$

$$= \begin{cases} \dfrac{B}{2} \sin (n+1)\omega t \\[2mm] \dfrac{B}{2} \cos (n+1)\omega t \end{cases} \qquad \begin{array}{l} \text{when } (n+1) = KB \\[1mm] K = 0,1,2,3 \cdots \end{array}$$

142

$$= \begin{Bmatrix} -\dfrac{B}{2} \sin (n-1)\ t \\[2mm] \dfrac{B}{2} \cos (n-1)\ t \end{Bmatrix} \qquad \begin{aligned} &\text{when } (n-1) = KB \\ &K = 0,1,2,3 \ldots \end{aligned}$$

where the two identities have been written in condensed form for convenience. The bending moments then become

$$
\left.
\begin{aligned}
\Delta M_x &= 0 && \text{when}\quad n \pm 1 \ \neq KB \\[2mm]
&= \frac{r\,\Delta T_o B}{2} \cos (n+1)\,\omega t && \text{when } n+1 = KB \\[2mm]
&= \frac{r\,\Delta T_o B}{2} \cos (n-1)\,\omega t && \text{when } n-1 = KB
\end{aligned}
\right\} \quad K = 0,1,2,3
$$

$$
\left.
\begin{aligned}
\Delta M_y &= 0 && \text{when } n \pm 1 \ \neq KB \\[2mm]
&= \frac{r\,\Delta T_o B}{2} \sin (n+1)\,\omega t && \text{when } n+1 = KB \\[2mm]
&= \frac{-\,r\,\Delta T_o B}{2} \sin (n-1)\,\omega t && \text{when } n-1 = KB
\end{aligned}
\right\} \quad K = 0,1,2,3
$$

$$\tag{165}$$

From this it is seen that the resulting moments about axes fixed to the engine do not exist when the order of excitation, plus or minus one, is not a multiple (or zero) of the number of blades. If the order, plus or minus one, is zero, or a multiple of the number of blades there is a vibratory moment on the engine whose frequency is the order of the blade vibration plus one or minus one. This moment causes a forward whirl of the engine if its frequency is $(n-1)$ times the propeller speed, and a reverse whirl of the engine if its frequency is $(n+1)$ times the propeller speed.

The table below has been prepared to show whether there is a vibratory moment or thrust on the engine for various numbers of blades in the propeller, and various propeller orders of vibration. A zero in the table indicates no vibratory force or moment while the symbol X indicates that there is a force or moment. In preparing this table, the rules developed in the previous paragraphs have been employed.

CONDITION FOR VIBRATORY MOMENTS OR THRUSTS

ON THE ENGINE WHEN THE PROPELLER IS SUBJECTED TO

AERODYNAMICALLY EXCITED VIBRATIONS

$B =$	2		3		4		5		6	
n	T_n	M_n	T_n	M_n	T_n	M_n	T_n	M_n	T_n	M_n
1	0	X	0	X(s)	0	X(s)	0	X(s)	0	X(s)
2	X	0	0	X	0	0	0	0	0	0
3	0	X	X	0	0	X	0	0	0	0
4	X	0	0	X	X	0	0	X	0	0
5	0	X	0	X	0	X	X	0	0	X
6	X	0	X	0	0	0	0	X	X	0
7	0	X	0	X	0	X	0	0	0	X
8	X	0	0	X	X	0	0	0	0	0
9	0	X	X	0	0	X	0	X	0	0
10	X	0	0	X	0	0	X	0	0	0
11	0	X	0	X	0	X	0	X	0	X
12	X	0	X	0	X	0	0	0	X	0

(s) steady bending moments
X = net force or moment
0 = no net force or moment

At one time, it was thought that reactionless modes which in-
volve no motions of the hub, crankshaft or engine might lead
to serious resonant stresses as any beneficial damping of the
crankshaft-engine nacelle system would be absent. However,
actual tests failed to disclose any abnormally high resonant
stresses incurred at a reactionless resonance. Reactionless
modes are tabulated in the following:

REACTIONLESS MODES

B	PROPELLER ORDER =N
2	None
3	None
4	2, 6, 10, etc.
5	2, 3, 7, 8, 12, 13, etc.
6	2, 3, 4, 8, 9, 10, 14, 15, 16, etc.

From this table it is seen that there are no reactionless
modes for the two and three-blades, but there are increasing
numbers of this mode for increasing number of blades in a
propeller.

The natural frequencies shown in Figure 50 were derived on
the basis that the propeller shaft was very rigid, both tor-
sionally and flexurally. Actually the propeller shaft, engine
and its mounts have certain flexibilities and masses, and when
the aerodynamically excited propeller vibration is not re-
actionless, the engine system will also vibrate, and the com-
plete vibration system must be considered in determining
resonances and responses. For this reason, the natural fre-
quencies (Figure 50) assuming perfect fixity of the hub are
approximate and must be modified depending on the mode and the
inertia and stiffness of the engine and its supports. Generally
the frequency of a propeller vibration is sufficiently above
the natural frequencies of the lower natural modes of the
engine motion, so that the "coupling" between the engine and
the propeller does not change the fixed-root propeller modes
by any large amount.

Past experience on conventional propeller installations has
shown that in the case of a periodic shaft reaction, a reduc-
tion in the calculated "fixed-root" blade frequencies, Figure
50, in the order of 10% can be expected.

It should also be noted that the previous discussion con-
sidered only the predominate thrust and moment reactions. The
periodic torque force can also produce a shaft reaction, nor-
mal force, in the x and/or y directions (Figure 51). Con-
sidering the drag force at r and resolving into its x or y
components, it is easily shown that the resultant shaft normal
force will follow the same pattern as given for the shaft
moment.

Torsional Resonance

As previously noted, it is possible to excite the fundamental
torsional resonance of a propeller blade. However, in practice
this mode of vibration is seldom, if ever, encountered except
in a condition of flutter. Propeller flutter is discussed in
more detail in a later section, and it is the purpose of this
section to present a method for computing the fundamental
torsional frequency.

The basic equation for the torsional stiffness of the blade
beam is given as

$$C_T \frac{d\theta}{dr} = Q \qquad (166)$$

where C_T is the torsional stiffness Equation (125) $\frac{\text{in.-lb}}{\text{rad/in.}}$

$\frac{d\theta}{dr}$ = rate of change of the torsional twist - rad/in.

Ω = applied torque - in.-lb

From the above equation, the angle of twist at any radius x can be written

$$\theta_x = \int_0^x (1/c_T)_s \, \Omega_s \, ds \qquad (167)$$

where   x = a given fixed radius

s = variable radius along the blade

Assuming a unit torque to be applied at some station j, the deflection at x is

$$\theta_x = \int_0^j (1/c_T)_s \, ds \qquad o \le j \le x$$

$$\theta_x = \int_0^x (1/c_T)_s \, ds \qquad x \le j \le R \qquad (168)$$

where R is the tip radius

Defining the above integral as $\int 1/c_T \, ds =\,^a(xj)$, the torsional deflection can be written

$$\theta_x =\,^a(xj) \, \Delta \, M_j$$

where ΔM is the incremental torque applied at station j.

In matrix form the above equation becomes

$$\left| \theta_x \right| \quad = \quad \left| a_{(ij)} \right| \quad x \quad \left| \Delta M_j \right| \qquad (169)$$

$\left| \theta_x \right|$ and $\left| M_j \right|$ are column matrices and $\,^a_{xj}$

is a square matrix, the elements of which are defined by Equation (168). For the free torsional vibration,

$$\Delta M_j = \quad \omega_o^2 \, \theta_j \, (I_p)_j \qquad (170)$$

146

where ω_0 = torsional frequency - rad/sec

θ_j = amplitude - rad

$(Ip)_j$ = incremental polar moment of inertia in.-lb

(Ip) = $(I_{max} + I_{min})\Delta s$

I_{max}, I_{min} = blade section moments of inertia - in.[4]

ρ = material density - slugs/in.[3]

s = incremental radius - in.

Substituting in Equation (169)

$$\left| \theta_x \right| = \left| \omega_o^2 \right| \left| a_{xj} \right| \times \left| I_{pj} \right| \times \left| \theta_j \right| \qquad (171)$$

Multiplying $\left| \theta_{xj} \right|$ by $\left| (I_p)_j \right|$ the above becomes

$$\left| \theta_x \right| = \omega_o^2 \left| A_{1_{(xj)}} \right| \left| \theta_j \right| \qquad (172)$$

The solution to (172) is obtained by assuming a normalized modal shape θ_j and solving for θ_x. The iterative process is continued until convergence and the frequency is then computed. Convergence of Equation (172) is straightforward and generally quite rapid. In order to present a complete spectrum of the fundamental frequencies, the fundamental torsional frequencies are generally plotted on the frequency curves as shown in Figure 50.

There are some points of interest in respect to the torsional resonance.

1. The effect of centrifugal force tends to increase the frequency. This effect is very small and neglected.

2. The value of C_T is a function of the blade pitch distribution, see Equation (125). Torsional amplitudes therefore change the pitch and can significantly influence the stiffness; the system is actually nonlinear. The nonlinear effect is generally

> very small and neglected. However, on
> very flexible blades, a decrease in
> frequency will be noted at large ampli-
> tudes of torsional vibration.

The higher torsional modes have been of no concern with re-
spect to propeller blades. If such modes and frequencies are
desired, they can be obtained by application of the principle
of the Holtzer method, which is available in any good text on
vibration theory.

Engine Vibrations

Engine excited vibrations are of particular concern only on
reciprocating engine installations. Due to the inherent
smoothness of the turbine, there has been little or no problem
of propeller vibration attributable to the engine on a turbo-
prop installation.

The engine can excite propeller vibrations in several different
ways. A reciprocating engine never delivers to the propeller
shaft a perfectly uniform torque; for this reason, the pro-
peller blades receive a periodic angular acceleration which
induces vibratory inertia forces on the blades in the torque-
wise direction. Since the blades are turned and twisted out
of the plane of rotation, these inertia forces will have com-
ponents perpendicular to the weakest axes of the sections and
will cause flexural vibrations of the blades.

When the engine is out of balance the center of the hub may
move back and forth in a lateral direction and such motion is
independent of the torsion and is associated with the displace-
ment of the center of gravity of the engine. Lateral motions
can also arise from the torque forces on the crankshaft which
cause it to deform laterally if it is flexible, or to have a
lateral motion if there is a clearance in the shaft bearings.

Furthermore, the engine or propeller shaft may be caused to
whirl from periodic forces on the engine or shaft. Whirling
motions of the propeller shaft can also arise if there is a
radial clearance in the propeller shaft bearings. In a whirl-
ing motion, the propeller shaft is rotating about some fixed
point along its centerline and as a result there are induced
on the blades periodic inertia forces in the direction of
flight. The origin of such periodic forces will be discussed
in a later paragraph.

The variation of torque supplied by the engine to the propeller
shaft is caused primarily by the variation of the gas pressures
on each piston. In reciprocating engines of the four-stroke
cycle type, the variation in gas torque will repeat itself

148

every two revolutions of the crankshaft. In other words, if the engine is revolving at "n" revolutions per second, there will be n/2 complete cycles of torque variations per second. For this reason, the variations in torque caused by the gas pressures can be expanded as a Fourier's series of sines and cosines of angles which are equal to multiples of half engine speed times the time. The greatest harmonic component is generally the "firing" frequency which is equal to half the number of cylinders times the rotational speed of the engine. For example, a nine-cylinder radial engine whose crankshaft is rotating at 30 revolutions per second will have a firing frequency equal to 9/2 times 30 or 135 cycles per second. If this particular harmonic frequency is coincidental with a natural frequency of the whole propeller system (including the engine), a resonance will occur. In most aircraft engines dynamic balancers or absorbers are installed on the crankshaft to eliminate or minimize this vibration having "firing" frequency.

Since a torque variation causes the same torquewise inertia on each blade at the same time, each blade will vibrate in phase with the others and since the blades are turned out of the plane of rotation, the blades will also have a fore and aft motion, and there will be a periodic thrust force on the propeller shaft.

As indicated previously, the resonance of the system will depend not only on the vibration characteristics of the propeller but also on the torsional characteristics of the propeller shaft and the engine crankshaft. A method of solving this particular problem is to consider that the propeller shaft is severed next to the propeller. A periodic sinusoidal moment is applied to the propeller at this severed section, and the response of the angular motion at this section is calculated for various frequencies at a fixed rotational speed of the propeller. A graph is made of this moment to its angular response against frequency, noting that only symmetrical modes can occur. This ratio of maximum torque to maximum angle is the mechanical impedance. For any frequency, Ω, of the exciting torque the exciting blade moment is

$$(m_z)_x = \Omega^2 \theta \int_x^R \int_s^R \rho A s\, ds\, ds \qquad (173)$$

$$m_y = 0$$

where θ is the maximum shaft angle - rad

149

A = blade section area - in.^{2}

s = blade radius (variable) - in.

x = blade radius (fixed) - in.

ρ = mass density of blade material - slugs/in.^{3}

These values can be substituted in Equation (136) and the values of M_Z obtained. The impedance is then:

$$\text{Impedance} = \frac{M \text{ shaft}}{\theta} = \frac{\text{No blades} \quad (M_Z)_O}{\theta} \qquad (174)$$

The term $(M_Z)_O$ is the value of M_Z calculated for the zero radius. Since the equations are linear in θ, the initial value of θ is immaterial. If the value of θ is doubled the moments are doubled and M/θ is unchanged. Similarly, a calculation is made of the torsional response of the engine crankshaft system by applying a vibratory moment at the same severed section of the propeller shaft. A typical plot of these responses is shown in Figure 52. When the moment-angle ratio of these two systems are equal, a resonance of the system will occur. For example, in Figure 52 resonances are to be expected at points A. The asymptotic values of frequencies for the propeller curves are the natural frequencies of the fixed-root propeller, while the frequencies where the curves cross the horizontal axis represent the natural frequencies of the propeller having complete torquewise freedom.

Vibrations Caused by Whirls

An analysis of the gas pressures on the pistons shows that there are periodic reaction forces on the crankshaft bearings. In single-row radial engines, the vertical and horizontal reactions have a frequency equal to a multiple of half the number of cylinders, plus or minus unity, times the engine speed that is, this frequency is equal to

$$\text{Frequency of whirl} = (k \frac{N}{2} \pm 1) \, \omega_e \qquad (175)$$

where k = integer
         N = number of cylinders
         ω_e = rotational speed of the crankshaft

These periodic reaction forces on the engine bearing will cause a whirling motion of the propeller shaft at a frequency given by the above equation.

A whirling motion imparted to the propeller shaft will cause

150
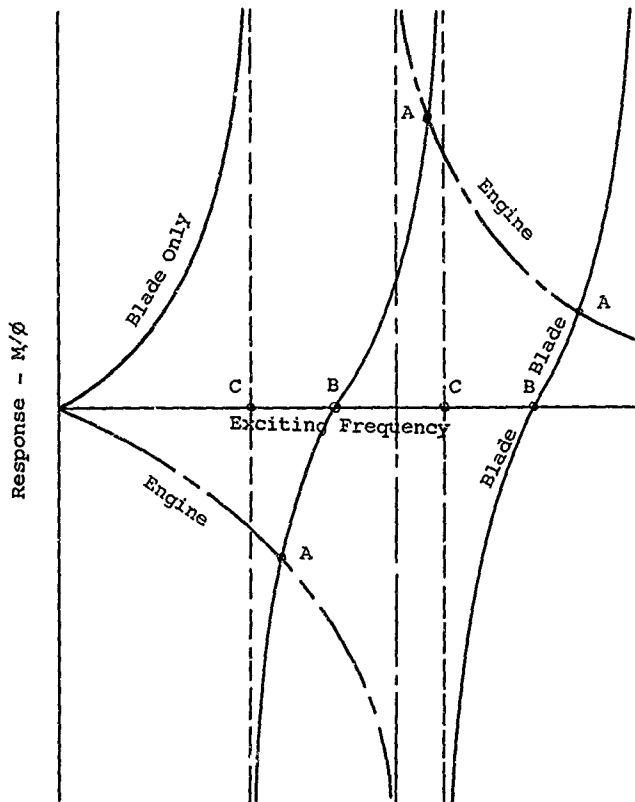
1. Fixed-root natural blade frequency occurs at C, while the free-root value is at points B.

2. Resonance of the complete system occurs at A.

Figure 52. Resonance of the Complete System.

151

the blade elements to receive a periodic acceleration in the
direction of flight as will be shown by the following explan-
ation.

Referring to Figure 53, it will be assumed that the blade
centerline is represented by the line OP, and the centerline
of the propeller shaft by OQ. Furthermore, it will be assumed
that the shaft line is "whirling" about the OZ axis at a speed
Ω, in radians per second, and that the propeller blade is
rotating about this axis at a speed, ω. Suppose that at some
instance in the whirl the shaft centerline, the axis OZ about
which it whirls, and the blade radii all lie in the same plane
(XOZ plane in Figure 53). Time will be referenced to this
position. At a small time interval later, a point, P, on the
blade will rotate through an angle to point, P_1, and a point,
Q, on the shaft will rotate through the angle α to a point Q_1
(see Figure 53). At this instance the point, P_1, will have
a downward velocity (opposite to the OZ direction) because the
velocity of the point, Q_1, in the OY_1 direction is pivoting the
line MP_1 about the line OX. This velocity component is found
by geometry to be

$$- \frac{d}{dt} (\overline{SQ_1}) \frac{\overline{MP_1}}{l} = - \frac{d}{dt} (\alpha l \sin \Omega t) \frac{r \sin \omega t}{l}$$

$$= - \alpha \Omega r \cos \Omega t \sin \omega t \qquad (176)$$

In a like manner, point P_1, has an upward velocity in the posi-
tive direction of OZ because point Q_1 is approaching the line
OY_1 and causing the line P_1N to pivot about line OY. This
velocity component is

$$- \frac{d}{dt} (\overline{TQ_1}) \frac{\overline{NP_1}}{l} = - \frac{d}{dt} (\alpha l \cos \Omega t) \frac{r \cos \omega t}{l}$$

$$= \alpha \Omega r \sin \Omega t \cos \omega t \qquad (177)$$

The vertical velocity of point P_1 is the sum of these two com-
ponents, or

$$- \alpha \Omega r (\sin \omega t \cos \Omega t - \cos \omega t \sin \Omega t)$$

$$= - \alpha \Omega r \sin (\omega - \Omega) t \qquad (178)$$

The vertical acceleration is obtained by taking the time
derivative of this last expression, or
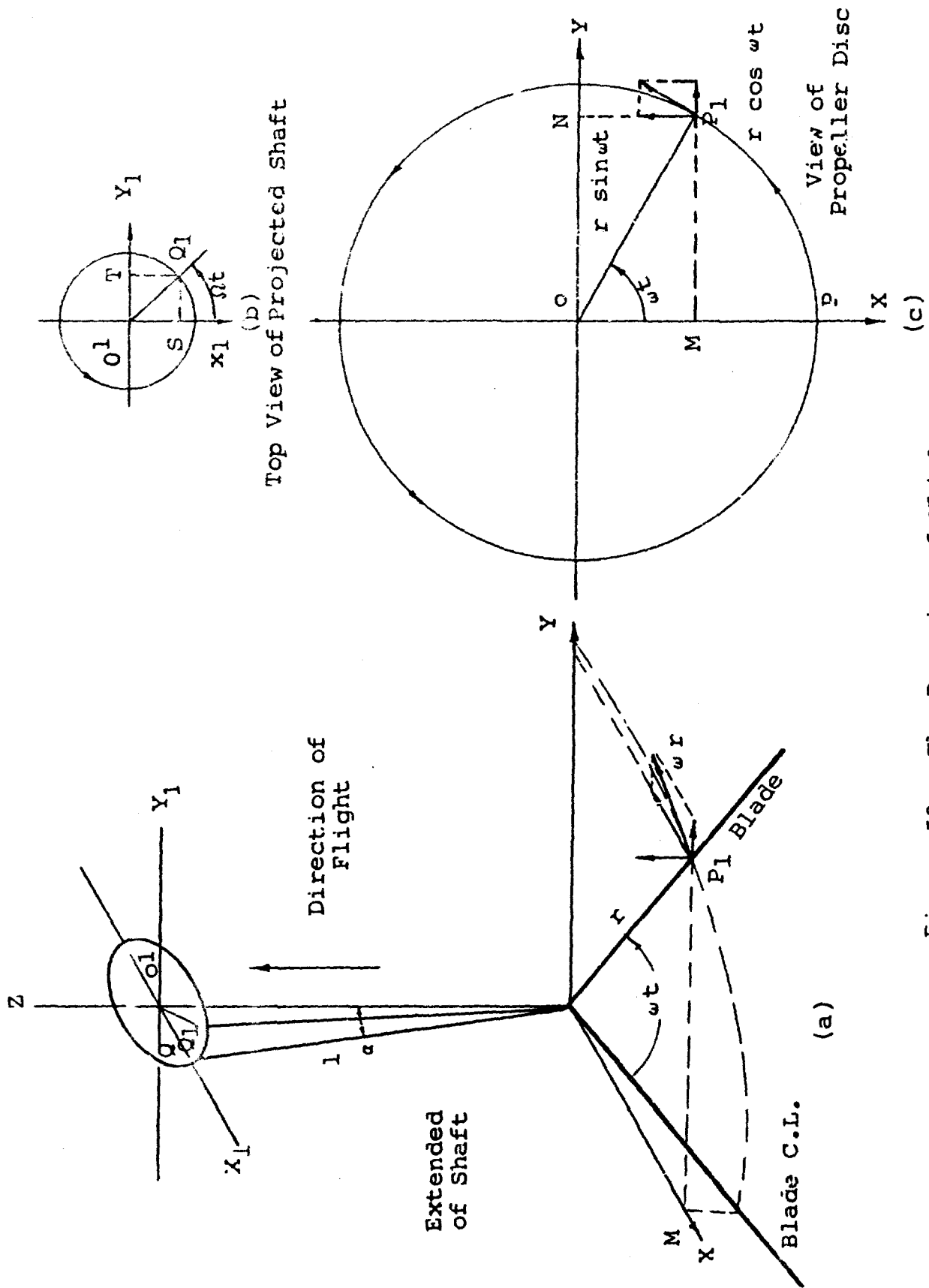
Figure 53. The Dynamics of Whirls.

Acceleration due to change in

$$\text{Vertical Velocity} = -\,\alpha r \Omega (\omega - \Omega) \cos\,(\omega - \Omega) \qquad (179)$$

There is still another acceleration in the vertical direction (i.e., along the OZ axis) which has, heretofore, been neglected and which arises from the change in the direction of the tangent speed, ωr, of the point P_1. After a very short time, the velocity components, $r \cos \omega t$ and $r \sin \omega t$ will change directions and have velocity differences (vectorial) in the vertical direction. The angle which the component, $r \cos \omega t$, makes with the horizontal plane is

$$\frac{\overline{SQ_1}}{l} = \frac{\alpha l \sin \Omega t}{l} = \alpha \sin \Omega t$$

Therefore, there arises a vertical acceleration equal to:

$$-(\omega r \cos \omega t)\frac{d}{dt}(\alpha \sin \Omega t) = -\alpha \Omega r \cos \omega t \cos \Omega t \qquad (180)$$

A similar acceleration component arises from the change in direction of the other component, and this is obtained by finding the rate of angle change of the line NP_1. This gives for this component:

$$(r \sin \omega t)\frac{d}{dt}(\alpha \cos \Omega t) = -\alpha \Omega r \sin \omega t \sin \Omega t \qquad (181)$$

Adding these two together with the former results leads to the following total vertical acceleration:

$$\text{Total acceleration} = -\alpha \Omega r \cos(\omega - \Omega)t$$

$$-\alpha \Omega r(\omega - \Omega)\cos\,(\omega - \Omega)t$$

$$= \alpha r(-2\omega\Omega + \Omega^2)\cos(\omega - \Omega)t \qquad (183)$$

This means that when the engine whirl is in the direction of the propeller rotation, the blades will receive a periodic fore and aft inertia force having a frequency equal to the propeller speed minus the whirling speed. This frequency is given by

$$\text{Blade Vibration Frequency} = \pm\,(\omega - \Omega)$$

where ω = rotation speed of the propeller

Ω = speed of whirl

On substituting the possible whirling frequencies of a radial engine Eq. (175), the above formula takes the following form:

$$\text{Blade Frequency} = \pm \left[\omega - (k\frac{N}{2} + 1)\omega e \right] \qquad (184)$$

$$= \pm \left[(k \frac{N}{2} - 1) - g.r \right] \omega_e$$

where g.r. = gear ratio

If the engine whirl is opposite to the propeller rotation, the last sign in the above is reversed.

To show what whirling frequencies are possible in a typical radial installation, consider a nine-cylinder radial engine having a gear ratio equal to 7/16. On substituting this information into the above relations, the following blade vibration frequencies are found to be:

$$(4\tfrac{1}{2} \pm 1 \mp 7/16)_e = (51/16 \text{ or } 3\,15/16) \times \text{Engine Speed}$$

These frequencies are generally high and are of primary concern with respect to plate resonance on hollow type blades.

Blade Flutter

The propeller blade like any aerodynamic surface can experience aeroelastic instability commonly referred to as flutter. The well-known classical flutter involves the coupling of the flexural and torsional modes and is important in the design of wings and control surfaces.

Theoretically, this classical type of instability can occur on the propeller blade. On conventional metal blades, the critical speeds have been well outside the propeller operating range, and therefore classical flutter has not been of concern to the propeller designer. In the early developmental stages of light-weight composite blades, there was some concern that this type of instability may develop, but to date there have been no incidents. However, if the more recent trend with respect to V/STOL propellers toward large diameter/narrow chord blades continues, the propeller designers will have to become familiar with the techniques of mass balance, etc., common to rotor blade design.

155

There are two types of flutter peculiar to the propeller. These are commonly called stall flutter and wake flutter. These phenomena are discussed in the following sections.

Stall Flutter

As the name implies, stall flutter is a self-sustained vibration that occurs when the propeller airfoil sections are operating at or near their stall angle of attack. Therefore, it generally occurs at the static takeoff condition where the propeller is generating maximum thrust, and consequently operating at high angles of attack. Once the aircraft experiences forward motion, the vibration dies out quite rapidly as the result of the forward velocity vector reducing the angle of attack.

It is a well known fact that when an airfoil is subjected to an oscillating angle of attack, C_L vs. α will be essentially linear up to the stall angle. In the proximity of stall, there is an abrupt loss of lift followed by a reestablishment of the basic lift curve. This is illustrated in Figure 54. Such a lift variation results in a hysteresis or energy that must be absorbed by the system. It is this action that is believed to be responsible for stall flutter. Obviously, the above simple description is complicated by frequency of oscillation, amplitude, etc.

The action manifests itself on the propeller blade as a self-sustained vibration involving the fundamental torsion mode. Fortunately this type of flutter does not increase in amplitude with time, but rather for a given angle and velocity the amplitude of vibration is constant. Because of this fact, some degree of flutter can be tolerated; the limits being set by the allowable working stress of the blade material. Figure 55 illustrates a stall flutter stress profile. Two types of stress gradient have been observed and these are shown in Figure 56 . The reason for these distinct characteristics is not exactly known, but it is believed to be due to material damping.

The primary problem of the designer is to predict the flutter boundary. Theoretical aeroelastic developments have been attempted, but as may be expected, these become quite involved and require a knowledge of the characteristics of airfoils oscillating in the vicinity of the stall angles; therefore, the use of such theories has not been too successful. However, a relatively simple semiempirical procedure has been developed which has proven very successful in predicting the flutter boundary of propeller blades. The details of the development would be superfluous for this report. It is sufficient to say that a considerable amount of blade flutter data
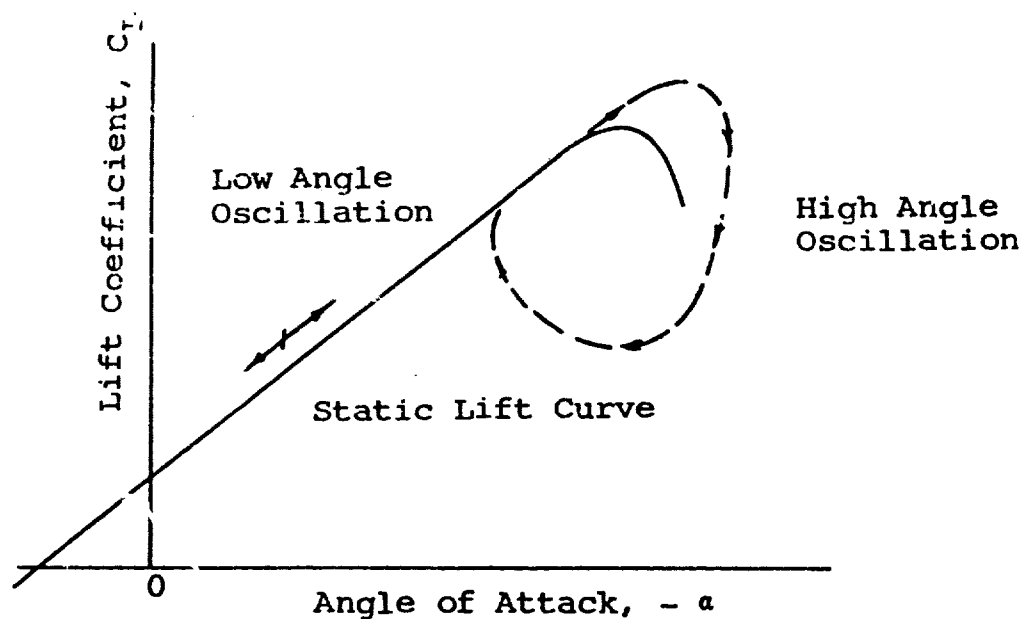
Figure 54. Lift Variation - Oscillating Airfoil.
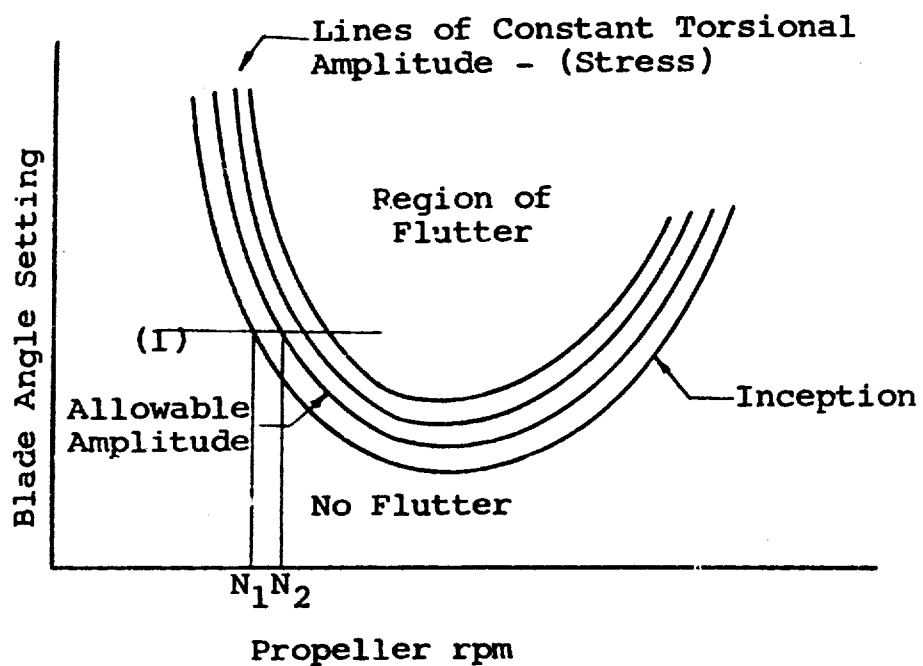
Figure 55. Flutter Boundary.

157
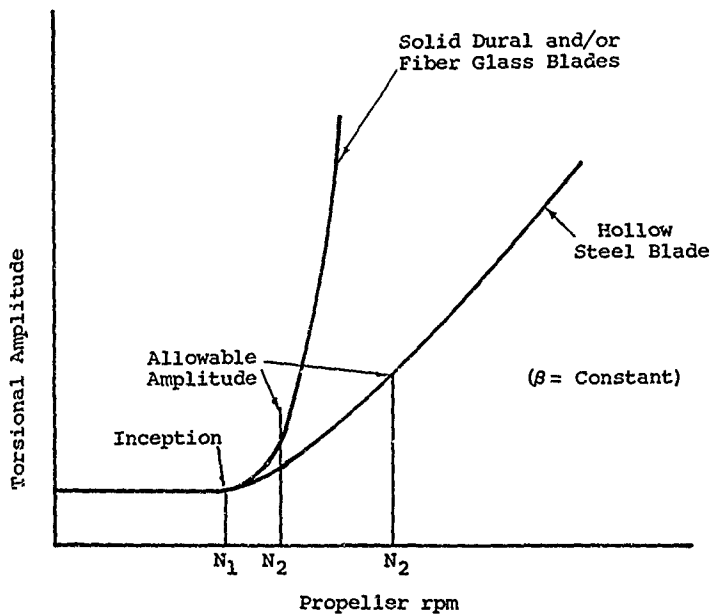
Figure 56. Variation of Flutter Amplitude
With rpm at a Blade Angle.

158

obtained from tests, including data generously supplied by a British propeller manufacturer, was analyzed. The results of that analysis are given in Figure 57 . This curve shows the variation of the angle of attack of a reference blade section at the 0.80 radius, with a parameter called λ for the onset of flutter. The angle of attack is measured with respect to the zero lift line, and λ is the reciprocal of the reduced frequency modified to include the Prandtl-Glauert correction

$$\lambda = \frac{(V) \sqrt{1 - M^2}}{(b \omega)_{.8}} \qquad (185)$$

where $\dfrac{(b \omega)}{(V)}_{.8}$ = reduced frequency at the 0.80 blade radius

b = semichord - ft

ω = fundamental torsional frequency - rad/sec

V = blade section velocity at 0.80 radius - ft/sec

M = Mach number corresponding to V

The value of λ_o, Figure 57, represents the value of λ below which stall flutter is not possible, or in a more practical sense the value of λ below which the flutter amplitude is an acceptable level. The value of λ_o is in the order of 1.0. The abcissa of Figure 57 shows a range of values and the significance of this will become clear later in the discussion. Figure 57 defines the flutter boundary of a propeller blade, but in terms of rather impractical parameters. The curve must be converted into more conventional terms of velocity and blade angle for a given propeller design.

For a given design, the chord at the 0.8 radius is known and the fundamental frequency is easily computed (Equation (172)). It has previously been noted that stall flutter is only of concern at the static takeoff condition; therefore the velocity is for all practical purposes equal to the rotational speed:

$$V = 2 \pi \frac{N}{60} r$$

where N = propeller rpm

r = radius to the 0.80 radius - ft

By using the above and Equation (185), the value of λ is

159

$$\lambda = \left(\frac{V\sqrt{1 - M^2}}{b\omega} \right)$$
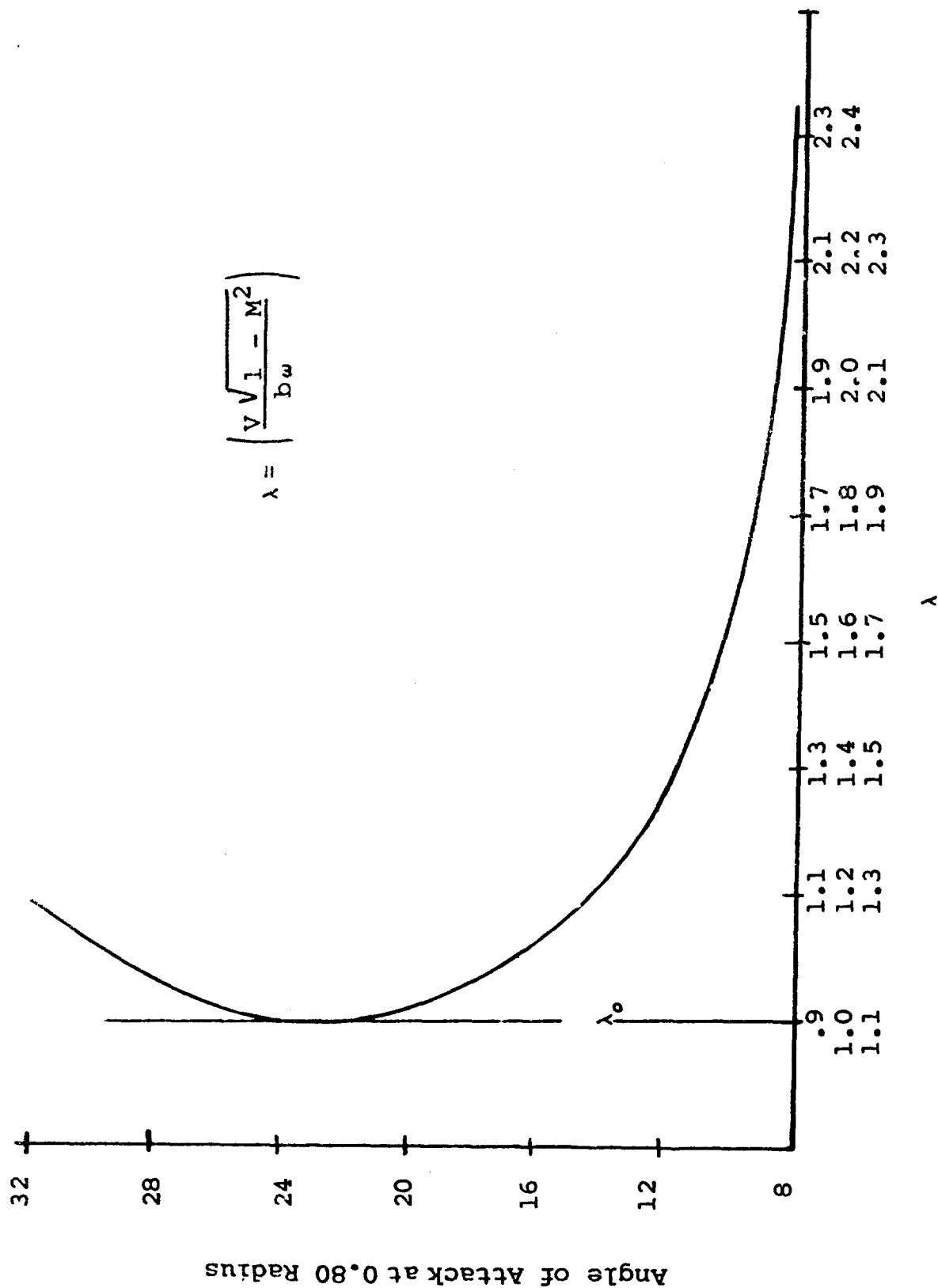
Figure 57. Angle of Stall Versus λ.

160

calculated for a series of rpm values and the flutter angle of
attack is read from Figure 57 . To establish the range of rpm
values, a value of λ_0 can be chosen and noting that $M = V/a$
where "a" is the speed of sound (1120 ft/sec at S.L.), Equation
(185) can be solved for the velocity corresponding to λ_0.
Solving for velocity results in a quadratic, and therefore
there are two values of velocity for a given λ_0.
The values of speed as a function of λ and (bω) are given in
Figure 58. Therefore, for a given value of λ_0 the end values
of the rpm range to be considered can be established by con-
verting the velocities read from Figure 58 to rpm. It will
also be noted that Equation (185) gives a maximum value of λ
at $M = 0.707$, and from Figure 57 the minimum angle of attack
will occur at the λ values corresponding to $M = .707$.

Experience has shown that in conventional hollow steel blades,
a value of $\lambda_0 = 1.1$ can be used to establish a practical
flutter speed range, and in solid aluminum and fiber glass com-
posite blades, limited test data indicates the practical
value of λ_0 is 1.0. It will be further noted that by choos-
ing a series of values of λ_0, a family of curves will result
similar to the constant stress curves illustrated in Figure
55.

The angle of attack read from Figure 57 represents the angle
of attack at the 0.80 radius of a standardized airfoil section
and this must be converted to the more practical corresponding
blade angle setting at the 0.80 radius.

The standard section had a static stall angle of 8.2 degrees,
and it is first necessary to correct for the stall angle of
the actual propeller section.

$$\alpha = \alpha_s + \Delta\alpha$$

$$\Delta\alpha = \alpha stall - 8.2^{\circ} \qquad (186)$$

where α = angle of attack of the 0.80 radius propeller
                section measured to the zero lift line - deg

α_s = angle of attack per Figure 57 - deg

$\alpha stall$ = static stall angle of the propeller 0.80 radius
                section - deg

The value of $\alpha stall$ should be obtained from appropriate air-
foil data. A good approximation can be made by using the
relation

$$\alpha stall = \frac{C_{L\ max}}{(dC_L/d\alpha)} \qquad (187)$$

161

$b^1{}_{ws}$, ft/sec. $\times 10^{-2}$
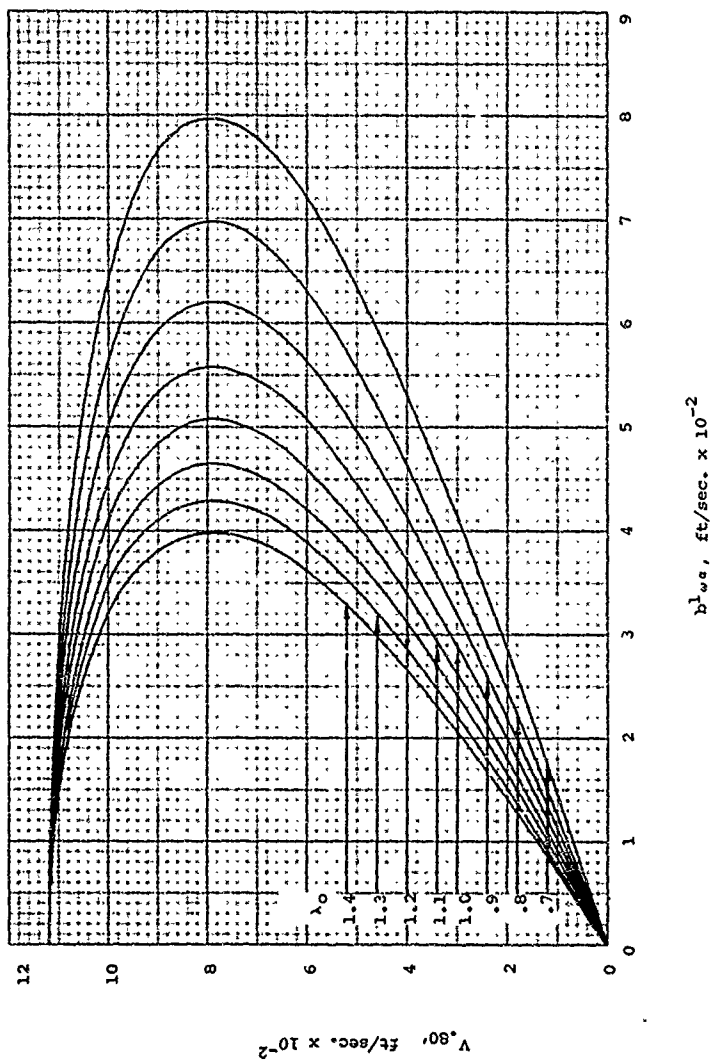
Figure 58. $V_{.80}$ Versus $b^1{}_{wx}$ for Various λ_o's.

162

Values of $C_{L\,max}$ and $dC_L/d\alpha$ can be taken from Figures 60 and 61.

As shown previously, the blade angle, β, is

$$\beta = \alpha + \alpha_i - \alpha_{LO}$$

where α is the value given by Equation (186) - deg

α_i is the induced angle - deg

$\alpha_{LO} =$ angle of zero lift

α_i can be obtained from aerodynamic strip analysis and α_{LO} is obtained from airfoil data. However, again a good approximation can be made by using Figures 62 and 63.

The blade flutter boundary is now defined by plotting the values of β versus rpm as shown on Figure 59.

The value of β calculated above is the operating blade angle and contains any torsional windup of the blade.
Since the operating blade angle is usually difficult to measure the static or unloaded blade angle β_S is the common reference. On the more conventional blades in the past, torsional deflection was relatively small and β was approximately equal to β_S. However, in the more recent propeller design, the difference has been significant and in order to use the static angle as reference, it has been necessary to evaluate the torsional deflection and define the flutter boundary as β_S versus rpm.

Figure 59 shows a typical variation between β and β_S reference flutter boundary. There have been instances on extremely flexible experimental blades where the torsional deflection was so large that the boundary closed. That is, there was an rpm limit at which the blade fluttered regardless of blade angle setting, and this type of boundary is shown on Figure 59. This situation is admittedly an exception, but it has happened. The torsional windup is found from Equations (193) to (196). Some attempt has been made in the past to predict the stress amplitude during flutter. There appears to be a relationship between stress and λ_0 of the form

$$\tau = e^{(m\,\lambda_0 + c)} \tag{188}$$

where $\tau =$ shear stress

m and c are constants for a given blade

163
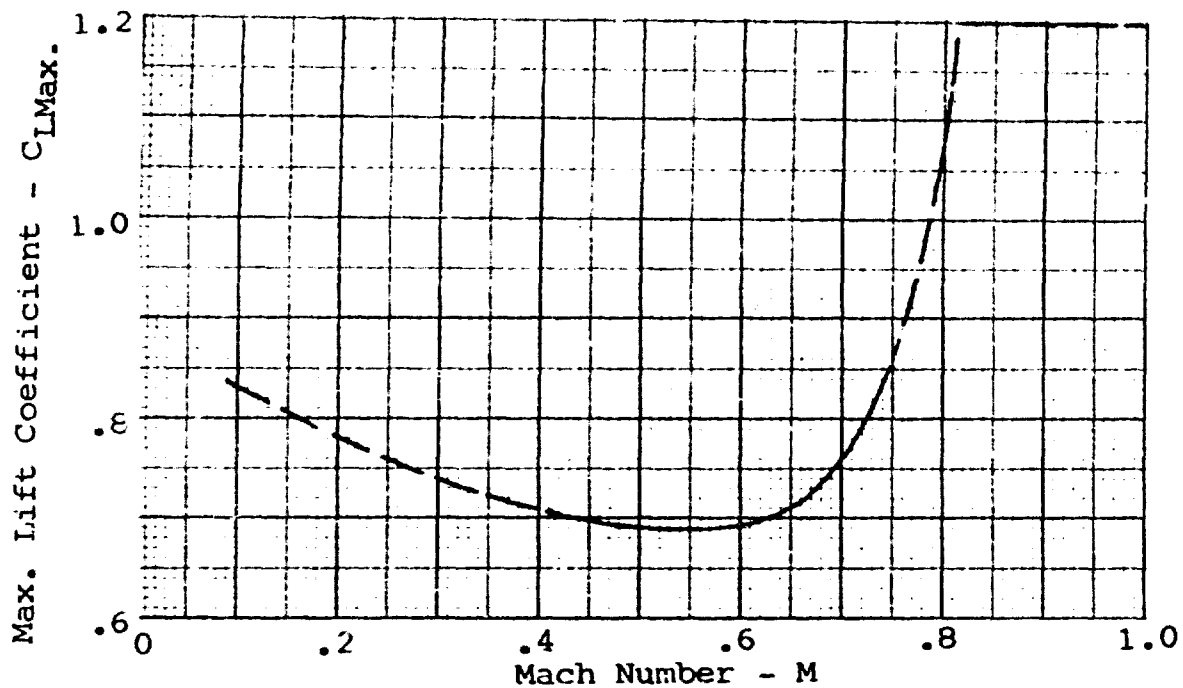
Figure 59. Average C_{LMax} Versus M For Flutter Calculation.
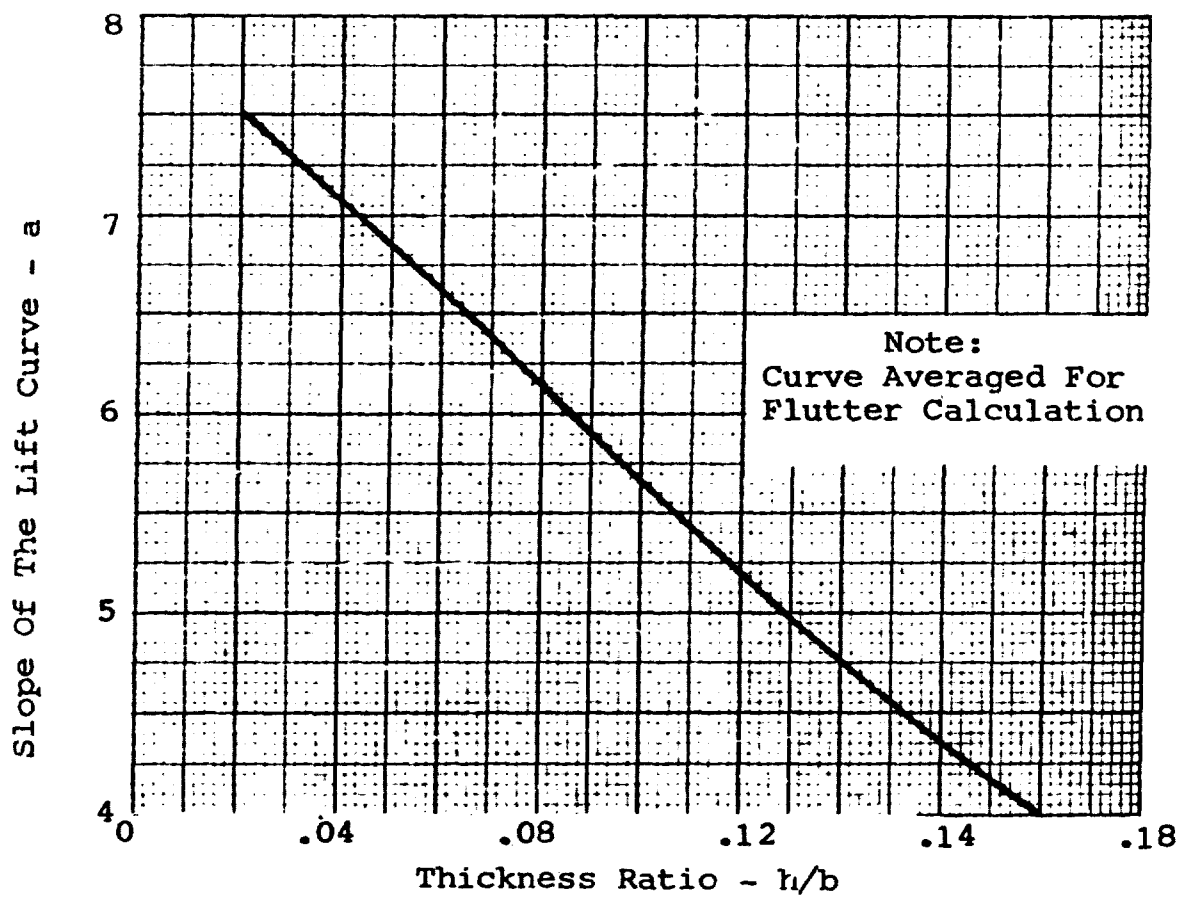
Figure 60. Slope of the Lift Curve Versus Thickness Ratio.

164
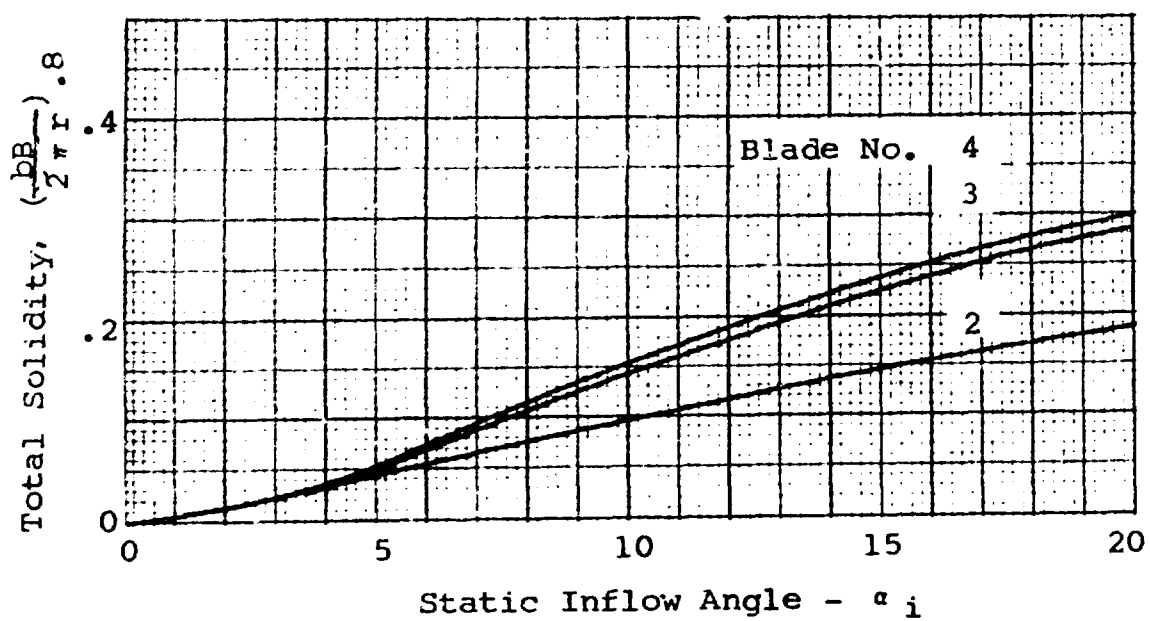
Figure 61. Static Inflow Angle α_i.
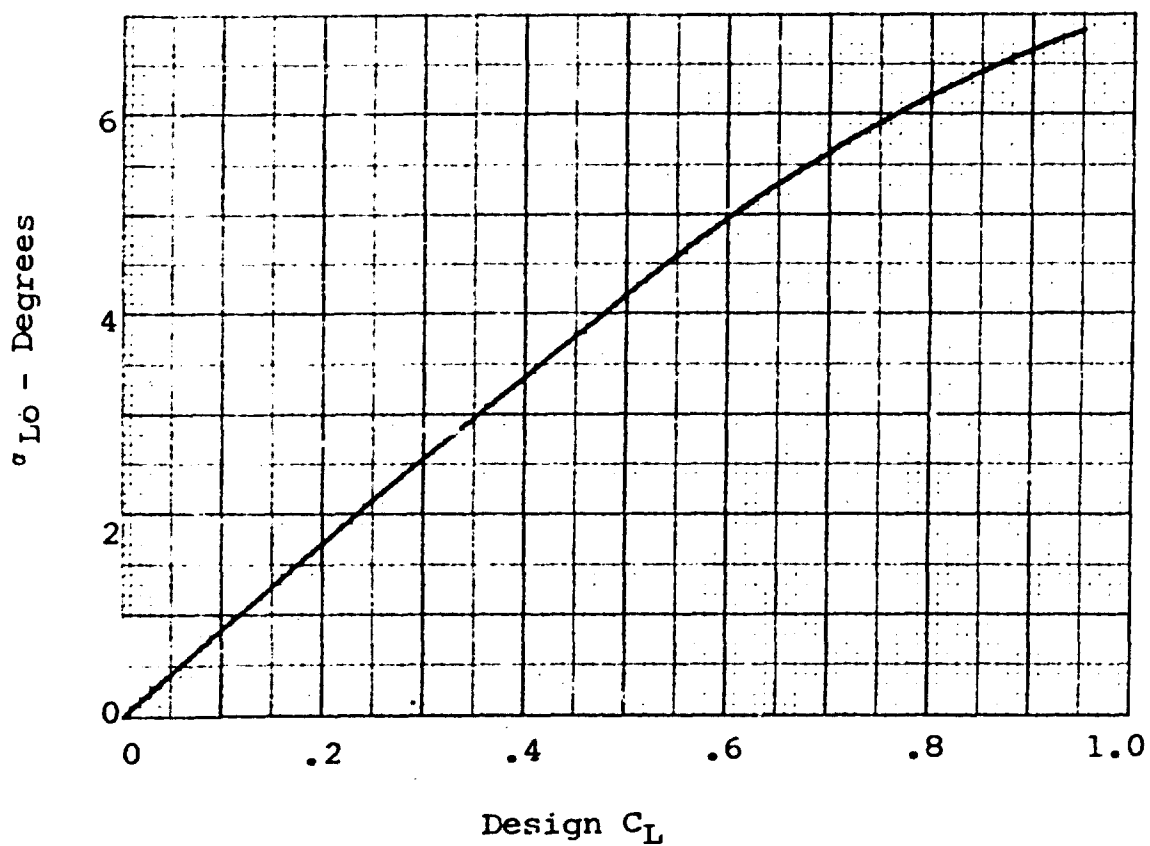
Figure 62. Average Angle of Zero Lift.
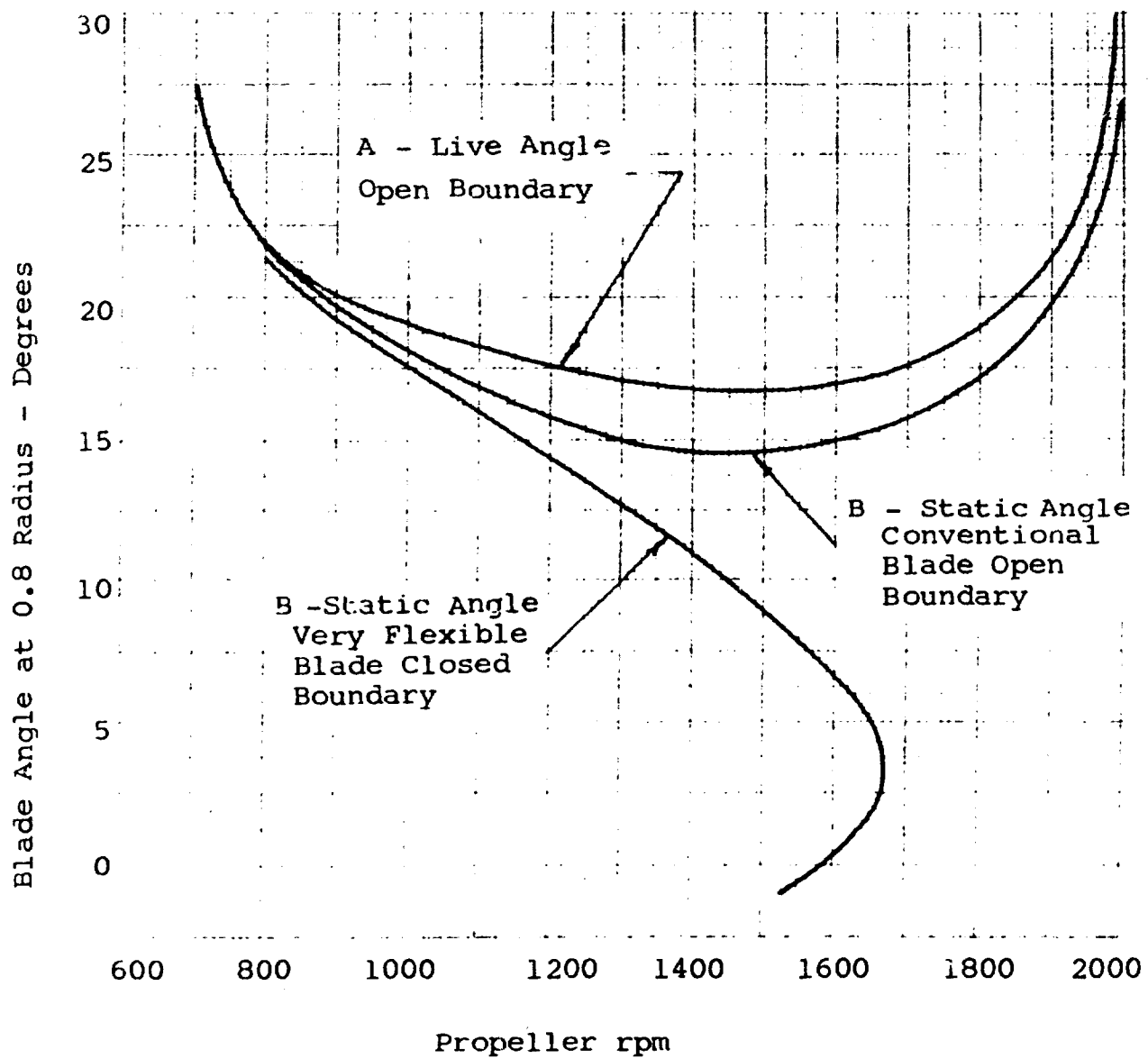
Figure 63. Typical Flutter Boundaries Showing
Effect of Live Blade Deflection.

166

It would appear that m and c are functions of the torsional frequency. The use of the above relation has not proved to be too reliable and the flutter amplitude must be verified by test surveys. Such tests have been standardized as part of propeller qualification testing and are specified in Reference 7.

To assist in locating the required instrumentation and in interpreting the results, relative stress distributions are usually computed.

Since the flutter involves the fundamental torsion mode, the maximum amplitude of the vibratory torque at any radius x is

$$Q_x = \omega^2 \int \theta_S \ (I_p)_s \ ds \qquad (189)$$

where Q_x = maximum torque amplitude at radius x - in.-lb

$(I_p)_s$ = blade section mass polar moment of inertia –
$$\frac{\text{in.-lb sec}^2}{\text{in.}}$$

$(\theta)_s$ = torsional amplitude of the fundamental modal shape – rad

I_p is obtained from the blade section data, and ω and the θ distribution are obtained from the frequency calculation. By assuming a value for the maximum amplitude, say 1.0 radian, a corresponding torque can be computed by Equation (189). The corresponding shear stress can be computed by using the appropriate equation of (153), thus defining the radial shear stress distribution and the location of maximum stress. For convenience this distribution can be normalized with respect to the maximum. If Equation (153) is divided by (154), the ratio of longitudinal and shear stress is obtained. For the hollow blade this gives

$$\frac{\sigma}{\tau} = \frac{E \ dB/dr \ (x^2 - k^2) \ (2kb_e h_e t)}{C_T} \qquad (190)$$

From the shear stress distribution this can be converted to a ratio of $\frac{\sigma}{\tau_{max}}$. With these stress distributions, the necessary strain gages can be located to verify the flutter amplitude during test. The safe operating limits of any given design must be established by evaluating the measured stress amplitude, shear and induced longitudinal, with respect to the allowable fatigue stress of the blade material.

If the required rpm and blade angle at static takeoff are within the calculated flutter boundary, Figure 55, or testing subsequently proves that the calculated curve was inaccurate, the blade must be modified. The easiest way to improve the flutter boundary is to increase the torsional frequency. This is most

167

easily accomplished by an increase in the blade section thick-
ness. This obviously increases the h/b ratio and may compro-
mise aerodynamic performance to some degree; in some cases a
change in airfoil section can be made. For the same mass a
16 section is slightly stiffer than a 65 section and will
therefore give a higher frequency.

Wake Flutter

Wake flutter is a self-excited blade vibration that occurs
when the propeller is operating at low blade angles. It is be-
lieved to be caused by the fact that a given blade is following
in the wake of the preceding blade and disturbances in that
wake excite and sustain the vibration. Strictly speaking,
therefore, the wake flutter is a forced vibration.

To understand the theory more completely, consider a single-
bladed propeller operating at a blade angle near zero degrees
so that the static thrust is zero and practically no inflow
exists in the outer portion of the blade. Suppose that a gust
excites a transient vibration of a natural mode of the blade,
either a flapping or a torsional vibration; in either case,
the blade will experience periodic lift forces and will leave
in its wake a disturbed airflow pattern. These patterns of
disturbed air are repeated around the circumference of the pro-
peller disc. If the number of these patterns exactly "fits"
the circumference of this disc, they will repeat in exactly the
same locations during the next revolution of the blade and this
will strengthen the first pattern. This condition is then con-
ducive to the growth and maintenance of the blade vibration.
If the pattern is not an integral subdivision of the disc cir-
cumference, there will not be a standing fixed pattern of dis-
turbed airflow and sustained blade vibrations are not likely
to exist. However, suppose that the number of wake wave lengths
is almost an integral number in one revolution. In this case,
the airflow pattern will revolve slowly in the direction of,
or opposite to, the propeller rotation. If this mismatch is
not too large, the successive revolutions of the blade may re-
inforce and maintain the strength of this wake pattern.

Based on the foregoing reasoning, "wake-excited" vibrations are
likely to occur at those rpm's where integral multiples of these
speeds are equal to (or nearly equal to) a natural frequency of
the blade. This means that wake-excited resonances can exist
for a given mode at consecutively higher rpm's, provided

$$i(n) = f_o \qquad (191)$$

where $i = 1, 2, 3, 4, \ldots\ldots$

n = revolutions per second

f_o = frequency of a natural mode of vibration
(including rotational stiffening).

As noted before the value of i need not be exactly an integer.

Although both bending modes as well as the fundamental torsional mode can be theoretically excited in the foregoing manner, it is unlikely that the bending modes will be actually excited since very large vibratory amplitudes are required to induce a strong wake pattern, and such amplitudes are unlikely in propeller blades. It is believed that this is the reason that the only significant wake-excited resonances have been those associated with the fundamental torsional mode.

In this foregoing analysis it was assumed that the propeller consisted of only one blade. However, the foregoing analysis equally applies to any number of blades in the propeller. When there is more than one blade, the other blades will vibrate with that special phase relationship between one another so that the wake pattern remains undisturbed.

An analysis of available data revealed that Equation (191) did not match observed data and from further analysis, that equation was modified to the following:

$$\frac{f_o}{i} = n\left[1 - (a + s_{0.8}) \right] \tag{192}$$

where   a is a value dependent on blade angle setting in Figure 64

s = blade solidity at the 0.80 radius

$s = (bB/2\pi r.)_{0.80}$

b = blade chord at 0.80 radius - ft

B = number of blades

r = radius to the 0.80 station - ft

If f_o is taken as the fundamental torsional frequency with an appropriate value of a, a series of rotation speed values can be found corresponding to $i = 1, 2, 3, 4, \ldots\ldots$ etc. These speeds will represent rpm values (rpm = 60n) where wake flutter is likely to occur. Experience has shown that at a particular rpm, resonance may or may not occur. If it occurs, it may be strong or weak. So far, no definite criterion has been

169
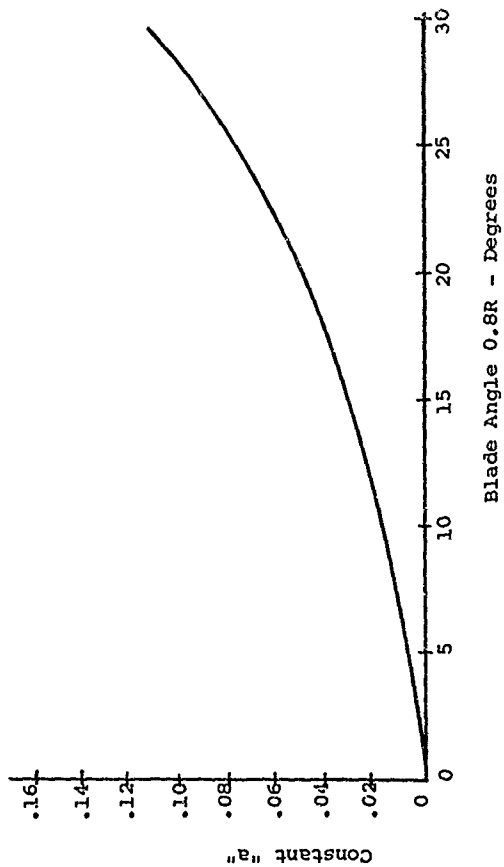
Figure 64.   Wake Flutter Factor "a" Versus Blade Angle.

established. Since such possible resonant points could be
serious, it is desirable to design the blade so that possible
resonances fall outside the operating speed (rpm) range. It
may be noted that solid dural and fiber glass blades have shown
a strong susceptibility to wake flutter whereas hollow steel
blades have shown only a mild or neglible response. However,
if any of the potential resonant rpm's are within the operating
speed range, a careful search for wake excited flutter should be
made in the vicinity of such speeds during the flutter survey
testing. As in the case of stall flutter, excessive amplitude
is corrected by changing the torsional frequency.

Miscellaneous Factors

The purpose of this section is to present certain miscellaneous
factors which may be involved in the structural design of the
propeller blade. These include: torsional deflection under
static load, buckling of hollow steel blades, and internal
pressure due to the centrifugal force on the air trapped in a
hollow blade.

Blade Buckling

Elastic buckling of the camber plate of hollow steel blades
occurs as a result of excessive compressive stress which acts
in the direction indicated on strip A-A of Figure 65 . These
excessive stresses can develop from water impact or impact with
snowbanks during tailing operations. This type of failure can
also occur under high amplitude flexural vibrations.

Plate buckling criteria have been investigated from the stand-
point of several criteria. A contributing factor is that the
buckling is most often associated with an initial depression
in the plate. These depressions can be attributed to impact
with some foreign object or manufacturing irregularities.

Plate instability has been evaluated by considering the trans-
verse section of the camber plate as a pin-end arch, Figure
65.

The collapsing forces acting on this arch are developed by the
force components resulting from a consideration of the com-
pressive stress acting along the longitudinal curvature of an
assumed initial dinge in blade surface. An approximate ex-
pression for the compressive stress to cause the collapse of
the arch has been developed as follows:

$$\tau_{CR} = \frac{E l^2 \ a t^2}{0.750 b_e^{\ 4} y_m} \tag{193}$$

171
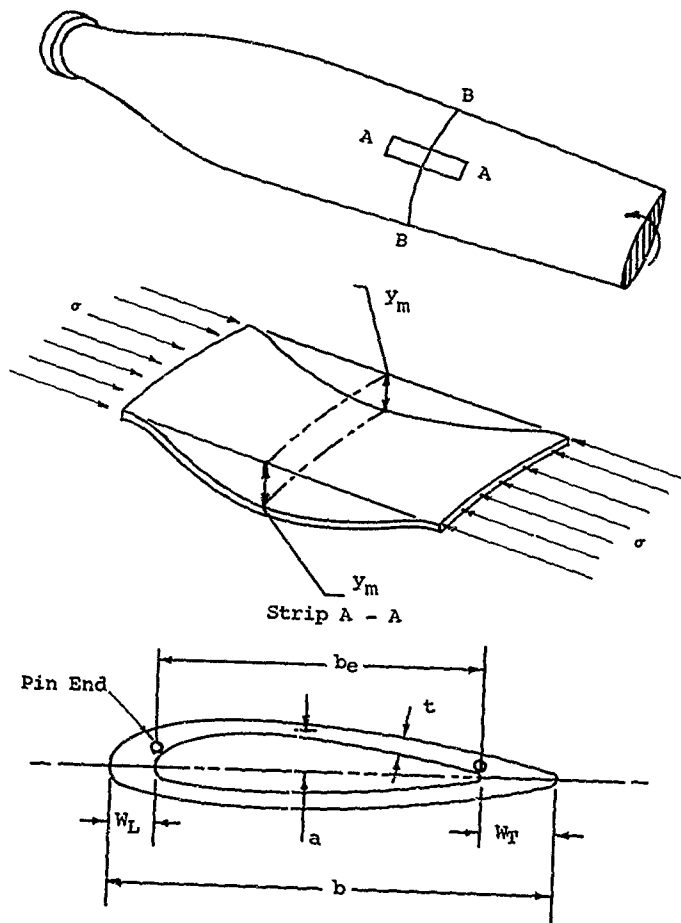
Figure 65.   Blade Buckling.

172

where σ_{cr} = the critical longitudinal compressive stress required for buckling - psi

           E = modulus of elasticity - psi

           l = length of blade segment considered (usually taken as 6.0")

       b_e = effective arch length - in.

        a = height of arch - in.

        t = plate thickness - in.

      y_m = the maximum depth of a longitudinal depression of the plate taken to be at midchord - in.

The value of 6.0 inches is usually taken for the length of blade segment based on good correlation with test results. The quantity y_m is used in the application of the equation to allow for slight depressions within manufacturing dimensional limits or a dinged area which may be caused by operational factors such as water impact, stone, bruises, etc. Based upon manufacturing tolerances and estimated depth of dinged areas due to other causes, it has become standard practice to calculate the stress for

$$y_m = 0.005 \text{ inch} \quad \text{and} \quad y_m = 0.015 \text{ inch}$$

Experience has shown that the foregoing equation is reasonably reliable in predicting the relative buckling characteristics of hollow steel blade designs.

Torsional Deflection

It has been previously mentioned that on the more flexible blades, the torsional deflection is important in establishing a manufacturing blade angle distribution (see section on Steady State Aerodynamic Loads) and also in evaluating the static flutter boundary (see Stall Flutter).

As previously noted, the steady-state aerodynamic loads thrust and torque are determined to satisfy a given condition of horsepower, velocity, rpm, etc. The result of aerodynamic analyses establishes a desired blade angle distribution. This is an aerodynamic angle and as such it includes any torsional deflection of the blade. The blade therefore must be manufactured with a pitch distribution such that:

173

$$\beta_{aero} = \beta_{mfg} + \emptyset \qquad (194)$$

where $\emptyset$ = torsional deflection

The designer therefore must establish a manufacturing pitch distribution, such that under load the blade will twist up to the desired aerodynamic angle. Obviously the above relationship can only be optimized for one flight condition, takeoff, cruise, etc.; at all other flight conditions the pitch distribution will vary slightly from that desired. With the optimum condition established, the aerodynamic loads and desired pitch distribution are known, and with this data the three components of steady torque are evaluated. These are aerodynamic torque, centrifugal twisting moment and the centrifugal straightening moment.

The aerodynamic torque at any radius x is

$$(Q_A)_x = \int_x^{tip} f_n \ (x_{cp}) \ ds$$

where   x = fixed radius - in.

      s = variable radius - in.

  x_{cp} = distance from section center of pressure to shear center - in.

  f_n = section normal forces - lb/in.

For most propeller sections the center of twist can be taken as coincident with the blade structured centroid. As a first approximation, the location of the aerodynamic center can be taken at the quarter chord point, or a more accurate location can be obtained from data given in the aerodynamic section, Figures 200 to 203, Volume I.

The centrifugal moment is given previously, page 39, as

$$Q_x = \frac{\delta}{2g} \ \omega^2 \int_x^R (I_{max} - I_{min}) \ \sin 2\beta_s \ ds + \int_x^R abA \ ds$$

and the centrifugal straightening moment is given, page 70, as

$$(\Omega_u)_x = \sigma_{CF} \frac{d\beta}{dr} (I_{max} + I_{min})$$

The total blade torque at any radius x is therefore

$$(\Omega_T)_x = (\Omega_A)_x + (\Omega_U)_x - (\Omega)_x \qquad (195)$$

The blade twist is easily calculated from the relation

$$\Omega_x = \int_0^x \frac{\Omega}{C_T} \, ds \qquad (196)$$

where C_T is the blade section torsional stiffness as defined in Equation (125)

The value of ϕ thus calculated is subtracted from the given aerodynamic angle to obtain a first estimate of the manufacturing angle, Equation (194). Since the centrifugal torques and the torsional stiffness are dependent upon the pitch distribution, it is desirable to repeat the computation using the calculated manufacturing angle distribution. The deflection, thus calculated, is then added to the assumed manufactured angle and the result checked against the desired aerodynamic pitch. Based upon the degree of agreement, the assumed manufacturing angle can be modified and the process is repeated until satisfactory results are obtained.

Calculation of the static flutter boundary is basically the same procedure. Two or three points are selected from the live boundary, and for the selected settings and rpm, the aerodynamic loads and the various blade torque components are evaluated. For this purpose the manufactured pitch distribution can be used. Equations (195) and (196) are used to evaluate the torsional twist, and the appropriate value is subtracted from the line blade angle to obtain the static boundary as discussed in the section on stall flutter.

175

Internal Blade Pressure

On hollow or monocoque blades there is a volume of air trapped in the internal cavity. Under rotation this air will experience a centrifugal force, and unless a tip vent is provided a significant internal pressure can develop in the tip region. Without going into details, the internal pressure due to the centrifugal effect on a column of trapped air is:

(1) Shank Open to Atmosphere

$$\frac{p_x}{p_o} = e^{\frac{1}{KT\ 2g}\ \omega^2(x^2 - x_o^2)} \tag{197}$$

p_x = pressure at a given radius x

p_o = atmospheric pressure - $lb/in.^2$

K = gas constant - $ft\text{-}lb/lb\ {}^oF$

K = 53.3 for air

T = absolute temp - ${}^oR$

ω = rotational speed - rad/sec

x = given radius - ft

x_o = blade butt radius - ft

g = gravitational constant - ft/sec^2

(2) Shank Sealed

$$\frac{p_x}{p_o} = \frac{V}{\left(\int_{xo}^{tip} A_s\, e^{\frac{1}{2gKT}\ \omega^2 s} ds\right)}\, e^{\frac{\omega^2\ x^2}{KT\ 2g}} \tag{198}$$

where V = the volume of the enclosed space - ft^3

A_s = cross-section area of enclosed space at station s - ft^2

If, in the foregoing equation, the value of x is the tip radius R, then $\omega^2 R^2$ equals the blade tip speed squared. It will also be noted that in Equation (197) x_o^2 is quite small with respect to x^2 for the pertinent outboard radii. Therefore, the foregoing equations can be written:

176

$$\frac{p}{p_o} = e^{\frac{1}{2KTg} \left(\frac{x}{R}\right)^2 (\pi nD)^2} \quad \text{(open shank)}$$

$$= \frac{V}{\displaystyle\int_0^{tip} A_s e^{\frac{1}{2KTg} \left(\frac{s}{R}\right)^2 (\pi nD)^2} ds} \; e^{\frac{1}{2KTg} \left(\frac{x}{R}\right)^2 (\pi nD)^2} \quad\quad (199)$$

$$\text{(closed shank)}$$

πnD = tip speed - ft/sec

Applying these equations to a typical hollow steel blade gives the following tip pressure for πnD = 1200 ft/sec.

Open shank - p_{tip} = 34.5 lb/sq in.

$\quad\quad\quad\quad\quad\quad = 19.8$ lb/sq in. (gage)

Closed shank - p_{tip} = 27.6 lb/sq in.

$\quad\quad\quad\quad\quad\quad = 12.9$ lb/sq in. (gage)

In assessing these pressures, one must recognize that on the camber plate the aerodynamic pressure on the external surface is negative. Therefore, the net force tending to distort the plate can become quite high.

In the past, blades were filled with low-density gas such as helium to minimize the centrifugal pressure. However, the more recent trend has been to vent the blade tip or fill the internal cavity with a low-density material such as foam.

RETENTION LOADS AND ANALYSIS

The primary design loads on the propeller blade retention are the blade centrifugal force, the steady-state bending moment and the 1xP vibratory bending moment. The centrifugal force is obtained by evaluating Equation (70) for the entire blade length, and the moments are obtained from the solution of Equations (137) and (143) at the assumed point of fixity. As previously noted, since the blade shank is round the resultant moment is

$$M_R = (My^2 + Mz^2)^{\frac{1}{2}} \quad\quad\quad (200)$$

177

and this resultant value is used in retention analysis. These forces are illustrated in Figure 66. As shown, the resultant of the steady and vibratory moments do not necessarily lie in the same plane. However, for conservatism in retention analysis it is generally assumed that the two load components directly add. The retention moment is therefore

$$M = M_{steady} + M_{1 \times P} \tag{201}$$

It is obvious that the retention must also provide the shear reaction for the blade thrust and torque loads, but as in most beam problems, these shear components are relatively unimportant for design purposes and can be neglected.

There are several types of propeller retentions and it would be impractical to attempt to provide a detailed analysis procedure for all types of designs. For the purpose of this report a somewhat detailed procedure will be given for the common flanged shank type retention, Figure 5. With these basic principles as a guide, modifications can be easily made for other retention types.

Equivalent Centrifugal Force

For convenience in analysis, the combined centrifugal and moment loads can be expressed as an equivalent axial load. If the moment is assumed to be reacted around the circumference as a cosine function, Figure 66, the value of the maximum unit load is

$$P_o = \frac{M}{\pi r^2} \quad \text{lb/in.}$$

The axial load necessary to give this same maximum unit value is

$$P = \frac{4M}{d} \tag{202}$$

The equivalent centrifugal force is therefore defined as

$$ECF = CF + \frac{4M}{d} \tag{203}$$

where   ECF = equivalent centrifugal force - lb

      CF = blade centrifugal force - lb

      M = retention moments steady and/or vibratory - in./lb

      d = appropriate load diameter - in.

178
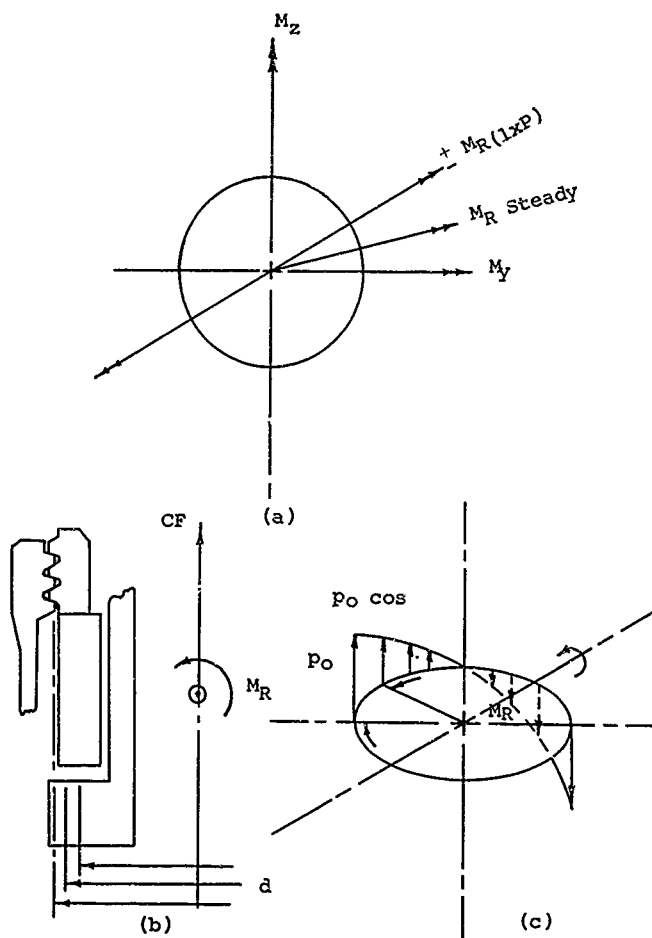
Figure 66.   Retention Loads.

179

If this load is divided by a circumference defined by diameter d, the unit load will obviously correspond to the maximum of the combined centrifugal force and moment.

This equivalent force also serves another important function, as will become obvious later; the retention stresses are essentially proportional to the value of ECF. Therefore, the effect of load changes on a given retention can be easily estimated by direct ratio of ECF values.

Blade Flange Analysis

The blade flange is a straightforward flange problem and the method of analysis is given in most handbooks on structural design. With reference to Figure 67 , the flange is considered as a tube and ring. R is the applied unit load and M_O and P_O are unit loads at the interface necessary for compatibility of deformation between the two bodies. Considering the loads and dimensions shown in Figure 67, if the deflections y and θ are computed for each section and equated, the following equations result

$$\left[\frac{Eh^3 \ln(d/c)}{24\beta^2 D} - \frac{hc}{2}\right]P_O - \left[\frac{Eh^3 \ln(d/c)}{12\beta D} + c\right]M_O + \text{Ret} = 0$$

$$\left(\frac{ca}{EA} + \frac{1}{2\beta^2 D}\left[\frac{h}{2} + \frac{1}{\beta}\right]\right)P_O - \frac{1}{2\beta D}\left[h + \frac{1}{\beta}\right]M_O = 0$$

(204)

where E = modulus of elasticity - lb/in.^{2}

$\quad\quad\quad\quad B = \left[3(1 - \lambda^2)/f^2 h_1^2\right]^{\frac{1}{4}}$

$\quad\quad\quad\quad D = Eh_1^3/12(1 - \lambda^2)$

$\quad\quad\quad$ ln = natural logarithm

$\quad\quad\quad$ A = h(d - c)

$\quad\quad\quad\quad \lambda$ = Poisson's ratio

all other values are defined in Figure 67.

180
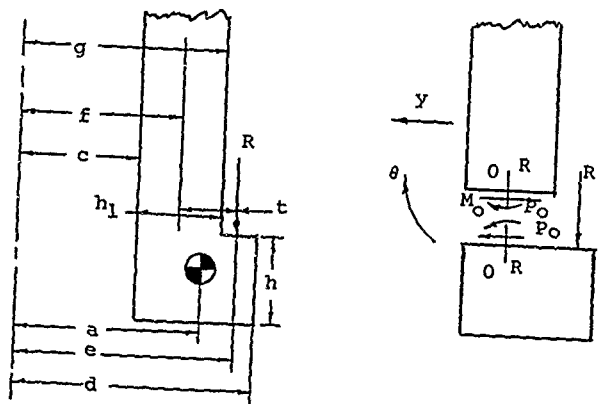
Figure 67. Blade Flange.

In practice it is common to solve Equation (204) for M_O as a function of R: $M_O = mR$

The basic fillet stress is therefore

$$f = R\left[(e/h_1 f) + 6\ mc/h_1{}^2 g\right] \qquad (205)$$

From Equation (203), R in terms of the dimensions of Figure 67 is:

$$
\left.
\begin{aligned}
R &= \left[\left(CF + \frac{2M_{steady}}{e} \pm \frac{2M_1 \times P}{e}\right)\right]\Big/ 2e\pi \\
R &= \left[\frac{CF}{\pi e} + \frac{M_{steady}}{\pi e^2}\right] \pm \frac{M_1 \times P}{\pi e^2}
\end{aligned}
\right\} \qquad (206)
$$

Correlation between the blade flange fillet stress thus calculated and experimental data indicates that for conventional proportions, see Table II, a fillet stress concentration factor is in the order of 1.10. In accordance with common practice in fatigue analysis the stress concentration factor is only applied to the vibratory component. The final stress

is therefore

$$f = C \left[\frac{CF}{2\pi e} + \frac{M_{steady}}{\pi e^2} \right] \pm C(1 \cdot 1) \frac{(M_1 \times P)}{\pi e^2}$$

(207)

where $\quad C \approx \dfrac{e}{h_1 f} + \dfrac{6mc}{h_1{}^2 g}$

Based upon the calculated stresses the flange factor of safety can be obtained from the appropriate working Goodman Diagram of the blade shank material. It has been mentioned earlier that in most propellers there are extraneous components such as higher order aerodynamic loads. These are generally unpredictable, and it has been common practice to design the retention components to a 1.3 factor of safety to allow for these miscellaneous load components.

Hub Thread Relief Analysis

Referring to Figure 68 it is seen that in the hub thread relief fillet area, the stress is a combination of flange bending and thread bending, and this area is probably the most critical section in the design of this standard type of retention.

Considering first the flange bending effect, Figure 69 shows a typical hub-thread equivalent flange. Analysis is identical to that used on the blade flange and the equations corresponding to 204 are

$$\left[\frac{hc}{2} - \frac{Eh^3 1_n \frac{c}{e}}{24 \beta^2 D} \right] P_O + \left[\frac{Eh^3 1_n \frac{c}{e}}{12 \beta D} + c \right] M_O - Ret$$
$$- Ru^1 \left[\frac{h}{2} - \bar{x} \right] = 0$$

(208)

$$\left(ca + \frac{EA}{2\beta^2 D} \left[\frac{h}{2} + \frac{1}{\beta} \right] \right) P_O + \frac{EA}{2\beta D} \left[h + \frac{1}{\beta} \right] M_O - u^1 Rea = 0$$

where $\quad E =$ modulus of elasticity

$B = \left[3(1 - \lambda^2)/d^2 h_1{}^2 \right]^{\frac{1}{4}}$

$D = Eh_1{}^3/12(1 - \lambda^2)$

$\lambda =$ Poisson's ratio

182

a) Typical Hub
   Thread System

b) Thread Relief
   Stress

c) Thread Bending
   Stress
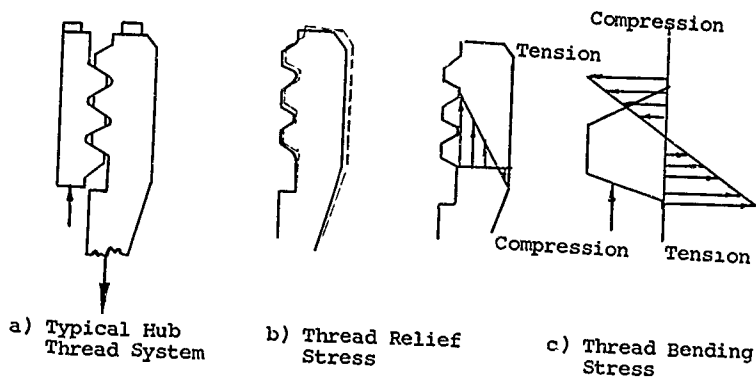
Figure 68.   Hub Thread Relief.

$u^1 = \tan\phi \pm u$

a) Method of Assuming
   Equivalent Section
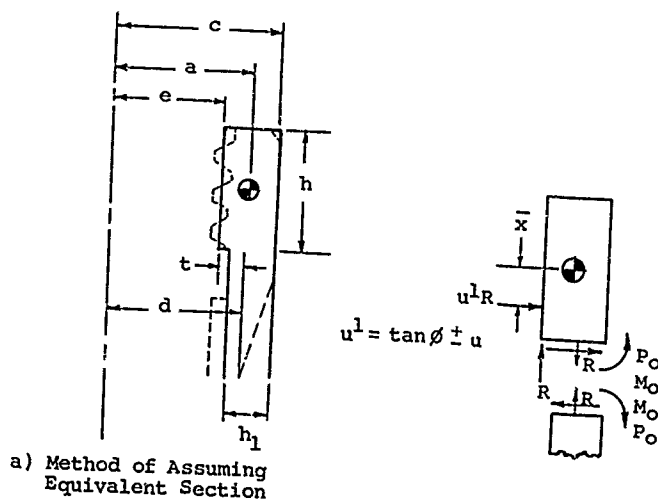
Figure 69.   Hub Thread Flange.

183

$$A = h(c - e)$$

$$u^1 = \tan \phi + u$$

ϕ = thread face angle

u = coefficient of friction between hub and nut threads

R is the applied unit loading;all other dimensions are as given in Figure 69

As in the case of the blade flange the above equation is solved for M in terms of R. However, the coefficient of friction contained in the u^1 term is not applicable for steady-state load. Therefore, two solutions are required: one for $u^1 = \tan \phi$ representing steady-state loads, and a second for $u^1 = \tan \phi + u$ representing a vibratory loading. Or, $M_o = mR$ for steady loads, $M_o = m^1 R$ for vibratory loads. The basic stress therefore is

$$f_{tr} = R_{steady}\ (e/h_{1d} + 6\ m/h_1^2)$$
$$\pm\ R_{vib}\ (e/h_{1d} + 6\ m^1/h_1^2) \qquad (209)$$

In terms of the dimensions of Figure 69,

$$R_{steady} = \frac{CF}{2\ \pi\ e} + \frac{M_{steady}}{\pi e^2}$$

$$R_{vib} = \frac{M\ 1xP}{\pi e\ 2} \qquad (210)$$

Based upon standard proportions, see Table IV, tests have shown an applicable stress concentration factor of 1.3. Also from average test data a value of $\mu = 0.15$ can be assumed.

In order to solve Equation (208) the value of $\bar{x}$ must be known, and this requires some knowledge of the load distribution within the thread system. It is well-known that in a normal threaded joint, the load is nonuniformly distributed with the first turn assuming the major portion. The distribution of thread load is treated at length in other literature, and one such development is given in Reference 8. Following a similar line of development, expressions have been developed for the thread load distribution and which retention testing has substantiated. These relations are given on the following pages.

184

First consider the simple thread system as shown in Figure
70.   In that   sketch R is the total load applied to the
system, Q is the load transmitted through the threads between
$x = 0$ and $x = x_1$, and FP is the load transmitted by the given
thread turn.   For this simple system, the relation for p with
the distance x is

$$p = \frac{k}{n} \left[\text{Cosh}\ k\ (L - x)/\sinh\ kL \right] \qquad (211)$$

where   x and L are dimensions defined in Figure 70

n = number of threads per inch

$k^2 = (\ \pi\,dn/KE)\ (1/A_f + 1/A_M)$

d = pitch diameter -- in.

K = thread flexibility constant equal to the
combined deflection at the pitch line of one
circumferential inch of an engaged pair under
a one-pound load - in.^{2}/lb

A_f = cross-section area of the female part (hub
section at the threads) - in.^{2}

A_M = cross-section area of the male part
(blade nut) - in.^{2}

E = modulus of elasticity
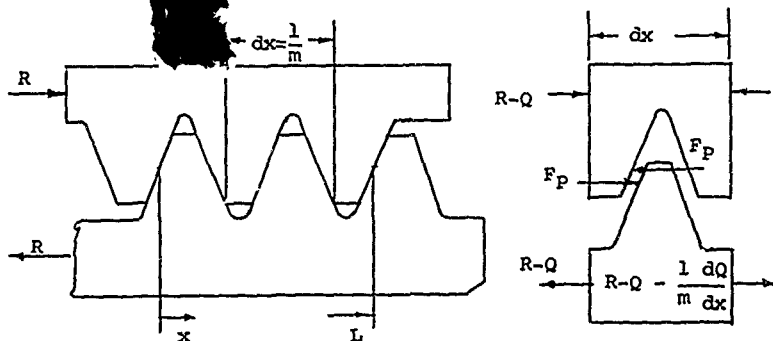
Figure 70.   Straight Thread System.

185

Solving the above equation for $x = 0$, first turn, and $x = L$, last turn, gives

$$P_O/P_L = \cosh \; kL \qquad (212)$$

This relationship shows that the first turn always carries the larger portion of the thread load. Using the distribution defined by Equation (211) the value of $\bar{x}$, see Equation (208) and Figure 69, is

$$\bar{x} = \frac{\cosh \; kL - 1}{k \sinh \; kL} \qquad (212)$$

A typical straight hub thread load distribution is shown in Figure 72. That curve indicates that about 40% of the load is taken by the first thread and 20% by the last thread. A more uniform distribution can be obtained in a straight thread by reducing L or the constant k. The k factor is reduced by increasing member areas, flexibility (K), or modulus (E), or by decreasing pitch diameter and thread pitch.

The thread flexibility, K, is a primary factor in the load distribution and attempts to evaluate it analytically have not proved satisfactory. For the standard four-pitch thread form commonly used on propeller hubs, experimentally determined value has been established. The value is $K = 35.4 \times 10^{-8}$ in^2/lb. For other thread forms corresponding values would have to be evaluated.

Another method for alleviating the high load on the first turn is to incorporate a tapered thread system. This is accomplished by tapering the nut thread, thereby forcing the outboard thread to pick up a higher portion of the load. Such a thread system is shown in Figure 71.
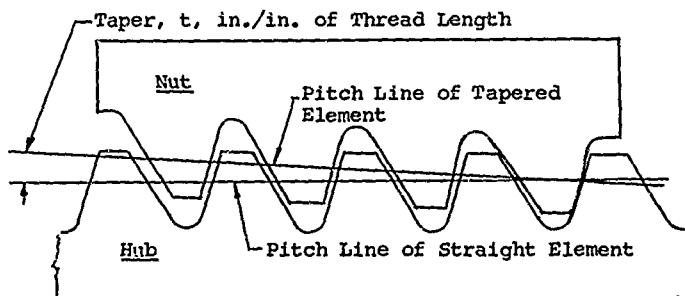
Figure 71. Tapered Thread System.

186
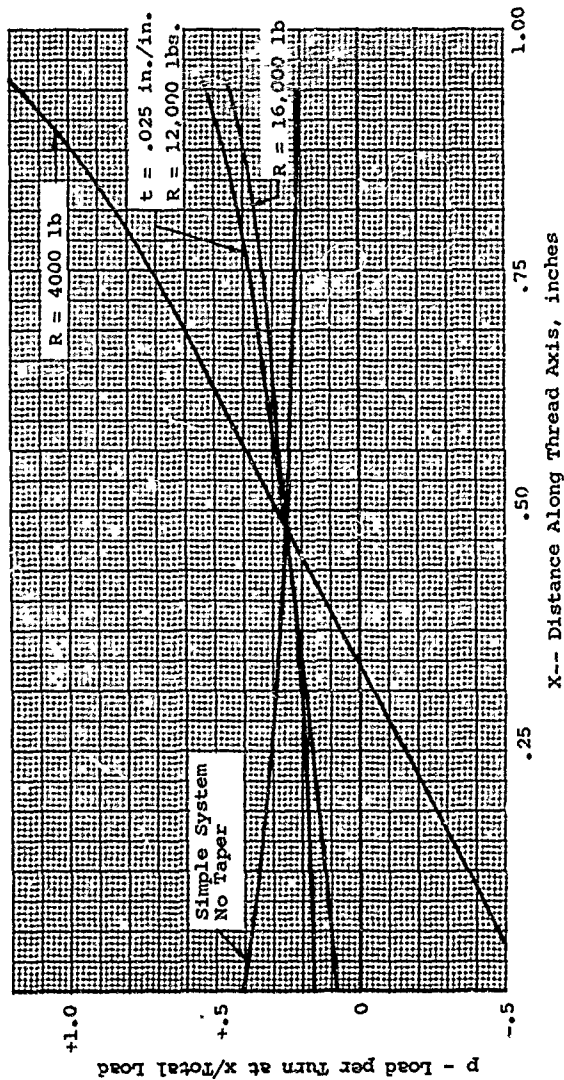
Figure 72. Typical Straight Hub Thread Load Distribution.

187

For this system the value of p with respect to the distance x is

$$p = \frac{k}{n \sinh kL} \left\{ \left[\frac{t \, n \, \tan \phi}{2 \, K \, R \, k^2} - 1 \right] \right.$$

$$\left[\cosh \, kx - \cosh \, k(L - x) \right] + \cosh \, k \, x \right\} \qquad (212)$$

and the value of $\bar{x}$ for this distribution is

$$\bar{x} = L \left[1 + \frac{h^2}{k^2} \right] + \frac{\left(1 + 2 \, h^2/k^2 \right)(1 - \cosh \, kL)}{h \sinh \, kL} \qquad (213)$$

where ϕ = thread face angle

R = applied load per inch of circumference

$h^2 = \dfrac{tn \, \tan \phi}{2 \, KR} - k^2$

t = thread taper, inch per inch of length

all other quantities are as previously
defined, Equation (211)

Examination of Equation (212) shows that the load distribution is now dependent upon: taper, flexibility, length and applied load.

A typical tapered thread load distribution is shown in Figure 72.   It will be noted that at low load a negative thread reaction is indicated. In practice there is generally sufficient clearance so that this condition could not exist. In such cases it is necessary to determine the distance x at which p = 0. Calling this value x'_0, the value $L' = L - x_0$ is substituted for L in Equation (212) and the distribution is recalculated.

With the tapered system it is obviously necessary to evaluate the thread load over the entire propeller load spectrum. At low loads the stress at the outboard thread fillet can be more critical than the stress at the inboard fillet under the high load. For such a thread system it is therefore necessary to analyze both the outboard thread fillet and the inboard fillet over the propeller load range for several degrees of taper until a so-called balanced design is obtained. The design is considered to be balanced when the minimum factor of safety at the outboard fillet is approximately equal to the minimum factor of safety at the inboard fillet. As noted earlier, the total fillet stress is a combination of flange bending and thread

188

bending. The flange bending at the outboard fillet is computed by applying Equations (205-210) to the flange defined by the outboard thread, Figure 73. In this case the radial load can be assumed to act at the distance x equal to h/2 without significant error.

Thread Bending Stress

The loaded thread is shown in Figure 74. The load pR is the unit load per inch of circumference and is assumed to be applied at the pitch line. From that figure the bending stress at the base of the tooth is

$$f_t = \frac{6 \ apR}{b^2} \tag{214}$$

For the standard four pitch hub thread this Equation reduces to

$$f_t = 11.8 \ pR \tag{215}$$

Experience has shown that a stress concentration factor of 1.86 is applicable to this calculated thread stress. The value of R is defined by Equation (210).

Combined Fillet Stress

The total stress in the thread fillet is a combination of the thread relief stress, f_{tR} Equation (209), and the thread stress, f_t Equation (214). However, the distribution of the two components around the fillet is such that they are not added directly. The respective distributions are given in Figure 75 . These curves have been normalized and the maximum value corresponds to the calculated value including the appropriate stress concentration factor when applicable.

The magnitude and location of the combined fillet stress is therefore obtained by applying the appropriate factor from Figure 75 to the calculated stress and adding. For example, at 40° location,

$$f_{40^\circ} = (.64 f_{tr} + .79 f_t)_{steady} \pm$$

$$\left[.64 \ (1.3)(f_{tr}) + .79(1.86)(f_t) \right]$$

where 1.3 and 1.86 are the appropriate stress concentration factors previously given. With the stress known, the factor of safety can be obtained from the material Goodman diagram.

189
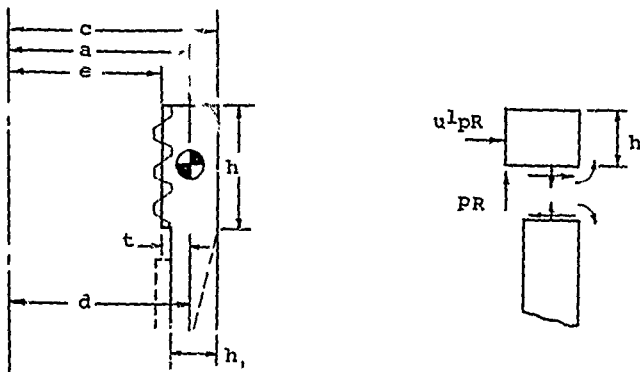
Note: All dimensions are the same as given on
Figure 69

Figure 73. Equivalent Flange - Outboard Thread.
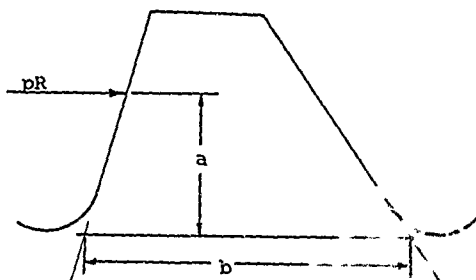
Figure 74. Thread Bending.
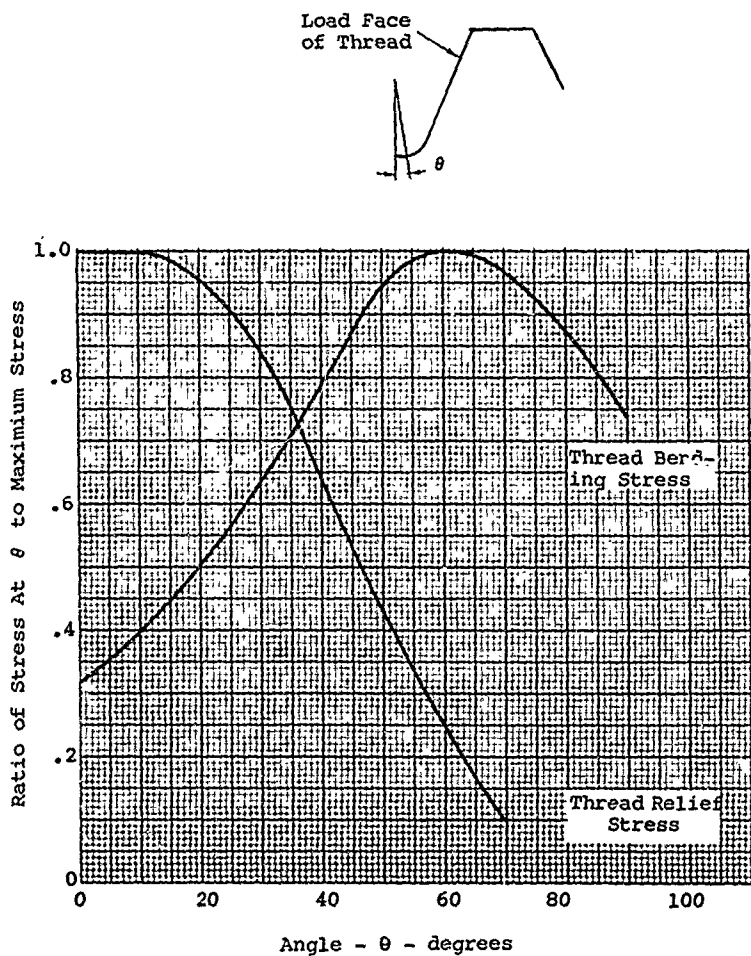
Figure 75. Nondimensional Distribution of Thread Relief and Thread Bending Stresses Around Base Fillet.

191

Blade Bearing Analysis

The standard blade retention bearing is a special angular contact thrust bearing and is usually designed with inner and outer races split as discussed on page 1 . The design is generally predicated on the mean Hertzian stress. A complete detailed procedure for the analysis of a bearing is found in Reference 1.

A detailed presentation is beyond the scope of this report; however, pertinent equations are presented for use in preliminary design. It is therefore recommended that a final design be coordinated with a bearing manufacturer.

Figure 76 shows a typical bearing race and pertinent dimensional data. The bearing contact stresses are dependent upon the bearing loaded contact angle, which in turn depends upon the deformation of the system.

For such a system the following equation is given for the final loaded contact angle.

$$(\sin\beta + C_1 \sin^{1/3}\beta) + C_2 - \cos\beta_o' \quad \tan\beta = 0 \tag{216}$$

where β = final loaded contact angle

β_o' = initial mounted contact angle

$\cos \beta_0' = \cos\beta_0 - (\Delta PD/2Bd)$

β_0 = unmounted contact angle generally specified

ΔP_D = total diametral mounting fit

$C_1 = \left[7.817(C_{\delta o} + C_{\delta i}) \times 10^{-6}/B\right](F_t/nd^2)^{2/3}$

$C_2 = F_t \sum k/Bd$

n = number of balls

$C_{\delta o}$ & $C_{\delta i}$ = constants for inner and outer race and can be obtained from Figure 77

F_t = total applied load and is taken as the total equivalent centrifugal force

$F_T = CF + \dfrac{4(Ms + Mv)}{D}$

192
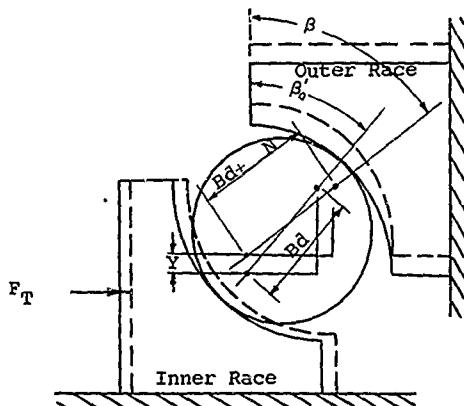
d = ball diameter, in.

β = operating contact angle, deg

β_o' = initial (unloaded) mounted contact angle, deg

B = bearing total excess curvature

f_o = curvature of outer race

f_i = curvature of inner race

r_o = radius of outer race, in.

r_i = radius of inner race, in.

Y = radial displacement of races under load

N = Hertz, or contact, deflection of ball and races under load

$f_o = r_o/d$

$f_i = r_i/d$

$B = f_o + f_i - 1 = (r_o/d + r_i/d) - 1$

Figure 76.   Bearing Geometry.

193
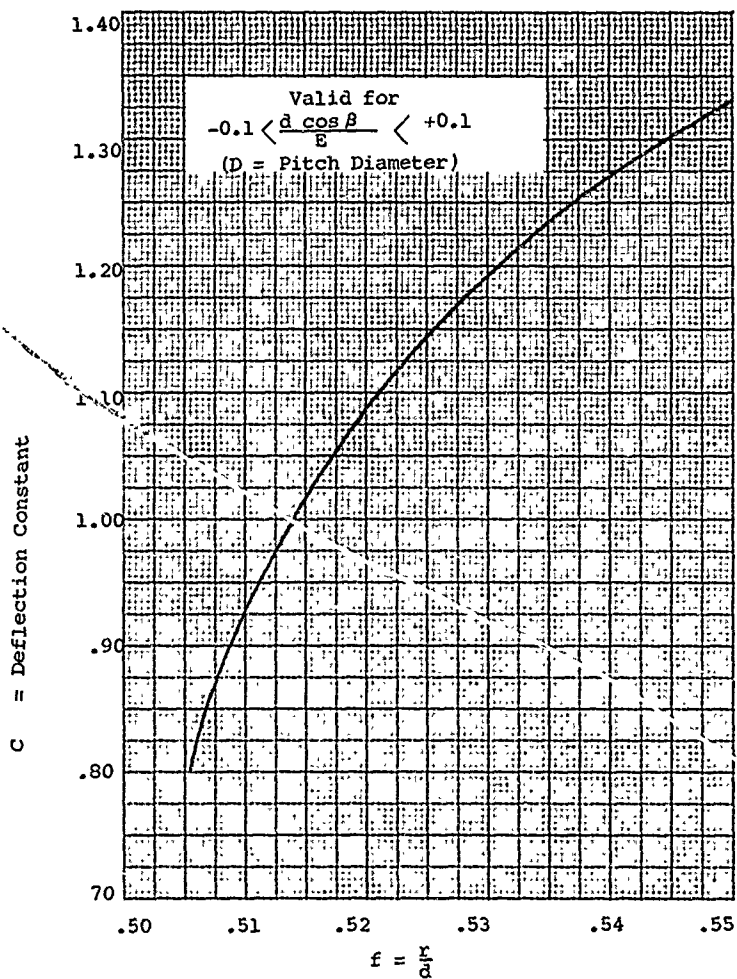
Figure 77. Bearing Deflection Constants $(C_{\delta_o} + C_{\delta_i})$.

194

D = bearing pitch diameter

M_S = steady bending moment at blade butt - in.-lb

M_V = vibratory moment at blade butt - in.-lb

The value Σk is the total radial flexibility of the bearing supporting structure, and must be estimated for the hub barrel and blade shank. Further, if the bearing races are not split, the hoop stiffness of the races must be combined in parallel with barrel and shank. The value of k for the individual ring elements may be estimated from the following:

$$k = \frac{1}{2\,\pi\,E\,L} \left[\frac{b^2 + a^2}{b^2 - a^2} \pm \lambda \right]$$

where   E = modulus of elasticity

b = outer diameter of the given body

a = inner diameter of the given body

L = effective length assumed to be supporting the bearing

λ = Poisson's ratio

With all factors known, Equation (216) is a cubic and the solution can be a tedious exercise.

Once β has been determined, the mean Hertz stress can be calculated by the well-known relation

$$s_m = 15079 f_S \ (F_T/nd^2 \sin\beta)^{1/3} \tag{217}$$

where f_S is a constant defined by Figure 78

For satisfactory operation, the maximum value mean Hertzian stress of the propeller retention bearing should be kept in the order of 350,000 psi. The operating range for propellers has been 325,000 to 405,000 psi. The foregoing has assumed a single row bearing. For multiple row bearings the analysis is made equally applicable by assuming the load, F_T, to be distributed equally between rows.

Bearing Overhang

If the bearing contact angle becomes too high the theoretical contact ellipse will overhang the race edge, such a condition will be prone to edge chipping. This condition is illustrated in Figure 79. The value of the projected semiaxis of the ellipse, a, can be calculated from

195
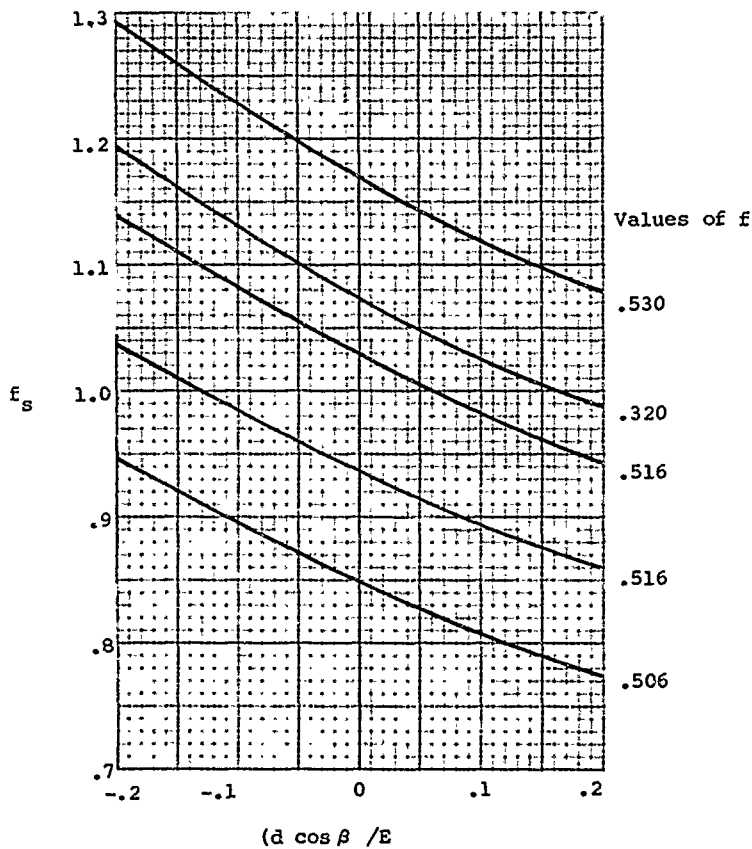
Figure 78. Bearing Stress Constant.

$$a = .0045944 \ K_a \ (F_T \ d/n \ \sin\beta \ )^{1/3} \qquad (218)$$

where K_a = constant given in Figure 80
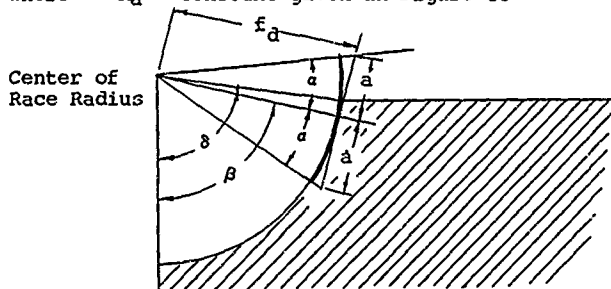
Figure 79.   Bearing Overhang.

Knowing the value of β and a, the degree of overhang can be determined from the bearing geometry and with reference to Figure 79, it is usually defined as

$$OH = (\alpha + B - \delta)/2\sigma \qquad (219)$$

$$\alpha = arc \ tan \ a/fd$$

Overhang to any degree is an undesirable feature and should be avoided. However, it does exist on most retention bearings. The adverse effect is minimized by generously bending the loaded edge of the race and using overlapping race ways. With such designs, overhang as high as 50% at the maximum loaded ball has proven satisfactory in test evaluation.

<u>Bearing Friction Alleviation of Load</u>

In the standard type retention, particularly those incorporating split inner and outer bearing races, a portion of the vibratory load is transmitted directly through the bearing by friction, thus bypassing the blade flange and hub thread. The so-called transmissibility factor is defined as

$$Q' = 1 - \frac{(\mu \ F_T }{F_V \ \tan\beta }) \qquad (220)$$

197
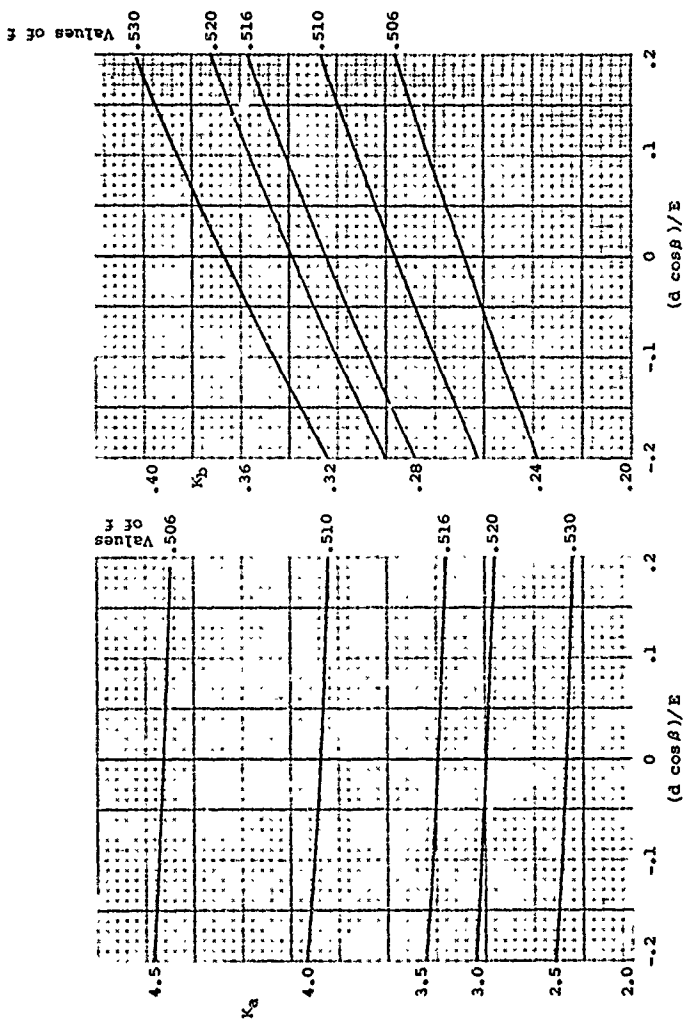
Figure 80. Bearing Contact Area Constants.

where Q = the transmissibility factor

F_T = total equivalent centrifugal force (see definition under Equation (216))

F_V = component of F_T due to vibratory moment

$F_V = (4 \ M_V/D)$

β = bearing contact angle

μ = coefficient of friction

To apply this factor, the vibratory component of the flange or thread relief load is multiplied by Q'.
This can significantly reduce the vibratory stress and thus increase the fatigue life. The value of Q' obviously depends upon the value of friction; from experiemtnal data, μ can vary from a minimumm of .052 to .212 depending on the configuration. Correlation between theoretical values of Q' and an experimentally established value is shown in Figure 81. This shows a very pronounced effect, indicating that only 60% of the vibratory load is reacted by the blade flange and thread system.

However, since there is some degree of unreliability with respect to the friction, there has been some reluctance to use Equation (220) to its full potential. It has been common practice to use a minimum value of $Q' = 0.90$ for installations having split inner and outer races, and $Q = 1.0$ for installations with an integral outer race.

Bearing K_T Factor

As a quick estimate of the adequacy of a given bearing with respect to Hertz stress the K_T factor may be used.

$$K_T = \frac{F_T}{\text{No balls} \ (d \times 8)^2} \tag{221}$$

where F_T = the total equivalent axial load - lb (see Equation (216))

d = ball diameter - in.

A value of K_T in the range of 150 to 200 would indicate that the bearing will have a satisfactory Hertz stress for the given load. Equation (221) can also be used for preliminary sizing.
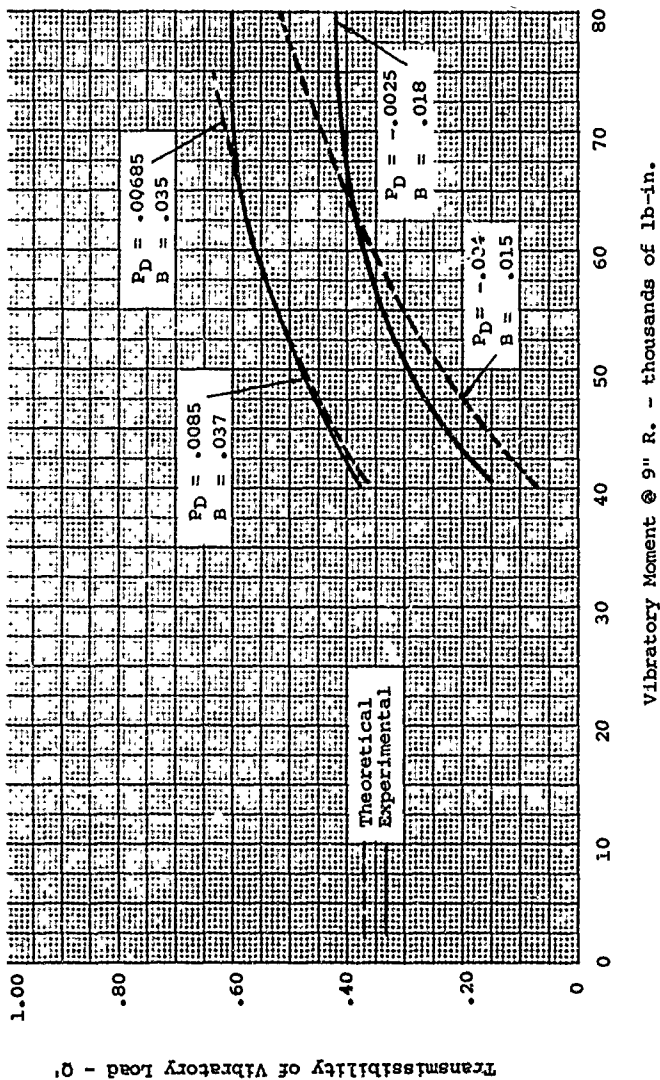
Figure 81. Comparison of Theoretical and Experimental Load
Transmissibility Factors, Q', for Two No. 2 Bearings.

Bearing Overturning

In developing the equivalent centrifugal force, Equation (203) and Figure 66 , the moment is reacted as a cosine function. It is seen that the moment forces add to the centrifugal on one side of the bearing and subtract on the opposite side. If the moment is high, one side can become unloaded, and under vibratory loads a pounding of the bearing would occur and considerable bearing damage would result.

The overturning ratio, OT, is defined as

$$OT = \frac{CF}{F_T}$$

$$= \frac{CF}{CF + \frac{4(M_{steady} + M_{vib})}{D}} \qquad (223)$$

where all terms have been previously defined.

Experience has shown that the value of OT should not be less than 0.40 for satisfactory bearing life. Propellers have been operated with OT value as low as 0.29. The resulting bearing damage was excessive – cracked balls and heavily spalled raceways. Such damage, while not catastrophic, is most undesirable and must be avoided.

It is quite apparent from Equation (221) that for a given set of retention loads, OT is dependent upon the bearing pitch diameter, D; therefore, this ratio can be used to establish the minimum bearing pitch diameter.

Hub Loads and Analysis

The basic structural elements of the propeller hub are illustrated in Figure 14. In the introductory discussion of the propeller structural elements it was noted that the hub is a highly redundant member. As such, it has not been subject to extensive analytical studies. Rather, it has been past practice to rely heavily upon experimental evaluation for the design of the propeller hub.

Initial or preliminary designs have generally been made by ratioing from previous designs. Prototype models were then subjected to elaborate test evaluation. For the purposes of this testing, the hub must be mounted so as to simulate the actual aircraft installation.

The steady-state blade loads and a static simulation of the vibratory loads are applied to the barrels through dummy blade shanks. Initial evaluations of the stress-strain patterns

201

are obtained by using strain sensitive coatings. Detailed
analysis of the more highly stressed areas is made by using
the wire strain gage. This experimental technique is obviously
time-consuming, and it is believed that as a future development,
the hub structure will be adapted to one of the more sophisti-
cated computer programs presently available for the analysis
of complex structures.

In the case of a new design where there is no past experience
to serve as a reference, the analyst must perform a preliminary
evaluation by making simplifying assumptions with respect to
the load paths and potential deformations under load of the
specific structure being considered. As a general rule, ex-
perience has shown the more highly stressed regions to be the
area between barrels, and the front ring (see Figure 14).

No standardized procedures have been established with respect
to such simplified preliminary analyses, rather the techniques
for a specific design have been left to the best judgment of
the analyst. As a qualitative guide to help visualize the
structural problem, Figure   82   has been prepared. These
sketches consider the hub as a relatively simple ring with the
various load components applied together with the appropriate
shaft reaction. For purposes of this illustration, a four-way
propeller has been assumed. The basic design loads are gener-
ated by the blade and are applied to the hub at the blade
barrels. These loads have all been previously defined, page
55. The basic loads are:

CF = centrifugal force

F_y = thrust force

F_z = torque force

M_y = thrust moment

M_z = torque moment

It must be remembered that the various load components can be
either steady state or vibratory; the predominate vibratory
component being the 1xP aerodynamic excitation. Therefore,
fatigue is a primary consideration in hub design.

The shaft reactions illustrated in Figure 82 are the loads
transmitted by the propeller to the airframe. There are
potentially six shaft load components: (1) thrust, (2) torque,
(3) normal force, (4) side force, (5) pitch moment, and (6) yaw
moment.

These loads are illustrated in Figure 14.   The source and
development of these various components have been previously

202
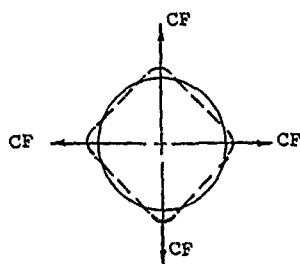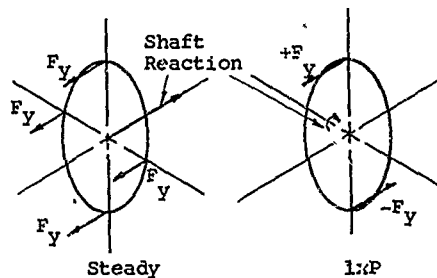
(a) Centrifugal Force   (b) Thrust Force
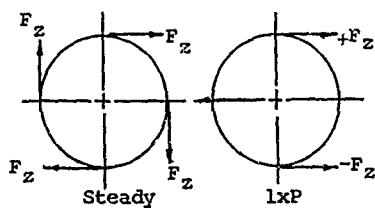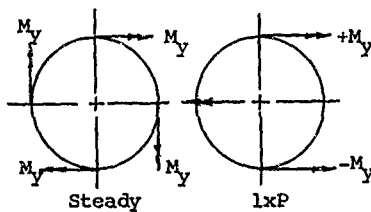
(c) Torque Force   (d) Thrust Moment
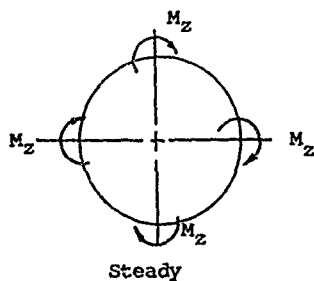
(e) Torque Moment
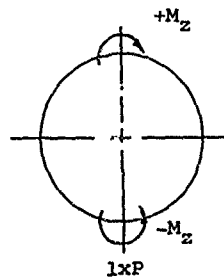
Figure 82.   Basic Hub Loads.

203

discussed in some detail in the sections on aerodynamic loads
and aerodynamic excited vibrations.

It should be cautioned that while the major components of the
shaft bending moments and radial forces are steady state, the
hub, shaft, or other supporting structure is rotating. There-
fore, a given point on the hub rear extension, propeller
shaft, etc., is subjected to a fatigue loading.

Propeller Materials

As has been noted repeatedly in the report, fatigue is the
primary consideration in the structural design of the high
performance aircraft propeller. As a basic prerequisite of
material fatigue, the designer is directed to the following
References 9 to 11.

Since fatigue is of primary importance, the propeller environ-
ment must be considered in establishing material working
stresses. During taxiing or other ground operations, stones
or other debris can be thrown through the propeller disc.
This results in bruises, nicks, scratches or other stress
raiser damage to the surface of the blades and hub. Further,
normal handling can inflict fatigue sensitive damage to the
propeller components. In addition to physical damage, atmos-
pheric conditions can influence fatigue characteristics. This
is particularly true on installations which must operate ex-
tensively in the proximitiy of sea water such as on Naval
aircraft. Manufacturing and design details can also influence
fatigue strength. These factors include such items as fillet
design, welding, plating, surface finish and residual stresses.
Considering all factors, the choice of a propeller material
should involve the guidance of a competent metallurgist or
materials engineer.

In the past the production high performance propeller blades
have used 2025-T6 or 7076-T6 aluminum alloys or steel,
SAE 4330 (UTS = 140,000 psi). Propeller hubs have been al-
most exclusively 4340 steel, 140,000 psi ultimate. The major
experience has been with these materials. Based upon extensive
material and full-scale propeller testing working Goodman dia-
grams have been established and are shown in Figures 84 and
85. It will be noted that the blade curves are based upon
nominal stress. Stress concentration effects have been included
in the curve. However, in using the diagram intended for the
blade flange, thread relief and hub structure, the theoretical
stress concentration factor should be included in the calcu-
lated stress. In the case of aluminum the 7075 material per-
mits a slightly high blade stress. However, this material has
one disadvantage: the yield stress is not too far removed
from the ultimate, and therefore any blade straightening

204

effort must be done with caution.

More recently, in attempts to reduce weight, higher hardness steels have been considered. The ultimate strength and the endurance limit increases with hardness, and a typical variation is given in Figure 86 . Some caution must be exercised, however, since certain alloys tend to become brittle at higher hardnesses. For example, 4340 steels should not be used in the 220,000 to 260,000 psi range. Working Goodman diagrams for such materials can be estimated by ratioing the allowable vibratory stress of Figure 85 by the applicable endurance limits in the case of the exposed blade. For the blade flange, retention and hub structure, the Goodman curve should be constructed which represents at least 95% probability of survival.

It has been previously mentioned that on hollow blades, high stress concentrations can exist in the region of the internal fillets at the leading and trailing edge. From a fatigue standpoint, this is further compounded by the common design practice of using a copper braze to smooth out manufacturing irregularities in the fillet radius. Tests on several typical blade sections as illustrated in Figure 83 have indicated the following nominal endurance limits for the transverse stress in these fillet areas:

Fillet Configuration	Minimum Endurance Limit psi
1. Good extruded fillet	20,000
2. Extruded with braze	12,700
3. Welded plate with braze	10,500
4. Braze, shot peened	26,000
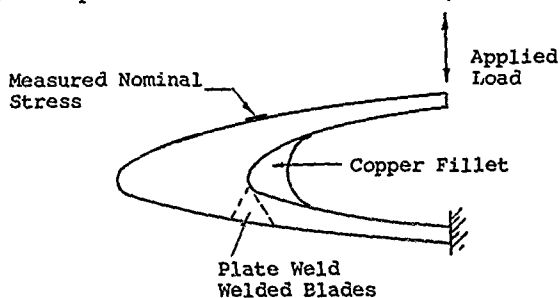
Figure 83. Typical Blade Fillet Endurance Test.

205
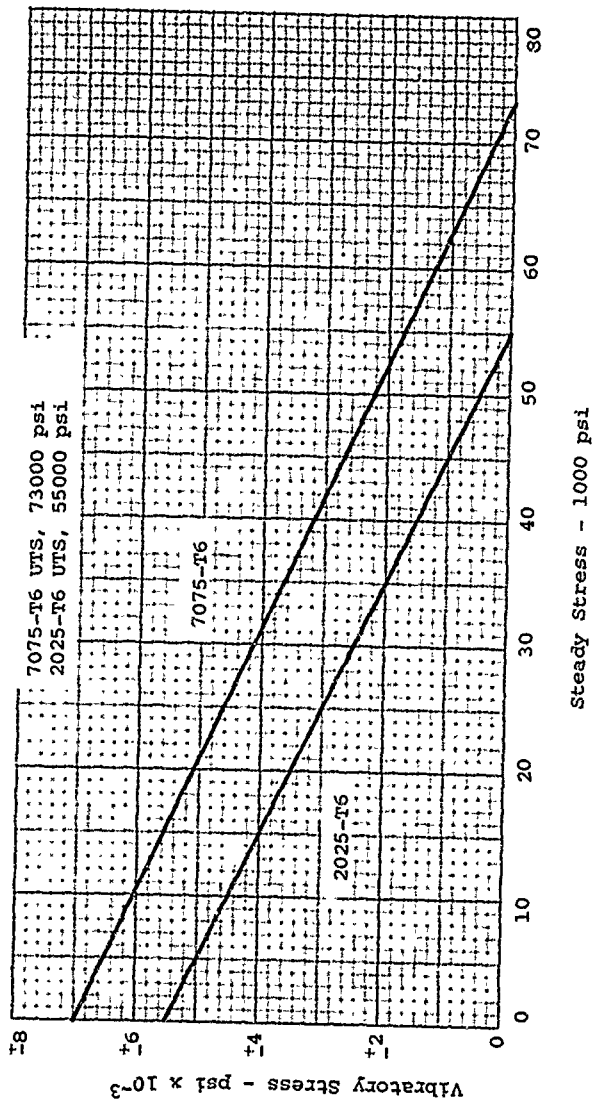
Figure 84. Working Goodman Diagram - Solid Aluminum Blades (Including Notch Effects and Factor of Safety).

206
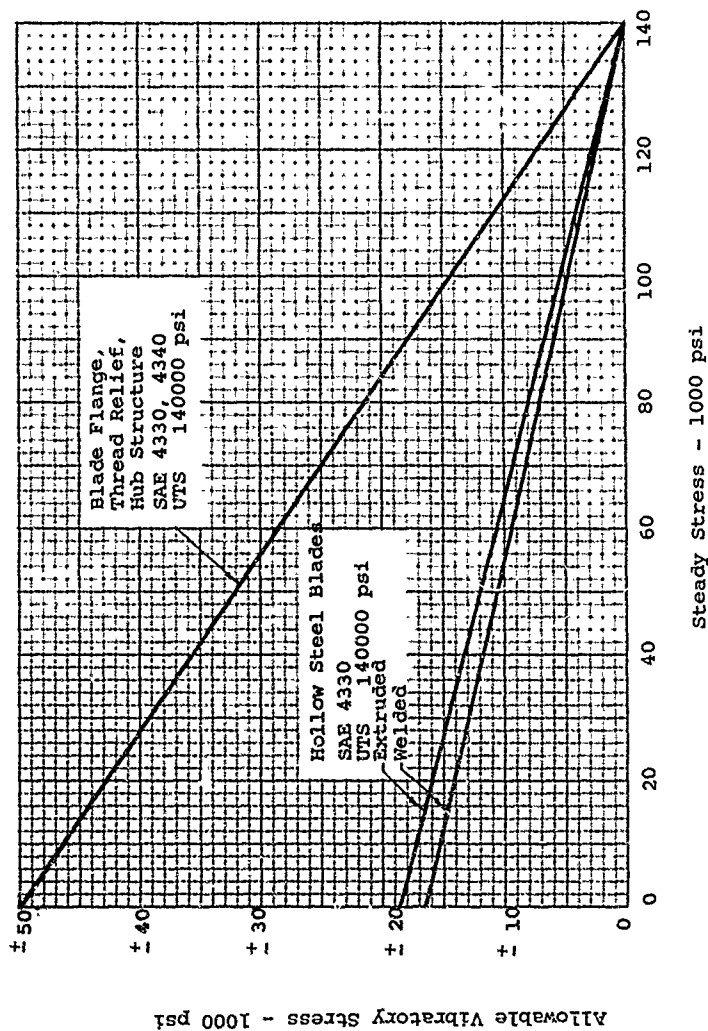
Figure 85. Working Goodman Diagram – Blade Curves Include Notch Effect and Factor of Safety.

207
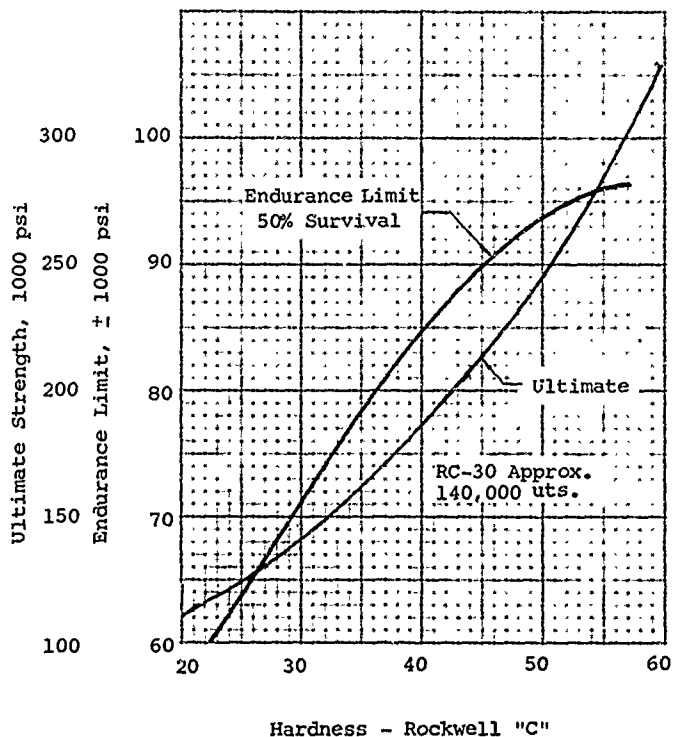
Figure 86. Variation of Material Strength
With Hardness Steel - 4340 Type.

It will be recalled that in the preliminary discussions on the
blade structural elements, it was noted that many of the high
stressed areas of the propeller were shot peened or rolled.
Such areas include the blade shank, retention thread area, and
areas of the hub. Shot peening and/or rolling is a cold
work process which improves the fatigue strength of a metal
significantly. Such cold work procedures should be used in
all high stressed areas if practical. With respect to struc-
tural design, the improvement due to shot peening is conserva-
tively neglected. And any benefit is regarded as an additional
margin of fatigue life. As a guide for shaft peening or roll-
ing, a summary of past practice is given in Tables VII and VIII.

Some preliminary design studies have been made using magnesium
and titanium as blade material. These have shown considerable
promise. However, work was not carried beyond the preliminary
stage. For reference purposes the blade Goodman Diagrams
tentatively established for two specific alloys are shown in
Figures 87.

It is believed that the next generation of propellers will
make extensive use of composites, particularly for blades.
Extensive material evaluation will be required to select the
optimum material. Successful prototype blades have been
developed using a fiber glass reinforced plastic. For the
specific layup selected the average material properties are
listed in Table IX, and the design Goodman diagram is given
in Figure 87 for reference purposes.

TABLE VII. SUMMARY OF SHOT PEENING SPECIFICATIONS

Application	Material	Shot Size	Intensity (Arc)
(1) Blade and power gear teeth	AMS 6263	SAE #P29	.0065-.0085 C 2 horizontal specimen .0055-.0075 C 2 45° specimen
(2) Bolts	AMS 6322	SAE #P28	.007 ± .001 C 2 horizontal specimen
(3) Hub extension radius	SAE 4340	SAE #P28	.006-.0075 C 2 45° specimen
(4) Hub threads	SAE 4340	SAE #P28	45° nozzle .016 A 2 $^{+.002}_{-.001}$ vertical specimen .020 A 2 $^{+.002}_{-.001}$ 45° upward specimen 15° nozzle .016 A 2 $^{+.002}_{-.001}$ vertical specimen .013 A 2 $^{+.002}_{-.001}$ 45° downward specimen
(5) Barrel ends and outside surface of barrel	SAE 4340	SAE #P28	.016 A 2 $^{+.002}_{-.001}$ horizontal specimen .016 A 2 $^{+.002}_{-.001}$ vertical specimen
(6) Blade shanks	SAE 4330 SAE 4340	Desired SAE #P28 See spec. for alter- nate	.70% or less carbon content .0200-.0250 A 2 outside gages .0200-.0250 A 2 inside round shank .0160-.0210 A 2 all other inside .90% carbon content .0188-.0238 A 2 outside .0188-.0238 A 2 inside round .0148-.0198 A 2 all other inside

TABLE VII. Continued

Application	Material	Shot Size	Intensity (Arc)
(7) Hub sections (webs, etc.)	SAE 4340	SAE #P28	.005-.0065 C 2 horizontal specimen .0035-.0050 C 2 vertical specimen
(8) Miscellaneous parts		SAE #P28	To be specified on drawing
(9) Hub barrel bore	SAE 4340	SAE #P28	.016 A 2 $^{+.002}_{-.001}$ vertical specimen .020 A 2 $^{+.002}_{-.001}$ 45° upward specimen
(10) Outboard blade sections internal and external (830-21C4 design)	SAE 4340 SAE 4330	SAE #P28	.011-.013 A 2 test specimens mounted as shown
Dural Blades	AMS 4130 AMS 4137	SAE 550 SAE 550	C2 .008-.010 axial specimens .010-.012 45° specimens .006-.010 parellel to butt face

NOTE: The time required is that to obtain the specified intensity

TABLE VIII. SUMMARY OF ROLLING SPECIFICATIONS

Application	Material	Roll Diameter-in.	Face Radius-in.	Load-lb
(1) Planet gear pin fillets	AMS 6322	2.50 2.00 2.00 2.00	Flat edge 0.023 0.030 0.035	300 500 500 500
(2) Steel blade shank	SAE 4340	2.625	0.120	645-685
(3) Dural Flade Shanks	AMS 4130	2.75 to 3.25	67% to 75% of fillet radius	2350
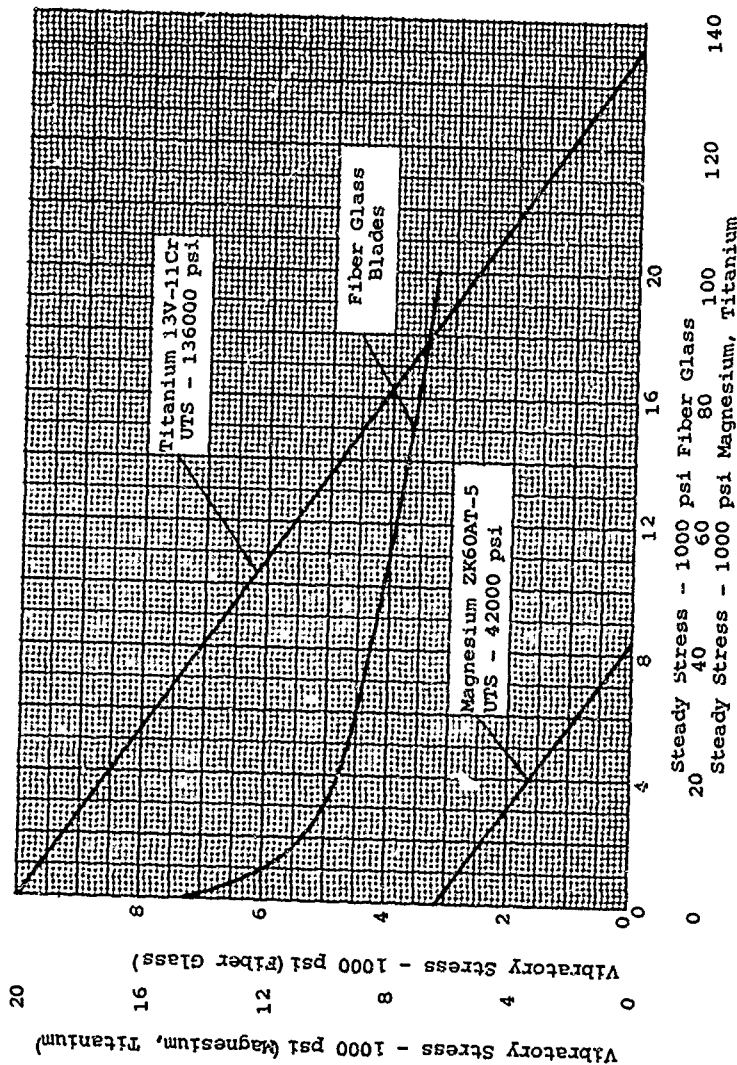
Figure 87. Working Goodman Diagram; Includes Notch Effects and Factor of Safety.

213

TABLE IX. PHYSICAL PROPERTIES FIBER GLASS REINFORCED PLASTIC BLADE MATERIAL	
Properties	Stress psi
UTS longitudinal	89,300
UTS transverse	33,500
UTS 45°	33,900
Shear ultimate	18,900
Modulus of elasticity longitudinal	4.8×10^6
" " " transverse	2.3×10^6
" " " 45°	3.2×10^6
Shear modulus	1.6×10^6
*Endurance limit, longitudinal	$\pm 11,000$
" " transverse	$\pm 5,900$
" " 45°	$\pm 7,000$
" " Shear	$\pm 3,800$
* 50 x 10^6 cycles	

PROPELLER BLADES

INTRODUCTION

A review of the recent background in propeller blade design
technology is presented to provide a basis for more advanced
blade designs of the future. The discussion will involve
design criteria, materials, construction concepts, design tech-
niques, manufacturing techniques, maintainability, reliability
and testing. Since new materials, processes and operating re-
quirements needed for V/STOL and tilt rotor aircraft will re-
quire new blade concepts, the material presented herein can be
useful as a base line to the design faced with the blade design
challenge.

BLADE DESIGN CRITERIA

Establishing design criteria is necessary to start a new
design or select a new concept of design. It sets forth the
designers goals and provides a ready check list for compromises
which will inevitably follow. For this report typical design
criteria are presented and discussed to provide a basis for
establishing the specific criteria needed for a given instal-
lation. The following are the typical design criteria, and the
specific criteria may be more or less comprehensive than shown.

Aerodynamics

    a. Aerodynamic parameters shall be chosen to be optimum
        for the installation in accordance with the latest
        state of the art.

    b. Noise will be held to a minimum by any practical means
        available. A specific level for allowable noise should
        be established.

Reliability

    a. Life of the blade shall be stated in hours or years.
        It should not be unusual to specify absolute safety of
        operation for 10,000 hours or 10 years of life.

    b. The allowable blade stresses should be selected which
        will assure that life will not be limited for this
        reason.

    c. Service damage and manufacturing imperfections will be
        considered in selecting the allowable stresses. These

allowances for service damage or manufacturing imper-
fections must be confirmed by component or full-scale
tests. A typical allowance might be the mean of a
modified Goodman curve minus 3σ divided by two.

d. Redundant load paths or an effective failure warning
system must be provided which will give warning early
enough to permit return to base or a safe landing be-
fore catastrophic failure occurs. For some instal-
lations a warning indication to shut down an engine may
be adequate.

e. Detectability of failure of a redundant load path be-
tween flights is required.

Survivability

a. Ground handling damage by unskilled personnel must be
anticipated and innovations provided for in the design
to minimize the consequences. External precision sur-
faces should be tolerant to ground handling damage or
be readily repairable.

b. Lightning protection systems shall be provided for
nonmetallic all weather blades. Protection for the
blade shall be adequate to resist repeated strokes of
100,000 amps and sacrificially one stroke of 160,000
amps.

c. Deicing systems shall be provided for all weather
blades covering at least the inboard 60% of the blade
radius and 20% minimum of L.E. chord. Heating capacity
of this area shall be equivalent to 8 watts/in^2 for a
typical cycle of 30 seconds on and 90 seconds off for
a typical installation.

d. Erosion protection shall be provided for on the entire
length of the leading edge of nonmetallic blades which
will resist both sand and rain erosion for the first 10%
of chord. The system must be field replaceable with-
out rebalancing. Metallic blades can also profit from
similar systems and should be specified where con-
ditions of the installation warrant and at least over
rubber deicing boot areas. For low ground tip clear-
ance on turboprop installations additional erosion
protection of the entire outboard 25% of tip may be
required.

e. Environmental surface protection systems shall be in-
corporated which will protect the blade inside and out
between overhauls from erosion, corrosion, fungus,

216

humidity and water. In addition composite blades must be protected from ultraviolet light and possibly ozone. The protection system and blade construction must survive temperature extremes of -65° to $+165^\circ F$.

f. Impact with foreign objects such as birds, stones, and nuts and bolts should not seriously affect the safe operation of the blade for one mission. Tests at full rpm for proving the tolerance to impact damage should be made with the items when applied at high stress blade areas. Blades thus damaged from these tests shall be fatigue tested in the laboratory to assure that adequate strength remains. Such tests may be supplemented by damaged coupon tests.

In the case of VTOL installations the ability of the blades to cut through hard wood tree branches up to some specified size such as $1\frac{1}{2}"-3"$ diameter may be required.

Extreme impact such as with a flight deck or runway shall not cause undue danger to ground personnel or the aircraft from flying debris.

g. Thermal shock resistance of the blade construction must resist repeated rapid cycling from -65° to $+165^\circ F$ without damage.

h. Bullet damage up to some caliber and type of hit must not cause a mission abort. Typically .50 caliber hits on the blade with ball ammunition tipped or untipped should be expected. It may be desirable to include larger calibers such as 20 mm and 37 mm.

i. Solvents normally found around aircraft including Mil 7808 type oils shall not damage the blade or blade finish.

Interchangeability

a. All blades of a given design must be completely and readily interchangeable dimensionally, for balance and for aerodynamic matching.

b. High service time blades may be balanced in matched sets for use where rapid blade replacement is not critical. Typically high time aluminum alloy blades which have been cleaned and repaired at overhaul a number of times but are still within service tolerances may have to be dimensionally matched and balanced against each other in propeller sets and so identified.

217

Producibility

A selected type of blade construction must be reasonably producible and cost effective. It should be reviewed against the following factors:

a. Skill level required to produce the blade which should include as much unskilled labor as possible.

b. Automation, especially of critical or time-consuming operations, should be a maximum. The use of NC machines for machining and layup of composites are examples.

c. Welds should be eliminated or at least minimized and should be automated when used.

d. Right-hand or left-hand blades should be producible with a minimum of additional tools.

e. Man-hours required must be a minimum and competitive since blades normally require more labor than material costs.

f. Work operations must be small in number.

g. Components required in a blade should be minimal. A one-piece blade is a desirable goal.

h. Compression molding shall be avoided in composite construction because of resulting wrinkling and fiber relaxation. Live pressurization expanding the laminate from the inner surface is desirable at a minimum of 100 psi. Tools must allow for raw composite room temperature bulk factors, heat up rates of heated tools must be compatible with the materials, and all surfaces to be later bonded will incorporate peel ply on the faying surfaces when fabricated or molded.

i. Reproducibility should be of a high order. Blades that are produced more identical one to the other are more desirable even though some tolerances from the drawing may be higher than desired. Tolerances must be established to suit the aerodynamic and dynamic requirements and the method of construction. Typically hollow steel blades require higher tolerances than solid aluminum alloy or molded composite blades. Molded blades are very reproducible generally.

Inspectability

Since prime reliability is mandatory in a propeller blade quality control and quality assurance are essential and the blade must be 100% inspectable.

a. Components must be inspectable.

b. Assemblies and the finished blade must be inspectable.

c. Metal components will be inspected for dimensions, contour, surface treatment and finish, and structural soundness by one or more NDT (nondestructive tests) methods for flaw detection such as magnaflux, X-ray, eddy current, ultrasonics, dye check, magna glo, etc. Sample forgings, plates, etc., will be destructively examined for grain structure, cleanliness, chemical composition and grain flow.

d. Composite components will be inspected for dimensions, contour, surface finish and structural soundness by one or more NDT systems for flaw detection such as X-ray, ultrasonics, infrared or other acceptable techniques. Fiber reinforcement may contain lead glass tracer fibers spaced at intervals as an aid to X-ray interpretation. Laminates must meet a specified size flat bottom hole ultrasonic sensitivity such as 1/4".

e. Ultrasonic sensitivity such as a 1/4" flat bottom hole will be met on all bonded assemblies.

f. Inspection procedures must be integrated with fabrication procedures to assure complete inspection and to avoid contamination of clean components.

g. Records of all inspections and quality control functions on materials, components, processes and blades must be maintained by serial number for a minimum of three years.

Maintainability

a. Finishes must be amenable to touch up in the field and should be capable of easy removal at overhaul.

b. Daily inspections and maintenance required should be limited to wiping the blades down, close visual inspection for impact damage and observation of failure warning indicators.

219

c. TBO (Time between overhauls) should be compatible with engine overhaul periods. A minimum of 2500 hours is required.

d. Component parts subject to deterioration must be field replaceable at forward bases.

e. Field repair systems and instructions shall permit minor repairs to be made on the line.

f. NDT (Non-destructive tests) must be feasible with portable equipment in the field, especially for those blade structural areas not protected by a failure warning system.

Materials

a. Aircraft quality materials shall be used throughout which have been fully qualified by coupon and full scale testing with the data statistically reduced to establish safe allowable stresses.

b. Temperature operating range of all materials shall be from $-65^\circ F$ to $+165^\circ F$.

c. Adhesive systems must conform with the specific application requirements. Adhesives which are not overly sensitive to heat up rate variations, bonding pressure and temperature ranges are required. Where dimensional variations exist between adherents, the adhesive should have good gap-filling qualities. Thermal stresses arising from the differential between temperature of polymerization and ambient shall be considered in the design.

d. Protection requirements of all materials shall be realistic.

e. Cost and availability of materials under wartime conditions shall be considered.

f. Metal selection shall consider as appropriate: cleanliness, chemical composition, forgeability, rollability, weldability, formability and ability to be cold worked for prestressing. Castings will not be used for structural components.

g. The selection of composite materials requires continuous review and aggressive programs for optimum utilization due to rapid advances in the state of the art. Materials must be chosen to be compatible with the

220

metals and adhesives used with it and the tooling and
processing concepts which will apply.

Design

a. Design concepts and constructions must be compatible
with the criteria set forth herein.

b. Weight shall not exceed the target.

c. Accuracy of design shall be maintained and methods
will be computerized wherever possible.

d. Compromises to the design criteria must be resolved
by trade-off studies.

e. Components shall be held to a minimum with internal
metal components in composite designs eliminated
wherever possible.

f. Concept selected should consider the future use of
advanced materials with minimal tool and process
changes.

g. Structural efficiency shall be optimized.

h. Tolerances specified must be realistic, keeping safety,
performance, and cost in mind.

i. Live twist allowance shall be built into the design.

Structural and Testing Considerations

a. Complete structural analysis shall include steady and
vibratory stresses, frequency diagram, and live deflec-
tions including twist and the flutter boundary.

b. Allowable stresses determined by test data and sta-
tistical reduction shall not be exceeded.

c. Resonances as shown by the frequency diagram shall be
moved outside the operating range wherever possible.
In no case will an operating rpm be within 50 rpm of
a resonance point.

d. Stall flutter and wake flutter must be avoided.

e. Full-scale laboratory fatigue tests of a minimum of
five blades, each tested in free-free flapping, free-
free torsion, fixed root edgewise and combined steady

221

and vibratory stress root end fatigue, shall be made. These tests must confirm the selection of the allowable Goodman diagram.

f. Qualification testing will include as a minimum aerodynamic calibration on an electric whirl rig, 20 hours at normal rated power or a multiple, 1 hour at 20% overspeed, 100 hours on the engine test stand at normal rated power and 10 hours at takeoff power using instrumented blades. In addition 10×10^6 cycles of overstressed endurance will be run on a 1xP gyroscopic test rig. The flutter boundaries shall be determined on the electric whirl rig.

g. Flight testing shall include a complete vibratory stress survey at all operating conditions as well as special conditions such as cylinder out operation. Resonance points will be confirmed. Performance will be confirmed. As a result of flight testing, operating restrictions, if any, will be specified.

Facilities

a. Facilities must be adequate for high quality fabrication of the design concept. All high temperature operations on metal components must be in atmosphere controlled furnaces; all composite, plastic and adhesive work must be done in dust free, temperature and humidity controlled rooms. Automation should be the maximum possible. Instrumentation shall be calibrated at frequent intervals.

BLADE MATERIAL CONSIDERATIONS

Before discussing types of blade construction it is first desirable to consider the available choices of materials. Many kinds of materials have been used for the primary structure of propeller blades. The most important of these have been wood, compreg (resin impregnated and compressed wood), Micarta (resin impregnated and compressed cotton duck fabric), aluminum alloy, steel, stainless steel (magnetic type), titanium alloy, magnesium alloy and fiber-reinforced plastic composites.

Of these various materials the ones remaining in common use are wood, aluminum alloy, steel and fiber-reinforced plastic composites (FRP). Since World War II the use of wood has been limited to low horsepower installations. Magnesium has never found much favor as a propeller blade material, although it too is used on some low power installations. Its low modulus

and softness have been limiting factors in its wider usage, but improvement in its properties is continuing and it may have future interest. Of the metals considered but not used for production blades, titanium showed much promise; active development of extruded hollow blades and solid blades was being carried out before propeller development was curtailed in this country.

With further propeller development there are some new possibilities which should be explored in the field of composites. These include the use of Boron fibers, carbon fibers and Dupont's PRD fibers. All of these materials have much higher moduli and tensile strength than either "E" glass or "S" glass. In a plastic matrix such as epoxy the broad dynamic design scope available to the designer by mixing these fibers and selecting various fiber orientations can be seen in Figure 88, compared to the narrow scope of metals. Going one more step and incorporating fiber reinforcement in metal matrices opens even further possibilities, perhaps the most important of all.

The FRP (epoxy/fiber glass) construction to be discussed later in this report is limited to a first-generation approach in which the glass material is woven "E" glass fabric used throughout the blade in a fixed orientation. On this basis both analysis and fabrication are greatly simplified and the material properties are identical throughout the blade. A more sophisticated approach to get maximum benefit from the material is to tailor the fiber orientation to each station on the blade as required and use unwoven material. When considering advanced composites such as Boron or Carbon fibers only unwoven material is available and the later approach also becomes most important because of material costs which tends to overshadow increased manufacturing complexity caused by the use of the unwoven material. Significant material improvement over the first-generation blades is possible by switching to "S" glass without a change in manufacturing technique.

Consideration of very large diameter propellers or prop/rotors approaching rotor blade characteristics and dynamics will very likely find the use of advanced composites advantageous, at least when mixed with other fiber types.

Material Considerations - Design

To meet the propeller weight specifications of new installations, especially for V/STOL aircraft, high strength to weight materials are required. This is true not only for ultimate tensile strength and yield point, but because of blade fatigue it must also have high endurance limits, especially in notch fatigue.
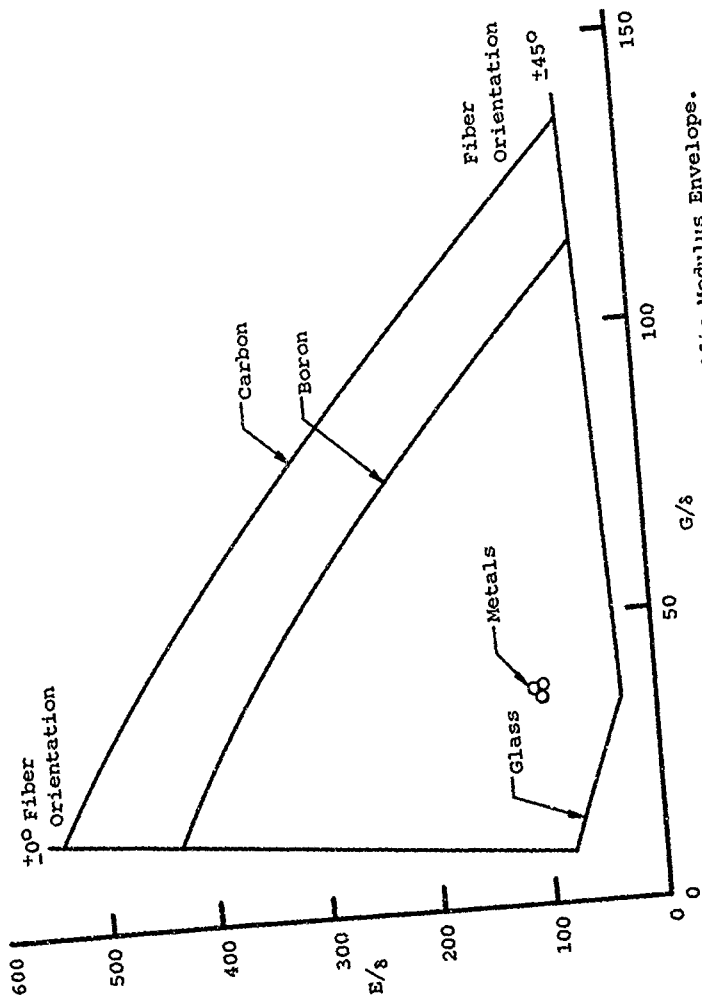
Figure 88. Mixed Fiber Composites Specific Modulus Envelope.

Notch fatigue problems are encountered with all types of propel-
ler blades due to service accumulated nicks and gouges. In
addition hollow blades have internal corners which are stress
raisers even when they are well blended with good radii. Manu-
facturing defects are another source of notches due to such
things as machining marks, metallic inclusions, porosity, hy-
drogen flakes, and weld cracks in metal blades and delamin-
ations, broken fibers and matrix bubbles in composite blades.
Stress corrosion and galling also contribute to fatigue re-
duction as well as lightning burns and arc pits. It is impor-
tant then to choose materials with low notch sensitivity and
it can be seen why brittle high hardness steels which have low
notch fatigue for example have found little favor by blade
designers despite very good plain endurance limits and high
UTS and yield characteristics.

The relatively soft fiber reinforced composites with an epoxy
matrix are very low in notch sensitivity, and the material is
thus very forgiving with respect to notch fatigue. On the
other hand these composite structures are very susceptible to
abrasion damage and must be properly protected or used in lim-
ited environments.

Young's modulus and the modulus of rigidity or shear modulus
of materials are important in connection with blade resonant
frequencies. While Young's modulus might be considered a
critical factor on blade bending due to aerodynamic thrust,
this bending load is offset by a centrifugal restoring force.
If Young's modulus is low the blade tilt or coning angle must
be increased to balance the thrust forces with increased cen-
trifugal restoring moment. In actual practice, however, blade
bending with low modulus materials has never been a critical
factor for propellers.

The more critical factor is the effect of shear modulus on
blade flutter. Since a high flutter frequency and high tor-
sional rigidity in a blade is desirable, a high shear modulus
or modulus of rigidity is needed with a low material density.
In a hollow metal blade the shear modulus is not adjustable,
thus an increase in wall thickness to get more torsional
rigidity will increase the major moment of inertia and give
little or no change in flutter frequency. The only recourse
here is to change the profile thickness. In a composite blade,
however, the designer can vary the amount of fibers oriented at
±45° to get the required torsional rigidity without increasing
the thickness ratio. This is important if the propeller is
operating at high Mach numbers where high values of thickness
ratio can cause high levels of drag.

While UTS/weight ratio has been shown to be important it should
be pointed out that in practice an allowable steady stress of
only about 1/4 to 1/3 of UTS is used to leave allowance on a

225

Goodman Diagram basis for a reasonable level of combined vibratory stress with a factor of safety. It should be kept in mind that good propeller blade design practice is to design for unlimited life allowing for all reasonable defects.

A further consideration that tends to hold down high steady stresses is establishing blade natural frequencies well above the propeller operating range. Further stress limiting factors are the need to hold manufacturing dimensions to practical levels, especially in the tip area of the blade and to control such things as plate distortion, plate buckling and resistance to impact.

Materials for use as internal support of blades and for internal vibration dampening and secondary structures such as shank fairings or cuffs must also be carefully selected. A widely used material for cuffs and fairings is urethane foam molded in place with a suitable protective cover such as fiber glass. Such fairings are considered replaceable at overhaul in order to inspect the underlying basic blade structure. They have been well proven in service and have replaced earlier sheet metal types.

Materials for use as internal cores for blades have been largely limited to those that are compatible with the basic blade processing. Most commonly internal propeller blade support has been provided by integral steel or partial ribs, internal spars, injection molded rubber ribs, foam plastic ribs and full poured-in-place foam plastic fillers. All of these approaches have had problems, and future research and development in this area could be most productive.

With organic core materials their high dampening and hysteresis can lead to severe destructive internal heating at high flutter frequencies. This is more of a problem during laboratory full-scale vibratory blade testing than it is in actual service.

All core filler material choices must consider their properties of moisture absorption, bonding, effect on corrosion, resistance to solvents and lubricants, high and low temperature resistance and low modulus to prevent overstressing.

Material Considerations - Blade Retention

Galling is a very vital problem associated with the blade retention. All blade retentions in common use are metal even on composite blades, largely because of the need for supporting the retention bearings. Wherever metal parts come in contact in a propeller galling can be a problem due to high loads and vibration. Control of galling has been accomplished by various

226

means including the use of phenolic chafing strips, cold roll-
ing, shot peening and various surface treatments such as
plating. All forms of lubricants have also been used. Com-
binations of cold rolling and shot peening have been found
very effective. In this case very high compressive surface
stresses are generated, greatly improving the fatigue strength,
and the shot peening texture retains lubricant well delaying
the onset of galling. Textured rolls have also been used.

Hollow steel blades having integral bearing races present a
special problem in local surface treatment. Normally such
blades use higher carbon steel and may make use of surface
alloying such as nitriding, cyaniding and carburizing to ob-
tain the required hardness. Such surface treatments require
special control of distortion and produce a relatively thin
skin. Flame hardening the local areas has also been used with
good results.

Material Considerations - Operational

Impact resistance of the selected material is important con-
sidering such possibilities as large foreign objects, birds,
sea water, snow banks, stones, and nuts and bolts. Impact again
tends to rule out the brittle materials and requires some de-
gree of material ductility. Material alone, however, is not
the only answer since impact resistance is often provided for
in design. Examples would be heavy thrust plates for water
impact on flying boats or snow bank impact on land planes and
solid leading edge allowances for bird impact on composite
blades and stone damage on metal blades. Impact implications
extend beyond avoiding blade flight failures and include con-
siderations of catastrophic impacts such as hitting the flight
deck where danger to deck personnel and the flight crew from
flying debris is most important. Here the blade must bend or
shatter without throwing lethal pieces over the area. Most
metal blades today meet this criterion as well as composite
blades which may shred and throw only relatively harmless light
weight core filler material. In VTOL blades impact of tree
limbs is often set as a design criterion.

The stress corrosion properties of a blade material are impor-
tant but are often taken care of by alloying or protective
coatings.

The abrasion resistance characteristics of propeller blade
materials is a most important consideration. Resistance to
rain, water spray and sand, or small particle erosion is re-
quired. Normally this type of abrasion resistance can be
provided with replaceable leading edge sheaths covering 10% -
20% of the leading edge. With a suitable leading-edge sheath
all of the blade materials are satisfactory. Steel and

227

aluminum alloy blades are often operated without any protective sheaths, but blade life can be improved with their use. Leading-edge sheaths are most often made of stainless steel or electro formed nickel and bonded directly to the blade or over rubber deicing boots which are also protected. Leading-edge sheaths have also been made of various elastomers such as neoprene and urethane and these do an excellent job in a sand erosion type of environment, better than stainless steel, but they are not very effective under rain erosion conditions up to this time.

While leading-edge sheaths will protect the blade L.E. from sand erosion, they do not protect the main surfaces which are subject to large particle abrasion such as from stones. Steel blades resist this type of damage best, but even on these added protection in the tip area is often provided in the outer 10%-25% in the form of nickel plating or a sheath. This is especially true on turboprops with high tip speeds and low ground clearance during taxiing. Aluminum alloy blades have been protected over a major portion of the blade by either nickel plating directly to the aluminum or by coating the blade with conductive rubber and then plating. Since there is a modulus difference the nickel is prone to cracking and could be a source of fatigue origin into the blade structure if direct plating is used. Plating over an elastomeric layer is better in this regard.

Composite blades are especially difficult to protect against abrasion damage. Metal leading-edge sheaths cemented to the blade tend to crack due to their much higher elastic modulus which causes high sheath stresses. While such cracks have never been shown to propagate into the basic blade they are certainly not desirable. Metal sheaths have worked on spar type blades with composite shells largely because the unit elongations are controlled by the metal spar. For a 100% composite blade, leading edge sheath protection remains a problem, at least with fiber glass composites. Urethane has been the best sheath material for composite blades so far, but frequent replacement when operated in a rain erosion environment is required. Work is continuing in this area because fiber glass rotor blades have the same problem. Titanium sheaths have been tried and may be a future possibility.

Protecting the entire blade surface of composite blades is also a problem, and requires not only protection from abrasion but from ultra violet light, ozone and natural weathering. Elastomeric urethane paints in a substantial film thickness of seven to ten mils has been effective.

228

Material Considerations - Processing

The major cost of manufacturing a blade is reflected in the amount of labor, tools and equipment needed. It therefore follows that a very important consideration is the processing properties of the material. Aluminum alloys for solid blades must be readily forged, preferably with a minimum of forging allowance to reduce machining, and they must resist warping during heat treatment and be readily bent for straightening when required. Early steel blades were made with steels like SAE 6130 which had to be oil quenched. The resulting severe distortion required excessive cold straightening with hammers and mandrels leading to gouging, cracking and high scrap. Switching to air hardening steels such as SAE 4320, 4330, etc., made possible the use of high pressure die forming and quenching which greatly reduced the hand straightening and scrap. Special attention had to be paid to weldability in choice of steels as well as cleanliness. Development of extruded hollow steel blades reduced the welding requirements somewhat but added extrudability to the list of requirements.

Composite blades require fewer tools and process steps than hollow steel blades, but more than solid aluminum alloy. The choice of the matrix material determines the curing cycle which can vary widely depending on properties. Molding pressure is generally associated with the limitations of the construction process chosen and can vary from vacuum bag molding to several hundred psi. Layup of the raw material can be costly and has been normally done by hand. Automatic layup, however, is feasible for the unwoven type of materials.

METHODS OF BLADE CONSTRUCTION - ALUMINUM ALLOY

The construction of solid aluminum alloy blades as the name implies is the simplest of all blade types and can be described as one piece solid forging machined and finished all over to final dimensions. Figure 89 shows a typical modern blade cross section and a typical root end.

The modern aluminum alloy root end is a major departure from the early double shoulder designs specified in U.S. Army Specification No. 98-29518-J. The early type was a carry-over from ground adjustable type propellers and when adapted to controllable pitch propellers required a heavy split steel sleeve with an integral blade gear.

In the modern root end the use of a flanged end requires a steel spacer ring or thrust washer in order to keep the flange proportions reasonable and the hub weight minimal while permitting a large flange root radius. The spacer thus becomes the platform for the hub bearings. Galling between the spacer

Typical Aluminum Alloy Section

Typical Aluminum Alloy Root End
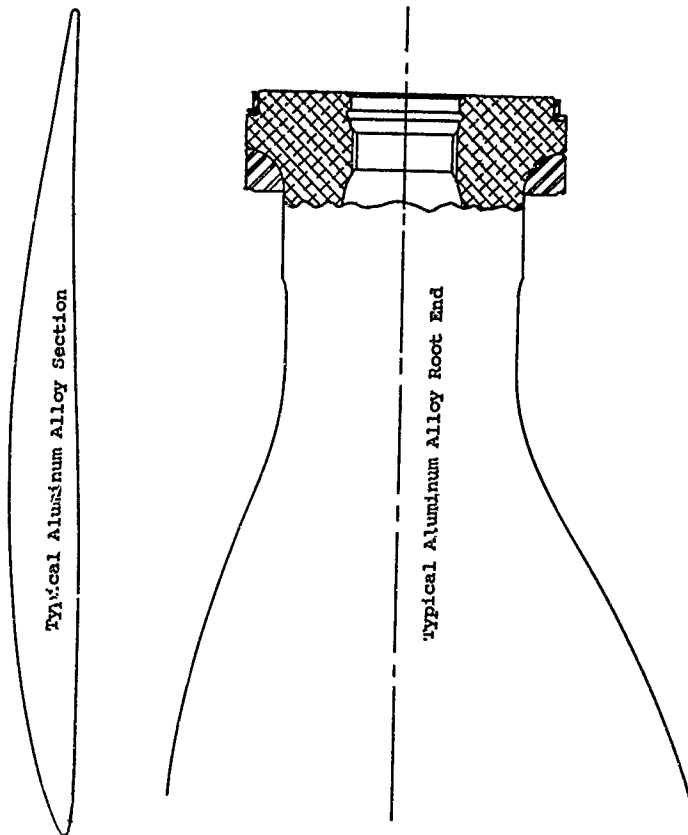
Figure 89. Aluminum Alloy Blade Details.

and the flange and under the hub bearings is controlled by heavy shot peening of the entire root end of the blade and suitable plating on the spacer and bearings. The spacer in some cases may be silver plated and in others may make use of a phenolic shim between the surfaces. It is apparent that the spacer must be a precision part and of one piece construction. It is therefore necessary to install the finished ring on the rough forging before the flange is upset, and then protect it throughout the blade processing.

Blade Finish

Shot peening of the blade surface is frequently carried out to about 30% radius to improve inboard fatigue strength. The use of highly polished blade finishes was largely discontinued during World War II and blades were given a satin finish. Surface protection normally consists of anodizing followed by painting.

Balance Provision

A shank hole is generally provided for holding balance weight such as lead or lead wool.

Fairings

Aluminum alloy blades frequently incorporate foam plastic blade shank fairings molded in place.

Development Time

Development time of solid aluminum alloy blades can be very low. Prototypes can be handmade from existing oversize forgings in many cases, or from handblocked forgings if a standard root end is used. This permits early testing aerodynamically and dynamically before committing costly forging dies and production tooling.

Survivability

Solid aluminum alloy blades like all metal blades provide a substantial radar cross section. Bullet type damage of solid aluminum alloy blades is frequently catastrophic and repair is normally out of the question except for minor edge or surface hits.

METHODS OF BLADE CONSTRUCTION - EXTRUDED HOLLOW STEEL

The extruded hollow steel blade is a structurally efficient one-piece metal blade. This conclusion is based on its efficient monocoque design and lack of welds in critical areas. While it is theoretically possible to build this type of blade with no welds, practical extrusion limitations usually mean adding trailing edge (T.E.) solid stock by the submerged melt welding technique in the outboard areas.

Basically the extruded blade concept consists of a one-piece structural blade shell supported internally by one or more rubber ribs. Because of the lack of critical welds higher allowable stresses are used than in its welded counterpart, and it is therefore also slightly lighter in weight for a given installation. Sizes up to 18'0" diameter and 2" in chord were produced. A design of 20'0" diameter and 26" chord was well under development before the program was terminated.

Extruded Tube

A typical extruded steel tube from which the blade is made is shown in Figure 90. As illustrated it can be seen that the tube incorporates leading- and trailing-edge ears with solid edges. The ears are not exactly 180° apart to give the required difference in mean perimeter between the thrust and camber sides. The external tube diameter and ear shapes are constant over the length of the ear portion of the tube. The tube I.D. varies along the length to give the required wall thickness values. The internal ear contour and depth also varies along the length to control internal edge radii and fillet thicknesses. Excess metal stock is allowed all over for finishing and removal of decarburized skins. After a series of forming operations including flattening and pressure die blowup and quench the tube is formed into its final blade shape.

Planform Shapes

Figure 91 shows that various planform shapes possible with extruded blades. The standard planform is trapezoidal as would be expected when flattening a constant O.D. tube where the resulting profile thickness is lower at the tip. The trapezoidal shape of the extruded blade is increased further because of thinner tip wall thicknesses and increasing internal ear depth which results in greater tip mean perimeters. Refined ear design reduced planform taper appreciably in later blade designs. Moderate planform shape adjustment is also possible by adding solid T.E. stock or so-called T.E. strips as shown in Figure 91.

Planform View

Enlarged
Cross Section

Thrust Side

Camber Side
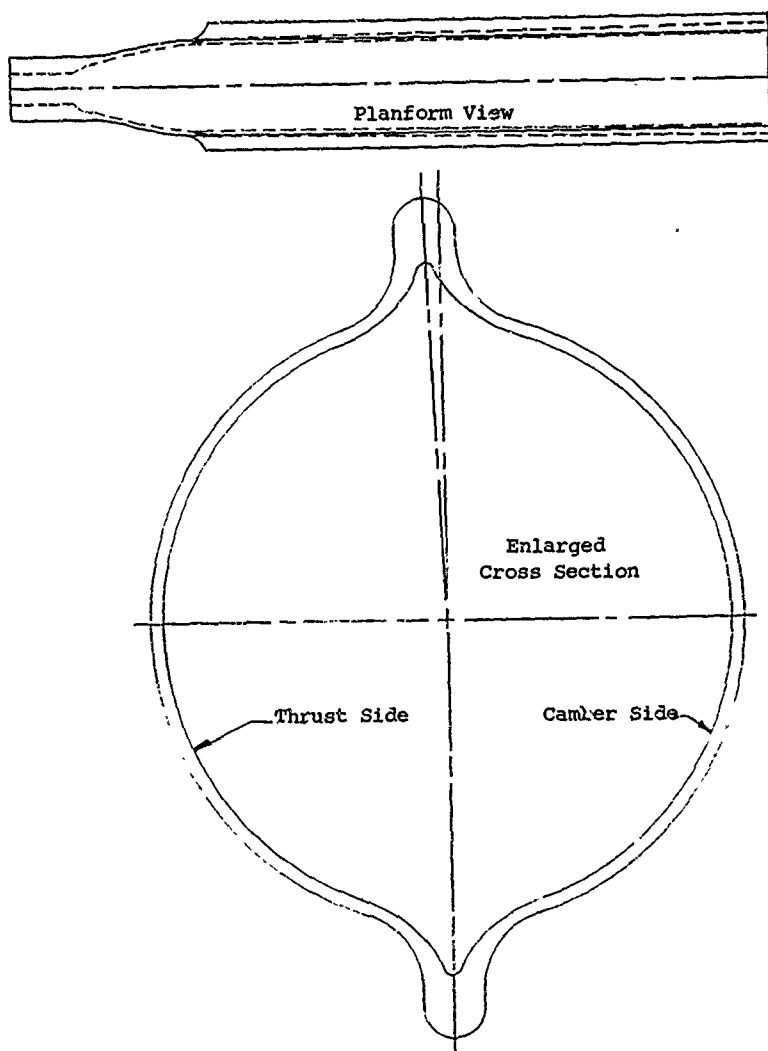
Figure 90. Extruded Hollow Steel Blade Tubular Blank.

233

With
Trailing-
Edge Strips

Standard
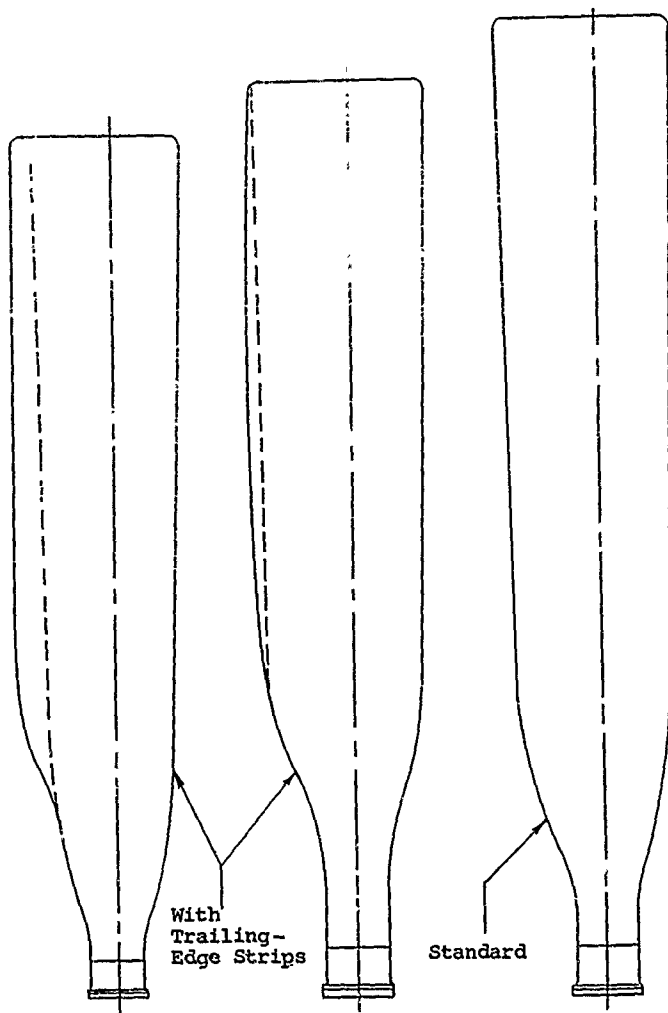
Figure 91. Extruded Hollow Steel Blade
Developed Planforms.

234

Cross Sections

Typical cross sections of extruded blades are shown in Figures 92 and 93. Figure 93 illustrates both inboard and outboard sections. The outboard section shows the normal T.E. butt weld used to join additional T.E. solid stock. On some designs this weld was very short and theoretically can be eliminated with proper extrusion capacity. It should be noted that this weld is away from the critically stressed fillet area.

While internal steel edge fillet radii of sound quality can be attained it is very difficult to magnaflux such fillets with 100% assurance, so it was common practice to add CuMn brazed edge fillets on most designs. The use of brazed fillets is a carry-over from welded blades and they do provide reliability from possible edge defects by moving the critical fillet stress away from the steel edge and into the CuMn meniscus. Such a brazed fillet does not have the fatigue strength of a sound steel fillet because of intergranular penetration of the steel by the CuMn. It does assure a consistent fatigue strength of the fillet area even if relatively gross defects exist in the steel edge. The resulting fatigue strength is one that the designer can rely on and design to.

Rubber ribs are the normal way of providing internal support to extruded hollow steel blades. As many as three ribs have been used. Such ribs can provide dampening of high frequency plate vibrations, stabilize the plates to resist buckling, support the plates against aerodynamic distortion, and provide a tip fillet to reduce the vibratory stresses at the tip clo-.sure. Rubber ribs have been used in some special cases to detune flapping or torsional frequencies of the blade.

Figure 93 also illustrates variations of extruded blade cross sections of particular interest. The center pad construction represents one way to maximize metal distribution to resist aerodynamic bending and 1xP forced vibratory stresses. The use of center pads also makes possible minimum edge fillets, and thus minimum solid edge widths. Such pads can also be an asset where impact with green water or snow is a problem. The theory, of course, is to place a higher percentage of the structure at the extreme fiber in bending. Centrifugal twisting moments are also held to a minimum with this construction while flutter frequencies can be raised.

The use of trailing-edge strips, see Figure 92, makes possible an easy way to make adjustments in activity factor. Frequently the strips are set at an angle equal to a line tangent to the basic section mean camber line. As discussed in the aerodynamic section the design C_L can be changed by varying flap angle over a very wide range in either direction. Developmentally T.E. strips can be easily added to a basic blade by
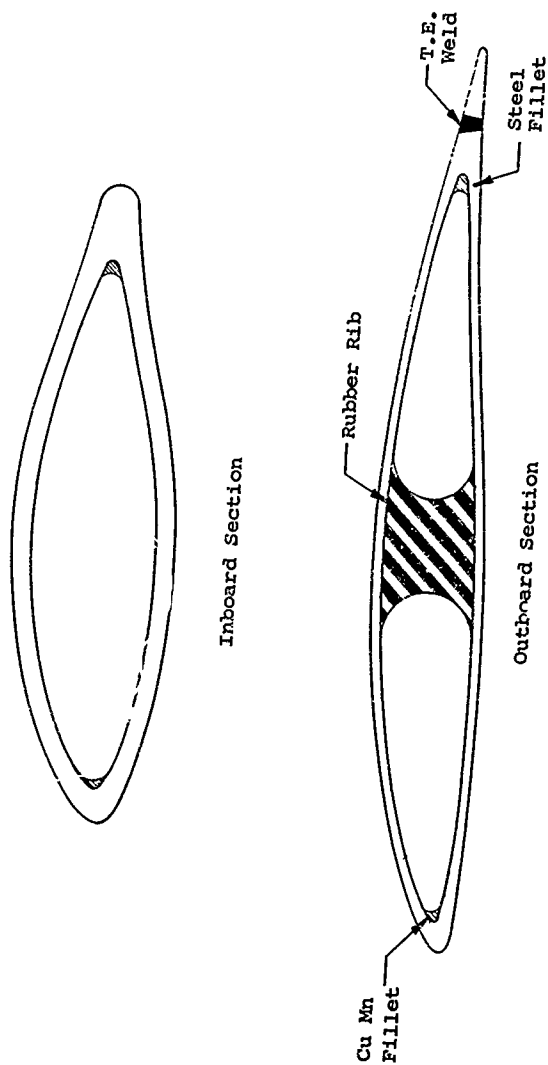
Figure 92. Extruded Hollow Steel Blade Sections.

Inboard Section

Outboard Section

Rubber Rib

Cu Mn Fillet

T.E. Weld

Steel Fillet

Section With Center Pads

Section With T.E. Strip
and
Double Rubber Ribs

Figure 93. Extruded Hollow Steel Blade Sections.

welding for limited testing aerodynamically and dynamically
to optimize the desired characteristics before making perma-
nent tooling changes. Obviously operational blades must be
made with proper tools and given the required heat treatment.

Outboard Construction

Figure 94 shows typical tip details for an extruded blade.
The normal arrangement of the rubber rib and tip fillet is
illustrated in the planform view. As shown, most rubber ribs
do not extend all the way inboard and the termination is based
largely on where the wall thickness/span ratio is high enough
to be considered stable against buckling, and where it is ex-
pected that plate diaphragming stresses will be acceptable.
Such a termination point is also usually one that is compatible
with acceptable aerodynamic profile distortion.

Also shown on Figure 94 is the typical tip closure for an
extruded hollow steel blade. This consists of a steel insert
welded and brazed in place. The braze, besides providing an
adequate fillet, penetrates between the plates and the insert,
contributing additional bonding of the insert. With the rub-
ber tip fillet and the brazed fillet plate, distortion stresses
are minimal. Other closure means have been tried such as just
the rubber fillet to seal the tip, however, in most cases the
added stiffness of the steel insert is required.

Also shown on the planform view, Figure 94, are the tip vent
holes which are an essential item on a hollow blade. Tip vent
holes are present to equalize internal pressure with atmos-
pheric pressure and minimize profile distortion. This leads
to some consideration of tip hole location to provide minimum
differential pressure, plus good drainage of internal con-
densation.

Environmental Protection

Environmental protection of extruded hollow steel blades must
be provided both internally and externally. Internally the
blade can be flushed with the adhesive used to vulcanize bond
the rubber ribs in place. The adhesive alone is good corrosion
protection but is black in color, which makes periodic inspec-
tion of the internal surfaces difficult. A light colored
paint, either white or grey, over the adhesive provides better
internal visibility and added corrosion protection.

The external surfaces of the blade after final polishing are
normally given a low intensity grit blast using fine grit and
then zinc plated followed by yellow anozinc and a clear plastic

Tip Vent Hole

Rubber Tip Fillet

Rubber Rib
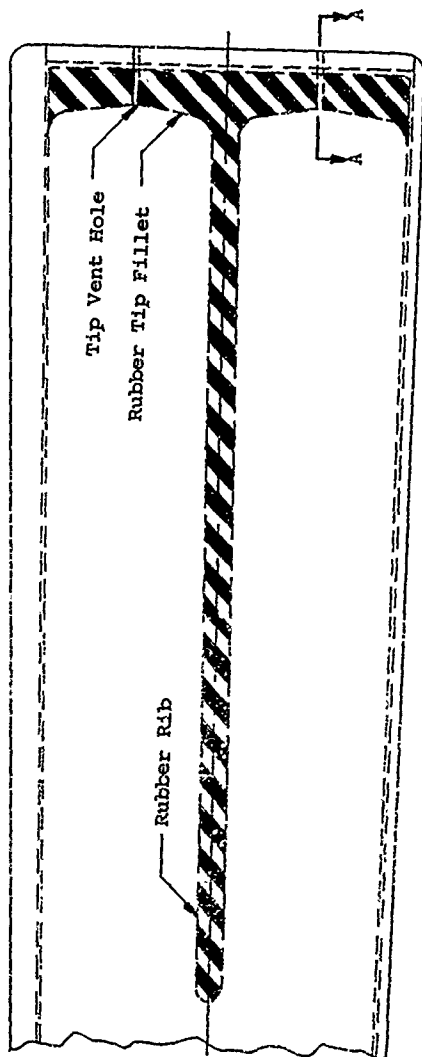
Developed Tip Planform View

Brazed Fillet

Tip Vent Hole

Weld
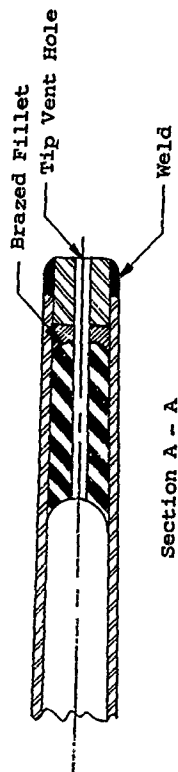
Section A - A

Figure 94. Extruded Hollow Steel Blade Tip Details.

finish. The use of this finish was specified by the U.S. Air Force after long experience with chrome plating, Houghto Black and paint and cadmium plating. Most plated finishes give rise to hydrogen embrittlement, and thus are detrimental to fatigue strength. Zinc plating is not too objectionable in this respect, and has the advantage of protecting the steel against corrosion even if bare spots develop in service because of galvanic action. The tendency for zinc to develop a white powdery oxide corrosion product in storage and under some service conditions is minimized by the anozinc and clear lacquer finish. It was felt by the U.S. Air Force that the clear finish also permitted easier visual examination of the blade surface for defects developed during service. Extensive commercial experience, however, indicated a grey painted surface was also desirable, especially for visual inspection for gouges and stone damage.

Root Ends

The root ends of extruded hollow steel blades were produced with a standard flanged shank as shown in Figure 95. Some work was done with integral race retentions also, but was never carried to production. The flanged shank has proven to be a very reliable retention with very extensive service experience. There is very little propeller weight savings with integral race retentions, and the flange shank makes use of replaceable bearings. In the event of brinnelling or other damage to an integral race retention the whole blade must be replaced. Handling of blades often results in shank damage and the flange shank retention is much less vulnerable. For this same reason blade gear splines are internal.

Typically the bearing surface and the flange root radius of the flange shank are cold rolled and shot peened for improved fatigue strength and resistance to galling. The bearing surface can be reclaimed if worn or damaged by chrome plate build-up using a special low hydrogen embrittlement type plating. The flange can be machined from the extrusion, but upsetting the flange will give better grain flow and material properties and is preferred.

Balance Provisions

Balance provisions are accomplished with a balance cup having an interference fit with the shank and sweat soldered as illustrated. A similar more readily removed balance cup with mechanical locking was also developed and widely used. This latter type was advantageous when internal inspection was required.

The area from the balance cup seat outboard several inches is

240

Balance
Cup
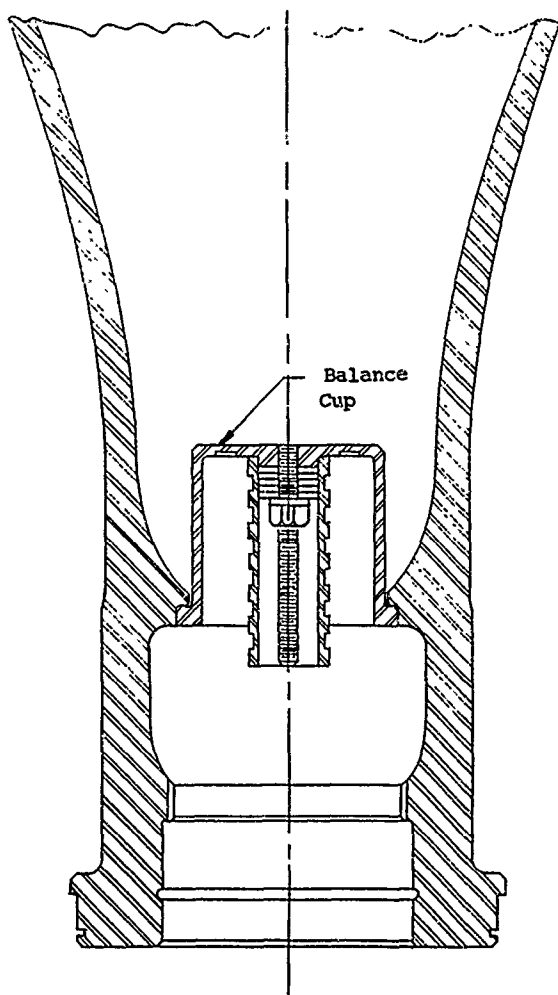
Figure 95.   Typical Hollow Steel Blade Root End.

241

normally tin plated for both types of cups and is an aid in sweating the type illustrated. In addition the tin plate protects the area between the cup and the blade on the outboard side from corrosion. It is apparent that this area is a natural pocket to accumulate moisture when a blade is in the up position.

To accomplish balance with this system lead is poured in the outer periphery of the cup for horizontal balance and for vertical balance the lead can be poured higher on one side than the other by the use of dams. The center cylinder and stud are provided for adding washers for propeller assembly balance.

Fairings

In order to continue effective airfoil shapes inboard as far as possible it is advantageous to make use of add-on shank fairings. As will be shown in the design section of this report, fairings are a weight saving and structurally desirable by eliminating abrupt changes in the primary blade structure and related detrimental secondary stresses.

Typical blade shank poured-in-place foam fairings are shown in Figure 96. Both the T.E. type of fairing and the full fairing have extensive operational experience. The foam used is a freon blown urethane type and it is self-bonding to cleaned and primed surfaces. Foam densities from 5 pounds per cubic foot to 17 pounds per cubic foot have been used with good results depending on conditions.

The full fairing normally makes use of a split fiber glass collar bonded to the shank. The collar simplifies locating the fairing mold and provides a hard point for locating and restraining deicing components.

The fairing can be protected in a number of ways such as premolded and formed covers of such things as ABS plastic, metal and fiber glass. Pending possible future developments the cover which seems to best fit the overall situation including allowance for blade tolerances is a fiber glass cover layed up and cured on the dressed fairing. Generally only one layer of a bi-directional cloth such as 181 is required with a room temperature curing epoxy resin. It is important when selecting covers and related bonding to run cyclic tests in an altitude chamber plus high and low temperature cycling. Covers may blister, bulge or crack under such conditions even though the foam has a closed cell structure. The fiber glass covers have passed such tests. Early experience with nylon reinforced neoprene covers grounded the C-124 fleet because of cover blistering.

242
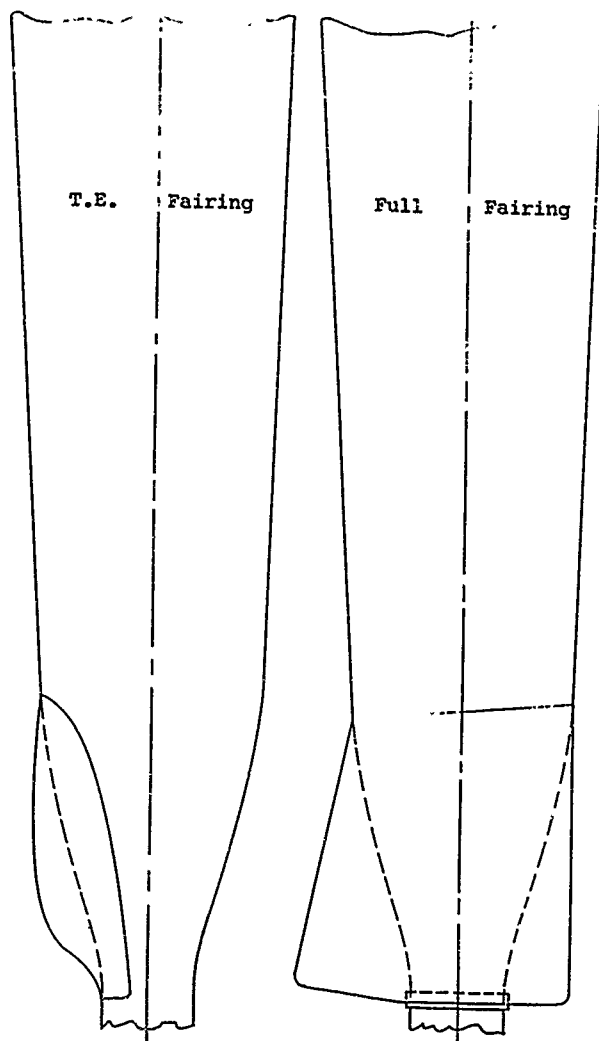
Figure 96. Shank Fairings.

Development Time

Development time on extruded hollow steel blades is quite
long compared with solid aluminum alloy blades. It is prob-
ably no longer than welded blades and reasonably competitive
with spar type blades. If the design is a minor variation not
requiring a new extruded tubular blank, development blades can
be produced quite fast for prototype work. Such variations
include design C_L adjustment, pitch distribution change, ad-
dition of T.E. strips and wall thickness adjustments. Only
the pressure form and quench die is affected by such changes.
T.E. extensions as mentioned can be handmade and welded to a
finished blade for limited test use and thus obtained very
fast.

Survivability

The radar signature of extruded hollow steel blades like all
metal blades is quite significant. Bullet damage is possibly
less catastrophic on hollow steel blades than on solid alum-
inum alloy. This is probably due to the relatively easy
penetration of the thin walls. Large numbers of hollow steel
blades returned to base during World War II with large holes
from .50 caliber and 37 mm hits. Such blades, as with all
metal type blades, are not repairable.

METHODS OF BLADE CONSTRUCTION - WELDED HOLLOW STEEL

The welded type hollow steel blade construction was for many
years the only successful hollow steel blade and was produced
in large quantities. It was gradually phased out in favor of
the extruded blade with its obviously greater structural in-
tegrity. However, the welded type blades had many advantages
and with the possible advent of improved welding may still be
of future interest.

Description - Side-Welded Blades

The original type of welded hollow steel blade developed by
Pittsburgh Screw and Bolt under the Dicks patent, and later by
Curtiss-Wright, was the so-called side-welded configuration
and constituted the bulk of welded blades produced. It con-
sisted of two formed plates welded together.

Welded hollow steel blades were produced in a broad variety of
configurations and in sizes up to 19'0" in diameter and chords
of 21". Planforms could be of almost any conceivable shape,
with curved edges, straight edges, round tips, square tips or
elliptical tips.

Figures 97 and 98 illustrate the most important variations
of this concept as fully developed. The early side-welded
blades had no thickening of the steel plates at the weld line
and no brazed fillet and no internal support with the early
narrow planforms. Longitudinal cracks developed readily at
the edge bond lines due to plate vibrations until the refine-
ments shown were introduced. With these refinements service
lives well over 30,000 hours are common.

A majority of side-welded blades were welded 100% by hand with
atomic hydrogen welding. Later atomic hydrogen was used solely
for the first tie in beads joining the two plates or shells.
The fill-in beads were then added automatically with submerged
melt welding. The use of thickened plate edges or steel fil-
lets greatly reduced the edge stresses at the weld line and
the brazed fillet displaced the peak stresses further away
from the tie-in weld bead with its irregular edges, lower
strength weld material and minor weld defects.

As shown in Figure 97, the use of partial steel ribs was effec-
tive for reducing plate distortion and vibrations on blades
with intermediate plate thickness/span ratios. The theory was
that while one station wanted to vibrate up, the adjacent sta-
tion wanted to vibrate down; and being tied together by the
partial ribs, the result was considerably dampened. As the
blade activity factors went up, it was necessary to use rubber
ribs or full steel ribs as shown in Figure 98. Full steel
ribs, of course, are not possible with extruded blades.

Variations possible with welded blades are further shown in
Figure 98. While an extruded blade can have center plate
pads, they must be equal in thickness or extrusion would be
impossible. The differential center pads shown make use of a
heavier pad on the camber side than on the thrust side of the
blade. With this arrangement the C.G. is moved more nearly to
the center of the section, equalizing the distance to the ex-
treme fibers and thus reducing the 1xP forced vibratory
stresses on the camber side where they otherwise would be a
maximum. Therefore, for equal section area, minimum 1xP
stress levels result.

The use of heavy thrust plates was effective for two types of
operating conditions. First, it resists green water impact
such as on flying boats;   second, it provides increased
abrasion damage allowance on installations with low ground
clearance since most such damage occurs on the thrust side.

Description - Edge-Welded Blades

A second type of welded blade was produced called the edge-
welded type of blade made from two clam shell plates. This

245

Weld

Inboard Section

CuMn Fillet

Weld

CuMn Fillet

Weld

Outboard Section With T.E. Strip

Partial Ribs

Weld

Weld

Outboard Section With Partial Ribs
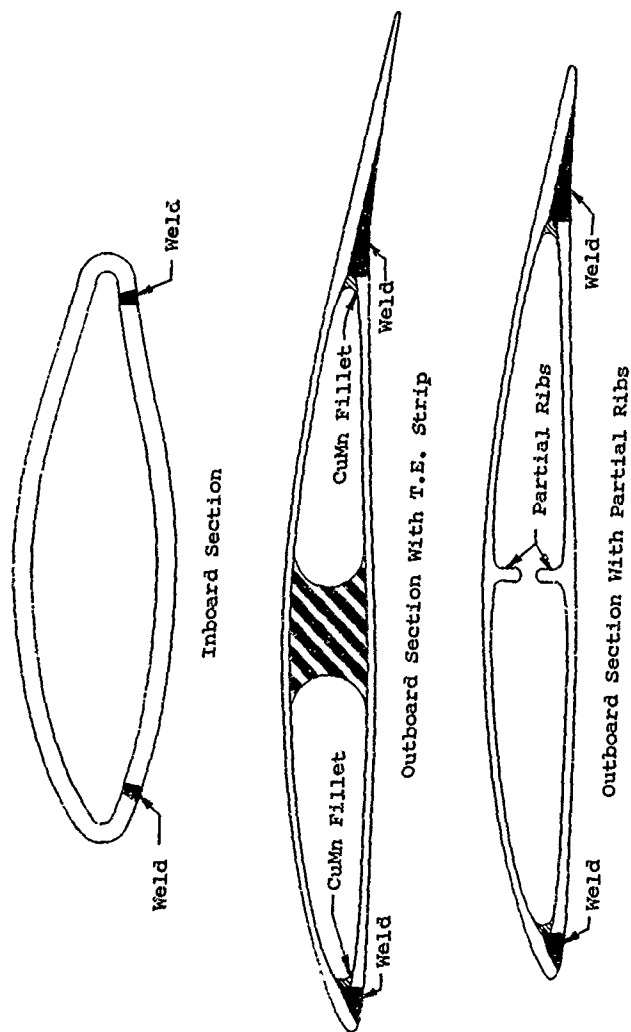
Figure 97. Side-Welded Hollow Steel Blade Sections.
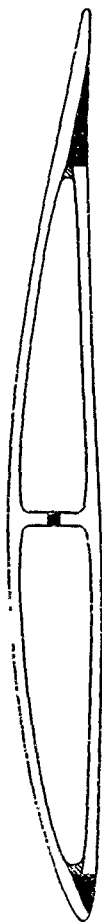
Steel Rib Section

Differential Center Pad Section

Thick Thrust Plate Section

Figure 98. Side-Welded Hollow Steel Blade Sections.

concept was conceived because it allowed for 100% automatic
submerged melt welding and resulted in very good internal
steel fillet radii. Figure 99 illustrates the basic concept.
While it had been hoped that this approach would eliminate the
need for internal edge brazing, it suffered the same internal
magnaflux interpretation problems as mentioned for the extruded
blade. Although a number of blades were produced without
brazed fillets, it became more economical to add them. Edge-
welded blades can be produced in all the configurations
mentioned for side-welded blades.

Inboard Weld Geometry

Figure 100 shows the general arrangement of the inboard weld
configurations on the two types of welded blades. Actually
the side-welded blade was also produced with two shank welds
instead of with the turnover construction shown. While this
was added to the weld metal in the root end it was more nearly
located on the neutral axis except at very high blade angles.
Of course, since all welded blades had the root end upset to
form the flange most of this weld metal had some refinement of
structure and better properties than ordinary welds.

Producing welded blades requires special care in getting steel
with good weldability both in plate stock and welding rod.
These must be closely controlled both by analysis and actual
weld tests before acceptance.

General - Welded Blades

The comments made under extruded blades covering retentions,
environmental protection, internal supports, T.E. strips,
radar signature, bullet damage and shank fairings apply equally
to the welded type blade.

Development Time

Development time of welded blades is perhaps slightly longer
than for an extruded blade because of the multiplicity of tool-
ing required. As in the extruded blade minor design variations
can be incorporated readily, especially minor plate thickness
changes.

METHODS OF BLADE CONSTRUCTION - COVERED SPAR HOLLOW STEEL

The covered spar type hollow steel blade has remained a major
hollow steel blade concept since shortly after World War II.
The basic concept goes back to patents by Brauchler and was

248
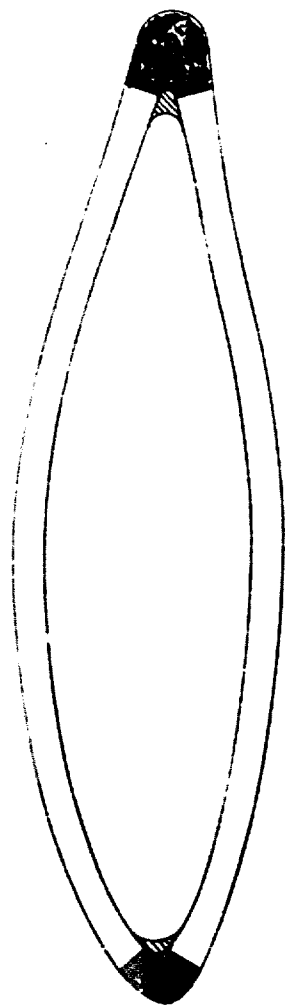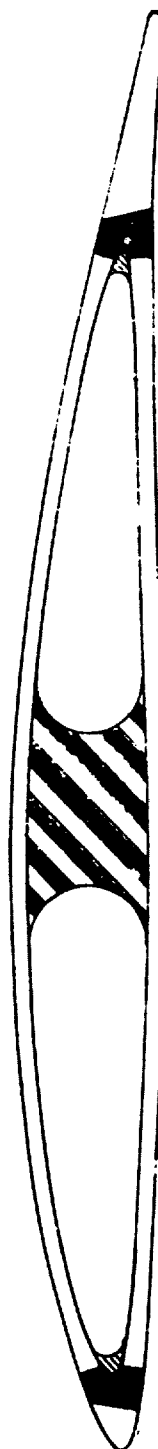
Inboard Section

Outboard Section

Figure 99. Edge-Welded Hollow Steel Blade Sections.

T.E.   L.E.   T.E.   L.E.
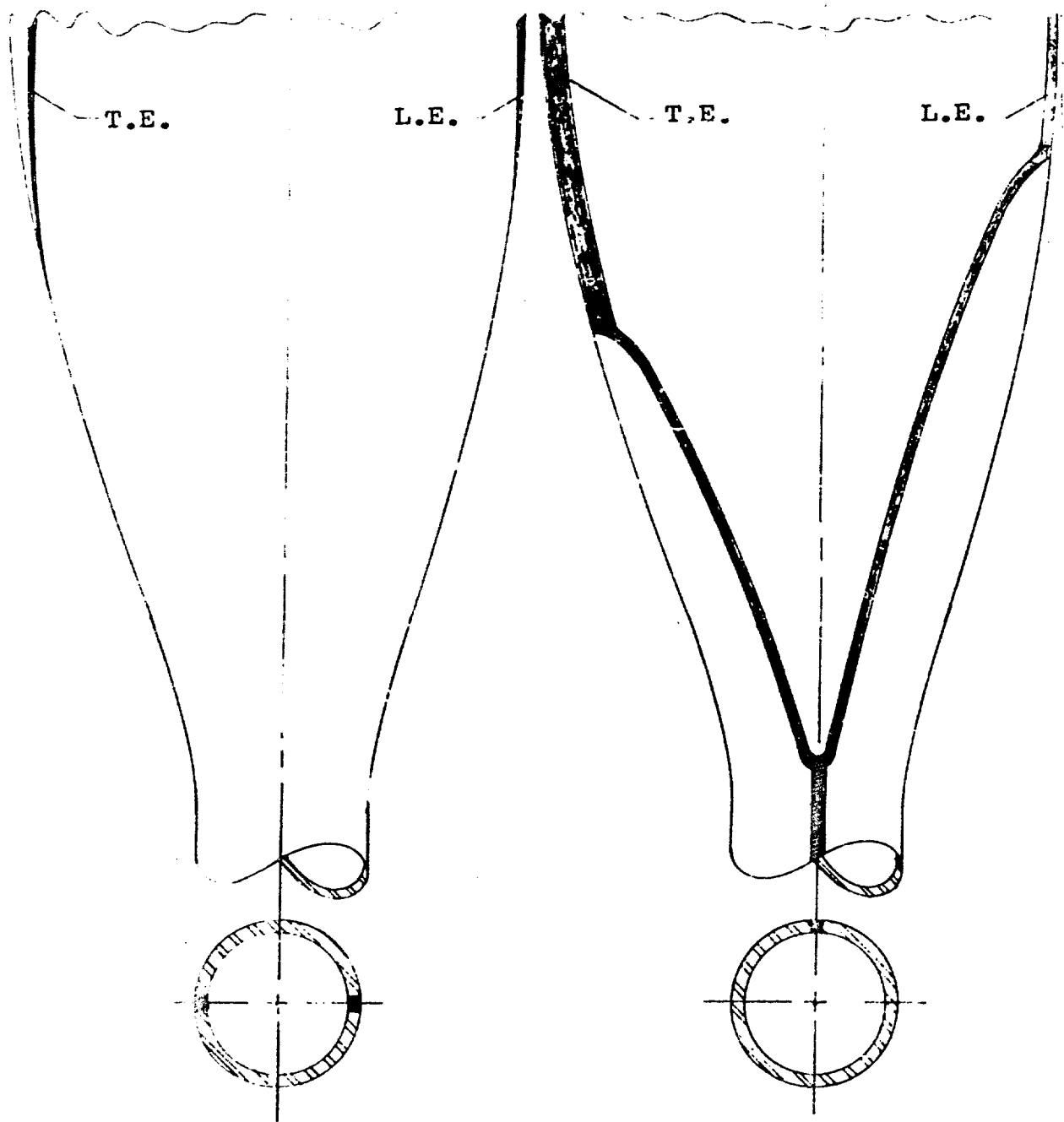
Edge-Welded Clam Shell   Side-Welded With Turnover

Figure 100. Inboard Geometry on Hollow Steel Blades.

250

evaluated by most of the major propeller producers and adopted and produced in quantity by one.

Description

Figure 101 illustrates the general configuration of the spar type of blade consisting of a single piece spar and an external shell. Considerable variations in detail are possible. The spar made from a seamless tapered wall tube is the major load carrying member and supports the thin walled shell which provides the desired aerodynamic shape. The two pieces are joined by brazing. Normally the planform shape is rectangular but variations with tapering tips are feasible.

Ideally the shell is made as thin as practicable but will not always permit unmodified leading-edge aerodynamic radii in the outboard profiles because of minimum internal bend radii requirements. Due to the thin shell at the leading edge a brazed fillet may be incorporated to provide support and resistance to stone impact. Additional erosion protection is often provided the thin shell. A resistance weld at the trailing edge of the shell requires a brazed fillet because of the sharp reentrant corner produced. While somewhat less durable than blades with a solid steel leading edge, the covered spar blades have given only fair service. Problems with cracks and corrosion have been encountered with this type, requiring complete blade replacement in the case of one installation.

Foam filler internal support is required to support the thin shell either side of the spar, and in some cases the spar itself may also be filled. Because of the thin shell and semi-resilient support of the foam, this type of blade is subject to foreign object impact denting to a greater degree than other types of hollow steel blades.

It is not known if T.E. strip airfoils have ever been incorporated on spar type blades, but it should be a feasible option. Adjusting C.G. position for best 1xP stress by the use of the differential pad effect appears to be very difficult.

Fairing

A shank fairing or cuff is a necessary requirement on spar blades because of the type of shell terminations used, and is accomplished similar to the foam fairings described earlier.
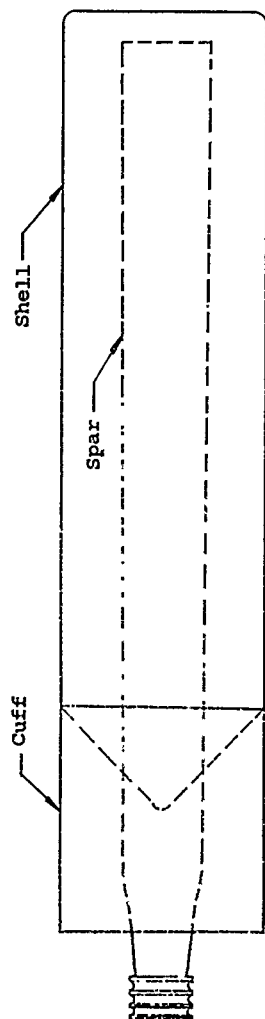
Developed Planform
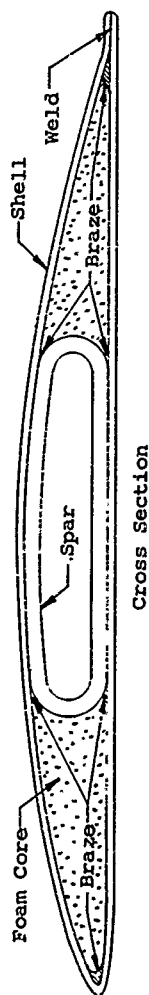
Cross Section

Figure 101. Covered Spar Hollow Steel Blade.

252

Root End

Root ends common on the spar type of blade generally were the integral race retention. As mentioned earlier damage in service or handling with this type of retention could mean rejection of the entire blade. Other type root ends such as the flange type can readily be incorporated.

Materials

It is apparent that the spar construction can be produced in a variety of metal choices such as aluminum or titanium, and has also been produced with fiber glass shells and a steel spar.

General - Spar Type Blades

The comments made earlier on environmental protection, radar signature and bullet damage of hollow steel blades also applies to the spar type hollow steel blade.

Development Time

Development time of spar type blades is competitive with other types of hollow steel blades. Minor design variations can be incorporated about as readily as on the other type of blades also.

METHODS OF BLADE CONSTRUCTION - FIBER-REINFORCED COMPOSITE COVERED SPAR TYPE

Fiber-reinforced composite-type propeller blades can be built in a variety of ways. The two most common are the monocoque and covered spar types. To date the composite material used has been epoxy/fiber glass but advanced composites such as Boron, Carbon, PRD and Borsic can be used for future blades where required.

It is apparent in the covered spar blade using a steel spar and composite shell that the reinforced plastic is used more as a fairing structure so that less than maximum benefit is gained from its excellent structural/weight properties. Its unit strain is limited by that in the steel spar and with a modulus ratio of close to 10:1 the unit stresses are about 1/8 to 1/10 that in the steel. The combination does have two advantages. One is that an electro formed nickel leading-edge abrasion strip can be used without excessive stresses in the nickel, and the other is that the shell protects the spar from

253

abrasion damage. Some weight reduction over an all steel spar
type blade can be achieved.

METHODS OF BLADE CONSTRUCTION - FIBER-REINFORCED COMPOSITE - MONOCOQUE TYPE

The monocoque fiber-reinforced blade as developed achieves a
significant weight reduction over its all steel counterpart.
Weight studies have shown reductions of the order of 35% to
50%. This is obtained in spite of the need for a hollow steel
stub root end. Elimination of the stub root end in future
development could give further weight reduction.

The development of fiber reinforced composite blades was stimu-
lated by the need for lightweight blades on early VTOL air-
craft such as the X-100, X-19, XC-142, CL-84 and X-22.
Development was further highlighted by the need for very high
static thrusts and ability to resist very high 1 X P loadings
due to high AQ's, especially during transition from hover to
level flight.

Figure 102 illustrates the monocoque fiber-reinforced blade
concept and its essential elements. The blade consists of a
tapered wall, seamless monocoque fiber-reinforced plastic
shell high-pressure molded around a bell shaped alloy steel
shank. The steel shank is designed for mechanical restraint
to the monocoque shell for fail safe reasons but is also bonded
to the shell. The internal blade cavity is partially filled
with a pour in place low density rigid foam plastic. A con-
ventional fiber glass covered foam plastic blade shank fairing
or cuff may be added if required. The blade cross section is
produced with excellent internal fillet radii. Because of the
use of a foam core thickened edge fillets are not required.
The cross section does incorporate the desirable solid edges
for durability. The strength of the solid L.E. is adjusted to
absorb bird impact.

Variations

Considerable design innovation is possible in monocoque fiber
reinforced composite blades. Center pads with or without dif-
ferential wall thickness can be incorporated as well as T.E.
strip profiles. While rubber ribs can be used they appear to
have no advantage with the low modulus composites as compared
to foam filling. The need for outstanding foam materials
should be stressed and much work can be done in this area.
Present foams must be considered marginal. Work has been done
on incorporating sandwich wall construction in composite mono-
coque blades using balsa for the sandwich core. A variety of
core material can be used in the sandwich wall including Nomex

254

Steel Shank

Foam Ending

Developed Phantom

Foam Core

Cross Section
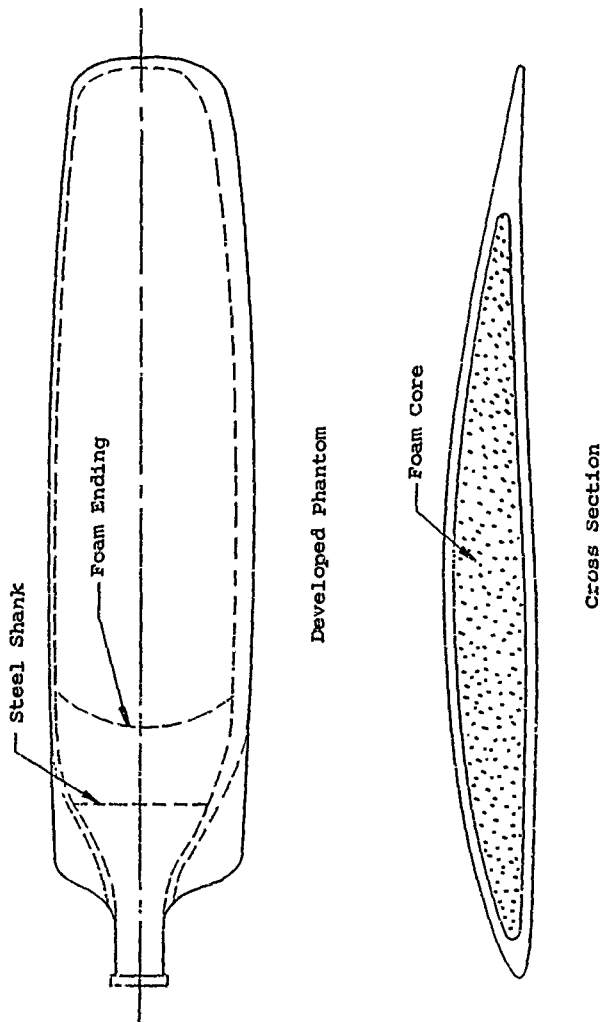
Figure 102. Fiber-Reinforced Composite Blade.

honeycomb and fluted fiber glass cores. This construction
leaves the internal cavity open for inspection. Future blade
development should give serious consideration to sandwich wall
construction for minimum weight designs.

Erosion Protection

A leading-edge erosion protection strip is mandatory on fiber-
reinforced composite blades which tend to erode in sand or rain
readily. Metal strips such as stainless or titanium can be
used but are prone to cracking under the high unit elongations
of low modulus composites although such cracking does not seem
prone to propagate into the basic blade structure. Elastomeric
urethane strips provide good protection but must be replaced
often if flown in rain. They resist sand erosion better than
most metals. Leading-edge erosion protection remains an area
where much research and development needs to be done not only
for composite propeller blades but rotor blades as well.

Environmental and Lightning Protection

Normal environmental protection of composite blades can be
provided with a heavy coat of elastomeric urethane paint.
This not only provides erosion protection but protection from
weathering, ultraviolet light and ozone. Perhaps the most dif-
ficult protection required on composite blades is lightning
protection. Laboratory full-scale lightning tests indicate
that an unprotected composite blade will be catastrophically
damaged by a lightning strike.

Grounding a metal L.E. erosion strip can give protection in
the laboratory, but the question remains, will natural light-
ning always be attracted to the grounded strip. It may be
found necessary to incorporate a Faraday cage effect, a metal
mesh over the blade or metallize the blade surface.

Survivability

With certain types of radar the all composite blade will allow
the waves to pass through, giving a minimal signature. However,
this is not probably true with most radar bands today. The
composite blade does offer some hope of incorporating radar
absorbing type structures which may be of future interest.

Bullet damage on composite blades will vary with the type of
construction and laminate. On a steel spar type blade with a
composite shell the problem of a hit in the spar area is of
major concern. On the monocoque blade away from the steel
shank and assuming high pressure molded fiber glass cloth the

256

structure permits very clean holes that are both highly sur-
vivable as proven by full-scale fatigue test and readily re-
pairable. If the structure is unwoven fiber glass molded at
relatively low pressures considerably more damage is experi-
enced in the form of delamination and brooming of fibers over
a much larger area.

Development Time

Development time of composite blades in the case of the mono-
coque type is very short compared to hollow steel blades.
Prototypes have been produced for test from preliminary design
drawings in as little as 90 days. The development of the spar
type composite blade is governed by the flow time for the spar.

RELATIVE BLADE WEIGHTS

It is difficult to make meaningful comparisons of relative
blade weights since practices by different manufacturers vary
as to design allowables, damage allowances, and durability
features. To further complicate the problem, data on weights
by different companies is not generally available and certainly
not for consistent design conditions. An added factor in com-
paring blade weights is that the advantage of one type of blade
over another will vary with blade size. For example, an old
rule of thumb says that hollow steel blades are advantageous
compared to solid aluminum alloy blades at diameters over 13 ft.
Since this rule is based on blades with fairly narrow planforms
it probably is not valid for modern high activity factor type
blades. For geometrically similar blades the solid aluminum
alloy blade will vary as follows:

$$\text{Weight} = K(AF)^2 D^3$$

For geometrically similar hollow steel blades the relationship
becomes

$$\text{Weight} = K(AF)D^2$$

where   K = a constant
       AF = activity factor
       D = diameter

Comparing the above relationships it is apparent that solid
blade weights increase much more rapidly with both solidity and
diameter than hollow blades. With modern high-solidity blades
it is likely that hollow blades have a weight advantage over
the usable spectrum.

Solid Aluminum Versus Hollow Steel

To estimate the weight of solid aluminum alloy blades compared to hollow steel blades of the same geometrical shape, the following approximate relationships are used:

where   h = profile thickness
           b = chord

Section area (solid) = .745 h b

Section area (hollow) = .186 h b

$$\frac{\text{Area (hollow)}}{\text{Area (solid)}} = \frac{.186}{.745} = .25$$

$$\frac{\text{Density (steel)}}{\text{Density (Aluminum)}} = \frac{.284}{.101} = 2.81$$

or $$\frac{\text{Hollow steel weight}}{\text{Solid aluminum weight}} = .25 \times 2.81 = .702$$

From this we can probably safely say that monocoque hollow steel blades weigh only 75% as much as solid aluminum alloy blades.

Relative Weights

If it is assumed that spar type hollow steel blades are about equal in weight with monocoque hollow steel blades, the following comparison can be made where the blades have been established for the same operating conditions.

TYPE OF BLADE	RELATIVE BLADE WEIGHT
Solid Aluminum Alloy	100%
Welded Hollow Steel	83%
Extruded Hollow Steel	75%
Covered Spar Hollow Steel	75%
Hollow Monocoque Fiber Glass	45%

RELATIVE BLADE COSTS

Blade costs can only be treated in a very general way and can vary widely depending on special features such as center plate pads, type of finishes, type of internal support and type of retention. Extruded hollow steel blades and welded hollow steel blades are close to the same cost with a slight advantage for the extruded blade due to lower manufacturing rejections. Spar type hollow steel blades are known to be

competitive, but may run more or less compared with extruded blades.

Data available would show very generally that solid aluminum alloy blades cost about 20%-25% as much as extruded hollow steel blades, and composite monocoque blades without ever reaching full production status can be forecast to run about 45% as much as extruded hollow steel blades.

BLADE DESIGN

The overall procedures and considerations for the design of propeller blades are presented to illustrate the steps necessary. In developing a basic blade design it is desirable to have a configuration that has smooth overall contours. Therefore, abrupt changes in blade contour should be avoided in both planform shape and profile thickness distribution. All blade surfaces should be smooth and well faired to avoid poor aerodynamics, structural instability or stress raisers.

Abrupt changes in planform shape are tempting, especially in the inboard areas in order to bring true airfoils as far inboard as possible for good performance and ram recovery. This is seldom warranted for the basic structure except possibly for a solid steel supersonic type blade where a fairing would not be durable enough. Flairing the shank area of a solid blade results in high stress concentrations at the juncture with the round root, high shear stresses and a weight penalty. For this reason separate cuffs or shank fairings are used which reduces weight and provides the needed contour.

In the case of a hollow blade, shank planform flair results in a more serious increase in secondary stresses. With such a condition the resulting flaired stress lines from the outboard blade loads want to realign themselves to be in line with the round shank. The blade edges overhanging the round shank therefore want to move outboard and towards the blade centerline resulting in a tendency for reduced chord and increased profile thickness and also resulting in high stresses at the juncture with the round shank.

The increased profile thickness also amplifies a tendency for a similar distortion due to the flair of the profile thickness distribution coming in to the round shank. This later condition is referred to as the bow string effect and can be visualized as a tendency for the blade loads to want to straighten the concave curve as seen in an edge view of the blade. The resulting total profile distortion produces high secondary stresses which are a maximum at the blade edges.

Abrupt changes in blade structural shape must be avoided in

259

the inboard area of the blade and the desired planform shape
for good blade performance or engine cooling obtained with the
use of a secondary cuff structure.

Blade Planform - Design Limitations

It has already been shown that basic planform shape is limited
for extruded hollow steel blades to a trapezoid with minor
variations possible by the use of T.E. strips. Internal con-
struction details and extruded tube ear design envelope will
have a bearing on the exact amount of flair in the edges. The
final planform shape can only be arrived at by some cut and
try by the designer with experience playing a large part in
his ability to select a producible shape.

Similarly, the spar type of blade is limited to what the de-
signer can do with the spar shape and the covering shell with-
out having excessive overhang of the shell to the spar and
maintaining structurally efficient shell/spar proportions.

All other blade construction types covered in this report are
relatively unlimited in choice of planform shape.

Choice of tip shapes for extruded hollow steel blades is lim-
ited primarily to the square or radial arc tip. Spar type
hollow steel blades are also limited in choice of tip shape,
since the external resistance welded seam coming around the
L.E. would produce a poor airfoil shape. Spar blades using
composite shells can be designed with almost any desired shape.
All the other types of blade constructions can be made in any
tip shape required.

The Number of Blades

As power and related solidity requirements go up it generally
becomes necessary to increase the number of blades in the pro-
peller. Very few blades have been designed with activity
factors over 200 and most are below 160. With high solidity
propellers, blade overlap inboard becomes a problem and recourse
must be made to the use of dual rotation types. From a propel-
ler weight point of view, it generally can be shown that the
fewer the number of blades the lighter the propeller weight
and the lower the cost.

Shank Size Selection

Propeller manufacturers generally build propellers for a lim-
ited number of standard shank sizes in their preferred reten-
tion types, as the cost of developing a broad range of shank

sizes even of the same design is prohibitive due to the large amount of testing needed for fatigue considerations. Retention bearings which are usually special and of limited production become costly as well as the related hub. Exhaustive full-scale laboratory testing and operational testing is also required before a new shank size and bearing is ready for production. The designer, therefore, in picking a shank size for a new blade design works within the established limited parameters of shank sizes. Gross loads for a new blade can be readily established and the shank size selected. When the new blade design is fully analyzed the shank may be modified in wall thickness to suit the conditions without affecting retention components.

With the standard shank size system it can be seen that some blade designs will be used in both 3 and 4 way propellers or even in dual rotation propellers without change.

BLADE CHARACTERISTIC DATA

Blade characteristic curves are a definition of chord distribution, thickness distribution, design C_L distribution, thickness ratio distribution and pitch distribution. These basic parameters are defined by aerodynamic analysis and structural considerations. The designer must first plot these curves to a large scale fairing out any discrepancies and arriving at accurate absolute dimensions. The curves, of course, are also completed into the selected root end. Figure 103 illustrates a typical set of characteristic curves as prepared by the designer.

Geometric Layout

The faired characteristic data is tabulated, and by using average factors face (FA) and edge alignment (LEA) are determined as shown in Figure 104, which also defines the various dimensions of a blade profile. The estimated values of FA and LEA, while not absolute, do permit making a layout of the developed geometric shape of the blade in planform and thickness views (see Figure 105). From this layout any required adjustments for fairness and smoothing of any abrupt contour changes can be made and fed back to the characteristic curves. Areas of the blade like the root end where contours are changing rapidly will be tabulated at closer station intervals.

Estimating Section Properties - Solid and Hollow Blades

Once the external blade parameters have been defined the blade section properties for structural analysis are estimated.

261
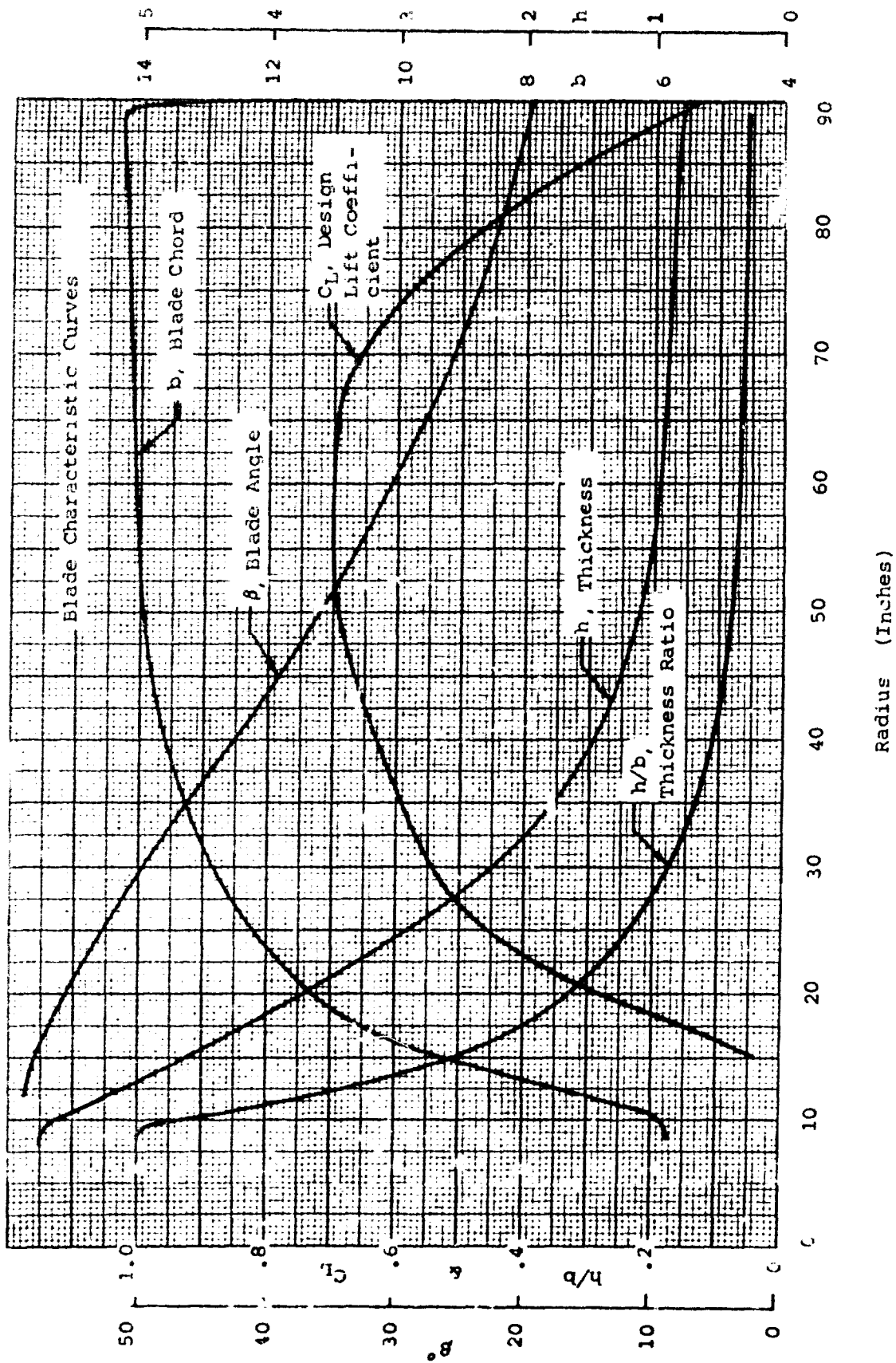
Figure 103. Blade Design Characteristic Curves.

Code For Blade Section

b   = Blade Chord
CG = Center of Gravity
FA = Face Alignment
LER = Lead Edge Radius
Y_T = Vertical Center of Lead Edge Radius
LEA = Lead Edge Alignment
h_u = Vertical Ordinate from Chord Line, Upper
h_L = Vertical Ordinate from Chord Line, Lower
x   = Horizontal Location of Ordinates
x_{cg} = Horizontal Location, CG
Y_{CG} = Vertical Location, CG
TER = Trail Edge Radius
β = Blade Angle
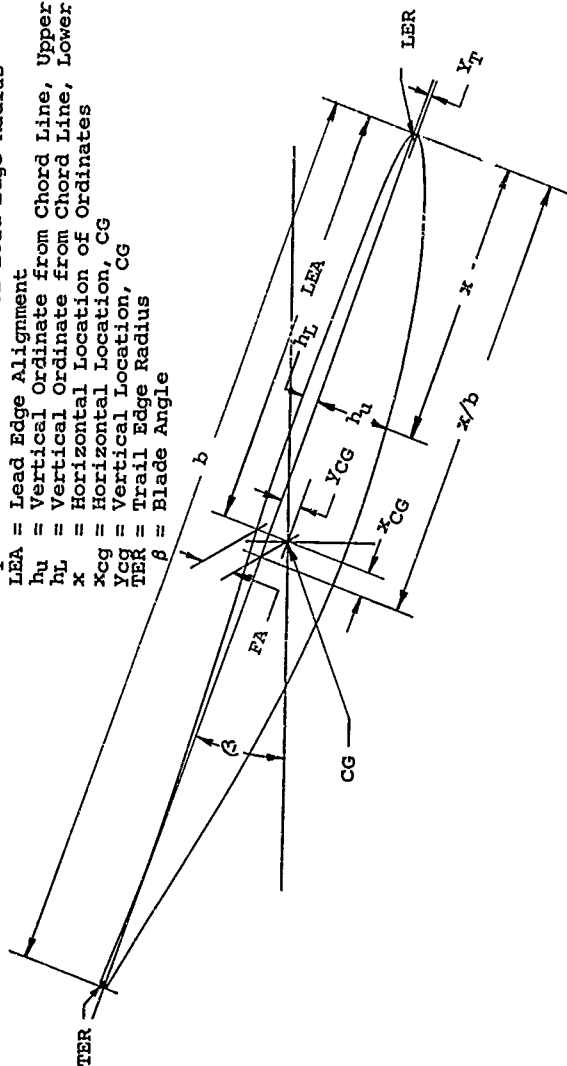
Figure 104. Illustrative Section.

263

Developed Planform View

Developed Thickness View
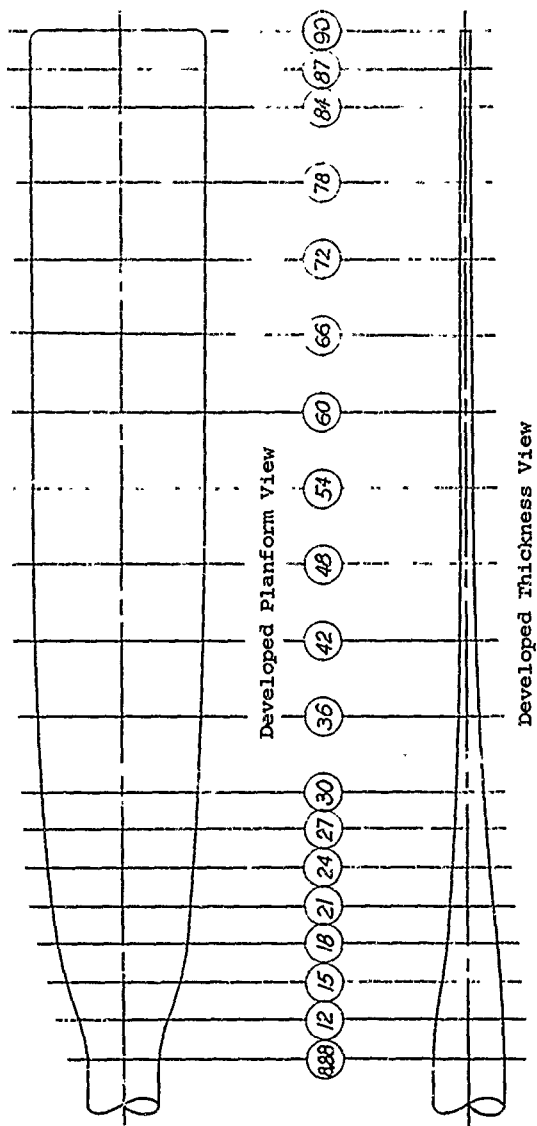
Figure 105. Geometric Layout.

264

These consist of area, I minor, I major, Z, C.G. location and
C distances for I/C camber and I/C thrust.

For solid blades the blade section properties can be obtained
readily from Figures 106 through 110.   For the older type
profiles, such as the RAF-6 and Clark Y, accurate results are ob-
tained with fixed constants on all properties. With the NACA
series profiles some of the properties vary with C_L and h/b
and these K values are shown in curve form.

Before section properties can be estimated for a hollow mono-
coque blade it is necessary to select a wall thickness distri-
bution for an initial trial. It has been found that wall
thickness distributions for a wide range of designs of hollow
monocoque blades form a narrow band and have a characteristic
shape. The minimum tip wall thickness will generally fall be-
tween .055" and .065" for a steel blade, depending on plate
span and durability desired. It is seldom selected on the
basis of stresses. From a manufacturing point of view it is
not practical to go much below .055". Higher tip wall thick-
ness will be selected where severe erosion problems are ex-
pected. The shank wall thickness is found from an estimate of
the maximum bending moment and centrifugal force based on a
target blade weight. Based on the characteristic shape of
wall thickness distribution a curve can be drawn between the
shank and the tip. Figure 111 shows a typical wall thickness
distribution for an extruded hollow steel blade.

The only way to determine accurate section properties of a
hollow blade is by integration as described under the struc-
tures section of this report. However, integration requires
a complete definition of the blade and is a lengthy procedure
until the blade parameters are more precisely established.
For preliminary design analysis short cut methods are used.
Ordinate calculations, structural layouts and integration can
be bypassed until the wall thickness is more closely defined.
To do this the section properties are estimated by the form
factor method. The form factor method for monocoque blades is
based on the following formulas and curves of constants aver-
aged from integrated data of a large number of fully designed
blades typical of the structure desired:

$$A = K_1 btp$$
$$Imin = K_2 btp(h - tp)^2$$
$$Imax = K_3 b^3 tp$$
$$Z = K_4 b^5 tp$$
$$c = K_5 h$$

265
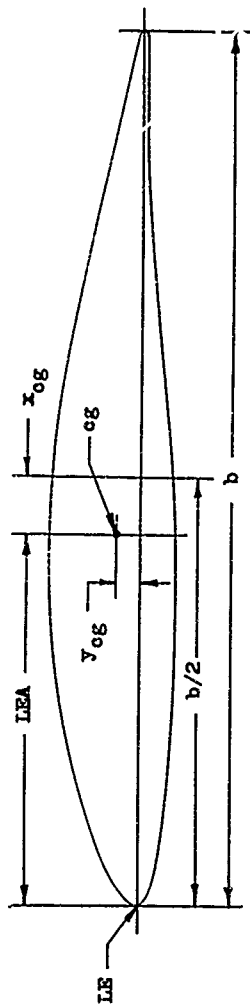
ILLUSTRATIVE SECTION

Section Property	Ellipse	RAF 6	Clark Y	Double Cambered Clark Y	NACA Series 16	NACA Series 65
Area	$.7854\ hb$	$.738\ hb$	$.725\ hb$	$.712\ hb$	$.733\ hb$	$K_2\ hb$
I major	$.0491\ hb^3$	$.0446\ hb^3$	$.0418\ hb^3$	$.0414\ hb^3$	$.0414\ hb^3$	$K_3\ hb^3$
I minor	$.0491\ h^3b$	$.0472\ h^3b$	$.0454\ h^3b$	$.0431\ h^3b$	$K_1\ h^3b$	$K_4\ h^3b$
x_{og}	0	$-.060\ b$	$-.060\ b$	$-.072\ b$	$-.018\ b$	$K_5\ b$
y_{og}	0	$.421\ h$	$.416\ h$	$.163\ h$	$.046\ bC_L$	$.045\ bC_L$
Z					$1.28K_6\ hb^5$	$K_6\ hb^5$

Figure 106. Solid Section Properties.
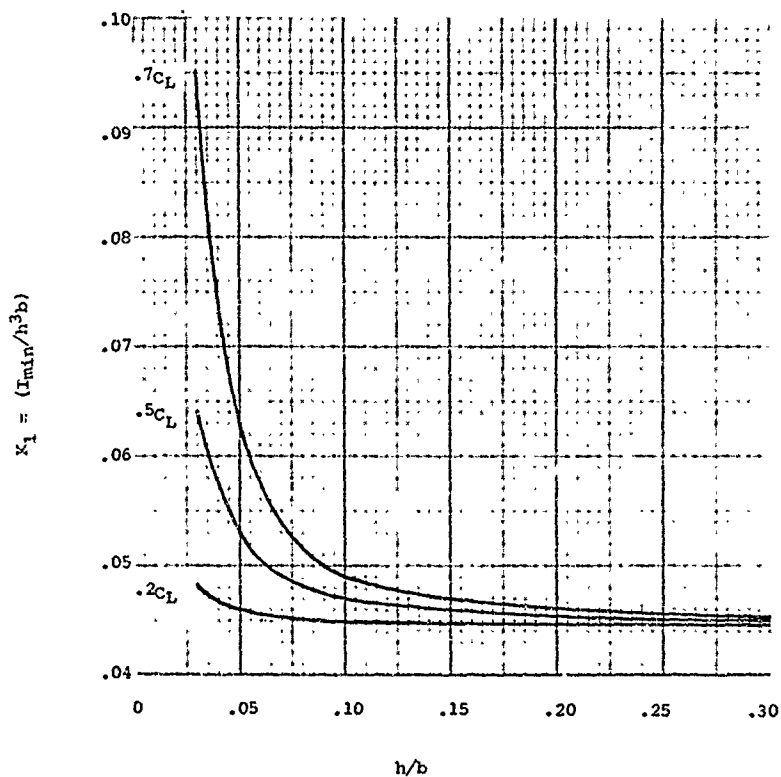
Figure 107. NACA Series 16
Solid Sections – Form Factors.

267
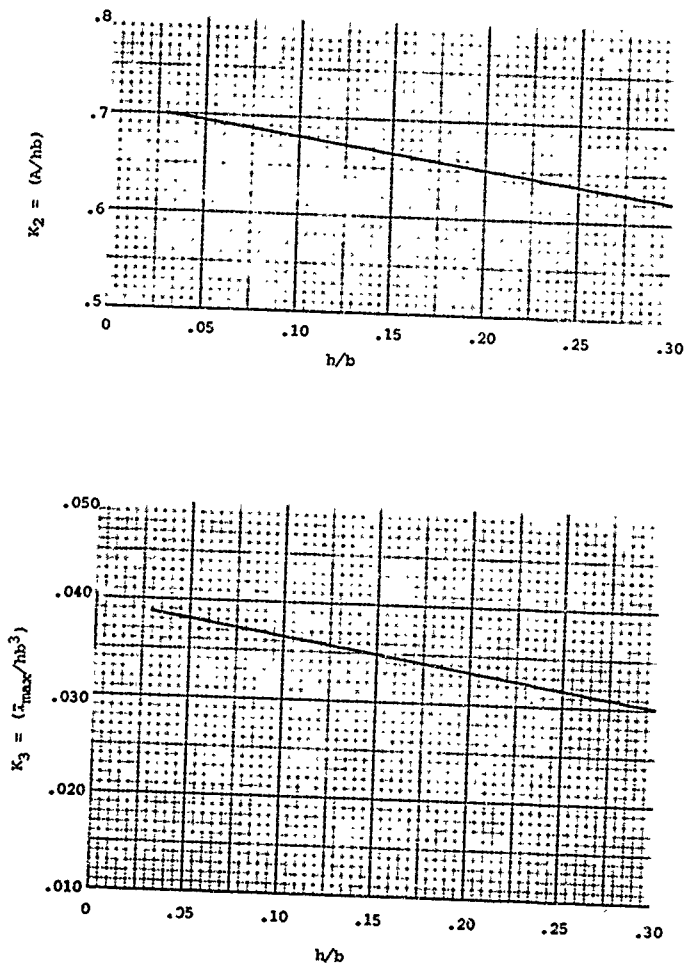
Figure 108. NACA Series 65
Solid Sections – Form Factors.
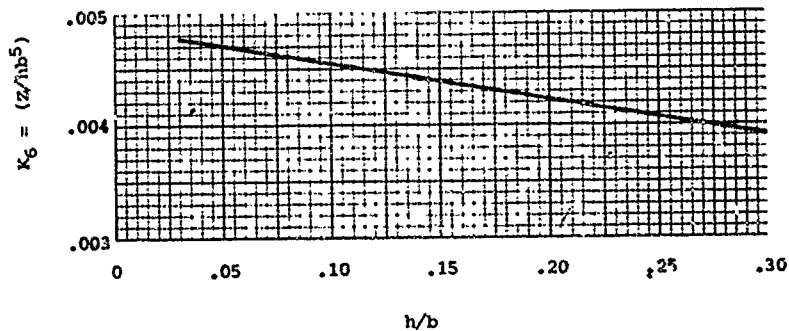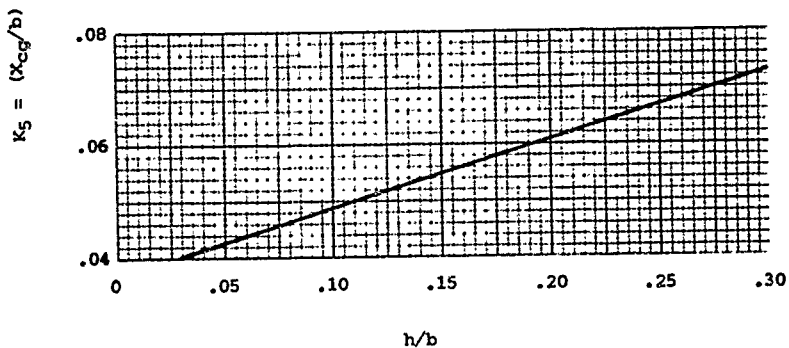
Figure 109. NACA Series 65
Solid Sections - Form Factors.
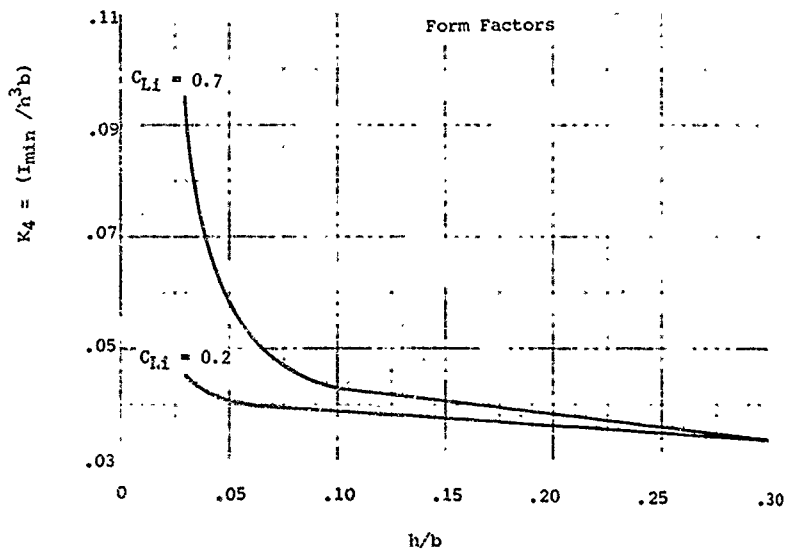
Figure 110. NACA Series 65
Solid Sections - Form Factors.
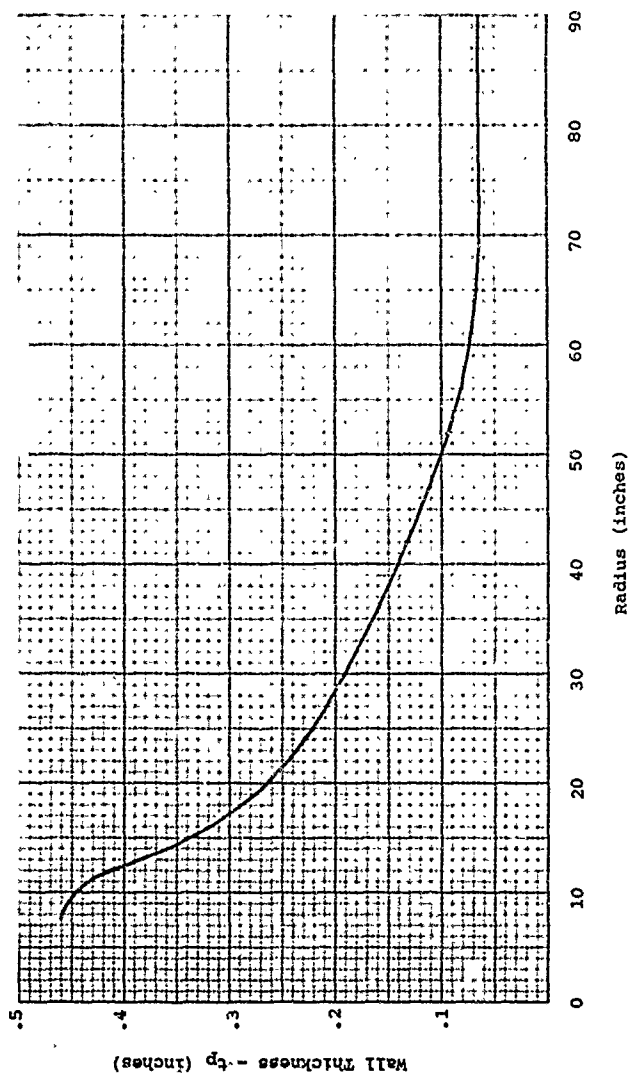
Figure 111. Typical Extruded Hollow Steel Blade
Wall Thickness.

where   b = chord
            tp = wall thickness
             h = profile thickness
             K = constants from integrated
                  sections (see curves)
             A = area
          Imin = I minor
          Imax = I major
             Z = induced torsional stiffness factor
             c = distance from C.G. to extreme fiber

The accuracy when using these factors should normally not be
expected to be better than 10%, although in many cases they
can be within 2%. I minor is generally more accurate than
I major or area. Figures 112, 113, 114, 115 and 116 are curves
of the constants used in the equations plotted against h/b.

It is generally best to estimate section areas first, based on
the form factors and the selected wall thickness distribution.
Knowing the areas and the basic shank weight the total blade
weight can be estimated and compared to any target weight for
the installation. Wall thickness adjustments can then be made
until the target weight is met. The remaining section proper-
ties can now be estimated, plotted and faired, and submitted
for preliminary structural analysis.

Optimizing Mass Distribution and Profile Thickness

After preliminary stress analysis it will be apparent that
stresses and loads are above or below the allowables, and
changes must be made for a new trial analysis.

Ideally the designer would like to have all of the blade oper-
ating at a constant stress equal to the design allowable stress.
However, even steady stresses cannot be made constant since
practical minimum wall thicknesses in the tip area for dura-
bility will result in lower stress values in the tip area.
When vibratory stresses are combined with the steady stresses
they must be considered on an allowable Goodman diagram basis.
Areas with high vibratory stresses must have low steady stresses
and vice versa. It is possible to get the major portion of the
blade operating at or close to an allowable Goodman curve, but
only for the maximum operating condition.

Generally speaking the designer has three options for adjusting
weight, stresses and loads. These are wall thickness, profile
thickness and forward tilt. Forward tilt of the blade center-
line is frequently resorted to in order to reduce steady bend-
ing moment stresses and loads. This can be done by building
it into the blade or the hub barrel. Its major drawback is
that it will increase reverse pitch braking stresses and loads.

272
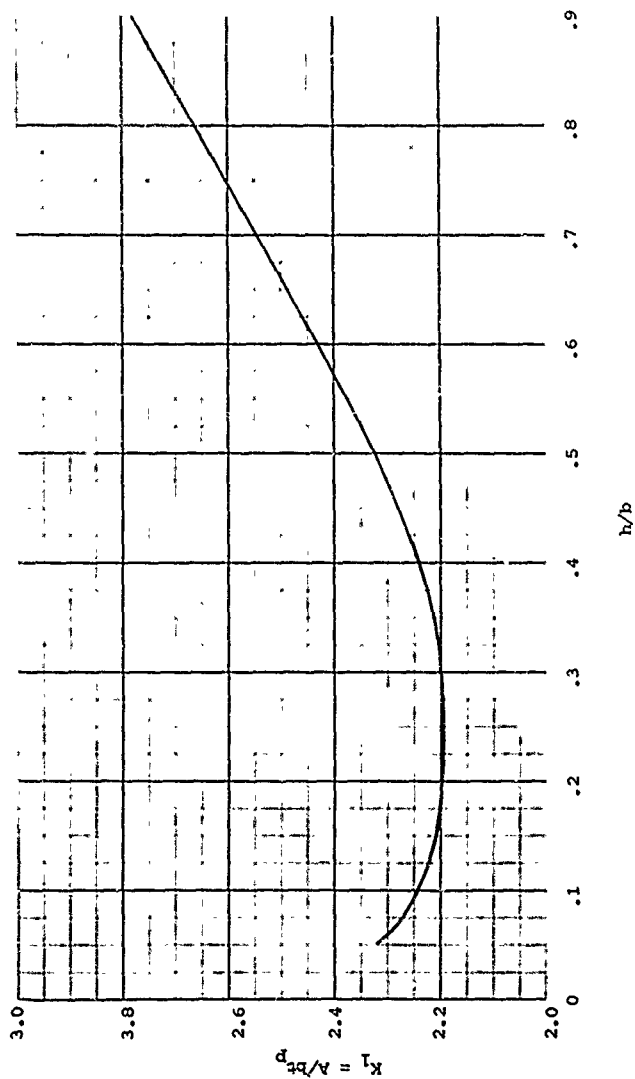
Figure 112. Form Factor Curve - Hollow Sections for Estimating Area.

273
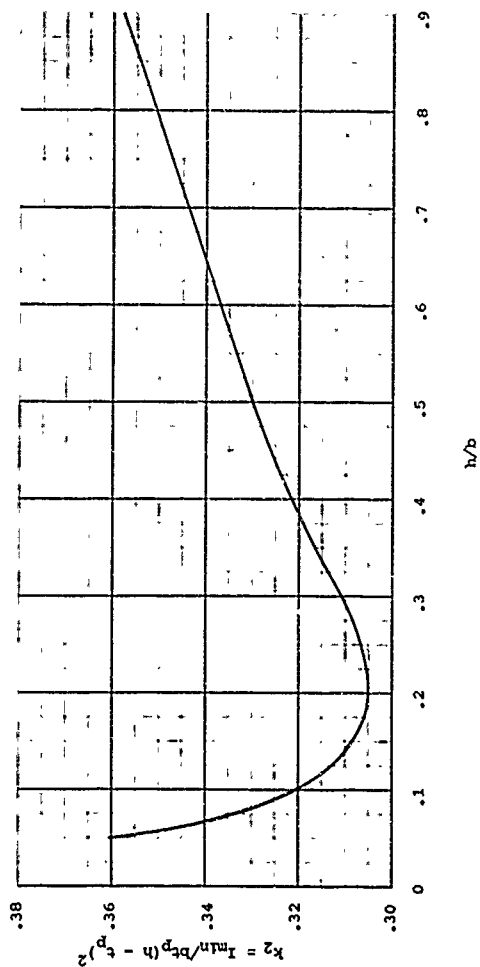
Figure 113. Form Factor Curve - Hollow Sections for Estimating I_{Minor}.

$$x_2 = I_{min}/bt_p(h - t_p)^2$$

h/b

274
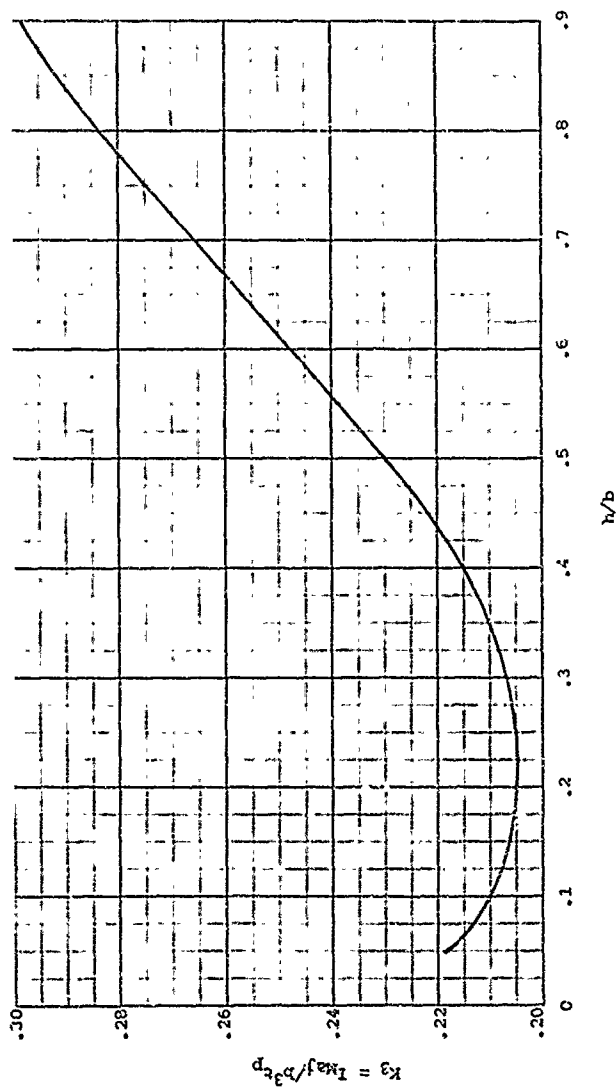
Figure 114. Form Factor Curve — Hollow Sections
for Estimating I_{Major}.

275
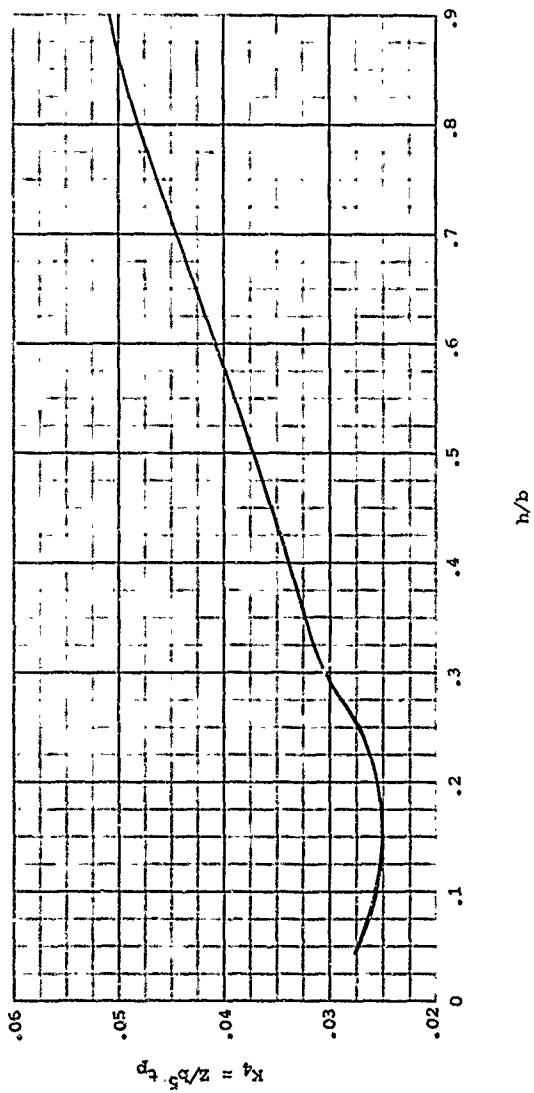
Figure 115.   Form Factor Curve – Hollow Sections
for Estimating Z.
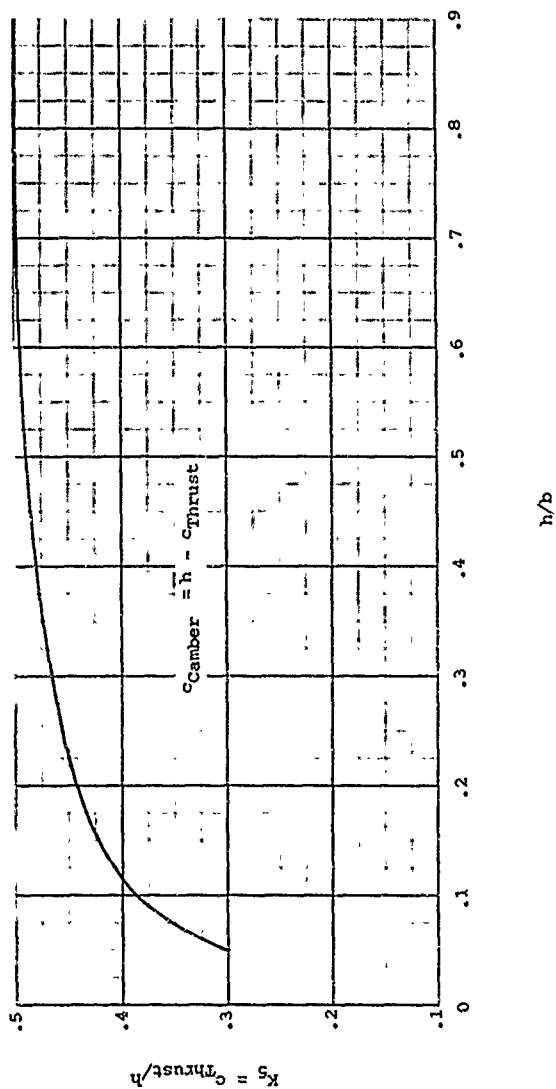
Figure 116. Form Factor Curve - Hollow Sections
for Estimating c_{Thrust}.

$c_{Camber} = h - c_{Thrust}$

h/b

$K_S = c_{Thrust}/h$

However, since reverse pitch is used for only a limited time in the life of a blade the increased loads can often be tolerated.

The designer's options and their resulting effects are:

Option		Will Affect
1. Wall Thickness	a.	Weight
	b.	C.F. loads and stresses
	c.	Bending loads and stresses including 1xP
	d.	C.F. restoring moment
	e.	Resonant frequencies (except flutter)
	f.	Centrifugal twisting moment
2. Forward Tilt	a.	Steady bending loads and stresses
	b.	Centrifugal restoring moment
	c.	Centrifugal twisting moment (slightly)
	d.	Reverse pitch bending loads and stresses
3. Profile Thickness	a.	Aerodynamics (efficiency)
	b.	Bending loads and stresses (including 1xP
	c.	Flutter frequency and stresses
	d.	Resonant flapping frequencies
4. Chord Width	a.	Aerodynamic loads and efficiency
	b.	Weight
	c.	All loads and stresses
	d.	All resonant frequencies

278

After the changes are selected revised section properties are
calculated either by going back to the form factor formulas
or by use of Figures 117 and 118. The revised values are
again put through stress analysis and the results checked for
acceptability.

Final Characteristic Data

After optimizing the design by estimating methods the final
characteristic curves are drawn and tabulated including wall
thickness. Accurate design procedures can now start.

Calculation of Ordinates

Once the characteristic data has been refined the blade design
can proceed with calculation of profile ordinate data. For
propeller blades using Clark Y and RAF-6 sections the ordi-
nates of the true airfoils from about 25% radius to the tip
are determined by multiplying a set of constants times the
design profile thickness. See Figure 119 for such ordinate
data on the RAF-6 and Clark Y profiles. The calculated ordi-
nates are then distributed properly over the selected chord
width. These types of airfoils, although still used, result
in a variety of mean camber lines and design C_L values over
which the designer has no control.

In the early 1940's the NACA developed a series of high-speed
airfoils, designated NACA 16, series where the design C_L could
be controlled. The NACA 16 profiles were first used
for propellers in the tip areas and because of their bene-
ficial high-speed characteristics. Inboard sections maintained
the classic Clark Y or double cambered Clark Y. Eventually
blades were and are produced with NACA series 16 profiles
throughout. As development continued, NACA series 64 and 65
profiles were introduced in propeller blade design with the
65 series being much specified in late designs by the aero-
dynamicist. The two airfoils most used today are the NACA 16
and 65.

Construction of NACA series profiles as defined by the NACA
does not result in calculated ordinates perpendicular to the
chord line as preferred by the shop. By laying out the pro-
file the ordinates could be scaled and specified in the con-
ventional manner. This was a lengthy process and subject to
many errors, so a method of direct calculation was developed
using empirical data.

Referring to Figure 120 it was found that correction factors
A and B were a function of h/b and C_L. Taking a given per-
centage chord ordinate point,
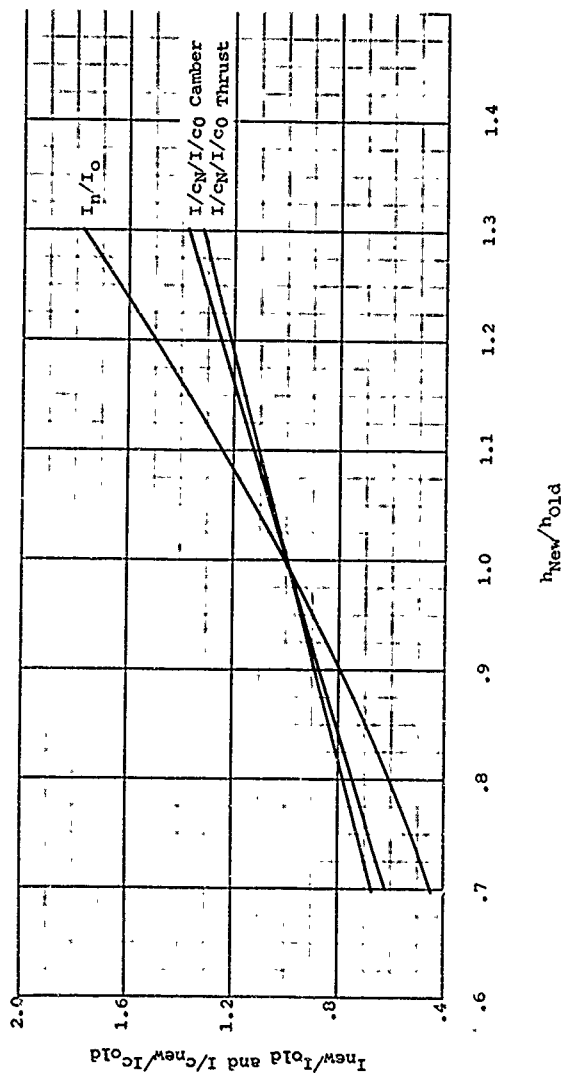
Figure 117. Estimating New Values of I_{Minor} and I_C When h is Varied.
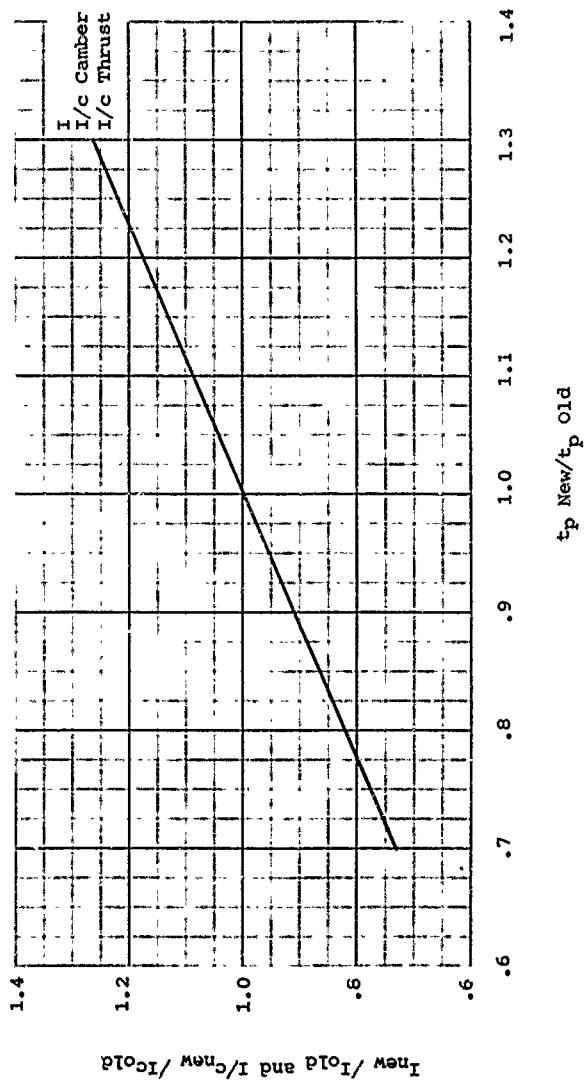
Figure 118. Estimating New Values of I_{Minor} and I/c When t_p is Varied.

281

RAF-6

x/b	Y_L	LER	.025	.050	0.10	0.20	0.30	0.40	0.50	0.60	0.70	0.80	0.90	TER
h_u/h	.100	.100	.410	.590	.790	.950	.998	.990	.950	.870	.740	.560	.350	.08

CLARK Y

x/b	Y_L	LER	.025	.050	0.10	0.20	0.30	0.40	0.50	0.60	0.70	0.80	0.90	TER
h_u/h	.295	.130	.549	.663	.806	.957	.995	.983	.928	.829	.684	.521	.338	.08
h_L/h			.128	.061	.038	.009								
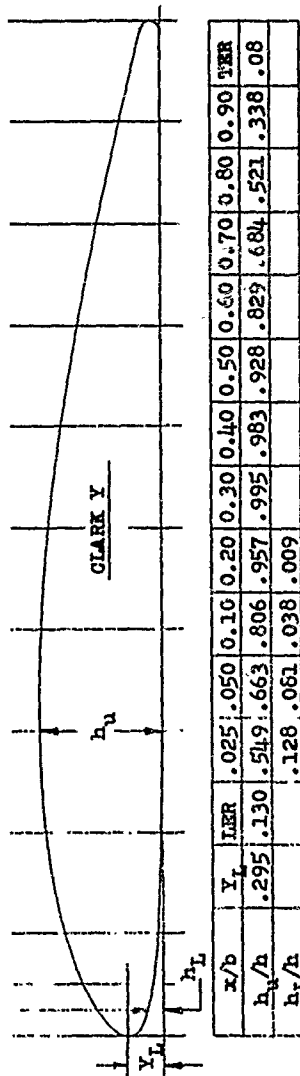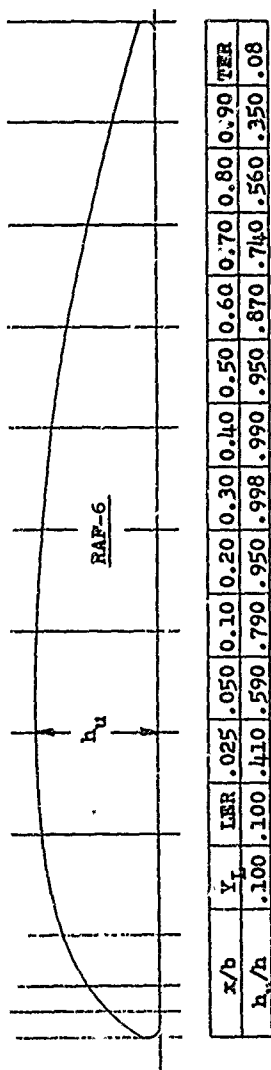
Figure 119. Early Propeller Airfoils.
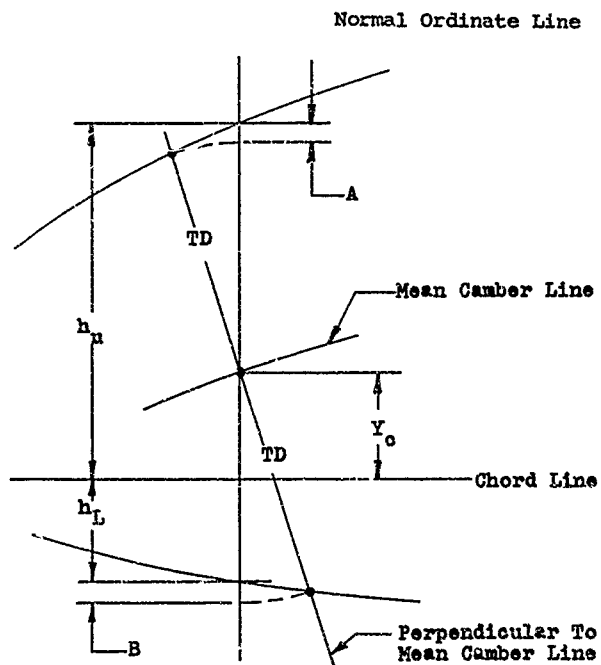
Figure 120. Construction of NACA Series Sections.

.283

$$h_u = Y_c + T.D. + h\left[f(C_L\ h/b)\right]$$

since $\qquad T.D. = Kh$

$$h_u = K + f(C_L\ h/b)\ h + Y_c$$

and $\qquad f(C_L\ h/b) = \dfrac{h_u - Y_c}{h} - K$

If we solve the latter equation for each percentage chord point for a number of known profiles selected across the board for C_L and h/b and then plot the $f(C_L, h/b)$ vs. $h/b \times C_L$ we get a straight line, or

$$f(C_L, h/b) = K_u \times C_L \times h/b$$

then $\qquad h_u = (K + K_u \times C_L \times h/b)h + Y_c$

Similarly, $\qquad h_L = (K - K_L \times C_L \times h/b)h - Y_c$

Taking the values of K_u and K_L from the straight line curves we can construct tabular ordinate calculation sheets which can also be programmed for the computer. See Tables X and XI . The chart for the NACA Series 65 section involves additional variables in the basic NACA construction than does the Series 16. As shown, the NACA Series 65 chart incorporates ordinate modifications in the T.E. area to make a more practical and thicker airfoil in this area with somewhat better I/c characteristics.

Before laying out the newly calculated profiles it is necessary to select the minimum TER or trailing-edge radius value. This will generally vary with the choice of blade material to assure durability. On steel blades it was common practice to go as low as .020". On aluminum alloy and fiber glass blades .030" minimum has been used up to 6% to 8% of h. Whatever the choice of TER the profiles can be slightly adjusted at the 90% ordinates if needed to fair smoothly into the selected TER when the profiles are laid out. The TER must increase from some radius outboard until it fairs into the radius of the round shank; similarly the LER.

Faired Intermediate Profile Ordinates

Early propeller blades had the faired inboard section ordinates between the round shank and the first true airfoil determined by water level line layout technique. This was effective but not very accurate and was time-consuming to do. It was inevitable that mathematical methods would be developed

284

TABLE X. FOR CALCULATING NACA SERIES 16 PROFILE ORDINATES

b =   h =   h/b = C_L =   h/b x C_L =   b x C_L =

Line Percent Chord	2.5	5	10	20	30	40	50	60	70	80	90	100
1. K_u	.1550	.1280	.0960	.0500	.0190	.0020	.0000	.0020	.0190	.0500	.0650	0
2. K_u x h/b x C_L												.0100
3. x	.1504	.2091	.2881	.3887	.4514	.4879	.5000	.4862	.4391	.3499	.2098	.0100
4. 2 + 3												
5. K_L	.0950	.0700	.0410	.0180	.0070	.0010	.0000	.0010	.0080	.0250	.1200	0
6. x	.1504	.2091	.2881	.3887	.4514	.487.	.5000	.4862	.4391	.3499	.2248	.0100
7. K_L x h/b x C_L												
8. 6 - 7												
9. K_y	.00930	.01580	.02587	.03982	.04961	.05356	.05516	.05356	.04861	.03982	.02587	
10. Line 8 x h												
11. K_y x b x C_L = Y_C												
12. Line 4 x h	-											
13. h_L = 10 - 11												
14. h_u = 11 + 12												

LER = .48889 x h x h/b =
          (fit to section)

TER =

Y_L = .62234 x C_L x LER =
Y_T =   (by subtraction)

TABLE XI. FOR CALCULATING NACA SERIES 65 PROFILE ORDINATES (MODIFIED TRAILING EDGE)

	2.5	5	10	20	30	40	50	60	70	80	90	95	100
1. x/c													
	.1635	.2214	.3052	.4134	.4745	.4995	.4884	.4440	.3745	.2875	.1805	.1100	.0100
2.	.0605	.0370	-.0123	-.0090	-.0145	-.0020	.0679	.2002	.3375	.3831	.3273	.2272	0
3. y_t × K_{TT} h/b													
4. K_{OO} K_{TT} h/b	0	0	0	0	0	0	.0006	.0143	.0333	.0508	.0555	.0425	0
5.													
6. y_t × K_{TT} h/b − K_h C_L	.1720	.1200	.0916	.0560	.0235	.0020	.0024	.0672	.1426	.1568	.1304	.1186	0
10. K_{SL} = π h/b × (10)	.00930	.01580	.02587	.03982	.04861	.05356	.05516	.05356	.04861	.03982	.02587	.01580	0
11. (8) + (10)													
12. (11) × h													
14. y_t × C_L													
15. h_u = (12) + (14)													
16. K_{OO} − K_{TT} h/b + K_h C_L													
17. K_{SSL}	.1220	.0910	.0645	.0340	-.0140	-.0020	-.0024	.0772	.1535	.1628	.1400	.1088	0
18. K_{SSL} × h/b × C_L													
19. (16) − (18)													
20. (19) × h													
21. h_L = (20) − (14)													

For h/b < .15, LER = .7 h × h/b = _____, For h/b > .15, LER = .25 h × $\sqrt{h/b}$ = _____, Y_L = .433 LER × C_L = _____

TER = .020 min. Y_T = .433 TER × C_L = _____

to computerize this work.

Where a full shank fairing is permanently incorporated, the most useful method preferred for maximum contact of the cuff cover to the blade involves calculating true airfoils into the root end assuming the cuff is in place. After laying these out with the cuff cover thickness shown, the LER and TER of the basic blade are fitted tangent to the inside of the cuff cover at their proper distances from the blade centerline. The basic blade ordinates are found by subtracting the thin cuff cover thickness from the cuff ordinates. It is not normally necessary to re-divide the resulting faired profile into the usual ten equal parts, and scaling new ordinates which would be a source of error.

LAYOUT OF OVERSIZE SECTIONS

It is desirable to lay out all of the airfoil sections to as large a scale as practicable, generally not less than 2:1. These layouts assure detection of minor ordinate errors or computer errors. They also permit any minor refairing into the TER. Accuracy in these layouts is a must because ordinate errors as small as .002" will be detected in the shop when making templates, and will cause shop delays while the error is confirmed and corrected, and the drawings changed.

If the layouts are of a large enough scale they may also be used in the next design step to determine structural geometry.

Structural Geometry

On a monocoque blade it is necessary to establish the struc-tural geometry by large-scale layouts of the leading and trail-ing edges of the profiles. Establishing the edge geometry starts with the wall thickness determined in the preliminary design stage. If the design is a welded or extruded monocoque hollow steel blade the edge fillets must be determined. Con-sideration of the plates acting as built-in beams subject to vibratory diaphragming with resulting peak stresses in the fillets is the basis for the fillet proportions. For welded blades the minimum fillets may run from 180% to 200% of the center wall thickness. Extruded blades can be less because of the absence of weld metal and sharp corners in the area. Fil-let lengths of 1.25" are normal. Weld gaps may run as low as .040" but can be much larger. On extruded blades the internal edge radii may go as low as .045" to .060". Foam filled fiber glass blades normally do not require fillets and internal edge radii may run as low as .050".

287

In conjunction with the edge fillets and the internal radii, minimum solid edge widths are also selected for durability and reasonable service repair allowances. These may run as low as .25" to .38" in the outboard area. In the inboard area solid edge widths gradually become equal to the center wall thickness except on edge-welded blades where weld fillets are maintained almost to the round.

With the edge parameters established, large-scale layouts are drawn to determine solid edge widths and proper fit of all factors. Figure 121 illustrates a layout of a typical edge construction. When these layouts have been accomplished for both LE and TE on all stations, the data is examined and plotted for smoothness and desired characteristics. Changes may be made and the layouts adjusted until the desired results are obtained.

Data for Integrated Section Properties

Before section properties can be integrated internal ordinate data must be tabulated. Values of k_u and k_L generally must be scaled in the edge area at all points of change such as at W_L and the start and stop of the fillets as shown on Figure 121 Most other values of k_u and k_L can be taken at the standard ordinate points by subtracting wall thickness from the external ordinates, plus some standard corrections where the airfoil has great curvature. The formulas for integrated section properties are given elsewhere in this report. Computer systems designed to by-pass layout and scaling of edges have been devised but need much more development.

In completing data for integrated section properties it is often necessary to lay out the root end area to be sure the selected wall thickness values will properly fit into the standard root end configuration.

Integrated Section Properties and Stress Analysis

After the computer has determined the integrated section properties they are tabulated and plotted for fairness and to check for errors. If a blade filler is used, both mass values and structural values must be determined equivalent to the basic blade material.

Generally the section areas are integrated first to see if the weight target has been met. A full stress analysis, 1xP analysis and frequency map can now be run as described elsewhere in this report. Analysis may be followed by minor changes depending on results.

288
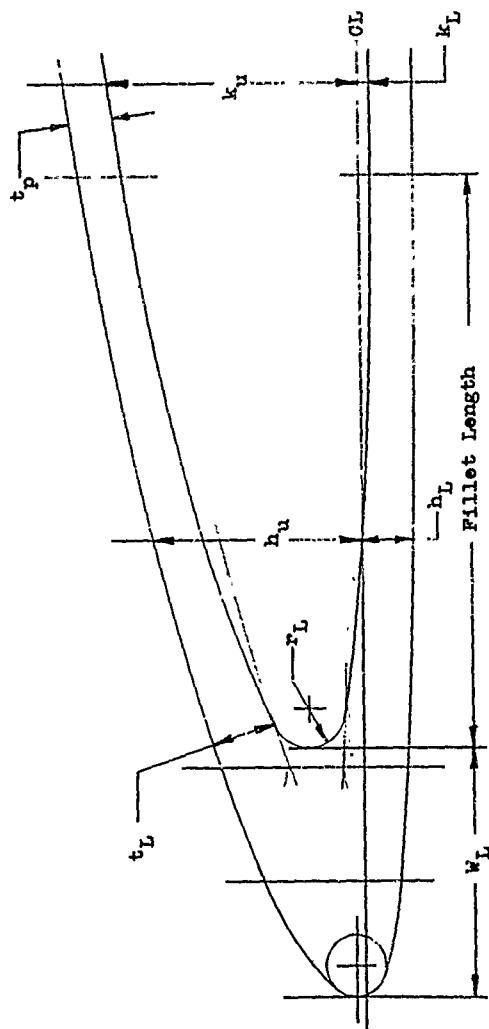
Figure 121. Typical Layout of Leading-Edge
Structural Geometry.

289

Weight and Balance/Volumes and Surface Areas/Polar Moment

In addition to the stress analysis a detailed weight and balance is calculated. This will include separate values for all components as shown in the following typical weight and balance breakdown:

WEIGHT AND BALANCE BREAKDOWN

Component	Weight	Moment
1. Shank to last round		
2. Balance Cup Assembly		
3. Blade Last Round to Tip		
4. Internal Support-Rubber Ribs, etc.		
5. Plating		
6. Paint		
7. Deicing Assembly		
8. L.E. Sheath		
	lb	in.-lb

TOTALS

```
         3% Manufacturing Allowance -
         Balance Lead Allowance -----
*        Blade Center of Gravity -
* Edge Unbalance @ β ref = 0° ----- in.-lb
* Face Unbalance @ β ref = 90° ----- in.-lb
* Does not include paint, deicing or sheath
```

While it is usually desirable to locate the sections' centers of gravity on the blade centerline for minimum centrifugal twisting moment and zero-zero vertical balance, this is not always possible with certain constructions.

Surface areas must be calculated from perimeter data before weights can be determined for plating and painting. Polar moment of inertia in slug ft^2 must be established for use in propeller load calculations.

Blade Drawings

Once the design has been finalized the blade drawings are prepared. The most important of these is a master blade drawing. The master blade drawing starting at the top consists of:

    a. Developed planform view with
       root end details

    b. Developed thickness view

290

c. All sections at angle and
   fully dimensioned.

Such a drawing frequently becomes top heavy with dimensions on
a monocoque blade, and section structural dimensions are often
tabulated in a separate section detail drawing. As a result
of this experience, master blade drawings have been evolved
which are much more practical, and include:

a. Developed planform and thickness
   views

b. Illustrative sections

c. Tabular chart of all section
   dimensions

d. Material and Process Specifications.

Standard dimensions for the retention can either be covered
separately on a blade root detail or on the master blade draw-
ing. Separate components such as balance cups, deicing boots
and erosion strips are covered on separate drawings. In the
case of composite blades, a separate layup detail is required
to define the fiber glass layers and joints.

Extruded blades also require an extruded tube design drawing
which only the blade designer can provide. On welded blades
the production engineer will normally define the plates and
shells required because of processing details which must be
included.

The extruded tube design, however, is based on establishing
leading- and trailing-edge ear envelope designs which permit
the varying ears on the extrusion mandrel to penetrate the
tube ear at a depth which will give the proper fillet thick-
ness. The resulting ear design is fitted to a tube diameter
which will give the proper total perimeters matching the blade
perimeters. The ears are then offset slightly from 180° apart
to provide the perimeter differential required on the thrust
and camber sides of the finished airfoil. The basic tube must
then be given allowances for blade manufacture, including de-
carb cleanup allowance.

Design Report

After a blade design is completed a design report should be
prepared covering all the aerodynamic and structural data on
the design. It is very important to fully cover the design
approach used for later reference and all the special consider-
ations incorporated. It will be found that such a report will

291

be very useful over the operational life of the blade.

BLADE ICE CONTROL

The need for ice control on propeller blades has been contro-
versial at times, with some feeling it is not required. There
can be little question, however, that it is highly desirable,
and ice control is incorporated on all propellers on all all-
weather aircraft.

Effects of Ice on Propeller Blades

Propeller blades and spinners will collect ice when operated
under 25,000 feet altitude continuously at temperatures from
0°F to 25°F in an atmosphere containing water droplets ranging
from 15 to 25 microns in size and a humidity of 0.5 gm/m^3
moisture content; Reference 12.

Ice accumulations will increase with exposure time, generally
unsymmetrically, causing distortion of the blade airfoils and
loss of aerodynamic efficiency. Such accumulations will be
accompanied by propeller unbalance which will be aggravated by
random disengagement of heavy ice masses due to centrifugal
force and the blade vibration. The disengaged ice is a hazard
to the airframe and personnel. With turboprop air inlets
directly behind the propeller disengagements from the spinner
and blade shanks can also be ingested under some conditions
causing possible damage and engine surge. Under emergency
conditions ice on a propeller without ice control can some-
times be disengaged by increasing rpm and centrifugal force.
It is interesting to note that ice is a pretty good adhesive
and sticks fairly well to most surfaces, including even such
things as Teflon and wax as determined by quantitative tests.

Surface Treatment and Compounds

There are many surface treatments, finishes and waxes that will
reduce ice adhesion and facilitate disengagement of ice, but
they all suffer from rapid deterioration when exposed to the
erosion environment of propellers, especially on the leading
edge where they are most needed. Various chemical compounds
in paste form have been used over the critical blade areas,
which both reduces ice adhesion and depresses the freezing
point of the ice at its interface, facilitating disengagement.
Unfortunately, these compounds are rapidly dissipated when
operated in rain, and also during actual icing conditions.

Fluid Anti-Icing

Ice control systems can be classified as either anti-icing or
deicing or a combination of the two. Anti-icing refers to a
system which prevents ice from accumulating while a deicing
system allows controlled amounts of ice to accumulate before
acting to disengage it.

Fluid systems are anti-icing and rely on keeping the blade
wet with a freezing point depressant fluid sometimes including
a lubricant. The most used fluid is isopropyl alcohol used
alone or mixed with glycerine. Isopropyl alcohol is inexpen-
sive but is very inflammable. The most common system for dis-
tributing the fluid to the blades consists of a tank, pump,
controls, slinger ring, blade fluid cup and a rubber fluid
anti-icing boot on the blade leading edge. Figure 122 illus-
trates schematically the propeller mounted components. The
metered fluid from the pump, typically $3\frac{1}{2}$ to 5 quarts per hour,
is fed to the slinger ring which acts like a centrifuge and
dispenses the fluid to the blade cup which will accept the
discharge at any operating blade angle. From the blade cup
the fluid flows through a tube or channel around to the leading
edge where it discharges onto the fluid anti-icing boot. The
fluid anti-icing boot contains grooves which terminate at pro-
gressive blade radii, assuring reasonable radial distribution
of the fluid along the blade leading edge after which it runs
back over the blade surfaces.

The grooves in the fluid anti-icing boot do cause undesirable
aerodynamic disturbances, but these are considered negligible
for the ice control provided. Fluid anti-icing without the
boot to aid distribution is not very effective. Boots normally
are installed with a termination at from 60% to 75% blade rad-
ius with the trend to the shorter boots coming in late years.

The fluid can also be distributed internally in hollow blades
through a manifold tube brazed in the leading edge and having
small holes drilled through the external leading edge to the
tube. Such a system was devised but never put into production.

Hot Air Ice Control System

Hot air ice control has had only limited application despite
the relatively lightweight sources of heat available as com-
pared with electrical generators. This is due in part to the
relative complications of the propeller structure required to
distribute the hot air and the slight loss of efficiency associ-
ated with the tip discharge of the hot air. Tip discharge
systems rely on centrifugal pumping action to circulate the
air to the blade tip at low pressures. If a system is used
where the air is returned from the tip to the inboard area

293
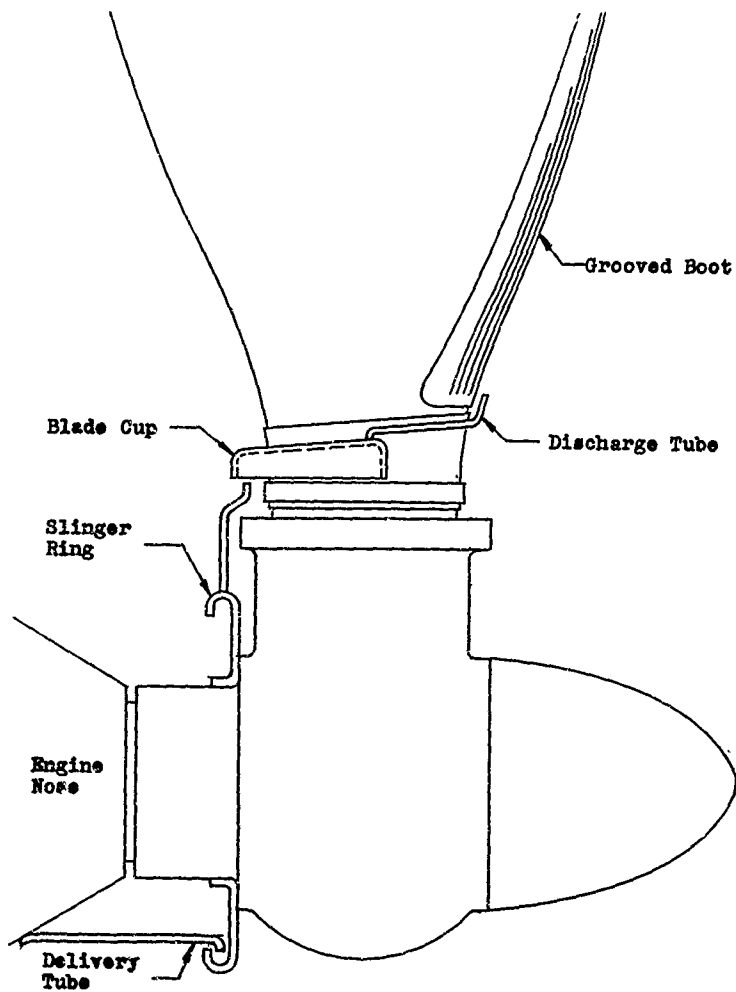
Figure 122. Typical Fluid Anti-Icing System.

294

before discharge in an effort to maintain full aerodynamic pro-
peller efficiency the blade will have to be under significant
internal pressure. Thin walled blades would then suffer pro-
file distortion and probably not maintain the aerodynamic
efficiency desired. The major production propeller instal-
lation using hot air deicing was the B-36 bomber and incorpor-
ated tip discharge.

The major components involved in a hot air ice control system
start with the source of hot air which can be,

                  a. Engine exhaust heat exchanger
                  b. Turbine engine compressor bleed air
                  c. A gasoline fired combustion heater

Engine exhaust gas is also a possible heat source, but has been
ruled out because of the additional corrosion problems. Tem-
peratures of 400°F are common for the inlet air to the propel-
ler.

The hot air is ducted to a volute manifold at the propeller
which requires a large carbon seal between it and the rotating
collector. The air is then fed to a muff around the blade
shank which has one or more holes penetrating to the blade
cavity, or it is fed into the hub and then out through a dif-
fuser tube in each blade balance cup. The B-36 used the latter
system. While the blade shank muff system might be simpler
the structural integrity of the blade is compromised and hot
air flow losses are increased. A control system is of course
also required. Estimates of heat requirements for hot air ice
protection of propeller blades may be found in Reference 13.

The propeller blade using hot air ice control with tip dis-
charge requires an air inlet system such as the diffuser tube
mentioned previously, a partition in the blade to direct the
air along the leading-edge portion of the blade and a discharge
hole in the tip. Figure 123 shows a typical arrangement of the
blade as used on the B-36. Many tip hole designs were studied
and tested in the wind tunnel, but the type shown was the best
aerodynamic and structural compromise. The structural steel
rib running down the blade centerline resulted in the entire
leading-edge half of the blade being heated. A supplementary
rib at 25%-30% chord would have been more effective for ice
control, but would have complicated the blade considerably.
Because of the nature of hot air ice control systems, it is
necessary to provide a very good protective finish inside the
blades for protection against corrosion. Baked phenolic fin-
ishes were reasonably effective on the B-36 but better finishes
should be available today. Resistance to 400°F air temperature
is required.

Tip Hole

Rubber Dam

Steel Rib

Hot Air

Diffusor Tube

Planform View

Hot Air

Shot Peen
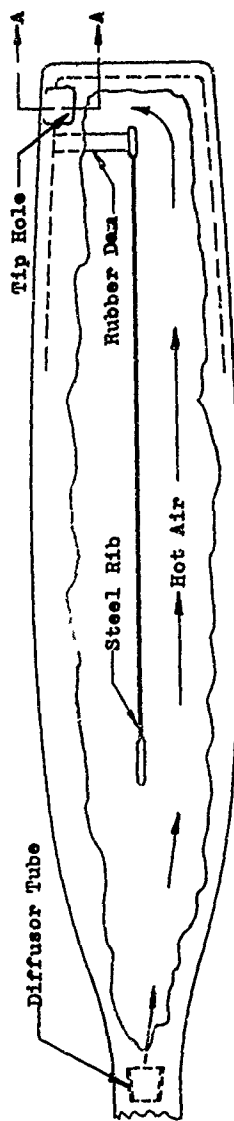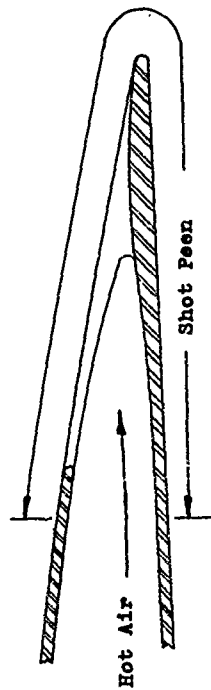
Section A – A

Hot Air

Figure 123. Typical Hot Air Ice Control Blade.

Because of the heat sink involved with hot air ice control, especially in the solid L.E., it is not practical to cycle the heat on and off as with electrical systems.

Electrical Ice Control

Electrical ice control is the most common system in use, and can be either a deicing or anti-icing type system. Blade heating elements may be mounted internally on the blade or externally. An electrical system will consist of a generator, either airplane supply system or hub mounted, the resistance heating element on the blade and spinner, and the system's controls and safety devices. Since hub-mounted generators are not practical on modern large-diameter low-rpm propellers, this discussion will assume aircraft power supply. Because power requirements are so high for propeller ice control, most installations rely on a balanced cyclic system controlled by a motor-driven cyclic time which sequences power to the various propellers and spinners in three balanced phases to match a 3-phase 115/200-volt supply. Overall weight is thus kept minimal, and balanced ice removal is obtained in a manner to avoid excessive vibration due to propeller unbalance.

Power requirements will vary depending on the use of internal or external heating elements. Internal elements require considerably more power to heat the blade from the inside out.

For full deicing control down to $0^{\circ}F$ temperatures, a power of 8 watts per square inch over the protected area has been used by the USAF assuming a standard rubber type deicing boot; Reference 15. One advantage of external deicing boots is that power is relatively independent of the blade construction except that composite blades, being good insulators and poor heat sinks, would require less. On metal blades it has been estimated that up to one-half of the heat is dissipated within the blade and is lost for deicing.

For economy of power and use only down to $25^{\circ}F$ elements have been designed for 6 watts per square inch; Reference 15. In some cases the watt density has been kept at 7 or 8 on the L.E. and reduced to 4 or 5 back from the L.E. The area of the blade covered will extend from the shank to 60% to 75% of the blade radius and from 20% to 25% of chord width. Some installations only protect out past the engine inlet, but these cannot be considered as giving good propeller protection.

Another advantage of external elements when using foam cuffs is that one deicing boot can be used over the cuff and blade, simplifying the wiring problem.

As mentioned, a higher watt density is required for internal

297

elements, and no flat figure can be given as the actual power
required will depend on the wall thicknesses and the mass of
the solid L.E. This total volume of metal must be brought up
to temperature, and in addition, lag in the system requires
longer heat-on times, thus reducing the effectiveness of cycling.
With heavy solid L.E. masses, it may be necessary to provide a
calrod at this point with continuous energization.

Typical Electrical Deicing Circuit

A typical electrical deicing circuit for a 4-engine aircraft
is shown in Figure 124 for a 3-phase 115/200-volt AC system.
Phases A and C are connected on for 30 seconds and off 90 sec-
onds for a total cycle of 120 seconds. Figure 124 shows the
cyclic timer schematic. Each phase absorbs an equal amount of
power. To accomplish this, the elements in each Phase (A, B and
C) are designed and combined as shown by the shaded areas in
Figures 126, 127, and 128 to get equal kw loads. The spinner
nose shown in Phase B, Figure 127 is anti-icing and is on full
time.

Deicing power is transferred to the propeller through slip
rings and brushes. The slip rings may be axial with respect
to the shaft or disc type in the plane of rotation. In either
case multiple brushes mounted in a block are used for reli-
ability and uniform brush pressure and complete bearing. With
the advent of higher aircraft supply voltages brush life has
been greatly improved.

Power is transferred from the propeller slip rings to the blade
either by slip rings on the blade shank or by pigtail flexible
leads. The use of blade shank slip rings is somewhat more
versatile in magnitude of pitch range possible, but recent pig-
tail designs have been able to provide the needed range also
without slip ring losses. Slip rings require attention to the
brush block design to permit easy removal of the blade from
the hub. Pigtails require care in design to resist centrifugal
and airstream blast forces.

While many types of heating elements have been conceived, only
two types are in common use. The most common is the rubber
sandwich around stranded resistance wires which resist fatigue
of the wires very well. The other type of element is based on
metal spraying a pattern of resistance conductors on preformed
fiber glass shapes and covering with fiber glass. This type
has been most used on spinners. Calrods are occasionally used
for anti-icing because of their high temperature capabilities
especially in spinner nose areas.

Internal elements consist of resistance wires securely mounted
inside the blade during its manufacture and are considered

Figure 124. Propeller Ice Control Schematic - Four Engine Airplane.

299
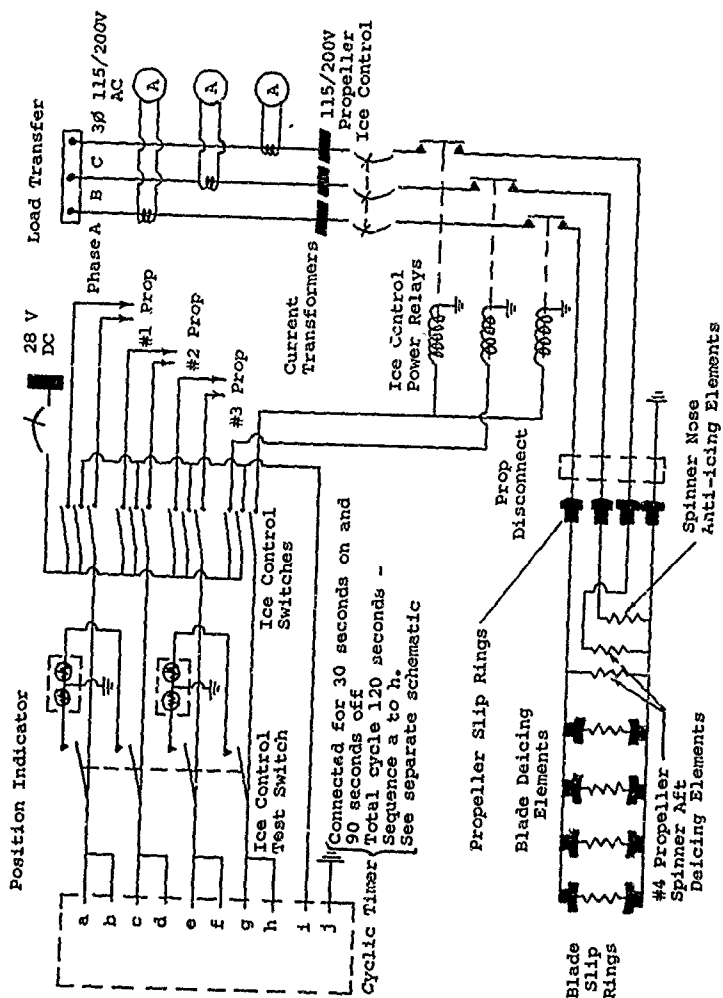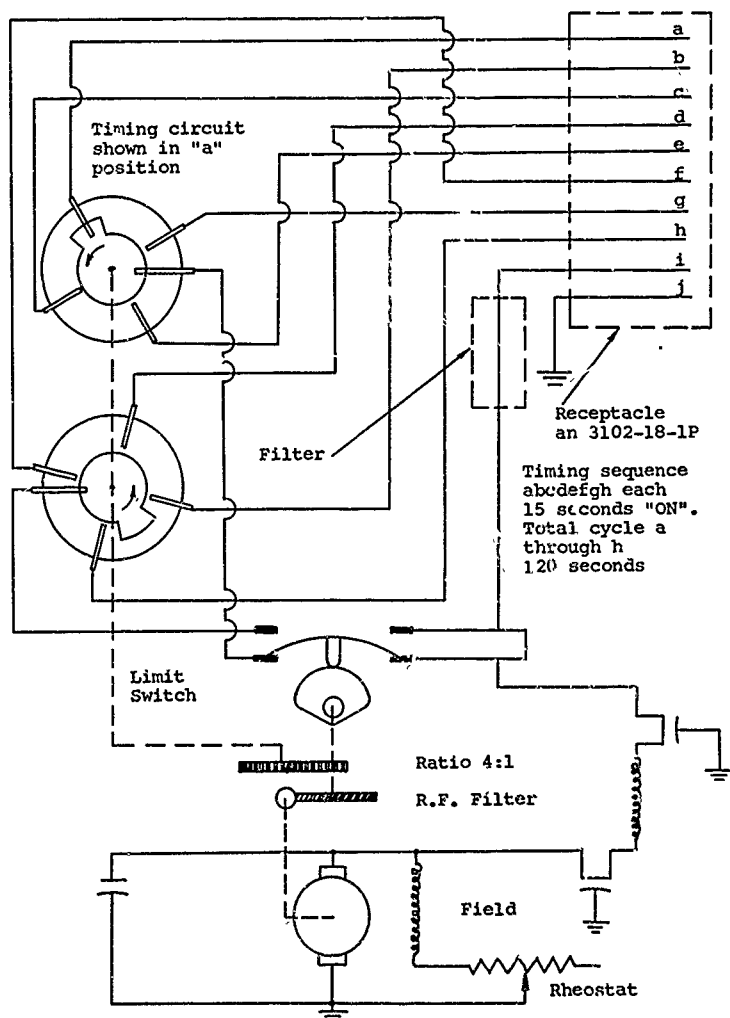
Figure 125. 28-Volt DC Ice Control
Cyclic Time Schematic.

300
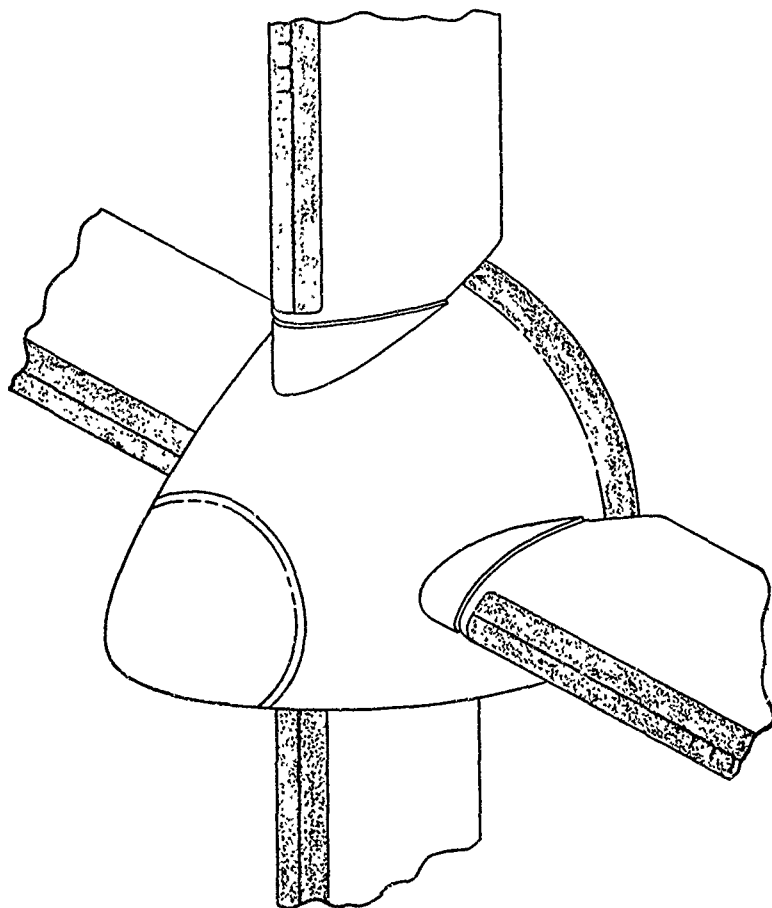
Each prop; on 30 sec., off 90 sec.
11 kw

Figure 126.   Phase A – Deicing.

301
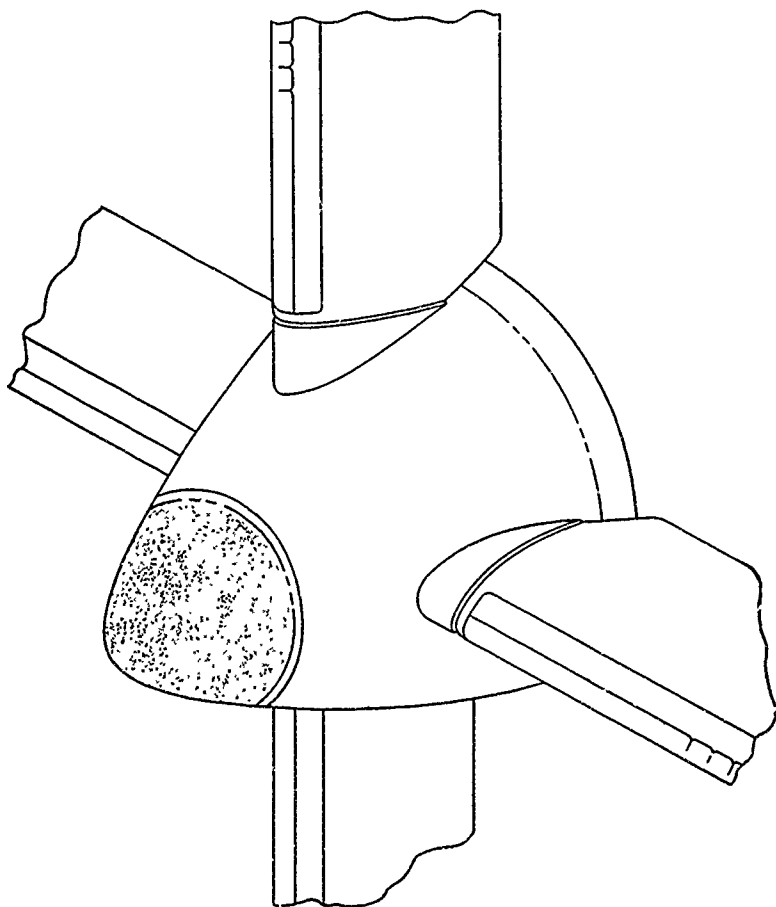
Four Spinners on Full Time
11 kw

Figure 127.   Phase B - Anti-Icing.
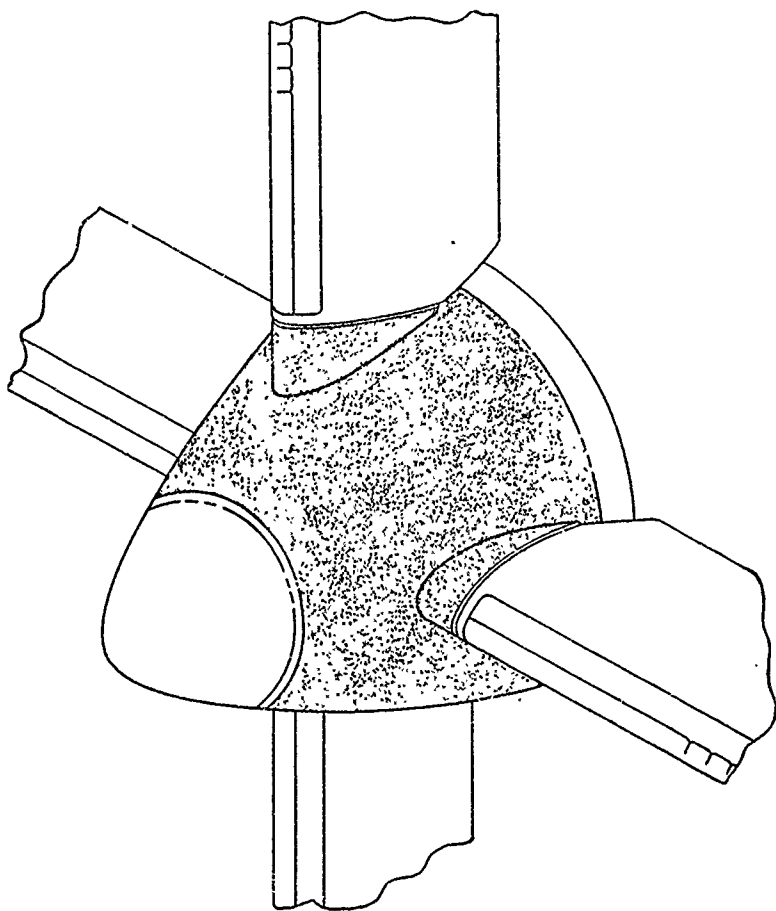
Each Spinner on 30 sec., off 90 sec.
11 kw

Figure 128. Phase C -- Deicing.

irreplaceable. Every effort must be made here to provide element designs with an unlimited service life since loss of the element could cause the entire blade to be retired.

The external rubber or neoprene element will normally contain stranded resistance wires woven into a fiber glass carrier and connected to bus bars at the root and tip ends of the element. Wire sizes are selected to provide the watt density required at the available voltage. The raw rubber cover of the element is sandwiched on each side of the resistance element and then molded together under heat and pressure on a flat plate. The rubber is tapered each side of the element to a feather edge for minimum airfoil discontinuity. An element of this type should withstand temperatures up to 200°F. Normally the rubber thickness next to the blade will be of the order of twice as thick as that on the outside surface. This puts the resistance wires closer to the iced surface and gives more insulation on the blade side.

Aerodynamically it is desirable to hold the heating element thickness as low as possible. The heating element will increase the operating L.E. radius an amount equal to its own thickness which can be a multiple of the desired LER. In addition 20-25% of the important L.E. area of the blade will have significant airfoil contour variations. Offsetting these airfoil modifications is the limiting of external boots to the inboard 60-75% of the blade, leaving the tip unaffected. In actual static thrust tests and flight tests aerodynamic losses due to deicing boots have been found to be negligible or within test accuracy. Nevertheless strong efforts have been made to limit deicing boot thickness and even rebate them in the leading edge. Figure 129 illustrates a normal and a rebated L.E. installation.

Despite efforts to minimize element thickness practical considerations of manufacture, durability and ability to pass hi-pot checks to prevent shorting to the blade require standard rubber deicing boots of .080" to .090" thick.

Being installed on the blade L.E., the heating element is vulnerable to erosion damage. While the rubber resists sand or small particle erosion very well it is highly susceptible to rain erosion and stone damage. It is therefore standard practice to protect the boot with about a .015" thick L.E. sheath of electroformed nickel or dead soft scalloped stainless steel. The nickel provides superior protection, but the stainless is adequate and much cheaper since elements are stripped and replaced at overhaul anyway to permit NDT inspection of the blade. The dead soft stainless sheath is easily fitted to the L.E., its only preform being the L.E. radius required and relief in bus bar areas.

304

Standard Deicing Boot
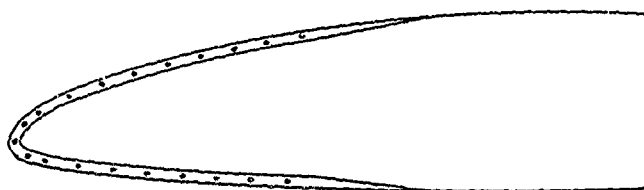
Deicing Boot

Figure 129. Deicing Boot Installation.

LIGHTNING CONSIDERATIONS

Metal Propellers

Propellers are subject to lightning strikes,especially in com-
mercial operation. While such strikes are common, only in a
relatively few cases has any significant damage been encountered
on metal propeller blades. Damage when it does occur results
in arc burns on the blade, sometimes several and in a string.
Most such arc burns are repairable by blending and polishing
as if it were a nick or gouge. The repaired area is then
etched for the severity and extent of the heat-affected zone.
Limits can be set for acceptability, preferably by sample
fatigue tests of representative damage.

Composite Propellers

The lightning problem on composite propeller blades is not yet
well known. With the advent of the use of fiber glass and ad-
vanced composites in major aircraft structures, much work is
being done to understand the phenomenon and develop protection
means which will undoubtedly apply to propellers and rotor
blades also.

At one time it was considered that 90% of lightning strikes
contained less than 50,000 amps. Recent data indicates that
10% of the strokes can be above 160 kiloamps, with some as high
as 300 kiloamps. By contrast an unprotected foam-filled fiber
glass blade tested in the G.E. lightning test laboratory when
hit by a 3-million volt 22,500 amp stroke was badly damaged
and split open down the leading edge. Other structures made
from advanced composites are reported to also be very suscep-
tible, especially Boron, which has tungsten wire at the center
of its filaments. In the case of foam-filled fiber glass blades
it was found that grounding a full length stainless steel ero-
sion strip to the steel shank protected the blade from repeated
hits by the 3-million volt, 10-foot arc at 22,500 amps and even
a 4" arc at 25,000 amps. By direct connection at about 40,000
to 50,000 amps the grounded erosion strip was vaporized at the
root of each scallop. The blade was undamaged except for local
scorching where the strip vaporized. Conductive paints gave
protection but the need for more conductivity was indicated.

It is really not known if in actual lightning conditions
whether a strike would seek out a conductive L.E. erosion strip
or an unprotected part of the blade. It may be necessary to
provide a protection network of conductive strips to form a
Faraday cage. In any event, capacity to handle 100,000 amps to
160,000 amps is needed, and perhaps as much as 300,000 for
some installations. The probabilities seem reasonable that

306

any system can be sacrificial since two strikes in one flight on one blade would appear to be unlikely.

The use of internal conductive structures such as metal spars or aluminum honeycomb cores will probably compound the problem of protection. It has been considered that an aluminum honeycomb core in a rotor blade may have to be grounded to an external metal T.E.

Lightning protection of composite blades remains a major area in need of future research.

MANUFACTURING METHODS - SOLID ALUMINUM ALLOY BLADES

Forgings

Solid aluminum alloy blades are fabricated from forgings of the alloy designed for. Alloys 2025 S, 7075 S or 7076 S are the most common. Full-length forging dies are used either in a drop hammer or press. Closer tolerances of the forging and thus less finish allowances are possible by press forging. It should be possible with development to forge a blade which would require only minimal skin removal plus shank machining. Typical forging allowances for blade finishing on drop hammer forgings run from 1/16" to 1/8" all over except up to 3/16" on the T.E. Blade angle tolerance is of the order of $\pm 1/2^\circ$. Press forgings should reduce these allowances about one-half. Forging size is limited by available equipment and surface area of the blade.

Flanged root ends are generally upset while using a piercing punch to get good grain flow around the flange root radius. If a spacer ring or thrust washer is used it must be protected and positioned before upset. As received the heat treated forgings must be inspected dimensionally and for forging defects. It is frequently necessary to bend the forging straight in a hydraulic straightener and to correct blade angles in a twist machine which can twist the forging between stations.

Master Blade

It is normal practice to produce a master blade before production manufacture is started. Master blades are produced by hand sinking stations to template with files and hogging off surplus stock, and then doing the close work with files again. The work is done on a heavy steel blade table with an accurate surface and marked stations. The machined shank is clamped in a head on the table so it can be rotated to proper blade angles and to position the blade for the hand working. Great skill is needed to do accurate work.

307

The blade surfaces are usually given a satin finish with an
orbital sander and possibly high polished. The finished master
blade is inspected to tolerances such as in Army Spec. 98-29520
-A as follows:

Blade length	$\pm$ 1/32"
Blade width	$\pm$ .010"
Blade thickness	$\pm$ .003"
Edge alignment	$\pm$ .020"
Face alignment	$\pm$ .020"
Template fit	$\pm$ .015"
Blade angle	$\pm$ .10°
Longitudinal location of stations	$\pm$ .010"

The accepted master blade is used to produce cams and patterns
for the tracer machines to be used to cut production blades
and it also may become the balance master.

Production Blade Fabrication

Starting with an acceptable forging the shank is first lathe
machined so that it becomes the locater for all subsequent
work. The forging is then positioned in a blade contour mach-
ine or series of machines and machined all over using the
master patterns or cams to control the work. These machining
operations are very fast and leave significant cutting tool
marks on the blade. Machines for this kind of work have been
produced by Sundstrand and Berliner among others.

Finishing

The rough machined blade is next ground with hand discers or
belt sanders to clean up the tool marks and finally given a
satin finish. A highly polished finish is seldom used. At
this stage it is necessary to check balance the blade to see
if additional stock removal is required for horizontal or ver-
tical correction. Horizontal balance may be checked in a
Gisholt machine set to the master and vertical balance in a
Toledo machine also set to the master.

A Gisholt machine consists of a horizontal cradle pivoted near
the center much like a scale balance. The blade is positioned
accurately with respect to the pivot on one end of the cradle
and a master balance weight on the other end. Provisions are
incorporated to directly read the blade error compared to the
master in inch-pounds and fractions. The Toledo type of ver-
tical balance machine consists of a table type platform pivoted
across one axis. The blade shank is clamped to the table and

in effect stands vertically. The unbalance of the blade is
checked first with the blade reference station at 90° to the
pivots for lead/trail balance, and then the reference station
is rotated 90° to read face/camber unbalance.

Before all stock is removed the blade will be dimensionally
checked to tolerances such as in Army Spec. 98-29518-J and for
fairness to be sure the best areas for further stock removal
are selected. In addition, the blade could be given a caustic
etch inspection for metal defects and/or a dye penetrant in-
spection. Final satin finish can then proceed.

Final Finishing and Balance

Final finishing on some designs will include shot peening with
large shot in critical areas such as the inboard one-third of
the blade. The shank area on flange type shanks is usually
shot peened also, sometimes after first cold rolling the bear-
ing area. Another practice is to grit blast the blade all
over before shot peening.

No matter what the final mechanical finish it is common to
anodize the blade all over as a final step. Anodizing will
disclose any further fissures or surface defects by staining
around such spots. Also, anodizing is a protection from cor-
rosion and provides a good base for paint and adhesives if
specified. Final balance is carried out before painting since
the paint is largely eroded away in service. If balance weight
is required at final balance it is usually provided by pounding
lead wool in the shank hole topped by a suitable stopper to
prevent it loosening in service. The total blade weight is
recorded.

The blade may receive a final dimensional inspection and ac-
ceptance stamps at this time.

Accessories, if any, such as shank cuffs or fairings and de-
icing boots are added, and the blade is painted if called for.
Balance variations from these additions are offset in propel-
ler assembly balance.

MANUFACTURING METHODS - WELDED HOLLOW STEEL BLADES

Fabrication of welded hollow steel blades starts with the pro-
curement of rolled steel plates. The steel is produced to
rigid specifications. Although the steel may be basically
chrome-nickel-molybdenum electric furnace SAE 4320 or 4330 it
will be modified especially to suit blade manufacture. Each
heat is carefully controlled for chemical analysis and kept

309

low in sulphur and phosphorus and other elements detrimental
for good weldability. Each heat's identity will be carried
through to the finished blade. While all the usual checks are
performed, special attention is given to actual weldability
tests before delivery; cleanliness and freedom from excessive
porosity, segregations, laminations and inclusions, fracture
grain size and minimum hardenability. The mechanical proper-
ties of the steel are also checked to see that they are
approximately the same for both longitudinal and transverse
specimens. As delivered the rolled plates will be free of scale
and surface decarburization or carburization beyond limits with
a smooth ground finish and with a full spheroidized anneal for
easy machining and forming. Naturally the plates will meet
dimensional requirements including flatness. Received plates
are also given a full inspection in house.

Plate Machining

The rough plates are given serial numbers listed against heat
numbers which remain throughout the manufacturing process.
This emphasis on identification of all materials and processes
is invaluable in the event a service problem develops. Cor-
rective action resulting, if any, can identify and limit the
number of blades involved. All operations are also dated and
operators identified for the same reasons.

The plates must first be surface ground on one side for assur-
ance of a flat working surface and to clean up any decarbur-
ization left from the steel mill. The plates then have accurate
holes made and closely located at each end of the plate on the
blade center line. These holes assure accurate location during
subsequent machining and forming. Both the camber plate and the
thrust plates are processed the same except for detailed dimen-
sions until they are welded together.

The shank end of the plates are broken down in a hydraulic press
to permit milling cutter clearance of this area to preserve
full stock thickness for later upsetting. See Figure 130. The
plate is next clamped to a tapered milling fixture in a large
milling machine and rough tapered milled as shown in Figure 130.
The milling cutter does not span the full width of the yet rec-
tangular plate in order to leave lips at each edge of the plate
for later clamping. A second and finishing taper mill cut is
usually required to obtain accurate taper dimensions. The
thickness of the taper cut at any station is equal to the re-
quired finished edge fillet thickness plus allowances for later
blade finishing. If the taper cut deviates only slightly from
a straight line, the plate can be brought down to the required
curve on the milling fixture by straight clamping. If a sub-
stantial curve is required this can be formed into the plate at
shank breakdown to fit the milling fixture. A climbing milling

310
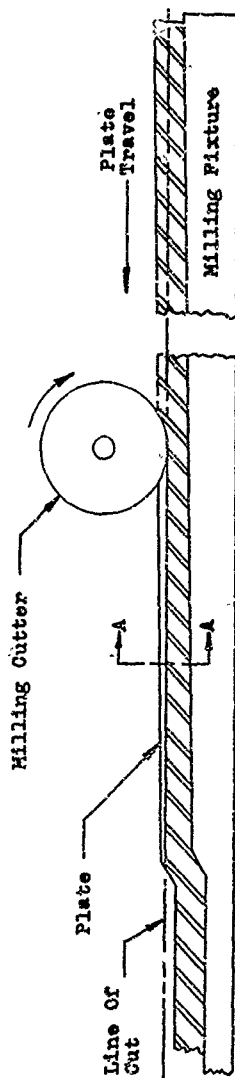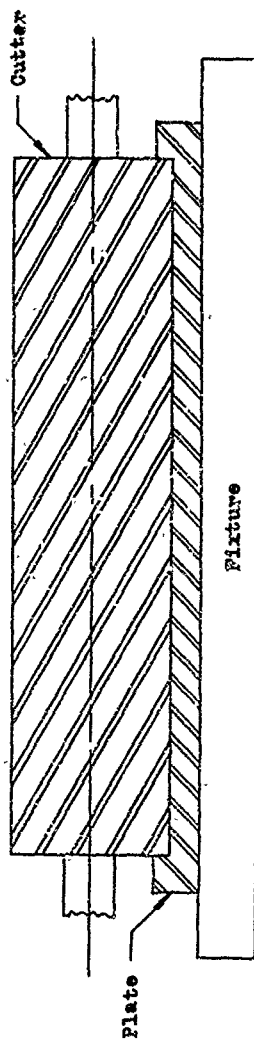
Figure 130. Taper Milling Operation.

cut helps keep the plate flat on the fixture. If the plate is to have ribs contoured straddle milling cutters split at the rib location are used which leave a stub rib with proper root fillets. On a full steel rib blade design the same technique is used but the plates can have had a rough rib rolled in at the steel mill to provide additional rib height.

Each plate is inspected for proper dimensions plus any visual metallurgical defects.

The tapered milled plate is next sent to the hydraulic press for another breakdown operation. This time the peripheral LE, TE and tip edges are bent down to permit milling the thinner center plate areas while maintaining proper edge fillet contours and thickness. See Figure 131. Again the plate is clamped to a contoured and tapered milling fixture where hydraulic clamps pull the plate down tightly to the fixture. The plate may have been given a slight convex transverse bow in the press operation to assure its laying flat on the fixture when clamped.

One or more milling cuts may be required to reduce the center plate area to size. The plate is then buffed or lightly ground to blend the characteristic milling marks and to obtain the desired surface finish. The plate is completely inspected dimensionally and visually.

The still rectangular plate is again returned to the large hydraulic press where it is blanked or sheared to its proper planform shape in one stroke. Figure 132 illustrates the operation on the plate, and the different width between the thrust and camber plates is apparent and reflects the construction shown in Figures 96 and 97. For edge welded blades the plates can be symmetrical and identical.

The blanked plates are now formed to the proper airfoil shape but without twist in the hydraulic press. Originally the plates were formed with twist but the advent of the pressure die eliminated this requirement. During the plate forming the edges are crimped over slightly to obtain proper restraint to assure proper strain of the metal. The plates are now called shells.

The formed shells must next have the crimped edges ground or milled to the proper configuration. Edge welded blades will have matching edges beveled for proper welding.

The finished shells are weighed and horizontal balance checked and paired with each other for best total balance. The paired shells are adjusted to fit each other properly by minor hand grinding if required. The shells are stress relieved and magnafluxed preparatory to welding.

312
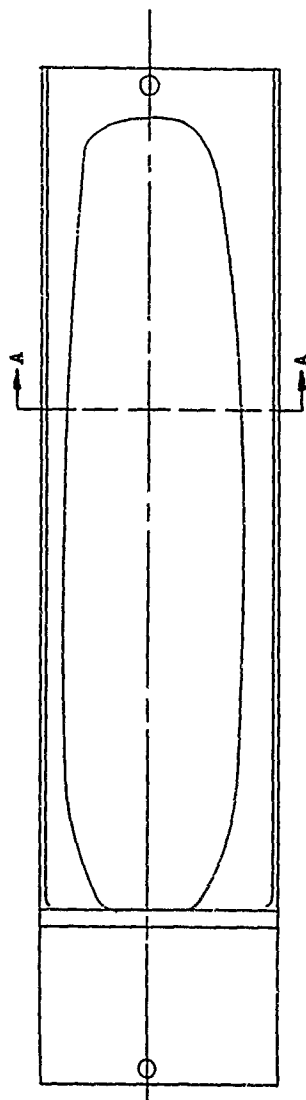
Finish Milled Plate

Cutter

Clamp

Plate

Milling Fixture

Clamp
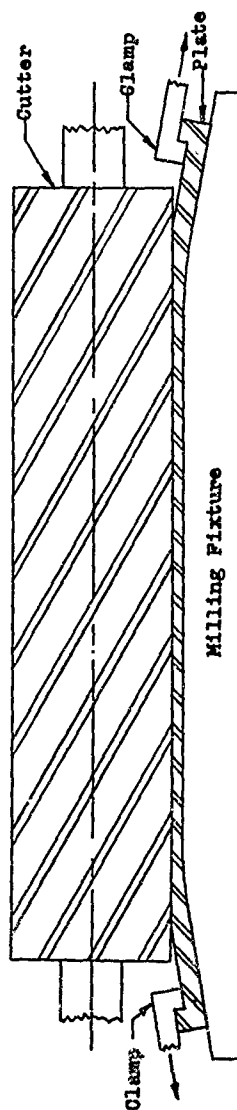
Enlarged Section A - A During Milling

Figure 131. Finish Milling of Plate.

313
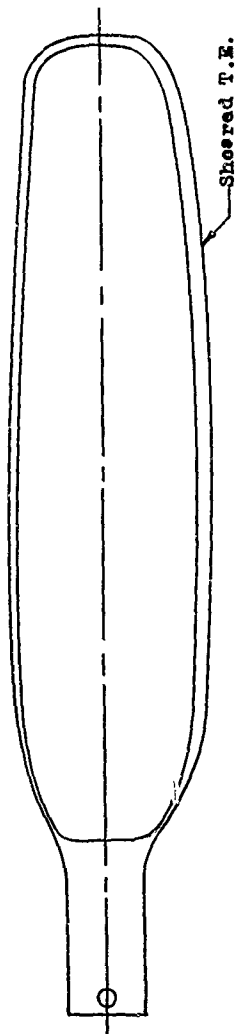
Blanked Camber Plate
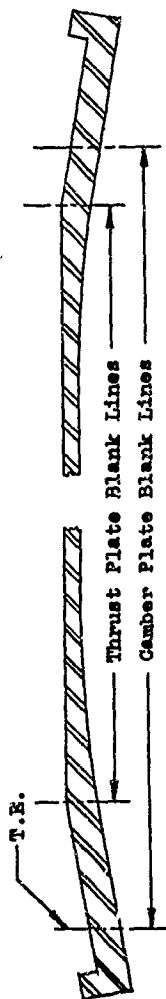
Cross Section Before Blanking

Figure 132. Plate Blanking.

Welding and Weld Grinding

For a side-welded blade the clean shells are assembled in a heated welding jig with a series of mandrels to hold the shells at their proper spacing (see Figure 133). After proper preheat of the assembly has been reached, hand tie-in welds are made simultaneously on each edge of the thrust shell. Burn back of the thrust shell has been allowed for. If the weld gap is large in some areas, a buildup bead or beads may be required to make the tie-in. The dual shank seams are not welded at this time. Highly skilled welders are required, and the high heat around the jig necessitates frequent rest periods. Very little metal is deposited. After suitable post heating, the mandrels are withdrawn through the shank, the blade is removed from the jig, and the weld is X-rayed and magnafluxed.

For an edge-welded blade, the shells are clamped in a vertical fixture with a copper mandrel which acts as a heat robber and chills the weld metal into a radius. Welding is done automatically by a submerged melt arc under a bed of granular flux which protects the weld from oxidation with a fused glass like covering. The entire weld seam from shank to tip on one side is welded and the fixture rotated and the second edge welded. Additional buildup beads are added as required. X-ray and magnaflux inspections are carried out.

The side-welded blade after tie-in is also automatically submerged melt welded to add the required fill-in beads and to make the dual shank seam welds.

The edge-welded blade needs no additional fill-in beads, but the edges must be ground and prepared for automatic welding the leading and trailing edge solid edge strips and hand welding the tip.

Both type blades are again X-rayed and magnafluxed after a radius grind operation to roughly remove excess weld metal.

Because of the heavy weld penetration required in the shank seam area, these welds require an internal washdown with the hand atomic hydrogen torch plus another X-ray and magnaflux of this area.

The finish welded blade is stress relieved as soon as possible and prepared for any weld repairs.

The high stress and fatigue environment of a propeller blade requires very high weld quality to be maintained. Such things as out of specification porosity, inclusions, cracks, hydrogen flakes and undercuts must be corrected. This is done by making local grindouts of the defect and atomic hydrogen or heli-arc hand weld repairing with suitable preheat and post heat followed by stress relieving and reinspection.

Welding Rod

Weld Fixture

Shell

Granular Flux

Copper Mandrel

Weld Fixture

Shell

Edge Welding

Shells

Weld Jig

Weld Jig

Side Welding

Mandrels
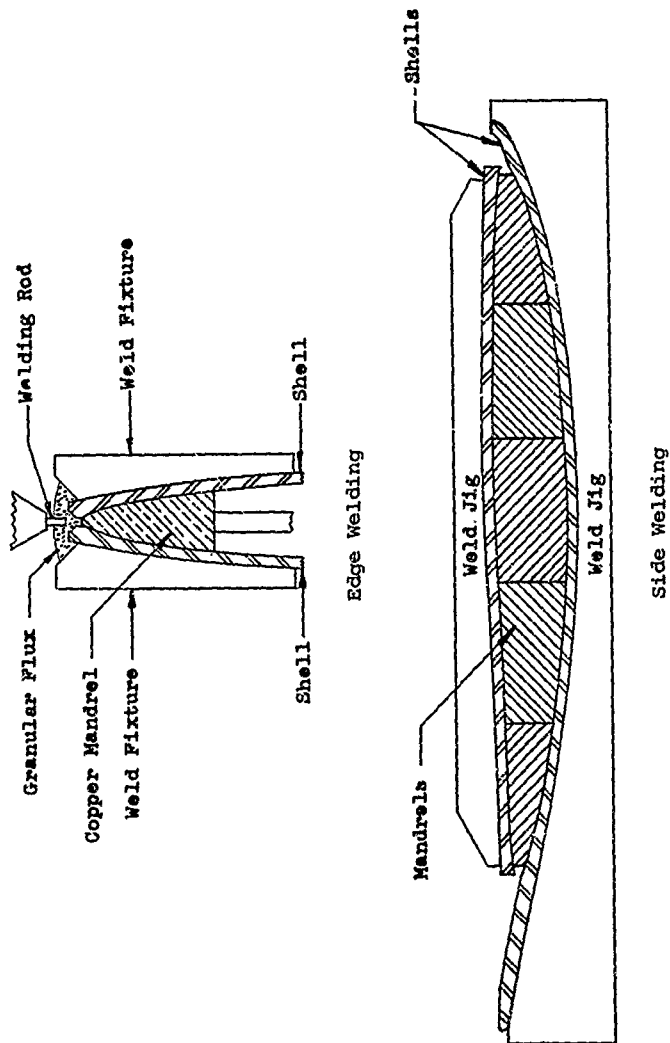
Figure 133. Two Methods of Welding Blades.

The rough blade edges must be notched for proper leading-edge alignment and chord width at each station. Reference may be made to the last X-rays to assure control of solid edge widths. After notching, the excess solid edge metal is ground off and the rough weld metal radius is ground to template fit, then the rough weld surfaces are cleaned. Too much oversize remaining can cause coining of the solid edges and incomplete closure of the pressure die later. Too little metal will preclude proper forming of the edges.

Shank Upset

The blade is prepared for upsetting the shank flange by hot swaging it round and welding a ring around the shank at the proper location by automatic submerged melt welding. The welded ring is then machined to properly fit the upset dies. The design is such at this operation that all ring weld material will be removed at final shank machining or if a cuff ring is called for on the finished blade the weld metal will be outside the cuff ring root radius and never in the basic blade surface. The shank is cut to proper length removing the locating hole.

The prepared shank is now induction heated, while surrounded by a protective atmosphere to prevent scaling, to proper forging temperature. The ring area is not heated. The heated blade is quickly located in a large Ajax upsetting machine and rapidly progressed through two or more upset dies, receiving one or more upset strokes in each cavity. The hot shank is slow cooled in a box of mica. The shank is illustrated in Figure 134 before and after upset. This operation is carefully controlled to give proper grain flow throughout, especially in the flange root radius area. After cooling the shank is rough machined.

Pressure Die Form and Stress Relief

Up to this point the blade has been produced without twist to simplify tooling, and in the case of an edge-welded blade even symmetrical - which permits the blade to be pressure die formed either right or left handed. The blade is heated to about 1600°F to 1700°F in a controlled atmosphere electric pit furnace. When the blade has soaked the required time it is rapidly transferred to a female steel die in a large hydraulic press. The die cavity is an accurate representation of the blade with a full twist. The die is closed and a breech block similar to that of a cannon is closed against the butt of the shank and simultaneously nitrogen gas is transferred to the blade cavity through the breech block at 1000 to 1500 psi.

This entire operation must be done in about 20 seconds. In this operation the die will lightly coin and shape the solid

Before Upset

After Upset
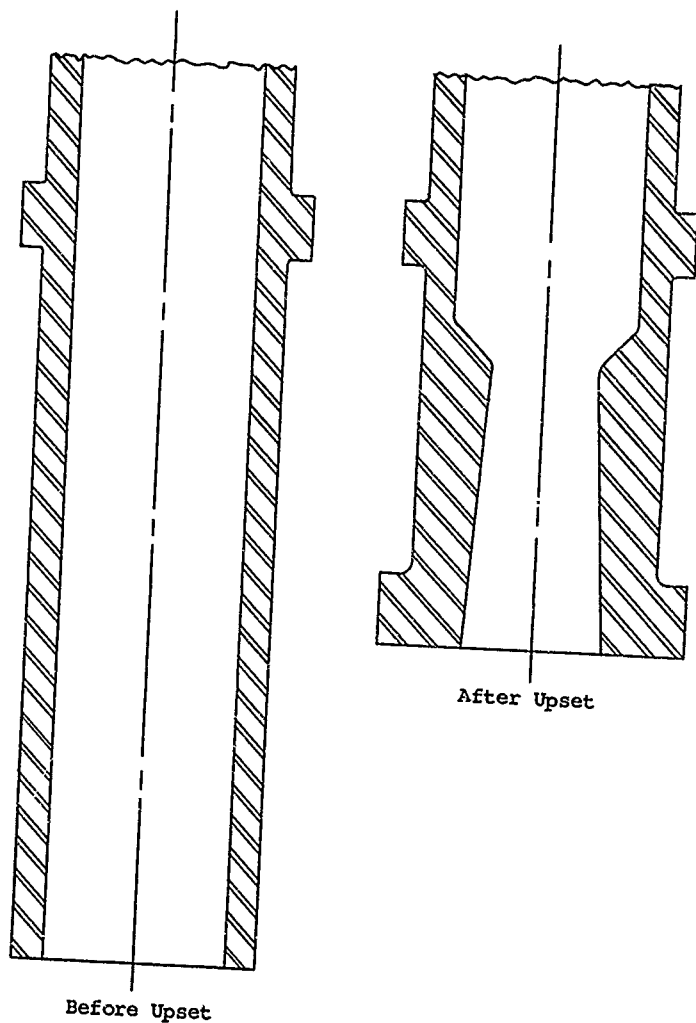
Figure 134. Shank Upset.

318

edges, and the nitrogen will inflate the blade cavity to the
shape of the die. After about two minutes the blade is re-
moved from the die and immediately placed in a stress relief
furnace. The blade is then steel grit blasted inside and out,
polished, and given a complete X-ray and magnaflux inspection
inside and out. Any weld repairs required are made
with the usual preheat, postheat and stress relief.   It should
be mentioned that weld repairs are limited to original weld
metal areas only. Welds are never permitted in the high-
stressed plate areas.

Clean and Braze Edges

The grit blasted internal edges are further cleaned and pickled
for braze and the blade is loaded in an automatic edge fillet
brazing machine. This machine consists of a small gas fired
furnace which concentrates its heat on the blade bondline from
both sides of the blade for about a 4"-6" length on one edge
at a time. A traversing mechanism is cam controlled to hold
the blade edge down and horizontal in the furnace, compensating
for the blade curvature. The traversing mechanism is auto-
matically actuated by an optical pyrometer mounted in the fur-
nace and can also be manually actuated by the operator.

After positioning the blade tip in the machine the edge to be
brazed is loaded with clean and fluxed CuMn pellets by a tube
device which meters the required amount of pellets at each
station.

Actual brazing starts at the tip end and when the optical
pyrometer senses that the melting point of the CuMn has been
reached it signals for traverse to begin. A small molten pool
of copper manganese is therefore maintained in the blade area
opposite the furnace as the blade traverse progressively moves
fresh unbrazed areas into the furnace. As the molten pool
leaves the furnace it progressively chills in the form of a
true radius or meniscus in the internal edge. The machine can
be programmed to do an almost perfect job of filleting the in-
ternal edges. When one edge is completed the blade is turned
over and the second edge brazed the same way. On some designs,
such as with square tips, the tip area may be brazed in a ver-
tical brazing machine first. During the brazing operation the
blade internal cavity is purged with a protective atmosphere
to prevent the formation of scale and decarb.

After the blade has been brazed and slow cooled and stress re-
lieved, it is grit blasted inside and out, and the the edges are
magnafluxed, X-rayed and inspected internally by visual bore-
scope examination. These inspections assure that no cracks
have been developed in the blade, and that the copper has the
proper width, the proper meniscus, and is free of shrinkage
cracks.

Pressure Die Quench and Draw

The brazed, cleaned and inspected blade is now ready for heat treatment and final form. It is heated in the controlled atmosphere electric pit furnace to the proper quench temperature and again rapidly transferred to the pressure die in the large hydraulic press. The nitrogen pressure is applied but this time additional quenching in the heavy wall shank sections is also applied. Depending on the wall thicknesses in the shank area and the alloy, either quench water or quench air is applied and distributed over the blade surface through waffle iron type grids in the die covering the affected areas. In the major portion of the blade the chilling action of the die at proper temperature is adequate for full quench, keeping in mind that chrome nickel moly steel is air hardening. After quench and form the blade is drawn in a pit furnace to the desired hardness level, generally Rockwell C 38-42.

The blade is now cleaned of all scale by the automatic Bullard Dunn process which is a carousel type machine that indexes the blade from one tank to another for the several steps in the process and includes acid stripping of the scale down to bare metal, at which time the bare areas are automatically coated with tin to stop the acid action. After descaling is complete the tin is stripped. The Bullard Dunn operation may be followed by another clean and pickle operation and grit blast. Rockwell hardness readings are then taken and the blade is magnafluxed. It should be explained that blade magnaflux is done both by direct connection of the tip and shank to detect longitudinal indications and by a coil to detect transverse indications. Properly used magnaflux will not only pick up surface and sub-surface cracks but thin plate, porosity, dirty steel, heavy copper fillets and inclusions.

Metal Finishing

The shank is now rough turned in a lathe to specified oversize dimensions and the blade sent to improve contour. Before the pressure die came into use this was a major operation, but since its use only minor corrections in contour are normally required, if any. When required this can mean driving internal mandrels into the blade plus external hammering followed by stress relieving. The blade edges are ground to template fit, and balance lines are scribed on the shank at $0°$ and $90°$ with respect to the reference station. The blade is now check balanced both horizontally and vertically. At this point the blade is marked for throw so that the shank can be finished on an axis to favor vertical balance.

The shank is finish turned and bored based on the previous balance check and finish ground. After inspecting the finished

shank it is blended at the outboard end of the machining and
given another check balance. Final notch and trim will follow
to obtain the best edge alignment and chord width while being
guided by the balance data. The blade is then polished all
over using carborendum impregnated cotton wheels and given
another check balance.

Blade Finish Operations

The polished blade is inspected ultrasonically for wall thick-
ness all over. In the heavy wall highly curved shank sections
deep throat dial micrometer readings must be taken. At close
intervals at each station wall thickness deviations from speci-
fication are marked ± on the blade. These readings are a guide
to where and how much stock can be removed. With this infor-
mation and the previous balance data the blade is ground down
to master balance plus allowance and check balanced again.

The blade is now given a fine finish to specified RMS quality
and check balanced again. Final X-ray inspection is made and
another magnaflux carried out. Tip vent holes are drilled, the
blade is lightly grit blasted inside, and the internal edges are
shot peened to specified intensity if called for, plus shot
peen of any other areas required. Shot peening of the copper
fillets may seem strange, but tests have shown significant im-
provement in fatigue strength in wishbone section fatigue tests
which simulate the effect of plate diaphragming at the internal
edge.

If a rubber rib or fillets are called for the blade is prepared
using a full internal flush of hot alkali solution followed by
a water rinse, steam and air dry. Using fresh clean unused
aluminum oxide grit or clean angular steel grit the entire in-
ternal surfaces are grit blasted and checked for complete
coverage. This cleaning must be followed immediately by flush-
ing with the proper adhesive primer and dried with hot dry air
before surface contamination or oxidizing can take place.
This is repeated using the proper adhesive for vulcanize bond-
ing of the rubber insert. Besides forming an excellent bond
with the injected rubber insert this adhesive system provides
excellent corrosion protection for the internal blade surfaces.

Rubber ribs are molded using segmented metal mandrels, usually
steel; these must be absolutely clean, free of burrs or rough
spots, and coated with a suitable parting compound.

The mill rolls must also be clean before milling the raw rubber
compound. Also the injector must be cleaned. The injector
consists of a hydraulic ram, a loading port, and a long heated
injector nozzle which connects to the main mandrel which also
has a distribution passage or passages bored in it.

The mandrels are inserted through the shank and properly positioned in the blade. The blade is placed in the heated steel rubber molding die. This is generally a partial die, covering only that part of the blade radius containing the insert. It normally is relieved over the solid edge areas. A gasket material may be placed between the die and the blade to absorb minor irregularities of fit. The injector tube is connected to the mandrels and the injector ram. Wires from warning sensors mounted in the tip of the mandrels are connected to external lights.

The raw rubber is now milled until it is completely broken down and rolled tightly into sausage-shaped pellets which will just fit the injector loading port. The blade temperature and injector nozzle temperature are brought up to heat, about 60° to 70°F below cure temperature. The weighed pellets are now fed one at a time through the injector, the ram making one stroke per pellet. Every effort must be made to exclude air between the pellets. Injection pressure will run from about 15,000 psi to 20,000 psi on the raw rubber. As the weight of injected rubber reaches the specified amount, the tip sensor light indicates that the rib cavity is nearly full. Usually a specified ram travel follows this signal. During cure the ram pressure is reduced sufficiently to just hold the position. Die temperature is raised to vulcanizing temperature and held for the specified cycle time.

After cure the mandrels are pulled and the rubber insert is inspected with a borescope and X-rayed for proper position, width and porosity. While ultrasonic inspection can determine complete lack of bond if it exists it has been found that by pressurizing the blade and taking readings of blade thickness over the rib before and after pressurizing, a more reliable check of the bond can be made and it also constitutes a sort of proof test.

Final Inspection, Operations and Aerodynamic Matching

The blade is now fully inspected with the finished external dimensions and angles read. The template fits are also checked. The operation is done on a propeller blade inspection table with the shank mounted in a head on the table to provide accurate centerline positioning over the table. The head is also indexed with a vernier angle reading scale for measuring blade angles. As part of this operation measurements are also made which are required to find the aerodynamic angles. The measurement of the aerodynamic angles is made by a caliper device which centers itself on the T.E. with jaws closing on the maximum thickness point of the profile, and in effect measures the angle between the T.E. and maximum ordinate of the mean camber line. With this data and the final read data an

aerodynamic calculation can be made resulting in a $\Delta\beta$ correction angle which will give aerodynamic thrust matching between blades in a propeller. The $\Delta\beta$ angle will indicate a ± degree correction at the reference station of each blade when assembling the propeller. The $\Delta\beta$ correction is steel stamped on the butt end of the shank.

A series of miscellaneous operations follows which include additional balance checks, compound or high finish to get the required balance, tin plate the balance cup bore, paint the inside with a light colored paint to cover the black rubber rib adhesive and give better visibility for service inspections and magnaflux, final ultrasonic and shank wall thickness inspect, machine splines and check concentricity, cold roll the shank bearing surfaces and flange root radius for improved fatigue strength and shot peen the bearing surfaces for better galling resistance.

Zinc Plate, Balance and Final Inspections

The blade is zinc plated with a coating normally .0005" to .001" thick. Some variation up to .001" may be permitted to aid in balance. Plating is followed by yellow anozinc treatment and a single coat of clear lacquer. The blade is baked for one hour at about 180°-200°F to drive off any hydrogen from plating and to dry the lacquer. The balance cup is installed and the blade final balanced with corrective lead added to the cup. All final inspections are made including final magnaflux and inspection stamps and identification numbers stenciled on the butt end of the shank. The blade is now complete.

MANUFACTURING METHODS – EXTRUDED HOLLOW STEEL BLADES

Extruded monocoque hollow steel blades are produced from chrome-nickel-molybdenum electric furnace steel basically modified SAE 4320 or 4330. Some designs may go as high as SAE 4340. As with welded blade steel the billets are produced to rigid specifications controlling chemical analysis, cleanliness, mechanical properties and moderate weldability. Billets are given substantial hot working before delivery by forging and are identified by heat number.

The forged billet is machined all over to precise dimensions including a central pilot hole. Because the extrusion process produces a tapered wall thickness the precise volume of the billet is important to assure that the extrusion mandrel position with respect to the extrusion die is maintained throughout the process. Without this control the desired wall thickness can be off station. Billets are checked for volume by the

323

water displacement method and by weight.

Extrusion

The extrusion process is carried out in three steps with salt
bath heating between each operation to control scale, decarb
and aid in surface lubrication. Press capacity will range from
5500 tons to 12,000 tons. Die and mandrel lubrication is
essential and involves proprietary high pressure and high tem-
perature lubricants. Die and mandrel materials are also pro-
prietary including special hard facings to withstand the
tremendous pressures of extrusion. Extrusion temperatures are
in the 2100°F range.

The heated billet is placed in the press container, the con-
toured conical shaped mandrel advances the billet to the die
face and as pressure builds the billet back extrudes over the
mandrel and then starts extruding out the die. Figure 135
shows the mandrel at the end of its stroke. The billet now
consists of the unextruded butt section and a constant O.D.
extruded stem with tapering wall thickness. The billet may
now be slow cooled to await the second operation.

The second step is an expansion and sizing operation which con-
verts the constant O.D. extrusion produced in the first step
to a tapering O.D., which forms the transition from the outboard
tube O.D. to the root end. Figure 134 shows how the contoured
mandrel expands the reheated billet to the shape of the die.
While no extrusion takes place the outboard ear starts of the
extruded tube are forged in preparation for the third step ex-
trusion. Again the billet is removed from the die and slow
cooled to await the final extrusion operation.

The third step is the final and most critical extrusion of the
constant O.D. and tapering wall outboard tube section with ears.
See Figure 90 for an illustration of the finished extruded tube
and outboard cross section. The reheated billet is placed in
the press which now has the die and mandrel with ears which
will give the outboard shape shown in Figure 90. Figure 135
illustrates the third step extrusion at the end of the stroke.
As the press ram advances and extrusion takes place, the shank
end of the tube is guided by the pilot bar and sliding guide.
The tapering shape of the mandrel is programmed by volume so
that the proper mandrel station is at the die lip corresponding
to the tube station then passing through the die. The result
is proper tube wall thickness taper. Similarly the tapered
ears on the mandrel provide the proper fillets and radii at
the internal tube ear edges.

At the end of the extrusion stroke the unextruded butt section
of the billet is cut off and the finished tube slow cooled and

324
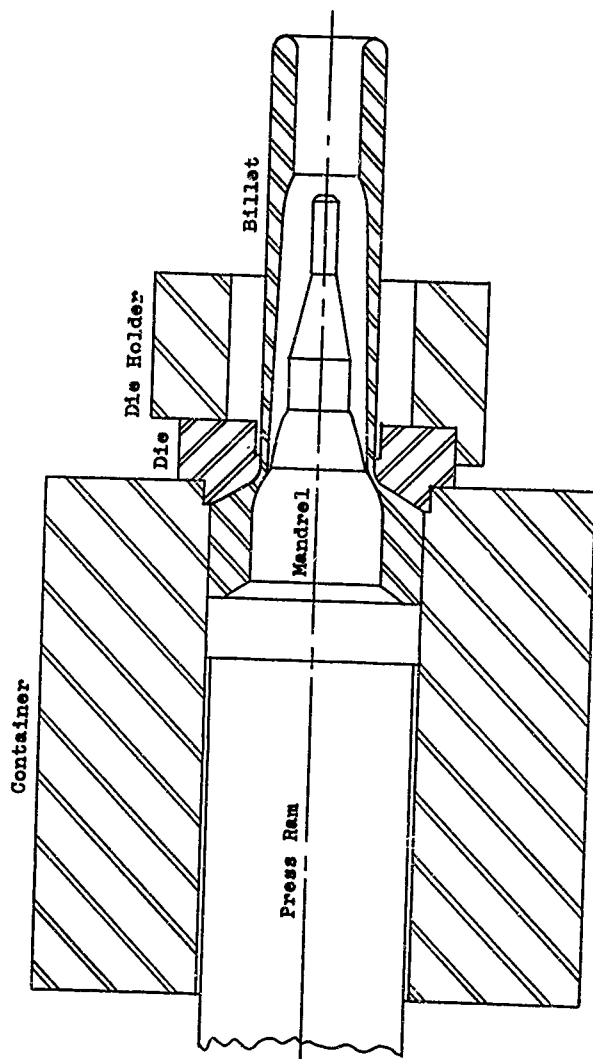
Figure 135. First Step – Extrusion.

Container

Press Ram

Die Holder

Die

Billet

Mandrel
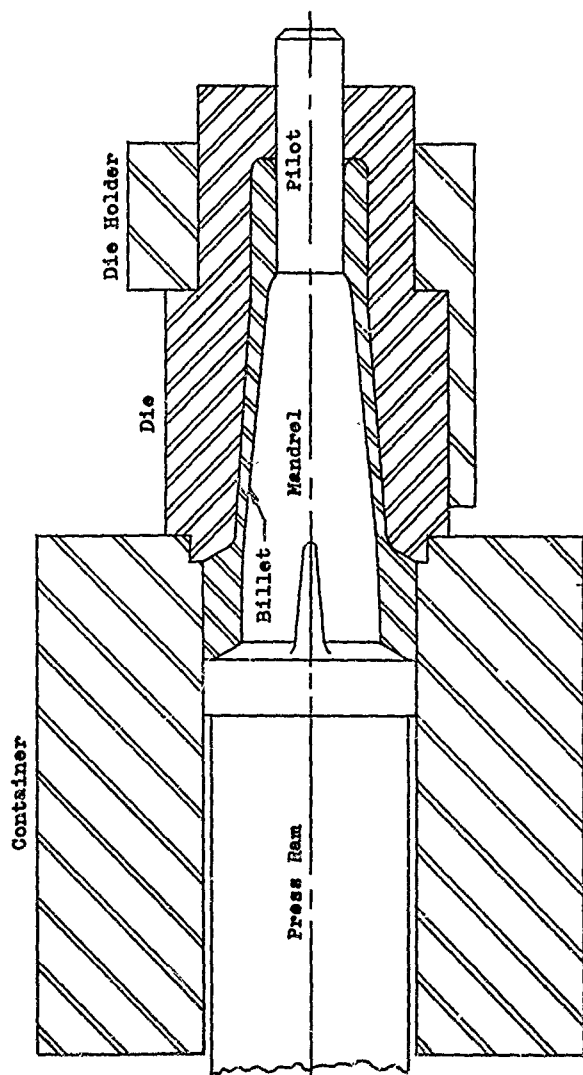
Figure 136. Second Step - Expansion.

326
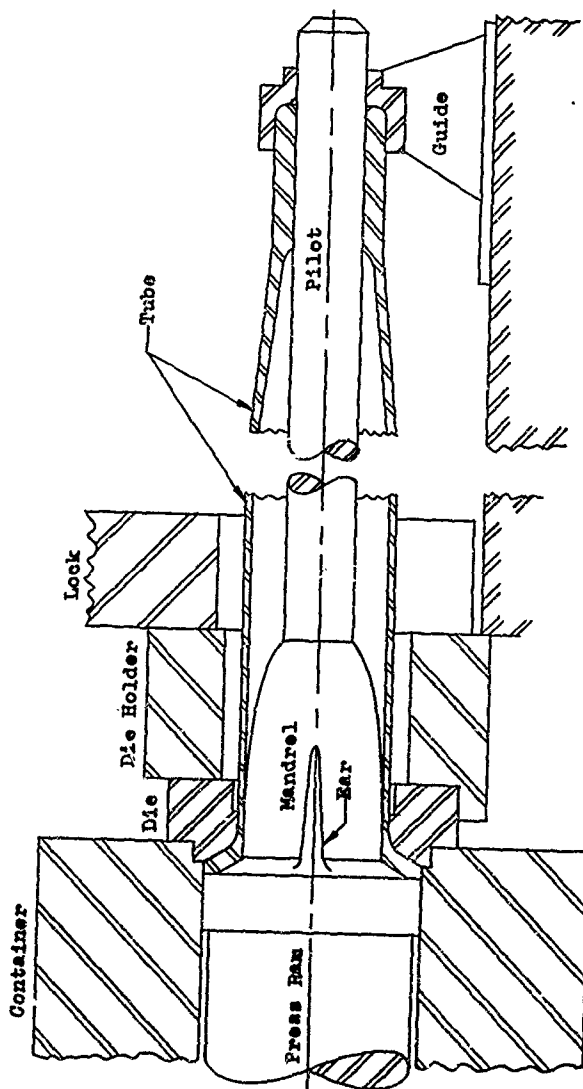
Figure 137. Third Step – Extrusion.

327

stress relieved. A serial number is assigned each tube after
this step. This number is merely an identification number and
not a blade serial number.

After cooling the tube is given a rough dimensional and visual
inspection before going to the blade line.

Tube Preparation

The tube must first be processed to remove decarb, improve sur-
face finish and reduce wall thickness dimensions to the proper
oversize for finish processing. After assignment of a blade
serial number the tube is prepared generally as follows:

a. Cleanup Tube

The tip of the tube is cut to length and then it is
given a Bullard Dunn cleaning to remove scale fol-
lowed by grit blasting inside and out.

b. Contour Turn and Bore and Upset

After checking wall thickness readings in the
shank and transition area and removal of a decarb
test piece from the ear start the shank and transi-
tion area is rough turned and bored on a cam con-
trolled lathe. Upset of the shank flange, if called
for, can now be done the same as for a welded blade
and the tube slow cooled.

c. Outboard Dimensional Check & Reduction to Dimensions

Using grinding and polishing equipment, the tube is
cleaned up free of surface marks to permit accurate
dimensional inspection. This is done using special
deep throat dial micrometers mounted on carriages for
the fillet areas and by the use of ultrasonic inspec-
tion devices in the uniform plate areas. Referring
to the decarb check, internal stock must now be removed
sufficient for clean up of any decarb. This is done
by a combination of hand grinding, belt sanding, grit
blast and polishing.

After internal cleanup and polishing the tube is given
another dimensional check. Special attention must be
paid to the ear fillet and solid edge areas to avoid
coining in later die operations. If stock removal in
the fillet areas is required it is done by spot dril-
ling with micrometer adjustment and then blended
to spots by hand grinding. Solid edges are ground to
template and thickness.

328

The center wall thickness area of the tube can now be belt sanded on proprietary machines which are wall thickness and cam controlled very accurately. All dimensions at this stage are process dimensions allowing for further stock removal.

Tube Partial Hot Flattened and T.E. Solid Edge Added

The tip of the tube is prepared to permit the partial hot flatten die to crimp it as it is closed so that the tube will hold high gas pressure. The partial hot flatten die is designed to bring the round tube down to a fairly thick elliptical shape without twist. To go from a round tube to an airfoil shape in one step is impractical and leads to gutters along the edges.

The tube is heated to approximately 1700°F in a controlled atmosphere electric pit furnace and rapidly transferred to the die mounted in a large hydraulic press. The die is closed and as in welded blade practice nitrogen is injected into the tube cavity at from 1000 psi to 1500 psi and held for 10-15 seconds. The internal pressure forces the tube to take the shape of the die cavity. The tube is removed and slow cooled in a cooling pit.

The tube will have the crimped tip cut off and is now in a more convenient shape for dimensional inspection and correction. The internal fillets can be polished and grit blasted and an internal magnaflux of the edges made. Fillet thickness inspection is made once again and further spot drilling is done if required to permit later controlled stock removal.

The T.E. may require addition of either a normal solid edge strip or a wide T.E. strip depending on the design. The strip is fitted to the partial hot flattened tube. After mounting the two pieces in a weld jig the strip is welded to the tube using automatic submerged melt welding and post heated and stress relieved.

The solid edges are now inspected for width and notched to proper width and planform shape followed by removal of the excess solid edge width. The solid edges are now radius ground to templates and the fillet areas ground down to any spots made earlier. Smooth contours are maintained.

The tube is now given a complete X-ray, magnaflux and ultrasonic inspection followed by any required discing or polishing.

Finishing Operations

The tip of the tube is once again prepared for crimping and then heated as before for full hot flatten. The operation is identical to partial hot flatten, but this time the die has the full airfoil shape but still without twist.

The blade is slow cooled, stress relieved and Bullard Dunn cleaned. Following tip cut off, inside grit blast and outside polishing the blade is once again X-ray and magnaflux inspected.

A solid contoured steel tip insert is fitted to the blade tip cavity by trimming for width only, and is hand welded in place and the tip locally stress relieved while purging the internal cavity with a protective atmosphere. After external grinding of the weld it is X-ray and magnaflux inspected.

The internal tip is grit blasted and cleaned and pickled for braze. Pellets of fluxed CuMn are positioned in the blade with the tip down and the blade placed vertically in a tip braze furnace and brazed while being purged with a protective atmosphere. Following local stress relief the tip is grit blasted and X-ray and magnaflux inspected again.

The leading and trailing internal edges are now grit blasted and cleaned for edge braze. Brazing is performed on the same automatic equipment and in the same manner as described under welded blades. After a stress relief operation the edges are grit blasted and X-ray, magnaflux and borescope inspected.

The blade is now pressure die quenched and formed with twist the same as for a welded blade and then drawn to the proper hardness.

From this point the blade is finished, using the same procedures as described under welded blades.

MANUFACTURING METHODS - COVERED SPAR HOLLOW STEEL BLADE

Discussion of the covered spar hollow steel blade will be limited to a general review of one possible basic technique since several options are open for manufacture.

Fabrication of the spar can start with procurement of an aircraft quality air hardening steel alloy tubular blank. The relatively short blank must have a thick wall and be fully annealed with a ground finish inside and out.

Processing Tubular Spar

The tubular blank is placed on a steel mandrel and cold worked down to correct wall thickness and length on a tube-reducing machine such as in the Rock Rite process. This process produces a tube with accurate wall thickness and good surface finish. Other tube-reducing processes may be used.

The still round spar may now be inspected for wall thickness and by magnaflux. Balance and weight must also be checked.

The tubular blank can be pressure die formed and quenched using the previously described technique. In this case however the tube will have a generally ovaloid appearing cross section with faces curved to proper partial airfoil shape. As in the extruded blade intermediate preforming may be required. The quenched and formed tube must be drawn to the required hardness.

The spar will receive a series of cleanup and inspection operations including dimensional and magnaflux inspections. The root end will be machined to finished specifications. If integral bearing races are incorporated the spar must be given special treatment for hardening the raceways such as flame hardening, carburizing or nitriding.

Shell

The shell can be made a number of ways. The dimensionally accurate plate can be rough stretch formed without twist or stamped bending about the seamless L.E.

The tip and T.E. seam must be welded and may be done using resistance welding. Welding will be followed by X-ray and magnaflux inspection.

If brazed fillets are called for these may now be added and inspected.

The shell may now be given a pressure die form and quench operation followed by proper drawing, cleanup and inspection. The root end of the shell will be trimmed to the proper termination shape.

Assembly

The spar and shell may now be assembled with fluxed brazing alloy between the parts. Brazing can be of the low temperature type below the draw temperature of the steel components. A special fixture is required to hold the parts in proper

alignment. If integral race ways are incorporated this area must be kept chilled. The assembly will be X-ray and magna-flux inspected.

Finishing

After internal cleaning, the poured in place foam core may be added and the blade processed through several finishing and balance operations including zinc plate, anozinc and clear lacquer. The covered foam cuff must be added to finish off the inboard root end.

MANUFACTURING METHODS - MONOCOQUE FIBER GLASS BLADES

There are several ways to produce a seamless monocoque fiber glass blade. The method described here is one which has been used successfully but the description will be limited to avoid proprietary details which have not previously been published, Reference 14.

Procurement of Materials

As with steel blades all materials are procured and received to rigid specifications. This is especially important when dealing with organic materials where a producer may vary the source of supply in producing resin formulations and thus the production technique. Such changes can often modify the blade fabricator's results and cause a great deal of searching as to why. Materials and sources should never be changed without qualification testing of the new materials. This can be a serious problem to the blade manufacturer who would normally like to have several optional sources of supply.

The most important material procured will of course be the preimpregnated fiber glass. Aside from the glass and resin used, the impregnation process must be carefully controlled not to contaminate the sizing or finish on the glass which assures proper wetting and bonding at the resin glass interface. After "B" staging or partial curing of the resin it is important that the pre-pregs have the correct resin content, resin flow proper-ties and tack. Pre-pregs normally are fully identified, dated and stored under refrigerated conditions as with many of the other materials for maximum shelf life.

Fabrication

The bell shaped hollow steel shank, see Figure 102, is fabri-cated much the same as a hollow steel blade using the pressure

332

die process. For high production there may be several cost saving options because of its simplicity.

A bladder is made from two pieces of fluorocarbon film heat sealed around the edges. The bladder is roughly the shape of the inside blade planform.

The bladder is prepared to be made into a bean bag by proprietary procedures and it is assembled with the steel shank which has been primed along with suitable plumbing. This assembly is placed in a vertical female mold or core box whose cavity is based on the inside blade shape less proprietary allowances. The bladder is inflated to take the shape of the core box cavity and filled with "beads" or pellets while being vibrated for compaction. When a vacuum is now applied to the bladder it becomes a hard mandrel and will retain its shape as long as the vacuum is held.

The evacuated "bean bag" mandrel is mounted vertically on a layup stand and is ready for layup of the preimpregnated glass cloth. The layup is done by hand tailoring each sheet for proper fit and type of joint. Type of cloth, fiber orientation and number of layers follows drawing specifications. All layers except for thickened center pads terminate over the steel shank.

The blade is now positioned in a female metal mold for cure and the hydraulic press is closed. Proprietary procedures assure that the glass fibers are tight and wrinkle free. Once in the press the "bean bag" vacuum is cut, the bladder cavity is filled with nitrogen under pressure, and heat is applied to the die. Cure is carried out to specified time, temperature and pressure cycles. The molded blade is now removed from the die, the "beans" or pellets are drained and the bladder is extracted. The seamless blade is trimmed and given a series of dimensional ultrasonic and X-ray inspections.

The internal blade surfaces are prepared for foam filling by a proprietary treatment and the blade cavity filled with poured in place urethane foam while being held in a die. After foam cure the blade is again X-ray inspected.

The shank fairing if called for is added much the same as for a hollow steel blade except that due to the high degree of reproducibility of fiber glass blades wet cover skins can line the mold before it is placed on the blade and the foam poured. With this procedure after cure the fairing is complete and requires only trimming. The fairing is X-ray inspected.

Blade balance is attained through process control and proprietary means. Complete dimensional inspection is made and the blade coated with an elastomeric finish. Deicing boots

and/or a L.E. sheath are added and the blade is complete.

SIZE CONSIDERATIONS IN MANUFACTURING

Considering the effect of blade size in the manufacture of pro-
peller blades it can be said that no limit is in sight. The
question is more pertinent if it refers to present plant facil-
ities. Any facility will have a maximum size limit. This will
largely be due to such things as heat treat furnaces, hydraulic
presses and machine tools. Size may also be limited due to over-
head clearance in the shop bays since many operations, such as
heat treat, are best done with the blade vertical. Increased
size also emphasizes the need for special handling equipment.
Some of the large 20' diameter extruded steel blades in the
past weighed over 375 pounds finished and much more in process
so all handling was mechanical.

It is also true that some innovation in process techniques will
be required with increase in blade size. An example could be
large composite blades layed up in the vertical position where
the large mass of material and extended layup time could result
in the layup saging before completion. This sort of problem
is another good reason for automatic layup machine development
in addition to the obvious economic advantages.

RELATIVE BLADE COSTS

Comparing relative blade costs as in comparing relative blade
weights is complicated by such things as lack of data on blades
of the same size in each category, unequal production rates and
variation in experience with different constructions placing
them at different points on their learning curves. Scrap rates
also play a major part in estimating costs. As automation
enters the picture more and more it would be expected that rel-
ative blade costs could change but it is unlikely that the
general order would change.

There is no doubt that solid aluminum alloy blades are the
least expensive of the metal blades discussed in this report.
A relative cost figure of 25% of the cost of a hollow steel
blade has been used in the past. It is also obvious that a
fiber glass blade cost will fall somewhere between the solid
aluminum and hollow steel blade cost. Depending on the type of
fiber glass blade, experience would suggest that they would run
between 40% to 60% of hollow steel blade costs. Use of unwoven
material without automation of the layup and/or the inclusion
of a metal spar would tend toward the higher figure.

334

BLADE RELIABILITY

Reliability of propeller blades is of very high order as would
be expected in a prime reliability component receiving the
most rigorous analysis and care in manufacturing. Reliability
has improved substantially over the years and is expected to
continue to improve as more engineering knowledge and better
materials become available. Even today with properly main-
tained equipment blade failures are extremely rare and can be
counted in terms of a failure in several blade years of oper-
ation. Reliability cannot be said to be 100%, but it is very
close.

Blade Life

Blade life of metal propeller blades has improved with use on
surfaced runways which are kept clean. Hollow steel blades
have operated in quantity above 30-40,000 hours and solid
aluminum alloy blades may go 10,000 hours before they "wear
out" due to erosion and repeated clean ups. In the case of
high time steel blades designers become concerned with low
cycle fatigue damage. Because of their extended life high
time blades accumulate a large number of cycles of high steady
stresses at a rate of one cycle/flight. Because these steady
stresses are high and the number of cycles number in the thou-
sands it can be seen that they must be treated on a low cycle
fatigue basis. While no known cases of blade retirement for
this reason exist it is inevitable that it will eventually
occur.

Blade incidents when they do occur are always studied in great
detail to pinpoint the exact cause. Virtually every known case
of blade failure in modern times has resulted from an undetected
flaw in materials or processing and/or poor maintenance prac-
tices. In each such case action has generally been taken to
improve quality control practices and equipment to prevent a
reoccurrence, and in many cases reinspection of the blades in
entire fleets around the world have been made.

Blade Durability

Hollow steel blades have an enviable record of durability.
Blades have flown the Atlantic when the outer 25% of the blades
were bent at nearly right angles from hitting a snow bank on
takeoff. Examples of extreme impact damage operating safely
to get a plane home have been commonplace. Perhaps the best
examples of such durability occurred during World War II.
Hundreds of blades returned to base with every conceivable
degree of battle damage. Figure 138 is a typical example of
such damage. In this case only the welded solid edges held
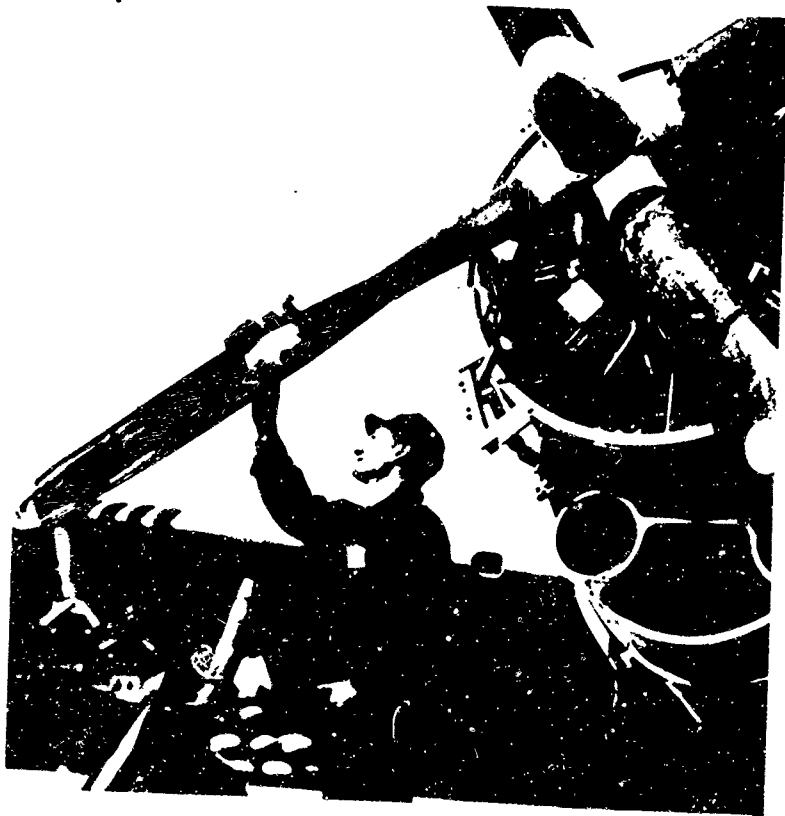the blade together after a direct hit by a 40mm explosive shell.

335

Figure 138. Blade Damage Due to 40mm Shell.

336

BLADE MAINTENANCE

Daily Inspections

Good maintenance of blades of any type involves daily visual
inspection for operational damage such as nicks, gouges,
scratches, dents, buckles, bulging, static discharge or elec-
trical burns, corrosion, cuff separation, damaged heating ele-
ments and cracks. For this kind of inspection the blades must
be kept clean and detection of damage aided by wiping the
blades with an oily rag. It is apparent that the type of blade
finish can greatly aid this kind of visual inspection.

While detection of cracks by visual examination is very rare
they have been found. In many cases suspected areas have been
confirmed by the use of dye penetrant or local magnaflux using
a permanent magnet on the flight line.

For the most part visual inspection will be looking for nicks
and gouges which are common to all types of blades plus dents,
buckles and bulges on hollow blades. Dents are the result of
impact damage while buckles may result from excessive tip load-
ing which may be caused by contact with snow, slush or solid
water during operation. Buckle damage is not necessarily
accompanied by surface abrasion in the area of such contact or
any noticeable change in blade track. A buckle can usually be
differentiated from a dent because it will have a distinct
crease through its center.

Damage Allowance Determination

Damage allowances are defined for each specific blade design.
The allowances are based on structural analysis and fatigue
tests of actual simulated damage of the type of blade involved
but not necessarily the specific design in question. The best
test data is acquired by simulating damage on a propeller run-
ning at speed in a test cell while introducing crushed stone
and nuts and bolts into the rotating disc at selected points
on the blades. Camber side damage is usually desired and is
obtained by running the propeller in reverse pitch, thus the
resulting damage will be at the extreme fiber or maximum stress
point in alternate bending. When the proper degrees of damage
have been obtained the critical areas are strain gaged and the
blades fatigue tested in the laboratory, usually in first mode
flapping. The data thus generated will be reduced and can be
generated into allowable damage values for a variety of oper-
ating stress levels. This method is preferred because it gen-
erates at the bottom of each gouge representative cold working
which greatly influences the fatigue strength of the gouge
compared with standard notched stress concentration factors.
Similar simulated damage can also be produced on test coupons

337

by such things as frangible glass bullets and rotating arms
with frangible glass wedges. In the latter test a coupon is
triggered into the path of the glass wedge on the end of a
rotating arm and receives one impact. Speed of impact and
depth of damage is adjustable. These simulated coupon tests
are helpful supplements to full-scale tests.

Other types of damage such as dents are also evaluated by both
analysis and experimental tests before allowances are estab-
lished.

Damage Allowances and Rework - Solid Aluminum Alloy Blades

Solid aluminum alloy blade damage allowances are generally
larger than for hollow steel blades and for a given exposure
the softer metal blades also incur greater damage. There are
two types of damage allowances normally established, those not
requiring rework and those that do. Typically for a solid
aluminum alloy blade damage allowances and local repair limits
might be as follows:

1. **Maximum Depth of Surface Damage Not Requiring Rework**

   a. Outboard - .018" except .008" in a previously
      reworked area.

   b. Inboard - .008" except .005" in a previously
      reworked area.

   c. Within 3" of tip - no limit.

2. **Maximum Depth of Rework on Face and Camber Sides -
   Local Repair Only**

   a. Shank to tip - .075" or up to 25% of section
      thickness at point of rework.

   b. Within 3" of tip - no limit.

   c. Rework General - All reworked areas shall have
      well rounded faired edges and smooth surfaces.
      All damaged metal shall be removed, but care shall
      be taken not to remove more metal than necessary.
      Reworked areas must be inspected to insure that no
      cracks, sharp edges or folded metal is present.

   d. Rework Proportions - All repairs must be faired
      out in the longitudinal direction of the blade.
      Length of rework must be blended over a distance
      of not less than twenty times the depth of the
      rework.

338

3. <u>Maximum Depth of Chordwise Rework on L.E. and T.E. -</u>
   <u>Local Repair Only</u>

   a. Inboard .25 R - .08"

   b. Inboard .60 R - .19"

   c. Inboard .80 R - .25"

   d. Tip area - .40"

   e. Last 3" of tip - no limit

   f. Rework General - Edge reworks shall be well faired
      into the original section shape. All reworked
      areas shall have well rounded edges and smooth sur-
      faces. All damaged metal must be removed but care
      shall be taken not to remove more metal than neces-
      sary. Reworked areas shall be inspected to insure
      that no cracks, sharp edges or folded material are
      present.

   g. Rework Proportions - All repairs must be faired
      out in the longitudinal direction of the blade.
      Length of blended rework in longitudinal direction
      must be no less than ten times depth of rework.

4. <u>Tip Reworks</u>

   a. Up to 3" of tip may be completely removed if re-
      quired and the tip reshaped as close to the origi-
      nal as possible.

5. <u>Scratches</u>

   a. Sharp line type scratches must be removed.

<u>Damage Allowances and Rework - Hollow Steel Blades</u>

As in the case of solid aluminum alloy blades two types of
damage allowances are established, those not requiring rework
and those that do. In addition to abrasion damage, however,
hollow steel blades must have allowances for dents, bulges and
buckles. In order to define allowances for hollow blades the
solid edge widths must be listed so that an inspector can tell
if damage is in the hollow area of the blade or in the solid
edges. Typically for an extruded hollow steel blade damage
allowances and local repair limits might be as follows:

339

1. <u>Maximum Depth of Surface Damage Not Requiring Rework</u>

   a. Hollow area - .005"

   b. Solid area - .010"

   c. Exception - Sharp line type scratches deeper than .003" must be repaired.

2. <u>Allowable Metal Removal Limits for Rework of Local Areas - When the Wall Thickness is Unknown</u>

   a. Hollow area inboard - .021"

   b. Hollow area outboard - .010"

   c. Solid area - .020"

   d. L.E. chordwise - .060"

   e. T.E. chordwise - .125"

   f. Tip longitudinal - .060"

   g. Rework General - All traces of damage in reworked areas must be removed. Magnetic particle inspection may be used with standard equipment or portable permanent magnet. All reworked areas shall have well rounded edges and polished surfaces such as with No. 240 grit emery paper. All rework depths must be measured.

   h. Rework Proportions - Since depth of reworks must be shallow, blending of the rework must also be shallow and well rounded. There should be no abrupt changes of contour. Minimum metal removal is required.

3. <u>Hollow Area Allowable Minimum Wall Thickness After Rework of Local Areas When Wall Thickness is Measured</u>

   a. Thrust and camber surfaces - 80% of drawing.

   b. From 75% R to tip - 70% of drawing if no repair exceeds 1" in diameter. No more than two such repairs in any 1" strip across the blade and no more than four such repairs per side.

4. <u>Repeening</u>

   Reworks in shot peened areas must be repeened with a vibrating hand tool with a bit having a spherical

radius of .013"-.018". Peening must be uniform in pattern and intensity and carry over .25" into existing peening.

5. Brush Plating

a. Reworked surfaces or damaged or worn plating should be touched up locally by "brush plating" with zinc. All such areas must be masked and treated with Iridite No. 8P until the yellow color matches the original anozinc. Flush with water and spray with lacquer.

6. Cracks

a. Cracks are not acceptable.

7. Static Discharge or Electrical Burns

a. Cause for removal from service for inspection and repair unless confined to 24" from tip and is in solid edge material. Such areas repair as above. Other areas may be repaired after etching with 10% ammonium persulfate solution to show heat affected material. If heat affected zone cannot be removed within limits herein,return to factory for stress relief and possible repair.

8. Dents

a. Any surface irregularity which does not have the identifying characteristics of a buckle but which is greater in depth than .040" as measured under a 6" straight edge shall be returned to the factory for possible repair.

9. Buckles

a. Any buckle identified with a crease through its center shall not be returned to service. Any blade maintained in operation after having been buckled is not repairable due to indefinite fatigue damage. Other buckles may be repairable at the factory.

10. Bulges

a. Bulges may be due to shifted rubber ribs or internal filler. Return to factory for possible repair.

All depth of damage above must be measured with
surface micrometers having pointed anvils and with
reference to adjacent undamaged surfaces.

Damage Allowance and Rework - Monocoque Fiber Glass Blades

Damage allowances have not been well established for fiber
glass blades due to limited service experience. However,
simulated damage tests and fatigue tests have been run similar
to those described for metal blades. A word about failure
modes may be in order as related to blades made with high
pressure molded woven cloth material. Unlike fatigue cracks
developed in unwoven material which include much delamination,
cracks in sound woven material are normally sharp and
well defined with little or no delamination between layers.
In either case they are readily detected visually through
clear transparent finishes. However, if the surface has been
abrasion damaged the failure origin may be at the root of the
nick or gouge and will first be evident as substantial delami-
nation at the interface of the damaged layers and the first
undamaged layer.

As fatigue progresses the sound layers below the nick or gouge
will develop the characteristic sharp line type crack. The
phenomenon just described may explain the low notch sensitivity
of woven fiber glass structures. Further research in this
area might show that fatigue strength is proportional to the
percentage of sound layers remaining after damage has occurred
since delamination of damaged surface layers would leave little
if any notch effect or stress concentration.

On a limited number of tests run on unprotected fiber glass
blades severely damaged in the test cell with 1/2 inch crushed
stone, the average endurance limit was more than for undamaged
blades. This is an unlikely fact and is probably due to test
scatter but may serve to emphasize that fatigue reduction is
small. More such tests should be run.

With foam filled fiber glass blades separation of the foam
core from the internal fiber glass surfaces may occur. This
is readily detectable by tapping, and sometimes visually, even
if no foam shift has taken place. Such separation will nor-
mally be evident on only one surface and is not usually serious
structurally. Blades have been run for several hundred hours
with almost total unbond on one side. Repairs are readily
made.

Typically for a foam filled fiber glass blade damage allow-
ances might be as follows:

1. <u>Maximum Depth of Surface Damage Not Requiring Rework</u>

   a. All areas - .010".

   b. Scratches - .010" deep and up to 2" long.

2. <u>Foam Separation Not Requiring Rework</u>

   a. All areas - Up to 10 square inches of unbond.

3. <u>Unbonded Root End</u>

   a. Unbonded root ends must be removed from service.

4. <u>Damage Repair Allowances</u>

   Unlike metal blades fiber glass blades can be repaired
   by adding new material. Even severe ballistic damage
   should be repairable. Many such repairs can be made
   in the field or in extreme cases at an overhaul base
   or at the factory.

   a. Field repairs - Local repairs up to a depth
      of 25% of the wall thickness.

      Rebonding local areas of foam unbonds.

   b. Base repairs - Local repairs up to a depth of
      100% of the wall thickness.

      Complete resurfacing and matched set balancing.

      Rebonding of large areas of foam cores.

5. <u>Damage Repair - General</u>

   a. Local repairs - The area to be repaired must be
      cut back to sound material. The foam core if
      damaged should be repaired by pouring fresh foam
      locally. The surrounding fiber glass ideally
      should b stepped back from the bottom of the
      hole in steps one to two layers of cloth thick
      with the width of each step sufficient for a bond
      area which will develop equal strength of the
      cloth layer. Cut cloth layers to fit step, im-
      pregnate with resin and fit to prepared repair
      area. Pressurize and RT cure. Refinish.

   b. Resurfacing - Remove all blade protective finish.
      Sand surface uniformly. Add wet impregnated layer
      of cloth. Vacuum bag if possible and RT (Room
      Temperature) cure. Or cover with PVA film and

343

rub smooth and RT cure. Refinish and balance
blades in sets.

c. Rebonding foam - Outline the unbonded area with
pencil or crayon. Drill two or more 1/16" to 1/8"
diameter holes at opposite ends of the unbonded
area. Connect a vacuum line to one hole and in-
ject epoxy resin system through the other hole.
A dye added to the resin helps to tell through
the translucent fiber glass if the unbonded void
has been filled. Vacuum bag the repaired area and
cure. Clean up and refinish the reworked area.

Base Overhaul of Blades

The overhaul of all types of blades is carried out desirably
at the same time as engine overhaul but may be only at every
other engine overhaul. There may occasionally be an interim
functional overhaul at unscheduled engine removal. Blade
time between overhauls (TBO) will normally run from 2500 to
5000 hours. Overhaul may be accomplished at a base or at the
factory. Some operations if required may have to be done only
at the factory.

Base overhaul will include all previously mentioned inspec-
tions and repair plus:

a. Remove blades from hub.

b. Remove sheaths and heating elements for inspection
and repair of concealed blade damage or corrosion.

c. Remove bearings, gears and seals for inspection, re-
pair or replacement. Inspect all root end details
internal and external.

d. Remove all blade cuffs or fairings (except on fiber
glass blades) for inspection and repair of concealed
blade damage or corrosion.

e. Remove balance cup if any and inspect internally for
corrosion

f. Inspect aluminum alloy blades with dye penetrant
method, anodizing, or 20% hot sodium hydroxide solu-
tion followed by neutralizing in a solution of 50%
nitric acid, 1% sulphuric acid and 49% water by volume
then rinse in cold water and then hot water.

g. Inspect steel blades by magnaflux both external all
over and internally at the root end.

h. Touch up all plating or strip and replate.

i. Inspect for soundness of all internal inserts.

j. Rebalance to master or in matched sets.

k. Install new fairings and deicing assemblies.

l. Return all useable components to blade.

m. Enter all information in the log book.

Factory Overhaul of Blades

Factory overhaul will include all items covered in a base overhaul plus several items that normally cannot be done at a base such as:

a. Straightening and stress relief or reheat treatment.

b. Burn out and replace rubber ribs.

c. Grit blast or vapor hone all over after surface repair. (Blends excessive minor nicks and gouges). Replate.

d. Cut down solid aluminum alloy blades all over to clean up accumulated surface damage. Profile thickness and chord may be reduced up to 5% of drawing values. Rebalance in matched sets.

e. Re-X-ray inspection.

f. Limited weld repairs in original weld metal and stress relief.

g. Reshot-peen as required.

The foregoing discussion on maintenance and overhaul only highlights actual service bulletin instructions which are normally very complete and descriptive and designed to be GI proof.

TESTING

Testing is the basis of safe operating propeller blades. Largely all testing is customized by each manufacturer. This is due mainly to the need for prime reliability and the high operating stresses and the novel processes often involved. While a company may rely on published data in making selections of materials and processes, in the final analysis it will establish its own data and subsequent controls based on

its own testing of materials, blades and components.

Basic Materials Testing

For use in propeller blades all structural materials must be qualified by complete physical property testing. Sufficient testing must be done in all categories to assure a good statistical base and repeatability. Testing will normally continue throughout the period of use of a material as improvements are sought.

The basic blade structural material should be tested to establish all normal physical properties. Testing should be sufficient for reliable statistical reduction. Emphasis must fall mainly on fatigue properties, S-N curves and Goodman diagrams. These tests must not only cover sound well polished material but should also include defective material such as inclusions, decarburized steel, simulated nicks and gouges, weld defects and rough finish. The effects of processing must also be evaluated such as welding, intergranular penetration of brazing, cold working, upsetting, and plating. The list can be much longer. The ultimate goal is, of course, a very reliable set of allowable physical properties. For a Goodman diagram, for instance, this may mean an allowable about one-half the mean minus 3σ limits to give a reasonable factor of safety for the unexpected.

Environmental effects should also be evaluated such as temperature extremes, fungus, rust and corrosion and the effects of service use such as galling.

A complete understanding of the materials and their properties cannot be over-emphasized as a basic requirement.

Core Material Testing

As with the basic material, core materials must be thoroughly evaluated. In addition to the usual physical and fatigue properties the core materials should be evaluated in their function as part of a sandwich structure. Abilities to bond well and resist water migration must also be checked. Thermal shock resistance can be an important factor as well as the ability to survive high altitudes without distortion. Under high frequency vibration, core materials may have high hysteresis and overheat, and this parameter should be checked on certain type cores or inserts. Post-cure gassing can also be a problem with some types of cores.

Fairing or Cuff Materials Testing

Although lightweight fairings if they fail may not pose a serious problem structurally, it is still important that they be fully reliable. Much testing similar to core materials is desirable. Processing tests can be very profitable.

Component Tests

Components in this instance refer to sections cut from blades. These may be in the form of cross-sections, longitudinal sections, 'wishbone" sections or any other section to assess a critical factor. Such sections may be tested as coupons for standard physical or fatigue properties representative of fully processed blades. The so-called "wishbone" section is a transverse section of a hollow blade which has the center area removed leaving a U-shaped edge specimen. Such specimen can be fatigue tested by mounting one leg on a resonance bar and tuning the other leg with small weights. For a hollow steel blade with brazed fillets, the failure mode and endurance strength can be established for this area of a finished blade by the "wishbone" test. Component sections can also be used for tests of core or insert bonds. Such sections are also useful for microscopic examination.

Full-Scale Laboratory Testing

Full-scale laboratory tests involve fatigue testing which will support the S-N intercept of the Goodman diagram, or they may involve combined stress testing which again should support the Goodman diagram. These tests are especially valuable since the results reflect the actual blade with all its manufacturing imperfections and built-in fillets and corners. In each group of these tests it is desirable to run a statistically significant number of specimen such as five. These tests are expensive and so are usually limited. However, they are not as costly as the combined stress tests common in the rotor blade field. Over the years they have proven to be entirely adequate for propeller blades. The tests are broken down as follows:

a. Free-Free Flapping - The fully strain-gaged blade is suspended tip down in a free-free manner and driven from the root end by an electro-magnetic vibrator. Endurance is generally run at resonance in first mode flapping which fatigue tests the outboard portion of the blade. Stress levels are controlled by varying power input. Test continues to failure.

347

b. Torsional Mode - In this test the gaged blade is sus-
pended by the shank from a crossbar. Vibrators are
mounted at each end of the bar and are excited out of
phase to produce pure torsional excitation. Endurance
is again run at resonance until failure.

c. Fixed Root Edgewise - For this test the shank of the
blade is mounted as rigidly as possible. The vibrator
i connected to the blade a suitable distance outboard
with its axis aligned from L.E. to T.E. Endurance is
run at resonance until failure occurs in the root area
of the blade.

d. Shank Retention Test - In this test the blade root
end is sawed off and fitted with special fittings at
its outboard end to apply the loading. The shank is
then assembled with a simulated hub barrel and bear-
ings and mounted in a collet on a special test machine.
Using pivoted draw bars a full centrifugal load is
applied by the levers off-center of the root so that
a steady bending component also results. A vibrator
or mechanical shaker is mounted at the outboard end of
the shank and adds the vibratory component of loading.
The hub is so mounted in the collet that it can be
torsionally oscillated so that the blade shank bearings
do not run in one position. This test obviously gives
valuable combined stress data on the blade shank and
retention and also tests the simulated hub barrel,
blade nut and blade bearings. Although retention com-
ponents may have to be replaced the blade root can be
run to failure.

Full scale laboratory tests in addition to testing
actual blades representative of the manufacturing pro-
cess can also be used to evaluate special defects
under study, simulated abrasion damage, or even high
time or damaged service blades.

Whirl Testing Blades

Electric motor whirl testing covers several areas of interest.
As the name implies, this group of tests is done on an elec-
tric motor whirl stand equipped with accurate means of meas-
uring thrust, power, rpm and deflections. These tests are
described elsewhere in this report.

Engine Testing Blades

Testing of blades on the engine for which they are designed is
important because of possible engine/propeller vibrations

which are not duplicated on the whirl stand. This is especially important if the engine is a reciprocating engine. The engine test stand should have a circular throat to obtain the best possible airflow without inducing unwanted airflow patterns and vibrations. Testing will normally be 100 hours at normal rated power and 10 hours at takeoff rating. Instrumented blades should be used. The actual conditions of the test may be run all or in part at the power condition which gives maximum blade stresses.

Gyro Rig Testing Blades

The gyro rig endurance test may be the most important proof testing done on propeller blades. Its purpose is to superimpose simulated 1xP loading on normal blade steady stresses. Two types of test rigs have been used. One involves running the blades in an evacuated chamber while the propeller is precessed around an axis at 90 degrees to the propeller shaft. No thrust loading is imposed on this type of rig but power required is low. The other type of test rig uses an aircraft engine to drive the propeller in open air while the entire rig is rotated about its vertical axis. This test rig simulates full C.F. loading, partial air load bending and 1xP gyroscopic moments. See Figure 139.

Both types of rigs induce 1xP gyroscopic moments which produce loads very similar to actual 1xP loads along the blade radius.

This type of testing most closely duplicates the major fatigue producing operating stress conditions on modern propeller driven aircraft.

Normally this type of test is run for 10×10^6 cycles of 1xP vibration.

Flight Testing Blades

Two types of flight tests are normally performed. One is conducted for aerodynamic performance and is discussed elsewhere in this report. The other involves flight vibration stress surveys and establishes the safe operating conditions of the blades.

Using fully instrumented blades the propeller is mounted on the highest stressed position on the airplane, usally No. 3 engine on a 4-engine aircraft. Data is first recorded for all normal ground operating conditions and powers including takeoff powers, all rpms, all wind directions and up to some minimum wind velocity since wind velocity and direction
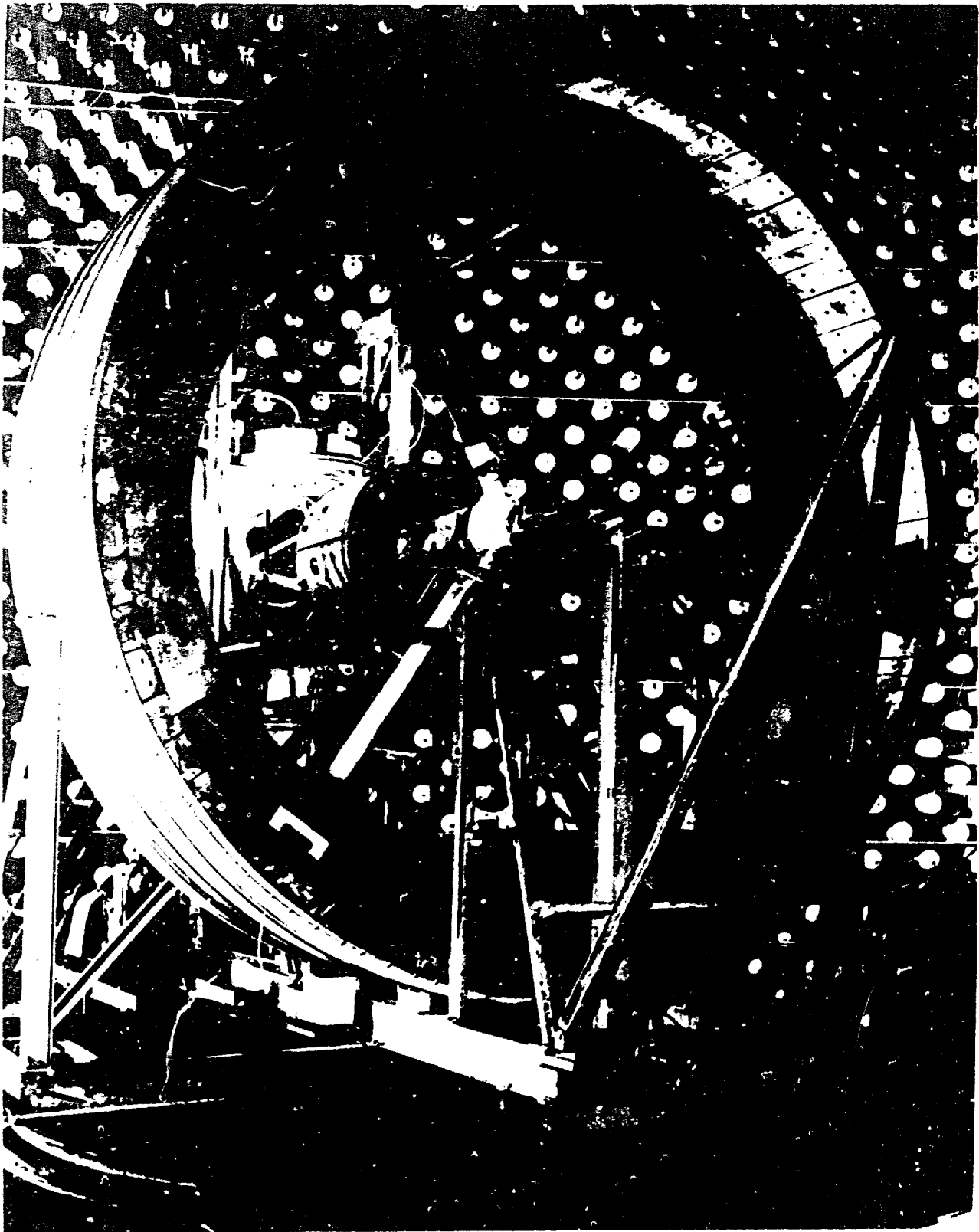
Figure 139. Gyro Rig for Blade Testing.

350

greatly affect blade vibratory stresses and types of vibration.

Flight vibration stress surveys are conducted for all aircraft operating conditions, loadings, maneuvers, and engine malfunctions such as cylinders out and altitudes. Later in the life of a reciprocating engine aircraft similar tests may be run on high time engines with worn dampers.

The vibratory stress data is reduced and plotted, and operating restrictions if any are noted and entered in the pilot's flight manual.

CONCLUSIONS

Based on the material presented in Volume II, it may be con-
cluded that:

1. Technology is available for the structural analysis to
determine the adequacy of the design of propellers suitable
for any conventional, STOL or V/STOL aircraft.

2. The success of a new propeller design is dependent on
the detailed knowledge of environment of the installation,
including the details of the flow angle, mounting and vibration
characteristics.

3. Proper lead time for the design analysis and tests of
new propellers must be provided to assure a mature design at
the time of the initial flights.

4. The application of new materials in composite structures
leads to large weight reduction of the propeller which im-
proves its competitive position relative to other systems.

LITERATURE CITED

1. Jones, A. B., ANALYSIS OF STRESS AND DEFLECTION, Volumes I and II, New Departure Co., Bristol, Connecticut.

2. Yaggy, Paul F., and Rogallo, Vernon L., NASA TN D-318, A WIND-TUNNEL INVESTIGATION OF THREE PROPELLERS THROUGH AN ANGLE-OF-ATTACK RANGE FROM 0° TO 85°.

3. Theodorsen, T., GENERAL THEORY OF AERODYNAMIC INSTABILITY AND THE MECHANISM OF FLUTTER, NACA TR-496.

4. Lehman, F. G., and Burke, P.R. GENERAL DYNAMICS ANALYSIS OF STOL/VTOL PROPELLER BLADES, WADC TR 58-371, 1959.

5. Taylor, J. Lockwood, AIRSCREW BLADE TWIST EFFECTS, Aircraft Engineering, December 1943.

6. Flanders, D. A., and Shortly, G., NUMERICAL DETERMINATION OF FUNDAMENTAL MODES, Journal of Applied Physics, Volume 21, December 1950.

7. Military Specifications MIL-P-26366A, PROPELLER SYSTEMS, AIRCRAFT, GENERAL SPECIFICATION FOR, 15 November 1962.

8. Stoeckley & Macke, EFFECTS OF TAPER ON SCREW THREAD LOAD DISTRIBUTION, ASME Preprint, 1951, Paper No. 51-S-15.

9. Cummings, H. N., Stulen, F. B., Schulte, W. G., INVESTIGATION OF MATERIAL FATIGUE PROBLEMS APPLICABLE TO PROPELLERS. WADC TR 54-531, 1955.

10. Cummings, H. N., QUALITATIVE ASPECTS OF FATIGUE OF METALS, WADC TR 59-230, 1959.

11. Cummings, H. N., SOME QUANTITATIVE ASPECTS OF FATIGUE OF MATERIALS, WADC TR 60-42, 1960.

12. Jones, A. R., and Lewis, W. RECOMMENDED VALUES OF METEOROLOGICAL FACTORS TO BE CONSIDERED IN THE DESIGN OF AIRCRAFT ICE PREVENTION EQUIPMENT, NACA TN 1855, March 1949.

13. Gray, V., and Campbell, R. G., A METHOD FOR ESTIMATING HEAT REQUIREMENTS FOR ICE PREVENTION ON GAS HEATED HOLLOW PROPELLER BLADES, NACA TN 1494, December 1947.

14. Modern Plastics, MORE LIFT WITH RP PROP, Modern Plastics May 1963, Breskin Publications Inc., New York.

15. AIRCRAFT PROPELLER HANDBOOK, ANC-9, September 1956.